Technische Universität München
Fakultät für Medizin

Screening of a drug library in *HDAC-2* proficient and deficient murine pancreatic ductal adenocarcinoma cells to identify new potential combination therapies

Marc Anwar Kidess

Vollständiger Abdruck der von der Fakultät für Medizin der Technischen Universität München zur Erlangung eines

Doktors der Medizin (Dr. med.)

genehmigten Dissertation.

Vorsitz: Prof. Dr. Wolfgang A. Weber

Prüfer*innen der Dissertation:

1. Prof. Dr. Günter Schneider
2. Prof. Dr. Gabriele Multhoff

Die Dissertation wurde am 06.10.2022 bei der Technischen Universität München eingereicht und durch die Fakultät für Medizin am 21.02.2023 angenommen.

TECHNISCHE UNIVERSITÄT MÜNCHEN

Klinik und Poliklinik für Innere Medizin II
Klinikum rechts der Isar
(Direktor: Univ.-Prof. Dr. med. Roland M. Schmid)

Screening of a drug-library in *HDAC-2* proficient and deficient murine pancreatic ductal adenocarcinoma cells to identify new potential combination therapies

Dissertation

vorgelegt von

Marc Anwar Kidess

aus München

2022

Contents

List of abbreviations

µl	Microliter
µM	Micromolar
°C	Degree Celsius
APS	Ammonium persulfate
ATP	Adenosine triphosphate
AUC	Area under the curve
BRCA	BReast CAncer-gen
BSA	Bovine serum albumin
CNS	Central nervous system
CO_2	Carbon dioxide
CTCL	Cutaneous T-cell lymphomas
Ctrl	Control
DAMPs	Damage-associated molecular pattern molecules
DMEM	Dulbecco's Modified DMEM
DMSO	Dimethyl sulfoxide
DNA	Deoxyribonucleic acid
EDTA	Ethylenediaminetetraacetate
EtOH	Ethanol
E8D	Ethanol treatment for 8 days; *HDAC-2* (+)
FCS/FBS	Fetal calf/bovine serum
FDA	U.S. Food and Drug Administration
FOLFIRINOX	*Flourouracil*, *Leucovorin*, *Irinotecan*, *Oxaliplatin*
g/gr	Grams
GSEA	Gene set enrichment analysis
GSH	Glutathione
GTP	Guanosine triphosphate
h	Hour(s)
HAT	Histone acetyltransferase
HCl	Hydrochloric acid
HDAC	Histone deacetylase
HDACi	Histone deacetylase inhibitor
HPV	Human papillomavirus
H_2O	Water
IC_{50}	Half-maximal inhibitory concentration
Ig	Immunoglobulin
IKE	Imidazole Ketone Erastin
IPMN	Intraductal papillary mucinous neoplasm
KRAS	V-Ki-ras2 Kirsten Rat sarcoma viral oncogene homolog
mA	Milliampere
MAPK	Mitogen-activated protein kinase
MCN	Mucinous cystic neoplasms
ml	Milliliter
mM	Milimolar
MS-275	Entinostat
MuSyC	Multi-dimensional synergy of combinations reference model
mTOR	Mechanistic target of rapamycin
NAC	N-acetylcysteine
NaCl	Sodium chloride

NAD^+/NADH	Nicotinamide adenine dinucleotide
nM	Nanomolar
ns	Not significant
KCl	Potassium chloride
PanIN	Pancreatic intraepithelial neoplasia
PARP	Poly-ADP-ribose-polymerase
PBS	Phosphate buffered saline
PDAC	Pancreatic ductal adenocarcinoma
Pen Strep	Penicillin, Streptomycin
PL-OH	Nontoxic lipid alcohols
PLOOH	Toxic lipid peroxids
PUFA	Polyunsaturated fatty acids
RAS	Rat sarcoma viral oncogene homolog
RNA	Ribonucleic acid
ROS	Reactive oxygen species
rpm	Rotations per minute
R0	In the microscope, no more remaining cancer cells remaining at the primary tumor site/on the resectate can be seen
SAHA	Suberanilohydroxamic acid/Vorinostat
SASP	Salazosulfapyridine
SDS	Sodium dodecyl sulfate
ST	Small T oncoprotein
TEMED	N, N, N', N' - Tetramethylethyldiamine
TRIS	Tris(hydroxymethyl)-aminomethane
T75	Medium-sized culture bottle
T8d	Tamoxifen treatment for 8 days; *HDAC-2* (-)
US/U.S.	United States of America
UV	Ultraviolet
V	Voltage
VDAC	Voltage dependent anion channels

Abstract

Pancreatic ductal adenocarcinoma (PDAC) is one of the deadliest cancer diseases in the human body, especially due to the lack of effective therapies in advanced stages. In the past, histone deacetylases (HDACs) showed to be applicable targets. Yet, HDAC inhibitors show no relevance in therapy of PDAC. Therefore, a drug-screening containing 101 agents with different mode of actions was performed using murine isogenic HDAC-2 proficient and deficient cell lines, and ferroptosis-inducer *Erastin* was found as a potential partner for a combination therapy with HDAC inhibition.

Zusammenfassung

Das duktale Pankreaskarzinom (PDAC) ist eines der tödlichsten malignen Tumorerkrankungen des Menschen, insbesondere wegen der eingeschränkten Therapierbarkeit in fortgeschrittenen Stadien. In der Vergangenheit erwiesen sich Histondeacetylasen (HDACs) als geeignete Angriffspunkte. Bisher haben sie keine Relevanz in der Therapie des PDAC. Daher wurde ein Screening mit 101 Wirkstoffen verschiedener Wirkmechanismen an murinen isogenen HDAC-2 -profizienten und -defizienten Zelllinien durchgeführt und hierbei der Ferroptose-Induktor Erastin als potenzieller Partner für eine Kombinationstherapie mit HDACInhibition gefunden.

Introduction

Anatomy and physiology of pancreas

The pancreas is a secondary retroperitoneal organ in the upper abdomen, which can be divided into head, body and tail. It has exocrine functions (98% of the pancreas) and endocrine functions (1-3%), which makes it a central organ in the human body (Welsch et al., 2014; Schünke et al., 2015). It is located on the height of the second lumbal vertebra and its head is located next to the descendent duodenum (Schünke et al., 2015) (figure 1).

The exocrine pancreas is a serous gland with epithelial cells organized in acini with apical zymogene granula, producing a lot of pancreatic secret (1500-3000 ml/day), enzymes (e.g. amylase) and proenzymes (e.g. trypsinogen), which are released into the pancreatic duct for secretion into the chymus in the duodenum to catalyze the digestion of proteins, carbohydrates or fatty acids (Pape et al., 2014; Welsch et al., 2014; Schünke et al., 2015). Besides the metabolic enzymes, the exocrine pancreas also produces bicarbonate in its epithelial cells of the intercalated duct to neutralize the acidic chymus coming from the stomach (Pape et al., 2014).

1-3% of the pancreatic tissue are the Langerhans insula, which represent the endocrine pancreas (Welsch et al., 2014). Depending on the metabolic situation, different hormones like insulin or glucagon are getting released into the blood and do their duty at the targeting tissue, e.g. hepatocytes (Pape et al., 2014). The main type of cells (60-70%) in the endocrine pancreas are the β-cells which produce insulin, followed by α-cells (20%) (glucagon) and 10-15 % δ-cells (somatostatin) (Pape et al., 2014; Rassow et al., 2016).

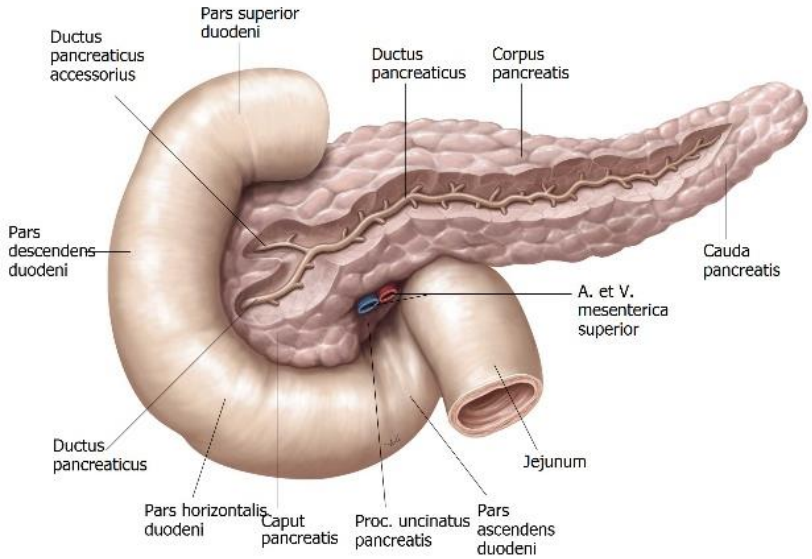

Figure 1: ***Anatomy of the pancreas.*** *From Gilroy, Atlas of Anatomy, 1st ed. Abb. 13.34. Illustrator: Markus Voll, ©2019 Thieme Medical Publishers. Inc. All Rights Reserved. (Gilroy, 2009).*

Pancreatic ductal adenocarcinoma (PDAC)

According to the recent 2022 cancer statistics, 32,970 US-men and 29,240 US-women will be newly diagnosed with pancreatic cancer (figure 2) in 2022 and with 25,970 estimated deaths of male patients and 23,860 estimated deaths of female patients (figure 3) in 2022, pancreatic cancer is one of the deadliest cancers (Siegel et al., 2022). In 2018, pancreatic cancer was the 4th deadliest cancer in the United States after cancers of the lung and bronchus, breast-/prostate cancer and cancer of the colon and rectum (Siegel et al., 2021).

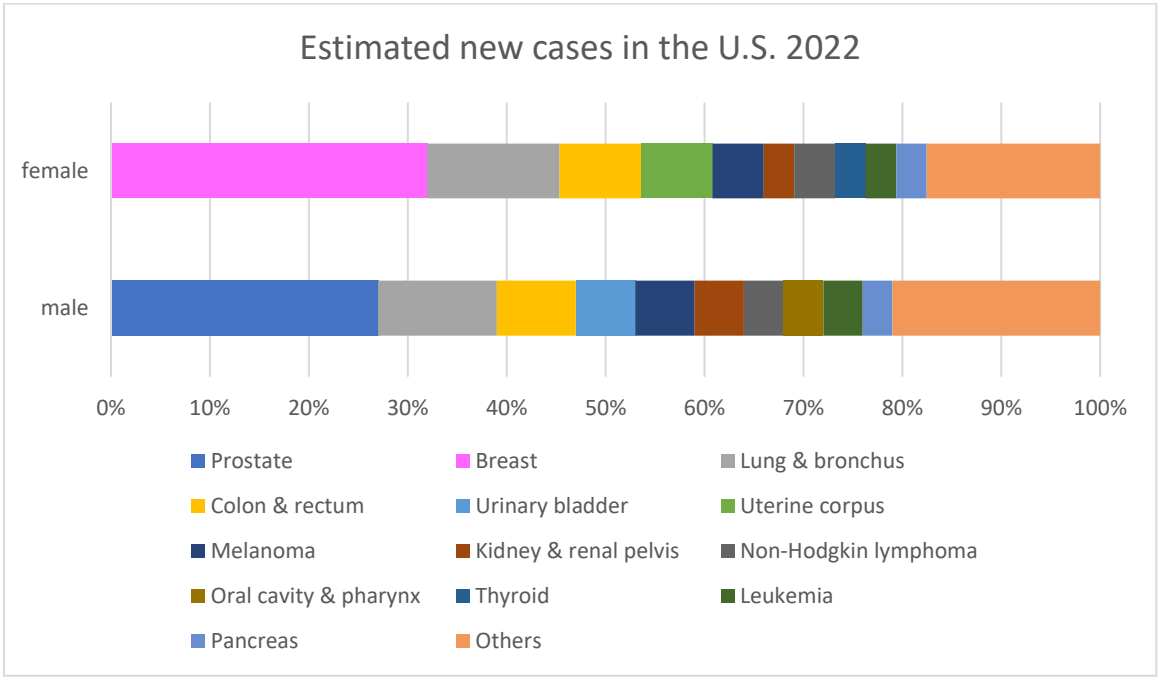

*Figure 2: **Estimated new cancer cases 2022**. With 3% of all new cancer diagnosis, pancreatic cancer is the 8th most common new cancer for women and the 10th most common new cancer for men. The results shown here are in whole or part based upon data generated by Siegel et al. CA: a Cancer Journal for Clinicians. 2022. (Siegel et al., 2022).*

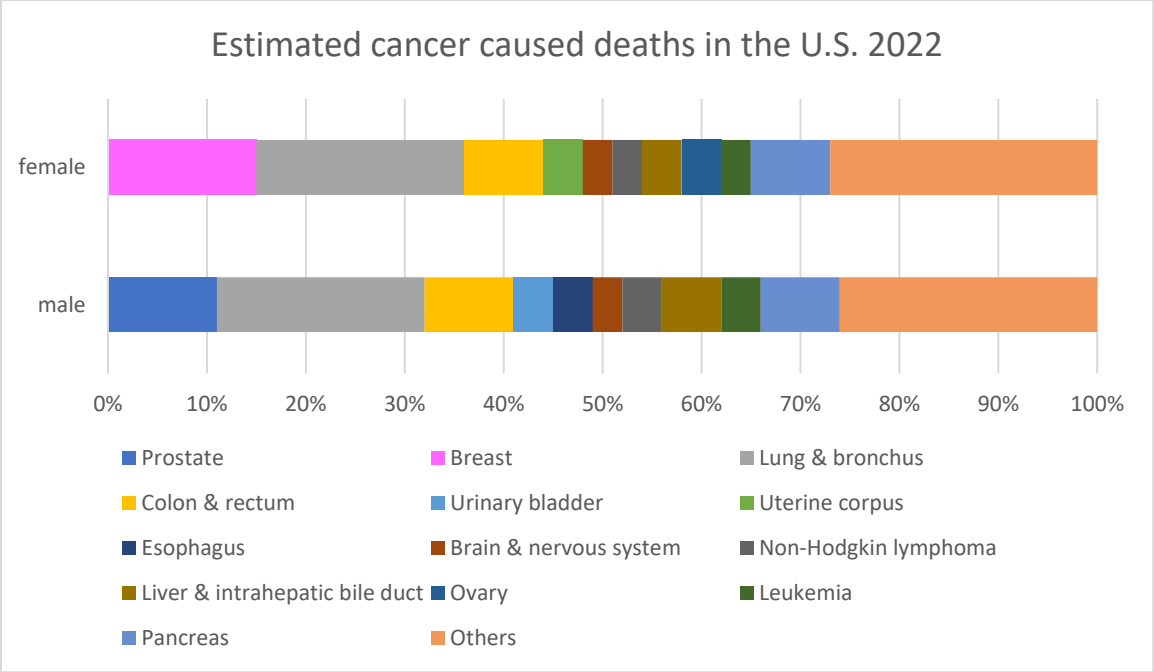

*Figure 3: **Estimated cancer caused deaths 2022**. Pancreatic cancer is the 4th deadliest cancer. The results shown here are in whole or part based upon data generated by Siegel et al. CA: a Cancer Journal for Clinicians. 2022. (Siegel et al., 2022).*

The 5-year-survival of pancreatic cancer is 11%, the lowest 5-year-survival percentage of all cancers (Siegel et al., 2022). Even if the cancer survival for the most cancers in general improved over the last years (e.g. because of new techniques of diagnosis, therapy or vaccinations like HPV-vaccination), it is not the case for pancreatic cancer: pancreatic cancer is mostly diagnosed at advanced or metastasized stages and therefore mostly has a poor prognosis and survival (Siegel et al., 2021).

The most common cancer of the pancreas is the pancreatic ductal adenocarcinoma (PDAC) (Cascinu et al., 2010; Renz-Polster et al., 2013). Typically for a cancer entity, PDAC also harbours many genetic mutations. The most frequent driver genes are *KRAS*, *CDKN2A*, *SMAD4/DPC4* and *TP53* (Jones et al., 2008; Hong et al., 2011; Zamboni et al., 2013; Esposito et al., 2014). Accumulation of genetic mutations lead to development and progression of precursor lesions, including pancreatic intraepithelial neoplasia (PanIN; most frequent precursor lesion) (figure 4), intraductal papillary mucinous neoplasia (IPMN) and mucinous cystic neoplasms (MCN) (Esposito et al., 2014).

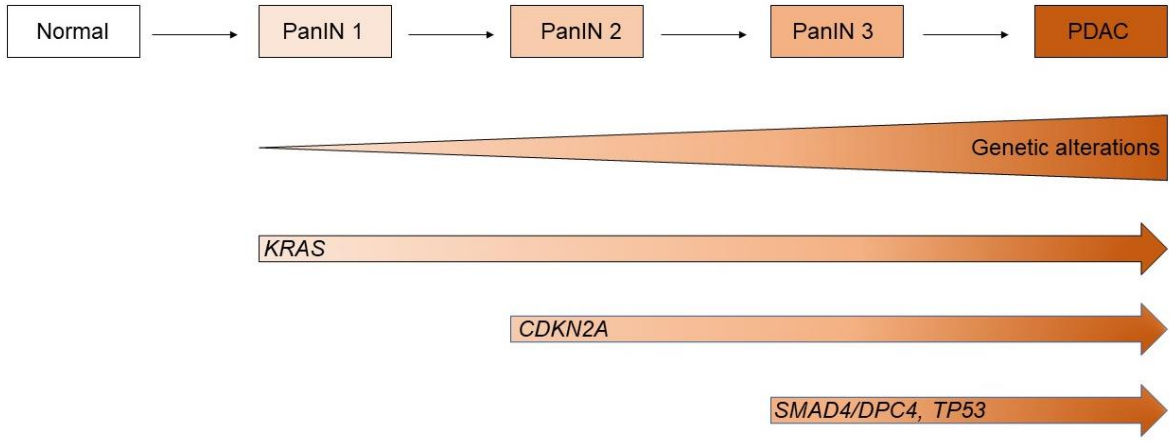

*Figure 4: **Development of PDAC**. Development of PDAC and its precursor lesions (PanIN) due to accumulation of genetic mutations of genes like KRAS, CDKN2A, SMAD4/DPC4 and TP53. The figure presented is based on a figure generated by Li et al. Cell stress. 2019. (Li et al., 2019)*

PanIN lesions can be classified into three grades: PanIN-1A and -1B as early and low-grade lesions, PanIN-2 are intermediate-grade lesions and PanIN-3 as carcinoma in situ (Zamboni et al., 2013; Distler et al., 2014). PanIN lesions are just detectable under the microscope (lesion usually < 5mm) and not reliable via imaging (computed tomography, magnetic resonance imaging or endoscopic ultrasonography) (Ott et al., 2007; Canto et al., 2012; Zamboni et al., 2013; Esposito et al., 2014). Although PanIN-lesions are not easy to detect, they offer an opportunity to cure a neoplasia before it develops into an invasive pancreatic cancer (Zamboni et al., 2013).

The most frequently mutated oncogene (>95 %) is *KRAS* (Hruban et al., 1993; Jones et al., 2008; Hong et al., 2011). *KRAS* codes for a membrane-bound GTP-binding protein, the KRAS protein, which fulfills several functions in the cell, e.g. proliferation or cellular survival: after bondage with GTP, KRAS protein gets activated. This leads to activation of more than 80 downstream signaling pathways and effector proteins, e.g. mTOR (mechanistic target of rapamycin), MAPK (mitogen-activated protein kinase), as well as activation of nuclear transcription factors (e.g. MYC) leading to stimulation of proliferation, dedifferentiation and tumor progression (Buscail et al., 2020). The activating *KRAS*-mutation leads to constitutive signaling of this pathway, as the mutation leads to reduced hydrolysis of GTP to GDP and reduced inactivation of KRAS (Waters and Der, 2018; Hafezi et al., 2021). Also found in the PanIN-lesions (PDAC precursor lesion), *KRAS*-mutation seems to be one of the earliest events in the genesis of PDAC (figure 4) (Tada et al., 1996; Moskaluk et al., 1997; Jones et al., 2008).

Current recommendations for treatment of PDAC

The recommendation for PDAC treatment depends on the clinical stage. In this context, a differentiation can be made between localized resectable disease (10-15% of the newly diagnosed patients), locally advanced disease (30-35%) and metastatic disease (50-55%). Resectability is defined as the ability to remove the cancer completely, considered when there is no or minimal contact with major vessels (e.g. hepatic artery) (Park et al., 2021).

The only possibility to cure patients from PDAC is surgery (Wagner et al., 2004; Doi et al., 2008; Leitlinienprogramm Onkologie, 2021). The goal is the complete resection in healthy tissue (R0), which shows the best long-term survival rate (Wagner et al., 2004; Fusai et al., 2008; Hartwig et al., 2011). The best surgical procedure depends on the tumors location within the pancreas (e.g. pancreaticoduodenectomy for tumors in the pancreas head). But even after reaching the R0-status after surgery, the 5-year-survival rate is 24,2% (Wagner et al., 2004; Leitlinienprogramm Onkologie, 2021). Although data varies between different observations, several studies in the past showed a benefit for patients receiving adjuvant chemotherapy (Principe et al., 2021). Patients with resectable disease should receive surgery in combination with adjuvant chemotherapy to increase the progression-free survival and overall survival after R0-resection. Therefore an adjuvant chemotherapy should be performed with modified FOLFIRINOX (fluorouracil, oxaliplatin, irinotecan, leucovorin) (overall survival 54,4% (Conroy et al., 2018)) or a combination of gemcitabine and capecitabine (overall survival 28% (Neoptolemos et al., 2017)) or gemcitabine alone (overall survival 25,5% (Neoptolemos et al., 2017)), depending on the patients functional status (Park et al., 2021).

Patients with borderline resectable or locally advanced tumors should receive neoadjuvant chemotherapy to eradicate metastasis or to increase the chances for downstaging and surgery. Therefore, these patients should receive modified FOLFIRINOX or a combination of gemcitabine and albumin-bound paclitaxel (Park et al., 2021).

Patients suffering from metastatic disease should receive palliative care, including chemotherapy (gemcitabine and albumin-bound paclitaxel or modified FOLFIRINOX), symptomatic therapy (e.g. with potent pain killers) and supportive care (e.g. placement of an endobiliary metallic stent in patients with biliary obstruction) (Park et al., 2021).

Not only in other types of cancer like chronic myeloid leukemia, also in PDAC targeted therapies start to establish: due to the POLO trial (U.S. Federal Government), Patients with BRCA-gen mutation and metastatic pancreatic cancer showed longer progression-free survival when treated with a PARP (poly(adenosinde diohosphate-ribose) polymerase)-inhibitor Olaparib (Golan et al., 2019). In 2019, the FDA approved Olaparib for maintenance treatment for patients with *BRCA*-mutated metastatic PDAC (U.S. Food and Drug Administration, 2019).

Histone deacetylases (HDAC), HDAC-inhibitors and their role in PDAC

Histones are proteins interacting with the DNA and after binding lead to regulation of DNA-packing. The binding of DNA lead to a tighter and more compact form of DNA, called heterochromatin, and reduces gene transcription (Mariño-Ramírez et al., 2005). The unit of DNA wrapped around histone proteins is called nucleosome (Mariño-Ramírez et al., 2005). Nucleosomes consist of 8 histone sub-units (H2A, H2B, H3, H4) and about 146 base pairs wrapped around (figure 5 A) (Singh and Mueller-Planitz, 2021). Besides of the mentioned function of controlled DNA condensation, they also play an important role in transcription process (Singh and Mueller-Planitz, 2021). Histone deacetylases (*HDAC*) are necessary to change the chromatin structure by removing the acetylation from the histone proteins (Venugopal and Evans, 2011). This

regulates the expression of target genes (Feng et al., 2014). Due to the removal of the acetylation from the Ɛ-amino group of lysines at the N-terminal tail of histone proteins, heterochromatin gets formed, which inhibits the transcription of genes (Yang and Seto, 2008; Haberland et al., 2009). Essential to fulfill their functions, HDACs (especially class I, see below) are part and catalytic core of multiple co-repressor complexes (Kelly et al., 2018). The three major co-repressor complexes are Sin3, CoREST (co-repressor for element-1-silencing transcription factor) and NuRD (nucleosome remodeling and deacetylation), all containing DNA-binding motifs, directing HDACs, with the help of transcription factors, to the specific chromatin regions (Kelly and Cowley, 2013).

HDACs also affect non-histone proteins, which are involved in different functions (e.g. chaperon proteins, enzymes for cell motility, enzymes of the adaptive immune system or metabolic enzymes) or transcription factors (e.g. *p53*) (Feng et al., 2014; Roche and Bertrand, 2016; Shvedunova and Akhtar, 2022). The deacetylation of histones also lead to epigenetic repression and is important for transcriptional regulation or the control of the cell cycle (Roche and Bertrand, 2016). The antagonistic reaction is catalyzed by histone acetyltransferases (HAT) (figure 4). They add an acetyl group to histones and thereby relax the structure of the chromatin (euchromatin) to increase the transcription of genes (Epping and Bernards, 2009; Lane and Chabner, 2009).

HDACs are zinc- or NAD^+-dependent enzymes which means, that they need Zn^{2+} (class I, II, IV) or NAD^+ (class III) for deacetylation (Yang and Seto, 2008; Seto and Yoshida, 2014; Roche and Bertrand, 2016). Phylogenetic analysis showed homology of the human HDAC with those of yeast, so that the 18 HDAC molecules can be classified into four classes (Schneider et al., 2010; Feng et al., 2014; Seto and Yoshida, 2014). Class I HDACs contain HDACs 1, 2, 3 and 8 and are homologue to those of yeast RPD3, class II HDACs contain HDAC 4, 5, 6, 7, 9 and 10, which are homologue to those of yeast HDA1, HDACs of class III are related to yeast Sir2 and class IV HDAC contains HDAC 11, showing homologies with class I and II HDAC's (Schneider et al., 2010; Feng et al., 2014; Seto and Yoshida, 2014; Damaskos et al., 2015). HDAC's are localized in the cytoplasm and/or the nucleus (Damaskos et al., 2015).

HDAC-expressions and -overexpressions, especially of class I HDACs, can be found in a lot of human malignancies (e.g. ovarian cancer and prostate cancer) (Weichert, 2009; Schneider et al., 2010; Li and Seto, 2016; Shinke et al., 2018; Rana et al., 2020). Also in 56% of PDAC, high expression of *HDAC-1* is reported (Miyake et al., 2008; Schneider et al., 2010). Together with the expression of HIF-1α, it could predict a poor prognosis (Miyake et al., 2008; Schneider et al., 2010). In their experiments, Wang et al. found the expression of class I and class II HDAC in all of their PDAC cell lines in variable levels (Wang et al., 2012). *HDAC-2* shows high expression in moderately differentiated and undifferentiated PDAC (Schneider et al., 2010) and seems to facilitate PDAC metastasis (Krauß et al., 2022). Depletion of *HDAC-2* can make PDAC cells more sensible to etoposide, a topoisomerase II inhibitor, or the tumor necrosis factor-related apoptosis-inducing ligand (TRAIL) (Fritsche et al., 2009; Schüler et al., 2010). *HDAC-7* shows high expression levels in PDAC too (Ouaïssi et al., 2008).

HDAC-inhibitors (HDACi) can inhibit all HDAC isoforms (pan-HDACi, e.g. Vorinostat) or specific isoforms (isoform-selective-HDACi, e.g. *MS-275, a class I inhibitor*) (Eckschlager et al., 2017). Based on their chemical structures, HDACi can be divided into five groups: hydroxamate/hydroxamic acid, short-chain fatty acids, benzamide,

cyclic peptide and sirtuin inhibitors (Seto and Yoshida, 2014; Damaskos et al., 2015; Roche and Bertrand, 2016; Eckschlager et al., 2017). A central mechanism of HDACi is the binding to the Zn^{2+} ion in the catalytic domain of class I HDAC, which is essential for the deacetylation catalyzed by HDACs, which leads to higher expressions of the target genes.

Inhibition of HDAC's prevent the deacetylation of lysine of histones which consequently leads to more acetylated lysine groups. Deacetylated lysine groups have a positive charge. With the binding acetylation, this positive charge gets neutralized, leading to reduced interaction with the negatively charged DNA (Damaskos et al., 2015). This leads to an increasing transcription of genes in the control of e.g. cell cycle (e.g. increased expression of *CDKN1A*), differentiation, angiogenesis (e.g. downregulation of *VEGF*) or apoptosis (e.g. by influencing the expression of death inducing genes) (Richon and O'Brien, 2002; Damaskos et al., 2015; Eckschlager et al., 2017) which in turn leads to an inhibition of cancer growth. Due to the relaxed chromatin structure, the access of polymerases or transcription factors to the DNA is much easier, leading to the described increase in transcription (Richon and O'Brien, 2002; Damaskos et al., 2015) (figure 5 B).

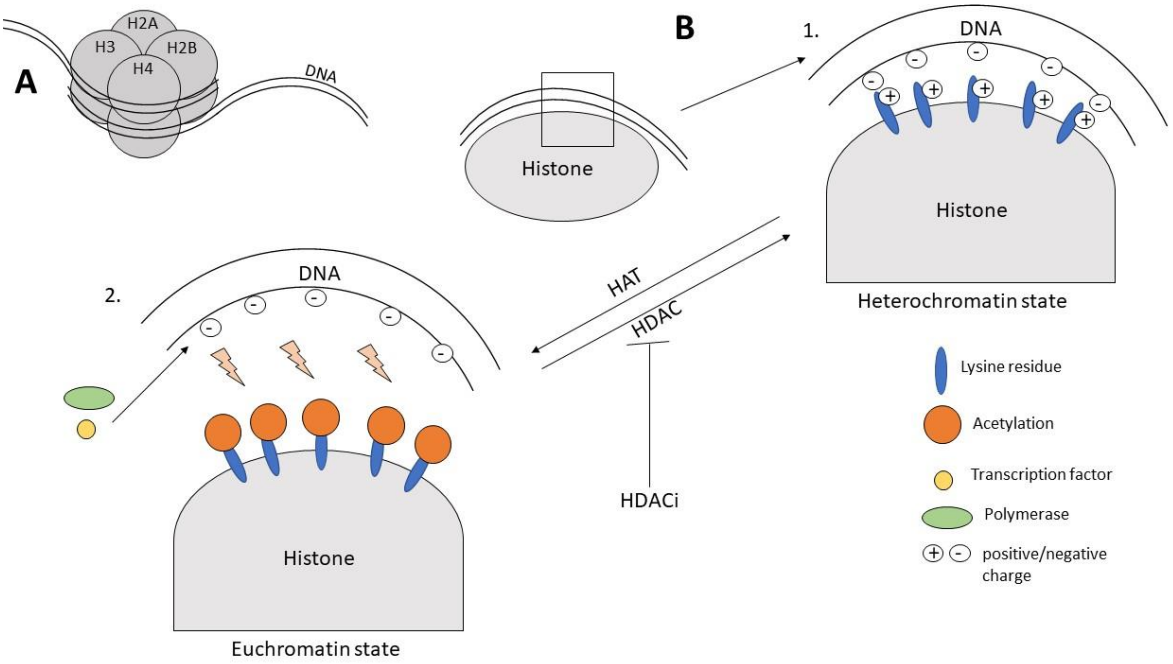

Figure 5: ***Nucleosome and mode of action of HDAC and HAT****. (A) Nucleosome consists of 8 histone subunits (H2A, H2B, H3, H4), formed by two molecules of each histone protein, and DNA wrapped around it. (B) Due to negative charged DNA and positive charged lysine residues from the histone, the histone binds with the DNA (heterochromatin, 1.). After acetylation of lysine, catalyzed by histone acetyltransferase (HAT), the positive charge gets neutralized, leading to lose DNA (euchromatin, 2.). Now, polymerases, transcription factors, etc. can access the DNA, leading to transcription. The antagonistic effect is catalyzed by histone deacetylase (HDAC), leading to compact chromatin structure. Inhibitors of histone deacetylases (HDACi) lead to increasing expression of proteins necessary for inhibition of the cell cycle, differentiation or apoptosis (Aktories, 2017).*

Another important effect of HDACi seems to be the regulation of proteins that are relevant for DNA repair (e.g. KU70 or FEN1) and are regulated by acetylation and may be increased by HDAC inhibition (Eckschlager et al., 2017), because due to the acetylation of proteins like KU70 (induces repair of double-strand brakes by binding the DNA endings), the binding to the DNA for its repair is reduced (Bose et al., 2014). Inhibition of *HDAC-1* and *HDAC-2* decreases the DNA-damage repair process (double

strand brakes), mediated by BAL-associated protein (BBAP) (Bhaskara, 2015; Eckschlager et al., 2017). BBAP is part of protecting cells against DNA-damage (see below) (Eckschlager et al., 2017). DNA-damage due to problems in DNA repairment causes genome instability, which can lead to cell death (Bhaskara, 2015; Li et al., 2020). HDACi can also induce reactive oxygen species (ROS), which could lead to higher oxidative stress and cell death (Ruefli et al., 2001; Trachootham et al., 2006; Wolf et al., 2014).

HDACi can be promising anti-cancer agents, e.g. *Vorinostat* has been approved for treating refractory cutaneous T-cell lymphomas (CTCL) by the U.S. Food and Drug Administration (FDA) (table 1) (Duvic et al., 2007; Falkenberg and Johnstone, 2014). Also recent studies show the potential of HDACi as effective drugs in solid tumors, e.g. triple negative breast cancer (Fedele et al., 2017).

*Table 1: **Overview of HDACi approved by the FDA or in phase-3-trials**. The results shown here are in whole or part based upon data generated by Nepali and Liou. Journal of biomedical science 28, 27. 2021 (Nepali and Liou, 2021) and Li et al. Frontiers in Cell and Developmental Biology 8:576946. 2020 (Li et al., 2020).*

FDA-approved HDACi		**HDACi in phase-III-trial**	
Vorinostat/SAHA (Cutaneus T cell lymphoma)	Pan HDACi	**Givinostat** (Polycythaemia vera)	Hydroxomate HDACi
Romidepsin (Cutaneus T cell lymphoma, peripheral T cell lymphoma)	Class I HDACi	**Abexinostat** (Renal cell carcinoma)	Pan HDACi
Belinostat (Peripheral T cell lymphoma)	Pan HDACi	**Entinostat/MS-275** (Hormone receptor-positive, locally advanced or metastatic breast cancer)	Class I HDACi
Panobinostat (Multiple myeloma)	Pan HDACi	**Tucidinostat** (advanced, hormone receptor-positive, breast cancer)	HDACi of HDAC 1, 2, 3, 10
		Pracinostat (intermediate/ high-risk Myelofibrosis)	Class I, II, IV (except HDAC 6) HDACi
		Tacedinaline (Non-small lung cancer, pancreatic cancer)	Inhibits HDAC 1-3
		Valproic acid (Flioblastoma)	Class I/II HDACi

Knock-out model: dual-recombinase system

Isogenic models offer the opportunity to determine the effect of individual genes on cancer development and to investigate and focus on the implications of addressing these genes. Therefore, PDAC cells of genetically engineered mouse models were used to evaluate the effect of *HDAC-2* knock-out. Therefore, an inducible dual-recombinase system has been developed in the past by combining flippase-*FRT* and Cre-*loxP* recombination systems (Schönhuber et al., 2014). This means, that the mice expresses Flippase (Flp)-recombinase, which is directed by (pancreas specific) *Pdx1* promoter, which activates the expression of CreER by removing the FSF-stop-cassette (FRT-stop-FRT). CreER is a recombinase fused with an estrogen receptor which can be activated by Tamoxifen (also called $CreER^T$ (Cre estrogen receptor tamoxifen)) (Kim et al., 2018). The FRT-stop-FRT cassette is located between the *CreER*-gene and its promotor $Rosa26^{CAG}$ and prevents the expression of CreER. After activation of Pdx1-Flp, the expression of CreER is induced (figure 6) (Schönhuber et al., 2014). The activation of oncogenic $Kras^{G12D}$ is similarly regulated, while exons 2-6 of the *Trp53* gene (Wu et al., 2017) are flanked by FRT sites leading to *Trp53* inactivation due to Pdx1-Flp activity. Both lead to development of murine PanIN lesions and PDAC (Schönhuber et al., 2014).

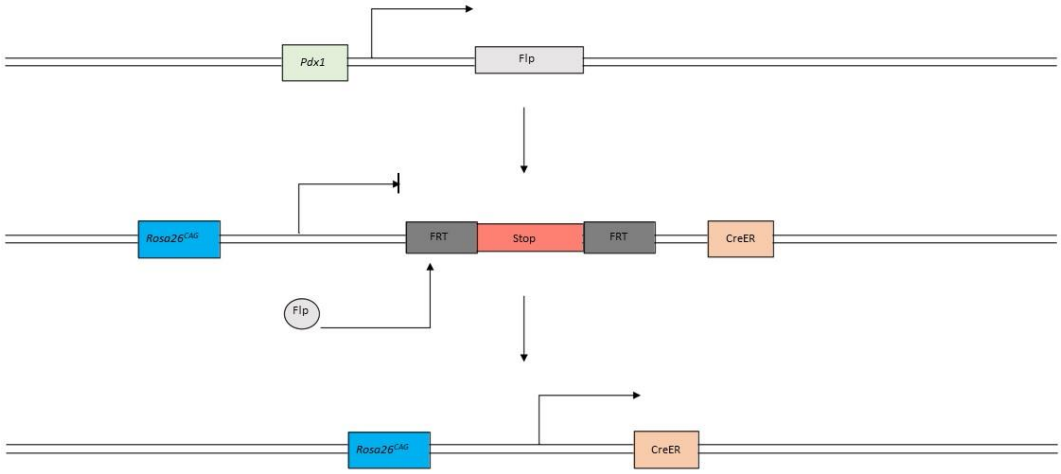

Figure 6: ***Knock-out model****. As "inhibitor" of CreER-expression, FSF-cassette is located between the CreER-gene and its promotor. After Pdx1-Flp activation, the FSF-cassette gets removed, leading to expression of CreER.*

The Cre/loxP-system can be used for selectively excising genes out of the DNA and binding the remaining DNA-endings together.

To get a Tamoxifen-inducible Cre/loxP-system, the Cre recombinase was fused with an estrogen receptor ($CreER^T$; see above). A new version of this fusion protein is called $CreER^{T2}$, a mutated form of $CreER^T$ which is more sensitive towards Tamoxifen treatment (Kristianto et al., 2017; Kim et al., 2018). Treatment with Tamoxifen leads to an induction of Cre activity, as $CreER^{T2}$ is normally located in the cytoplasm and bond to heat shock protein 90 (Schönhuber et al., 2014; Kim et al., 2018). Tamoxifen disrupts

this interaction between CreER^{T2} and heat shock protein 90, which leads to translocation of CreER^{T2} into the nucleus for interaction with *loxP* sites (Schönhuber et al., 2014; Kim et al., 2018). *loxP* sites are necessary for recognition of the target gene region by Cre as the targeted gene region is flanked by the genetic sequence of *loxP* (flanked by *loxP* = floxed). After recognition, Cre excises the floxed sequence of the targeted gene(s) (figure 7) (Kim et al., 2018). The floxed regions used in our model were *HDAC-2 exons 2-4*. Consequently, after a treatment with Tamoxifen, the cells were deficient of *HDAC-2*.

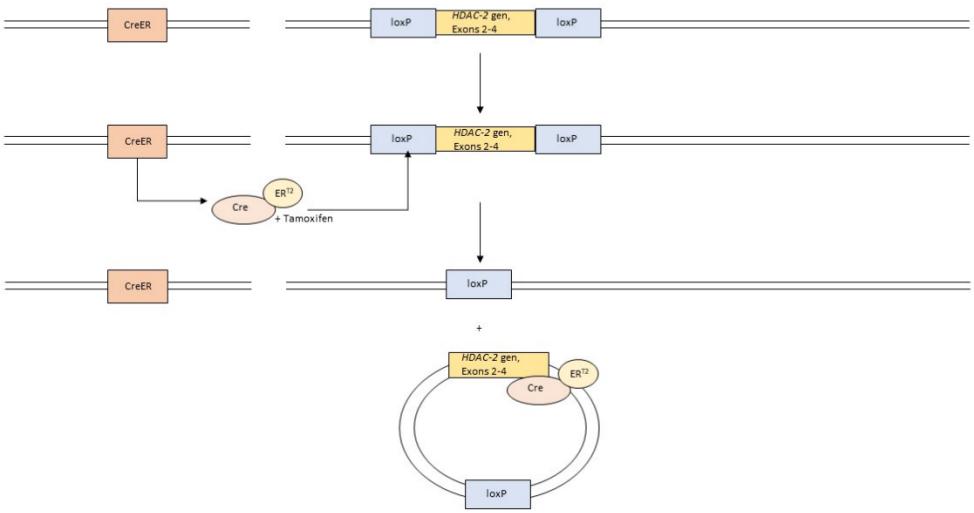

Figure 7: ***Scheme of the HDAC-2 knock-out mechanism****. Exon 2-4 of HDAC-2 gene is floxed and gets exercised by CreER^{T2} after Tamoxifen treatment. This leads to HDAC-2 knock-out.*

Objective

In the past, HDACi as anti-cancer drugs in pancreatic cancer failed in clinical studies regarding relevant antitumor effects (Arlt and Schäfer, 2016). To find effective, specific and novel combination therapies, an unbiased drug screen was implemented containing 101 drugs with different mode of actions (tables 1 – 9). Therefore, two *HDAC-2* proficient (*HDAC-2 (+)*) and deficient (*HDAC-2 (-)*) murine cell lines were treated with the drug library. The goal was to find new potential therapies against PDAC with an HDAC-2 inhibitor as a combination partner. Goal of this thesis is to explore new possibilities and potential therapeutical solutions in the fight against PDAC. The results are presented in the following.

Material and Methods

Material

Cell lines

Table 2: ***Cell lines****.*

Cell line	Genotype	Morphology	Date isolated	Source
PPT-F1648	*FSF-Kras$^{G12D/+}$, FSF-Trp$^{53del/+}$, Pdx1-Flp, R26$^{CAG-FSF-CreERT2/+}$, Pdk$^{loxP/+}$, Hdac2$^{loxP/loxP}$*	Mesenchymal	01.06.2012	Department of Internal Medicine II, Klinikum rechts der Isar, Technical University of Munich
PPT-F2612	*FSF-Kras$^{G12D/+}$, FSF-Trp$^{53del/+}$, Pdx1-Flp, R26$^{CAG-FSF-CreERT2/FSF-CreERT2}$, Hdac2$^{loxP/loxP}$*	Epithelial	17.04.2013	

Reagents

Table 3: ***Reagents****.*

Product – Reagents	Manufacturer
30% Acrylamide/Bisacrylamide-stock solution (29:1)	Carl Roth, Karlsruhe
4-Hydroxytamoxifen	Sigma-Aldrich, Steinheim
Ammonium Persulfate (APS)	Sigma-Aldrich, Steinheim
Agarose	Sigma-Aldrich, Steinheim
Aqua 1000 ml	B. Braun Melsungen AG, Melsungen
Bovine serum albumin	Sigma-Aldrich, Steinheim
Bradford reagent 5x	Serva, Heidelberg
Crystal Violet	Sigma-Aldrich, Steinheim
ddH_2O	SAV Liquid Production GmbH, Flintsbach am Inn
Dimethyl sulfoxide (DMSO)	Carl Roth, Karlsruhe
Dulbecco's Modified DMEM; high glucose	Sigma-Aldrich, Steinheim
Dulbecco's Phosphate Buffered Saline	Sigma-Aldrich, Steinheim
Ethanol Absolut	Otto Fischar, Saarbrücken
Ethanol 100%	Merck, Darmstadt
Ethylenediaminetetraacetate (EDTA)	Invitrogen GmbH, Karlsruhe
Fetal Calf Serum (FCS)	Gibco, Schwerte
Glycerol	Sigma-Aldrich, Steinheim
Glycine	Sigma-Aldrich, Steinheim
Isopropanol	Carl Roth, Karlsruhe
Methanol	Carl Roth, Karlsruhe
PageRuler Prestained Protein Ladder	Thermo Scientific, Schwerte

(Penicillin-Streptomycin-solution (Pen Strep)	Gibco, Schwerte
Phosphatase-Inhibitor-Mix	Serva, Heidelberg
Potassium chloride	Merck, Darmstadt
Powdered milk	Carl Roth, Karlsruhe
Protease inhibitor cocktail tablets	Roche Diagnostics GmbH, Mannheim
RLT-Buffer	Qiagen GmbH, Hilden
Sodium Chloride	Merck, Darmstadt
Sodium Dodecyl Sulfate pellets	Serva, Heidelberg
Sodium hydrogen phosphate	Fluka, Steinheim
Tetramethylethylenediamine (TEMED)	Carl Roth, Karlsruhe
Tris Pufferan	Carl Roth, Karlsruhe
Trypan Blue 0,4%, 0,85% NaCl	Lonza, Walkersville, MD
Tween 20	Carl Roth, Karlsruhe
β-Mercaptoethanol	Carl Roth, Karlsruhe

Kits and Assays

Table 4: ***Kits and Assays.***

Kits and Assays	Manufacturer
***CellTiterGlo* Luminescent Cell Viability Assay**	Promega Corporation, Madison

Antibodies

Table 5: ***Antibodies.***

Antibody	Dilution	Species of origin	Catalogue number	Manufacturer	RRID
Anti-mouse IgG (H+L) (DyLight™ 680 Conjugate)	1:10000	Goat	5470	Cell Signaling Technology, Leiden	AB10696895
Anti-rabbit IgG (H+L) (DyLight™ 800 4X PEG Conjugate)	1:10000	Goat	5151	Cell Signaling Technology, Leiden	AB10697505
Hdac2 (D6S5P)	1:500	Rabbit	57156	Cell Signaling Technology, Leiden	AB2756828
β-Actin	1:5000	Mouse	A5316	Sigma-Aldrich, Steinheim	AB476743

Drugs

All drugs used for the screening (listed under “b. Methods – Cell culture: Drug screening”, table 12-20) were purchased from *Selleck Chemicals Llc* (www.selleckchem.com).

Table 6: ***Drugs.***

Product – Reagents	Manufacturer
Entinostat (*MS-275*) E-3866	LC Labratories, Woburn

Buffer/Medium/Solution

Table 7: ***Buffer/Medium/Solution.***

Buffer/Medium/Solution	Composition
Dulbecco’s Modified DMEM, high glucose (supplemented with FBS and Pen Strep)	- 500 ml DMEM - 10% (v/v) FBS - 1% Pen Strep
EDTA-Solution (0.05%) for cell culture, 50 ml	- 2,5 ml EDTA 1% - 47,5 ml PBS
Freezing Medium	- 70 ml DMEM - 20 ml FCS - 10 ml DMSO
IP-Buffer (pH 7,9)	- 150 mM NaCl - 1 mM EDTA - 1% Triton X-100 - 50 mM TRIS
Laemmli (1x), 100 ml	- 20 ml Laemmli (5x) - 80 ml ddH_2O
Laemmli (5x)	- 0,3 M TRIS - 50% (v/v) Glycerine - 0,35 M SDS (pH 6,8) - 50 mg Bromophenol blue - 5% (v/v) β-Mercaptoethanol
Lysis buffer	- 200 µl IP-Buffer - 2 µl Phosphatase inhibitor - 8 µl Protease inhibitor (25x)
PBS (10x) 1l, pH 7,4	- 80 gr. NaCl - 2 gr. KCl - 14,4 gr. Na_2HPO_4 - 800 ml ddH_2O - with HCl to pH 7,4 - fill up with ddH_2O to 1l
Protease inhibitor (25x)	- 1 protease inhibitor cocktail tablet - 2 ml ddH_20
RIPA-buffer	- 4,206 gr. NaCl - 3,028 gr. TRIS - 2,5 gr. Sodiumdeoxychelate - 0,5 gr. SDS - 5 ml NPO_4 - 25x Protease - 100x Phosphatase

	- H_2O
Running buffer (10x) 1l	- 10 gr. SDS - 30 gr. TRIS - 144 gr. Glycin - fill up with ddH_2O to 1l
Separation gel (10%), two gels	- 6150 µl ddH_20 - 3900 µl separation gel buffer - 4950 µl acrylamide 30% - 150 µl SDS 10% - 75 µl APS 10% - 22,5 µl TEMED
Separation gel buffer (1,5 M TRIS/HCl pH 8,8), 100 ml	- 18,171 gr TRIS - 50 ml ddH_2O - with HCl to pH 8,8 - fill up with ddH_2O to 100 ml
Skim Milk	- 500 ml PBS - 25 gr Powdered milk
Stacking gel (2x), two gels	- 4500 µl ddH_20 - 1950 µl collection gel buffer - 1125 µl acrylamide 30% - 75 µl SDS 10% - 37,5 µl APS 10% - 15 µl TEMED
Stacking gel buffer (0,5 M TRIS/HCl pH 6,8), 100 ml	- 6 gr. TRIS - 50 ml ddH_2O - with HCl to pH 6,8 - fill up with ddH_2O to 100 ml
Transfer buffer 1l, pH 8,3	- 2,9 gr. Glycin - 5,8 gr. TRIS - 700 ml ddH_2O - 3,7 ml SDS 10% - 200 ml Ethanol - fill up with ddH_2O to 1l

Devices

*Table 8: **Devices**.*

Product	Manufacturer
Anthos Photometer 2001	Anthos Mikrosysteme, Krefeld
AxioCam MRc	Carl Zeiss, Oberkochen
Axiovert 25 Inverse microscope	Carl Zeiss, Oberkochen
Centrifuge 5415 R	Eppendorf, Hamburg
Centrifuge 5451R	Eppendorf, Hamburg
CLARIOstar Plate Reader	BMG Labtech, Ortenberg
CO_2 Incubator	Sanyo, München
Combitips advanced 0,2 ml, 1 ml, 2,5 ml, 5 ml, 10 ml	Eppendorf, Hamburg
FLUOstar optima	BMG Labtech, Ortenberg
LI-COR Odyssey	LI-CO, Lincoln, NE
Mini-PROTEAN Tetra Cell	Bio-Rad, Hercules

Mini-Trans-Blot Cell	Bio-Rad, Hercules
Multipette E3x	Eppendorf, Hamburg
Multiscan RC	ThermoFisher Scientific, Waltham
Nebauer chamber	Assitent, Sondheim vor der Rhön
Pipettes 10 µl, 100 µl, 200 µl, 1000 µl	Eppendorf, Hamburg
PowerPac HC Power Supply	Bio-Rad, Hercules
Rotina 280	Hettich Zentrifugen, Tuttlingen
Rotina 46 R	Hettich Zentrifugen, Tuttlingen
Shaker	Henning GmbH, Berlin
Stripettor Ultra Pipet Controller	Corning, Corning
Thermomixer compact	Eppendorf, Hamburg
Vortex Genie 2	Bender & Hobein AG, Zurich

Software

Table 9: ***Software****.*

Product	Manufacturer	RRID
Axio Version 4.3	Carl Zeiss, Jena	SCR_021351
Flourstar optima Programm Version 1.30-0	BMG Labtechnologies, Ortenberg	-
Graph Pad Prism 5	Graph Pad Software, La Jolla, CA	SCR_002798
Image Studio Software Version 5.2.5	Li-COR, Lincoln, NE	SCR_015795
Microsoft Excel 2016	Microsoft Corporation, Redmond, WA	SCR_016137
Microsoft PowerPoint 2016	Microsoft Corporation, Redmond, WA	-

Online Tools/Databases

Table 10: ***Online Tools/Databases****.*

Product	Internet-adress	RRID
ClustVis	https://biit.cs.ut.ee/clustvis/	SCR_017133
Gene set enrichment analysis 4.0.3, BROAD Institute	https://www.gsea-msigdb.org/	SCR_016863
SynergyFinder 3.0	https://synergyfinder.fimm.fi	SCR_019318
Venny 2.1	https://bioinfogp.cnb.csic.es/tools/venny/	SCR_016561

Various materials

Table 11: ***Various materials****.*

Product	Manufacturer
5 ml Polystrene Round-Bottom Tube	BD Falcon,
Assay Plates, 96 wells	Corning, Corning
Cell Culture Flasks 50 ml, 250 ml, 550 ml	Greiner Bio One, Frickenhausen
Cell Scraper	Sarstedt, Newton

Cellstar tubes 15 ml, 50 ml	Greiner Bio-One GmbH, Kremsmünster
CellTrics 30 µm	Sysmex, Görlitz
Clear Line Filter Tips 10 µl, 100 µl, 200 µl, 1000 µl	Biosigma, Cona
Injekt-F 1ml	B. Braun Melsungen AG, Melsungen
Pasteur Pipettes	Hirschmann Laborgeräte GmbH & Co. KG, Eberstadt
Serological Pipette 2 ml, 5 ml, 10 ml, 25 ml, 50 ml	Greiner Bio-One GmbH, Kremsmünster
Tissue Culture Dish 100 x 20 mm	Corning, Corning
Tissue Culture Plate 96 Well	Corning, Corning
Whatman Papier 3MM Chr	GE Healthcare Life Sciences, Freiburg
Amersham Protran 0,2 µm NC	GE Healthcare Life Sciences, Freiburg
100 Sterican 0,45 x 25 mm Gr. 18	B. Braun Melsungen AG, Melsungen

Methods

Cell culture: preparing Medium

The medium used for the experiments was *Dulbecco's Modified Eagle's Medium – high Glucose* 500 ml bottles (DMEM). 50 ml fetal calf serum (FCS) and 5 ml of the Penicillin-Streptomycin solution was added to DMEM prior to use.

Cell culture: washing cells and exchange of medium

After aspirating the DMEM from the T75-cell culture flask, 5 ml PBS was added to wash the cells and to remove media residue. After 30 seconds of incubation the PBS got removed. Finally, 10 ml of new DMEM was added.

Cell culture: freezing cells

To freeze cells, the cells were grown till 80% confluency in a T75-flask. First, the cells were washed (see Cell culture: washing cells/exchanging of medium). After removing the PBS, 1 ml EDTA 0,05% was added to the cells to detach them from the flask, followed by resuspending them in 10 ml of DMEM. After detaching, the suspension was filled into 15 ml falcon-tubes and centrifuged at 1000 rpm for 5 minutes. Subsequently the supernatant was aspirated, and the cell pellet was resuspended and singularized with 4 ml freezing medium. After preparation of the cryo-tubes, 1 ml of the suspension was filled in each of the tubes. The tubes were frozen at -80°C and transferred into liquid nitrogen tanks after one week.

Cell culture: thawing cells

The frozen samples were thawed in the 37°C water bath. After thawing, the samples were transferred into a falcon tube filled with 5 ml DMEM. Subsequently they were put

into the centrifuge at 1000 rpm for 5 minutes. Afterwards the supernatant was aspirated and another 10 ml DMEM was added to the tubes to resuspend and singularize the cells. Afterwards the whole suspension was transferred into a T75-culture flask and put into the incubator.

Cell culture: splitting cells

To split cells, the cells were grown till 80% confluency in a T75-flask. First, the cells were washed (see Cell culture: washing cells/exchanging of medium). After aspirating the PBS, 1 ml EDTA 0,05% was added to the cells to detach them. While the cells detached from the bottom of the flask, the new flasks/dishes were prepared by filling them with DMEM:

- T75 bottle: 10 ml
- 10 cm-dish: 5 ml

Depending on the cell line, after 5 (F1648) to 10 (F2612) minutes of incubation with EDTA, the cells were detached with 10 ml DMEM and singularized. Next, 0,5-1 ml of the suspension was transferred into the previously prepared flask respectively 0,5 ml in the 10 cm-dish.

Cell culture: drug screening

The drug library was divided into nine screens, containing 5-12 different compounds. The following descriptions of the drugs are copied from the official descriptions of www.selleckchem.com (viewed October 13th, 2019) where the compounds were bought (Selleck Chemicals).

Table 12: ***Drugs of screen 1 with mode of action (Selleck Chemicals).***

Veliparib	Potent inhibitor of PARP1 and PARP2
Linsitinib	Selective inhibitor of IGF-1R
Pelitinib	Potent irreversible inhibitor of EGFR
Galunisertib	Potent inhibitor of TGFβ-receptor I (TβRI)
GDC-0152	Antagonist of XIAP-BIR3, ML-IAP-BIR3, clAP1-BIR3 and clAP2-BIR3
UNC1999	Selective inhibitor of EZH2 and EZH1
SF1670	Highly potent and specific PTEN inhibitor
4EGI-1	Competitive eIF4E/eIF4g interaction inhibitor
CB-839	Potent and selective glutaminase inhibitor
Ulixertinib	Potent and reversible ERK1/ERK2 inhibitor
Sabutoclax	Pan-Bcl-2 inhibitor, including Bcl-xL, Bcl-2, Mcl-1 and Bfl-1
Saracatinib	Potent Src inhibitor

Table 13: ***Drugs of screen 2 with mode of action (Selleck Chemicals).***

Alisertib	Selective Aurora A inhibitor
Ispinesib	Potent, specific and reversible inhibitor of KSP (kinesin spindle protein)

Indirubin	Potent cyclin-dependent kinases and GSK-3β inhibitor
Birinapant	SMAC mimetic antagonist, mostly to cIAP1
Crenigacestat	Oral Notch inhibitor
WZ4003	Highly specific NUAK kinase inhibitor
PTC-209 HBr	Hydrobromide salt of PTC209, a potent and selective BMI-1 inhibitor
AZD6738	Selective ATR kinase inhibitor
LJH685	Potent pan-RSK inhibitor
UNC0638	Potent, selective and cell-penetrant chemical probe for G9a and GLP
Lapatinib	Potent EGFR and ErbB2 inhibitor
CUDC-101	Potent multi-targeted inhibitor against HDAC, EGFR and Her2

Table 14: ***Drugs of screen 3 with mode of action (Selleck Chemicals).***

Orantinib	Potent against PDGFR autophosphorylation
Trametinib	Highly specific and potent MEK1/2 inhibitor
GSK2656157	ATP-competitive and highly selective inhibitor of PERK
RO5126766	Dual RAF/MEK inhibitor
HTH-01-015	Potent and selective NUAK1 inhibitor
UNC0379	Selective, substrate competitive inhibitor of N-lysine methyltransferase SETD8
STF-083010	Specific IRE1α endonuclease inhibitor
NVP-CGM097	Highly potent and selective MDM2 inhibitor
RI-1	RAD51 inhibitor
Elesclomol	Potent oxidative stress inducer
Vemurafenib	Inhibitor of B-RafV600E
Pracinostat	Potent pan-HDAC inhibitor

Table 15: ***Drugs of screen 4 with mode of action (Selleck Chemicals).***

Milciclib	Potent, ATP-competitive CDK inhibitor for CDK2
AZD1208	Potent Pim kinase inhibitor
Erastin	Ferroptosis activator by acting on mitochondrial VDAC, exhibiting selectivity for RAS-mutated tumor cells
CW069	Allosteric and selective inhibitor of microtubule motor protein HSET
GSK2830371	Allosteric Wip1 phosphatase inhibitor
GSK503	Potent and specific EZH2 methyltransferase inhibitor
Spautin-1	Potent and specific autophagy inhibitor, and inhibits the deubiquitinating activity of USP10 and USP13
GSK591	Potent and selective inhibitor of the arginine methyltransferase PRMT5
Enzastaurin	Potent PKCβ selective inhibitor
BX-795	Potent and specific PDK1 inhibitor
Adavosertib	Potent and selective Wee1 inhibitor
Sapanisertib	Potent and selective mTOR inhibitor

Table 16: ***Drugs of screen 5 with mode of action (Selleck Chemicals).***

Pevonedistat	Small molecule inhibitor of Nedd8 activating enzyme (NAE)
JIB-04	Pan-selective Jumonji histone demethylase inhibitor
JSH-23	Inhibitor of NF-κB transcriptional activity
LLY-507	Potent and selective inhibitor of protein-lysine methyltransferase SMYD2
MI-463	Potent inhibitor of Menin-MLL interaction
Epacadostat	Potent and selective indoleamine 2,3-dioxygenase (IDO1) inhibitor
MS023	Potent, selective and cell-active Type I PRMT inhibitor
Luminespib	Highly potent HSP90 inhibitor for HSP90α/β
BX-912	Potent and specific PDK1 inhibitor
AZD7762	Potent and selective inhibitor of Chk1
Alpelisib	Potent and selective PI3Kα inhibitor
PYR-41	Cell-permeable inhibitor of ubiquitin-activating enzyme E1, with no activity at E2

Table 17: ***Drugs of screen 6 with mode of action (Selleck Chemicals).***

NMS-873	Allosteric and specific p97 inhibitor
EPZ004777	Potent, selective DOT1L inhibitor
GSK-J1	Highly potent H3K27 histone demethylase inhibitor
MI-503	Potent and selective Menin-MLL inhibitor
Napabucasin	Stat3 and cancer cell stemness inhibitor
NSC87877	Cell-permeable inhibitor of SHP-1 and SHP-2
MK-2206 2HCl	Highly selective inhibitor of AKT1/2/3
Rigosertib	Non-ATP-competitive inhibitor of PLK1
Selisistat	Potent and selective SIRT1 inhibitor
BI-D1870	ATP-competitive inhibitor of S6 ribosome for RSK1/2/3/4
PFI-2 HCl	Potent selective and cell-active lysine methyltransferase SETD7 inhibitor
P22077	Inhibitor of ubiquitin-specific protease USP7 and USP47

Table 18: ***Drugs of screen 7 with mode of action (Selleck Chemicals).***

Poziotinib	Irreversible pan-Her inhibitor
BRD4770	Histone methyltransferase G9a inhibitor
SGC707	Potent, selective and cell-active allosteric inhibitor of protein arginine methyltransferase (PRMT3)
A-196	Potent and selective inhibitor of SUV420H1 and SUV420H2
ML264	Selectively inhibitor of kruppel-like factor 5 (KLF5)
Abexinostat	Pan-HDAC inhibitor mostly targeting HDAC-1
Ruxolitinib	Potent and selective JAK1/2 inhibitor
KU-60019	Improved analogue of KU-55933 (specific ATM inhibitor)
Salubrinal	Selective inhibitor of eIF2a dephosphorylation and inhibits ER stress-mediated apoptosis
C646	Inhibitor for histone acetyltransferase, and inhibits p300

ML324	Selective inhibitor of Jumonji histone demethylase (JMJD2)
OTX015	Potent BET bromodomain inhibitor

Table 19: ***Drugs of screen 8 with mode of action (Selleck Chemicals).***

PX-478 2HCl	Selective hypoxia-inducible-factor-1α (HIF-1α) inhibitor
BI-847325	Selective dual MEK/Aurora kinase inhibitor
Entrectinib	Pan-TrkA/B/C, ROS1 and ALK inhibitor
BI-78D3	Competitive JNK inhibitor
SMER28	Small-molecule enhancer (SMER) of autophagy
EED226	Potent and selective allosteric Polycomb repressive complex 2 (PRC2) inhibitor
Thiomyristoyl	Potent and specific SIRT2 inhibitor
PRT4165	Bmi1/Ring1A inhibitor
CPI-455 HCl	Specific KDM5 inhibitor
LY2109761	Selective TGFβ-receptor type I/II (TβRI/II) dual inhibitor
AZD5153	Potent and selective BET/BRD4 bromodomain inhibitor
A-1210477	Potent and selective MCL-1 inhibitor

Table 20: ***Drugs of screen 9 with mode of action (Selleck Chemicals).***

Erdafitinib	Potent and selective pan fibroblast growth factor receptor (FGFR) inhibitor
Ralimetinib	Potent inhibitor of p38 MAPK
MX69	MDM2/XIAP inhibitor that binds to MDM2 RING protein
BAY-876	Potent and selective GLUT1 inhibitor
LLY-283	Potent and selective SAM-competitive chemical probe for PRMT5

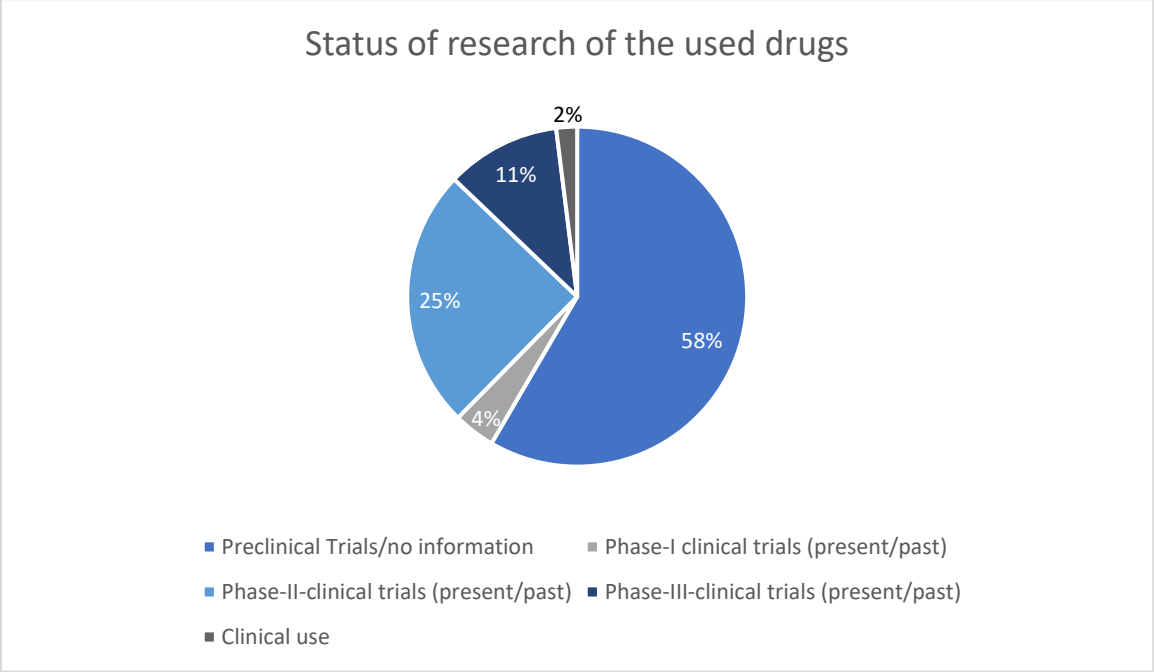

Figure 8: ***Developmental status of the drugs used in the screening.***

One screen needed 5 days to be completed:

Day 1:

After splitting the Tamoxifen (*HDAC-2* deficient)- and ethanol-treated (*HDAC-2* proficient) cells (see cell culture: splitting) to one 10 ml bottle and two 10 cm-dishes (for harvesting proteins), the cell suspension was put into a 50 ml Falcon-tube and singularized. Afterwards, 20 µl of the suspension was put into a 0,5 ml Eppendorf-Tube and 20 µl of Trypan Blue 0,4% was added, followed by another singularization of the cells. Next, the cells were counted with a Neubauer-chamber (see counting cells with Neubauer-chamber). In order to seed 1000 cells in 100 µl per well in the 96-well-plate later, dependent on the counting result, the cell suspension was diluted to 10000 cells/ml. The next step contained seeding the cells with a multistep pipette into the wells. After finishing this procedure, the cells were put in the incubator (37°C; 5% CO_2) until the next day.

Day 2:

To treat the cells with the drugs, the preparations of the right concentrations were necessary. The drugs were added to the cells on the 96-well-plate following the scheme in figure 9.

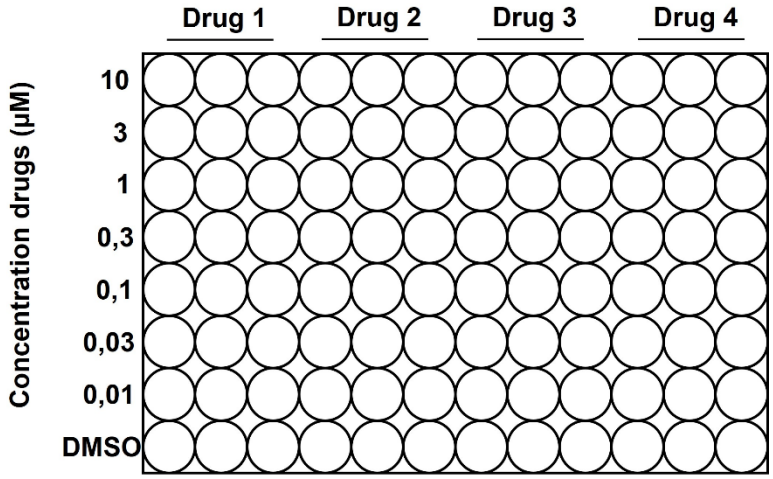

Figure 9: ***Layout of drugs and concentrations on a 96-well-plate.*** *On each plate, four drugs were tested. For every concentration, technical triplicates were performed. The prepared seven-point drug dilutions contained the indicated concentrations. Additionally, the cell lines were treated with the vehicle (DMSO/water) as control.*

In the beginning, the 1,5 ml Eppendorf tubes for the drug dilutions series (seven-point drug dilution: 10 µM – 0,01 µM) were prepared. The stock solutions of the drugs (10mM, frozen at -80°C) were thawed and diluted to 60 µM in DMEM. Afterwards the dilution series were prepared in a 1:3 manner. The DMSO-control was prepared similarly as the stock solutions of the drugs were dissolved in DMSO (exception *Ralimetinib*, which was diluted in H_2O).

20 µl of the drug dilution series and the control dilutions (DMSO/H_2O) were added to each well to achieve the final drug concentrations indicated in figure 9. In the end, the plates were incubated (37°C; 5% CO_2) for 72 hours.

Day 3 + 4:

Incubation in the incubator (37°C; 5% CO_2).

Day 5:

Initially, the *CellTiterGlo* was prepared following the instructions of the manufacturer (Promega Corporation), filled into aliquots and put into the freezer until further use. Prior to use, the *CellTiterGlo* aliquots were thawed. Afterwards, 25 µl *CellTiterGlo* was added to each well in a darkened room. Next, the plates were covered with aluminium foil and put on a shaker for 10 minutes. Afterwards, the plates were incubated for additional 20 minutes, followed by the measurement of the luminescence with the *Fluostar optima-photometer*.

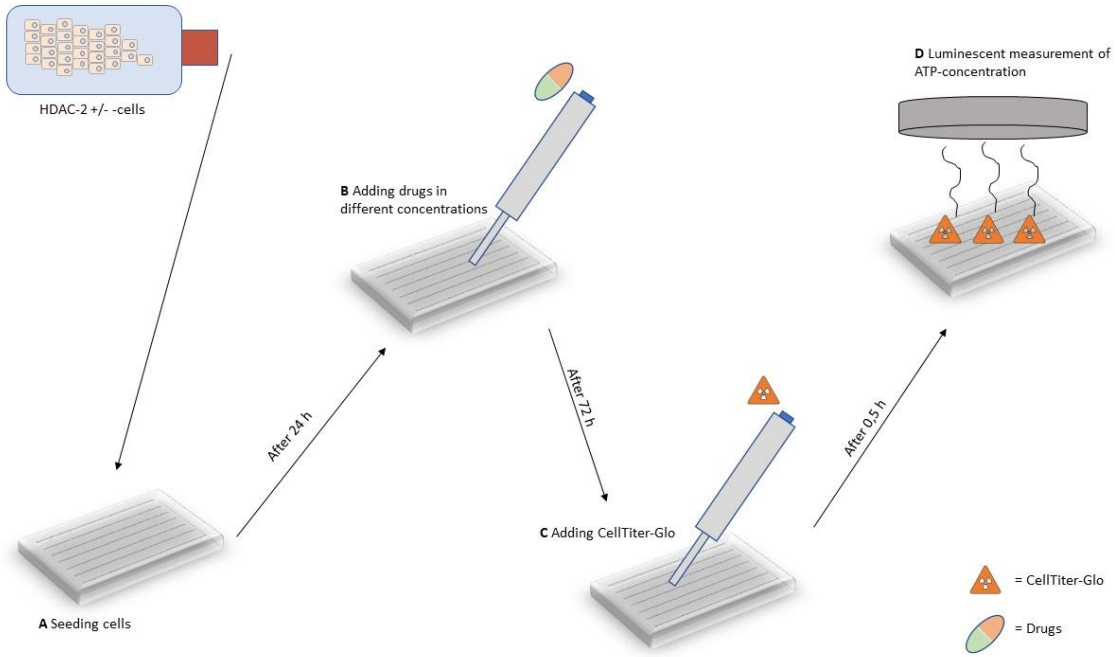

*Figure 10: **Scheme of the screening procedure**. 24 hours after (A) seeding the cells into 96-well-plates, (B) the drug treatment was started. (C) After 72 hours, the CellTiterGlo reagent was added to the wells and after 30 minutes of incubation, (D) the cell viability was measured.*

The results were analyzed using the program *GraphPad Prism 5* after normalizing the raw data to the DMSO control. A scheme of the screening procedure can be viewed in figure 10.

Cell culture: counting cells with Neubauer-chamber

20 µl of the singularized cells were put into a 0,5 ml Eppendorf tube and mixed with 20 µl Trypan blue 0,4%. The chamber and the necessary cover glass were prepared by cleaning them with 80% ethanol, followed by fixing the cover glass on the chamber. Furthermore, 10 µl from the cell-dye suspension was applicated between the cover glass and the chamber. Subsequently, all cells in the 4 quadrants were counted. After counting, the following formula was used to calculate the cells per ml (x = number of cells, counted in all 4 chambers):

$$\frac{x}{2} \times 10^4\ cells/ml$$

For every screening, 100 µl containing 1000 cells were seeded in every well of the 96-well-plates per cell line. Depending on the result, the cells were diluted to 10000 cells/ml (see above).

Cell culture: harvesting proteins

When the cells were seeded on day 1 of the screening, additionally cells were seeded to 10 cm dishes with 0,5 ml cell suspension into 5 ml DMEM. At 80% confluence in the dishes, the proteins were harvested to confirm the *HDAC-2* knock-out with WesternBlot later. Therefore, the lysis buffer was prepared, which contained 200 µl of IP-buffer, 2 µl phosphatase-inhibitor x100 and 8 µl protease-inhibitor x25 per 10 cm-dish. After aspirating the medium and washing the dishes with 5 ml PBS, 200 µl of the lysis buffer was added on each dish, the cells were collected using a cell scraper. The cell suspension was filled into 1,5 ml Eppendorf tubes and they were blast-froze in liquid nitrogen before storing them in a freezer at -80°C until further use.

Cell viability assay *CellTiterGlo*

The *CellTiterGlo* assay is a method to indirectly measure the viability of cells by measuring the adenosine triphosphate (ATP) level of a cell population via luminescence. The assay binds and reacts with ATP: Catalyzed by luciferase, luciferin reacts together with ATP and O_2 to the luminescent product oxyluciferin (Promega Corporation). The luminescence emission signal is directly linked with ATP-level and cell viability (Promega Corporation).

The *CellTiterGlo* assay consists of 2 components which needed to be prepared prior to use according to the instructions of the manufacturer (Promega Corporation). The prepared reagent was frozen until further use.

The day the prepared *CellTiterGlo* was needed, aliquots were thawed 4 to 5 hours prior to use and therefore put into a darkened place. After thawing, the reagent was added to the 96-well-plates from the screening by adding 25 µl *CellTiterGlo* in each well under light-protection. Afterwards the plates were put on the shaker for 10 minutes, followed by 20 minutes incubation time without shaking, both under light-protection. After incubation, luminescent measurement of the plates with *Fluostar optima-photometer* was performed (gain: 1500, luminescent filter: lens from the top, room temperature).

Bradford reagent and measurement of the protein concentration of samples

The Bradford reagent is an assay used to measure the protein concentration of samples by a photometric measurement. The reagent contains triphenylmethane dye which builds complexes with nonpolar and cationic rests of the tertiary structure of proteins. The resulting complex shows an absorption maximum at 595 nm, the reagent

itself has an absorption maximum at 470 nm. By change of absorption maximum of a probe, protein concentrations can be measured by comparing them with a calibration curve.

First, the Bradford reagent was mixed with sterile water in a 1:5 manner in a 50 ml falcon tube. Meanwhile a 96-well-plate was prepared. The first 6 wells were necessary for the calibration curve, which was generated by adding BSA 1 µg/µl into the wells in indicated concentrations (figure 11). Meanwhile the protein samples for the measurement were thawed and centrifuged at 4°C for 15 minutes (16000 rpm).

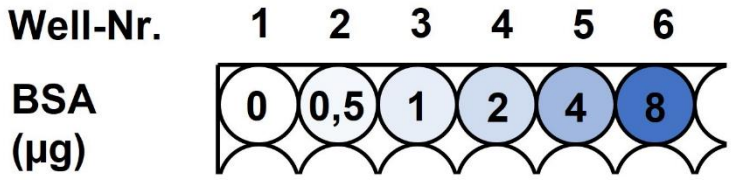

Figure 11: ***Occupancy for the BSA calibration curve****. To receive a calibration curve for the photometric measurement of protein concentration, the first six wells of the plate were used. Therefore, bovine serum albumin (BSA) in different concentrations was added to the prepared Bradford reagent: no BSA was added to the first well, the concentrations of the remaining five wells were 0,5 µg – 8 µg.*

For the sample wells, 1 µl of each sample was added into the prepared 300 µl Bradford reagent (n=3). A change of the color from green to blue was observed after adding standard or sample. Afterwards, the plate was put into the *Anthos-photometer* to measure the absorption at 595 nm.

Gel electrophoresis and WesternBlot

First, the electrophoresis chambers were prepared. Next, the separation gels were prepared and filled into ¾ of the electrophoresis chambers. To prevent formation of air bubbles, a few drops of isopropanol was added on top of the separation gel. After the separation gel polymerized entirely, the stacking gel was prepared and filled on top of the separation gel. A spacer was put into the polymerizing separation gel to form pockets for protein loading.

After the stacking gel polymerized, the protein samples were prepared. Depending on the protein concentrations of the harvested samples (measurement with Bradford reagent, see above), Laemmli-reagent and the protein samples were mixed in an eppendorf tube, to receive 2 µg/µl protein of each sample in the aliquot. Afterwards the aliquots were boiled up for 5 minutes at 95°C to denaturate the proteins. Meanwhile the gels were prepared by removing the spacer and the *Mini-PROTEAN Tetra Cell* were prepared by filling the trough with running buffer.

After the aliquots were boiled up for 5 minutes, 60 µg of protein per sample were filled into the foreseen pockets in the stacking gel. In one of the pockets 1 µl of the *PageRuler* marker was loaded to determine the size of the bands. After the gels were put in the trough, the electrophoresis was started using 80 V. After the samples reached the separation gel, the voltage was raised to 120 V.

Prior to use, one blotting membrane and six prepared Whatman papers were briefly incubated in transfer buffer. In the next step, three Whatman papers were stockpiled, followed by the gel and the blotting membrane, topped with the remaining three Whatman papers. To prevent air bubbles, the pile was smoothened and chucked into the blotting device, which was put into the blotting chamber filled with transfer buffer. The blotting was started for 120 minutes at 350 mA.

After the blotting was completed, the blotting membrane was washed in PBS two times for 5 minutes, followed by a blocking process with 5% Skim Milk for 30 minutes. Furthermore, the blotting membrane was shrink-wrapped in plastic foil, followed by adding 3 ml of the primary antibody (solved in 5% skim milk/PBS) and putting it on a shaker at 4 °C overnight.

The next day, the primary antibody was aspirated and the membrane was washed two times with PBS for 10 minutes, before the membrane got shrink-wrapped again, followed by adding 3 ml of fluorescent secondary antibody. Again, the membrane was wrapped into aluminum foil to protect the antibodies from light and put on the shaker for 1 hour.

Afterwards, the antibodies were aspirated and the blotting membranes were washed two times with PBS for 10 minutes, before the blotting membrane were shrink-wrapped one last time in plastic foil and 3 ml of the prepared mixture of anti-β-Actin-antibody and the fluorescent secondary antibody were added, followed by wrapping the membrane into aluminum foil and incubating it on the shaker for 1 hour. Finally, the membranes were washed two times with PBS for 10 minutes, prior to scanning them by using *Li-COR-Odysee* (figure 12).

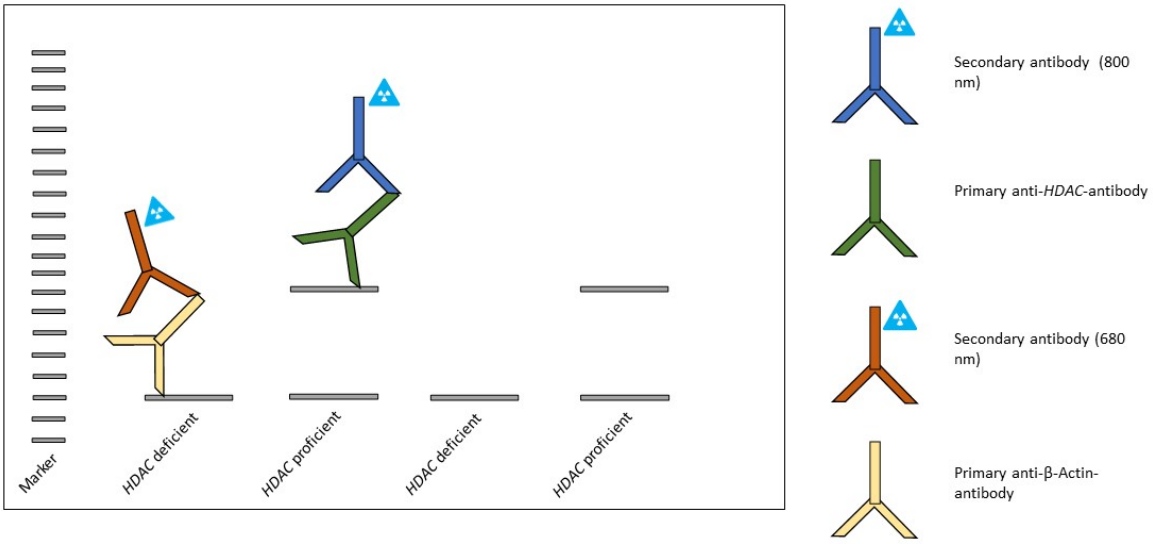

Figure 12: ***WesternBlot****. Draft of the knock-out measurement, exemplary for HDAC-2 knock-out: After the blotting, the membrane gets blocked with skim milk, to prevent untargeted bindings of the antibodies. The primary antibody binds the proteins. The secondary fluorescent antibody binds the primary antibody. The primary anti-β-Actin-antibody and the fluorescent secondary antibody were already mixed together in advance and are added to the membrane in the following step.*

RNA-sequencing

Previously generated and normalized RNA-sequencing data of the *HDAC-2* cell lines F2612 and F1648 were used. Briefly, mRNA was extracted from the Tamoxifen treated cell lines and control cell lines. After quality control with densitometry, RNA-sequencing was carried out by the facility for genomics and proteomics of the *Deutsches Krebsforschungszentrum*. For more explicit description see Krauß et al., 2022.

The changes in gene expression between *HDAC-2* proficient and deficient cell lines were analyzed using the Log2 fold changes. To generate the Log2 transformed fold changes, the DeSeq2 package in RStudio was used (Krauß et al., 2022).

Cell culture: Tamoxifen treatment for *HDAC-2* knock-out

The dual recombinase system, used to induce *HDAC-2* knock-out in murine PDAC cell lines, has already been described previously (Schönhuber et al., 2014; Kim et al., 2018).

First, cells were seeded on 10 cm dishes and treated with 4-OH-Tamoxifen (diluted in 100% ethanol) for 8 days. This induced *HDAC-2* knock-out due to the recombinase system. Since 4-OH-Tamoxifen (dissolved in ethanol 100%) is less stable in solution and when exposed to UV-light, 600 nM 4-OH-Tamoxifen was added each day by changing the media supplemented with 4-OH-Tamoxifen and the cells were split every 2-3 days. The control cell lines were treated simultaneously with the same amount of vehicle (ethanol). After finishing the treatment, the cells were labeled with T8d (treatment with 4-OH-Tamoxifen -> *HDAC-2* knock-out) or E8d (treatment with ethanol -> no *HDAC-2* knock-out) and proteins were harvested to confirm the knock-out of *HDAC-2* with WesternBlot.

Cell culture: Clonogenic assay

24-well-plates were used and 1000 cells/well (*HDAC-2* proficient or deficient) singularized in 500 µl of DMEM were seeded. 24 hours later, the drug dilutions of *Erastin* (100 µl 6-fold concentration of the final indicated concentrations) were added to the wells (figure 13).

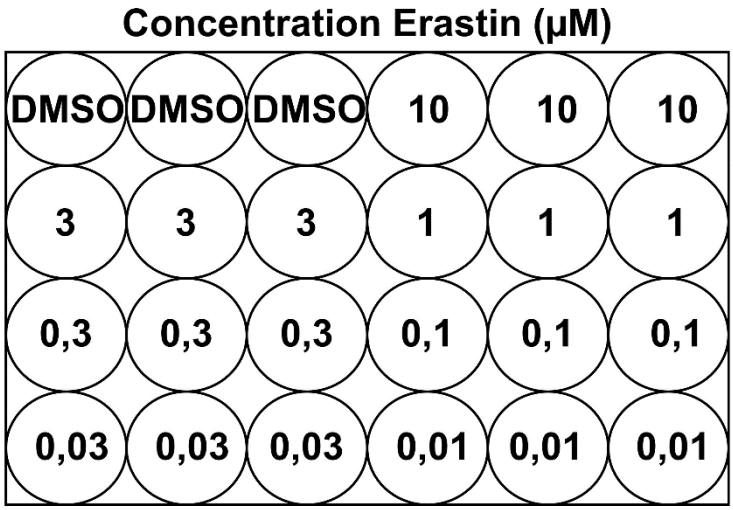

*Figure 13: **Clonogenic assay**. Layout of the 24-well-plates for the Erastin concentrations: after seeding 1000 cells in every well, drug dilutions of Erastin (0,01 µM – 10 µM) and, as Erastin was solved in DMSO, the DMSO control was added to the wells. To achieve technical triplicates, three wells were needed for every concentrations/control.*

DMEM was changed every second/third day. On day 7 after seeding the cells the medium was removed and the wells were washed carefully using 1 ml of PBS. After removing the PBS, each well was carefully filled with 200 µl of 0,2% *CrystalViolett*-solution, to fix and stain the cells. After 10 minutes of incubation, the *CrystalViolett* solution was removed, followed by washing the wells two times with 1 ml of water for 60 minutes. After the second washing process, the water was removed, and the plates were left for drying. After the plates were dry, they were scanned and subsequently 600 µl of 1% SDS was added to every well to solubilize the *CristalViolett* staining in the wells. After incubation of 2,5 hours, the *CLARIOstar-photometer* was used for photometric measurement.

Calculation of the z-score and definition of hits in the screening

The results of the IC_{50}-values and the AUC-values of the screening were analyzed by calculation of the z-scores. The z-score (z_i) is the amount of standard deviations (s) above or below a certain data (x_i) from the mean ($\bar{x}$).

$$z_i = \frac{x_i - \bar{x}}{s}$$

For example: $z_{IC50-Erastin\ F2612E8d} = \frac{x_{IC50-Erastin\ F2612E8d} - \overline{x_{IC50\ of\ Erastin\ in\ all\ tested\ cell\ lines}}}{Standarddeviation\ IC50\ all\ cell\ lines}$

Afterwards, the difference between the z-scores of the Tamoxifen-treated cell lines and the corresponding ethanol-treated cell lines was calculated:

$$\Delta z = z_{Tamoxifen} - z_{Ethanol}$$

A drug was defined as a hit when Δz-score of IC_{50} as well as Δz-score of AUC-values in both *HDAC-2* cell lines were <0. A negative Δz indicated a higher sensitivity of the tested drug in *HDAC-2* deficient cell lines. Afterwards the dose-response curves of the drugs were analyzed manually to confirm the observed results.

Cell culture: Combination treatment of *HDAC-2* proficient cells with *Erastin* and *MS-275*

To further validate the results from the screening, *HDAC-2* proficient cell lines F2612 and F1648 were treated with a combination treatment of *Erastin* and *MS-275*. Therefore, we performed cell viability assays using *CellTiterGlo* (for more information regarding *CellTiterGlo* see “Cell viability assay *CellTiterGlo*”). The cell lines were treated with *Erastin* (10-0,01 µM) and *MS-275* (2 µM or 4 µM) (figure 14). To determine the differences between the combination and a treatment with each compound alone, the cell lines were simultaneously treated with only *Erastin* or *MS-275*.

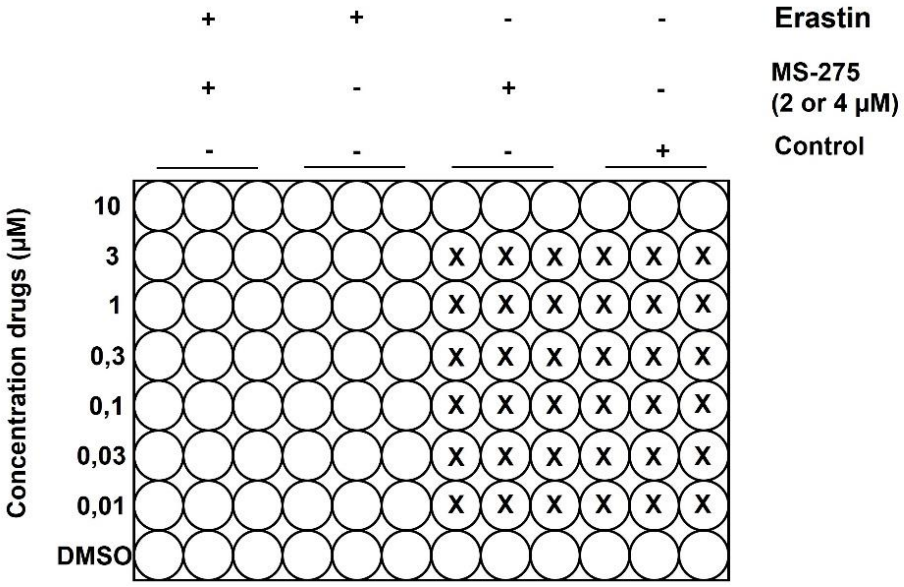

Figure 14: ***Layout for the validation experiments (Erastin + MS-275) with a 96-well-plate using cell viability assay****. HDAC-2 proficient cell lines were simultaneously treated with a combination of Erastin and MS-275 (2 or 4 µM), Erastin only and MS-275 only.*

Synergy Finder

To identify a potential synergy between *Erastin* and *MS-275*, the online tool *SynergyFinder* was used (https://synergyfinder.fimm.fi). It compares measured drug responses with expected drug combination responses calculated by means of synergy scoring models. The used synergy scoring model was the *Zero interaction model* (*ZIP-model*), which quantifies the degree of synergy and the expected response as if the single compounds wouldn’t affect the potency of each other and models the drug interaction by comparing the change in potency of each drug with the dose-response curve of the combination (Yadav et al., 2015; SynergyFinder, 2020; Ianevski et al., 2022).

Clonogenic assays (n=3) of F2612 were performed and measured as previously descirbed (see “Clonogenic Assay”), six 24-well-plates were seeded, and the cells were treated with *Erastin* (3 µM – 0,1 µM) and *MS-275* (4 µM – 0,0625 µM) in technical triplicates (figure 15).

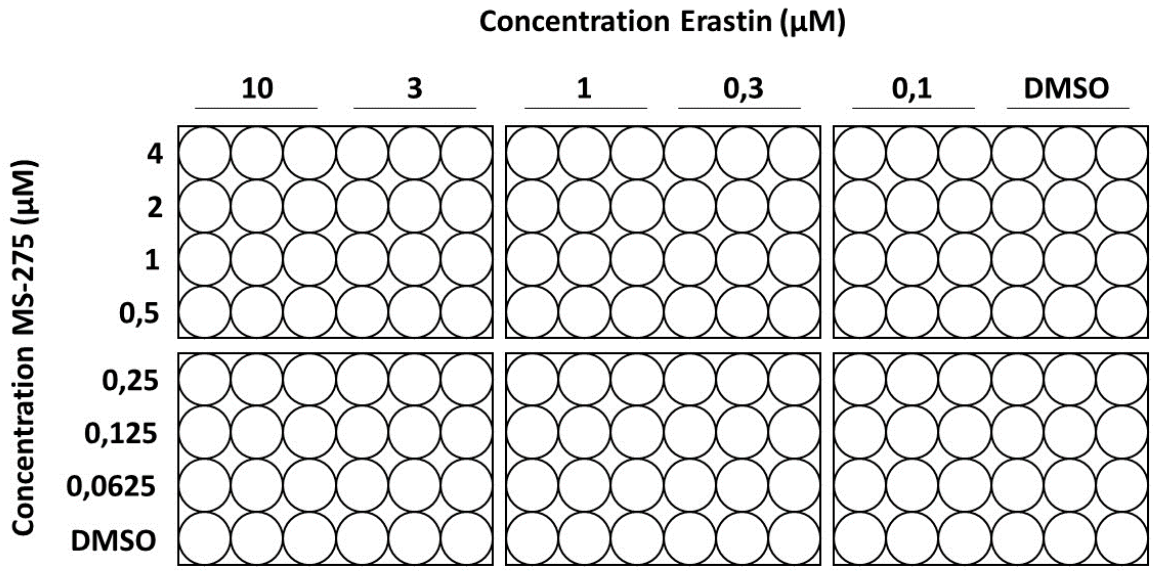

*Figure 15: **Clonogenic matrix for synergy finder**. Layout for the cell treatment with Erastin and MS-275 with indicated concentrations.*

To receive representative synergy scores after measurement, the highest (and lowest for MS-275) concentrations (10 and 3 µM for Erastin, 4 µM and 0,0625 µM for MS-275) were removed prior to analysis. Next, the values of the individual concentration treatments were uploaded as a table to the *SynergyFinder*-tool. "ZIP-model" as reference model and "Inhibition" as readout was chosen. All other settings were set to default. The tool consequently calculated synergy scores (mean and highest), dose-response curves, dose-response matrix and visualized the synergy scores with 3D and 2D models. Furthermore, dose-response curves of the multi-dimensional synergy of combinations (MuSyC) reference model were created by the tool. MuSyC reveals if an observed synergy is caused due to enhanced potency or/and efficacy of the compounds (Ianevski et al., 2022).

Gene set enrichment analysis (GSEA)

GSEA offers the possibility to compare *HDAC-2* proficient and deficient PDAC cells (F2612 and F1648) regarding significantly enriched pathways. Previously generated RNA-sequencing data were used and analyzed, using the software *GSEA 4.0.3* (Mootha et al., 2003; Subramanian et al., 2005). Briefly, rlog transformed countmatrix of RNA-sequencing data was used to compare *HDAC-2* proficient and deficient cell lines.

To detect overlapping positively or negatively enriched pathways in F2612 and F1648, the pathways with adjusted p-values <0,05 in F2612 and F1648 were compared using *Venny 2.1*.

Statistics

Unless stated otherwise, experiments were done in at least biological and technical triplicates. The screening was performed as one biological replicate in technical triplicates. Validation experiments were additionally performed in biological triplicates. For comparison of two independent kind of cell lines (*HDAC-2* proficient and deficient cell lines) regarding the consequences of the treatments, unpaired t-test (two tailed) was used to explore statistical significance, except for the evaluation of significance towards the findings from *SynergyFinder* (one-way analysis of variance with Bonferroni's multiple comparison test was used to determine significance). *GraphPad Prism 5* was used to visualize the results and perform the statistical calculations. No statistical method was used to predetermine sample size. The experiments were not randomized. The investigator was not blinded to allocation during experiments and outcome assessment.

Results

Drug screening and validations

To identify new HDACi-based combination therapies against PDAC, an explorative unbiased drug screening using 101 drugs targeting a variety of targets (see tables 12 – 20 in materials) in different concentrations was performed in two *HDAC-2* proficient and *HDAC-2* deficient PDAC cell lines (F1648, F2612). The knock-outs were confirmed on protein level by performing WesternBlots (figure 16).

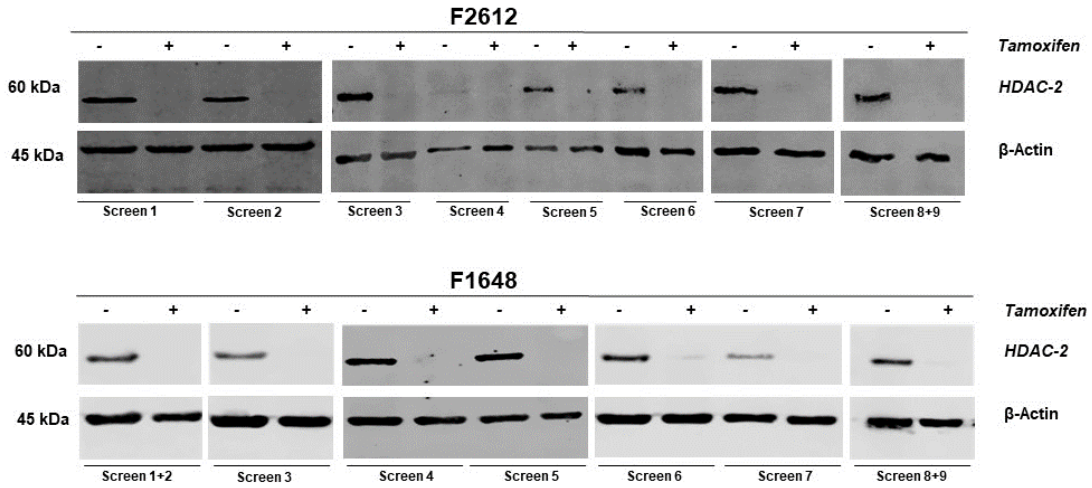

Figure 16: ***Tamoxifen induces HDAC knock-out in murine PDAC cell lines****. Indicated murine PDAC cell lines were treated with ethanol or Tamoxifen (600 nM, 8 days). Knock-out of HDAC-2 was confirmed on a protein level using Western Blot analysis. β-actin was used as a loading control.*

As a screening result, we observed differences in drug sensitivity between proficient and deficient cell lines. For analysis the IC_{50}- and AUC-values of the dose-response curves were used (tables 25 - 26) and the z-scores were calculated (table 27). Based on the IC_{50}- and AUC-values, the z-ratios (Δ z-scores) between proficient and deficient cell lines were calculated (table 28). A drug was defined as a hit, if z-ratios of IC_{50} and AUC were both negative in the *HDAC-2* cell lines F2612 and F1648, indicating increased drug sensitivity in *HDAC-2* deficient cell lines (figure 17 B, C and D).

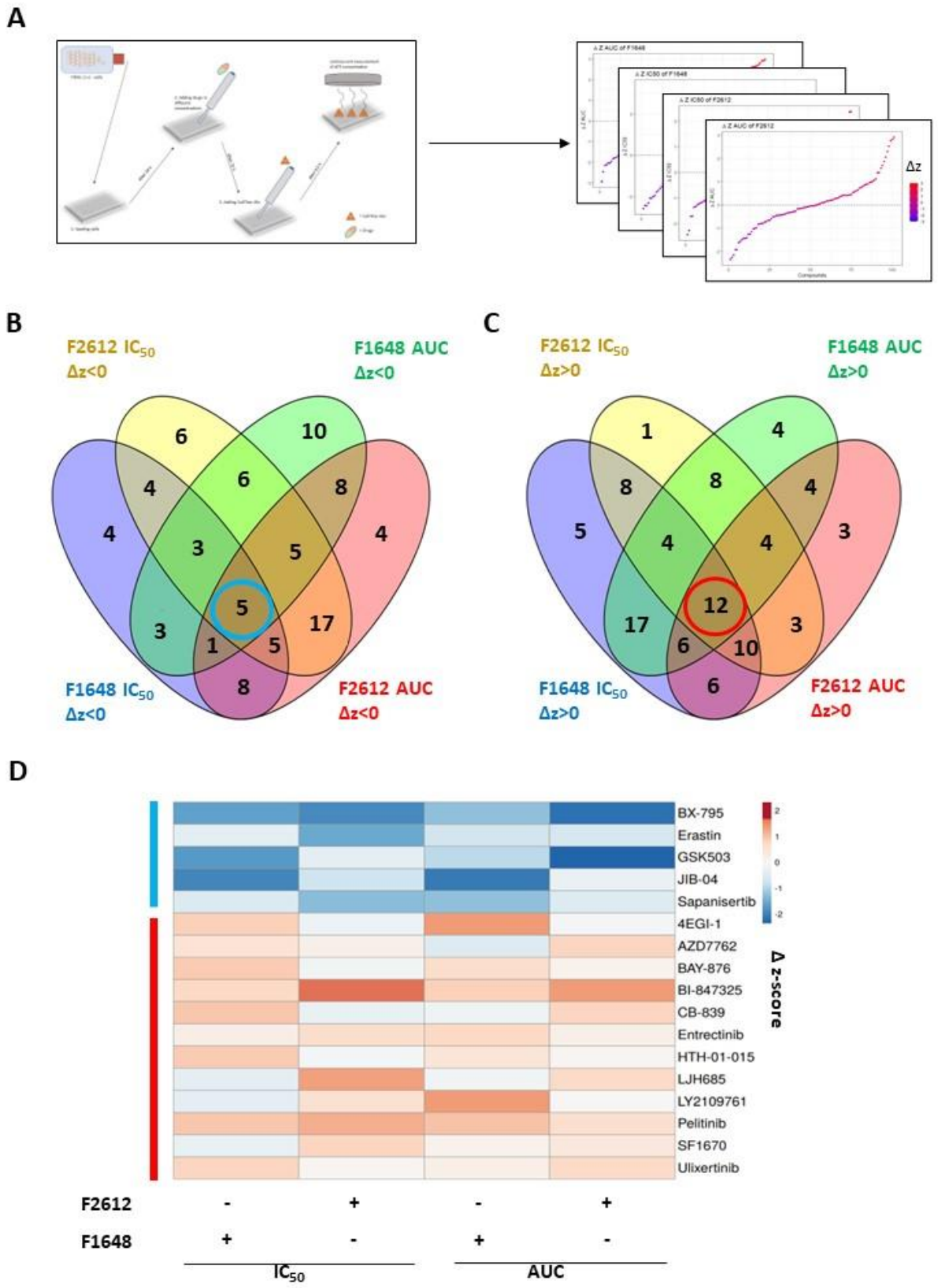

*Figure 17: **Definition of screening hits in HDAC-2 cell lines**. (A) Visualization of screening hits and analysis of the results. (B) shows the overlap of the calculated negative z-ratios. (C) shows the overlap of the calculated positive z-ratios. (D) Heatmap of the overlapping compounds (negative z-rations shown in blue, positive z-rations shown in red).*

Consequently, five drugs were identified as hits (figure 17 B and D and table 21). Furthermore, curve fitting was confirmed manually.

Table 21: Overview over Δz-scores of identified compound hits.

	Δz IC_{50} F1648	Δz IC_{50} F2612	Δz AUC F1648	Δz AUC F2612
BX-795	-1,881	-1,346	-1,021	-2,171
Erastin	-0,030	-1,062	-0,305	-0,505
GSK503	-1,958	-0,051	-0,595	-2,321
JIB-04	-2,327	-0,418	-2,131	-0,103
Sapanisertib	-0,251	-0,831	-1,015	-0,359

In order to validate the identified hits, we first repeated the viability experiments (figure 18) and were able to confirm the results of *Erastin* and *JIB-04*. For *Erastin*-treatment in *HDAC-2* deficient cell lines we observed a significant reduction of IC_{50}-values of 38,11% in F2612 and 39,85% in F1648 as well as a reduction of AUC-values of 9,22% in F2612 and 15,70% in F1648 compared to the *HDAC-2* proficient cell lines. For *JIB-04*-treatment in *HDAC-2* deficient cell lines we observed a significant reduction of IC_{50}-value of 29,77% in F2612 and 57,94% in F1648 as well as a reduction of AUC-value of 7,42% in F2612 and 36,78% in F1648 compared to *HDAC-2* proficient cell lines (table 22). To calculate the reduction of AUC- and IC_{50}-values, the following equation was used: $\text{Reduction}_{IC50/AUC} = (1 - \frac{T8d}{E8d}) \times 100$ [%].

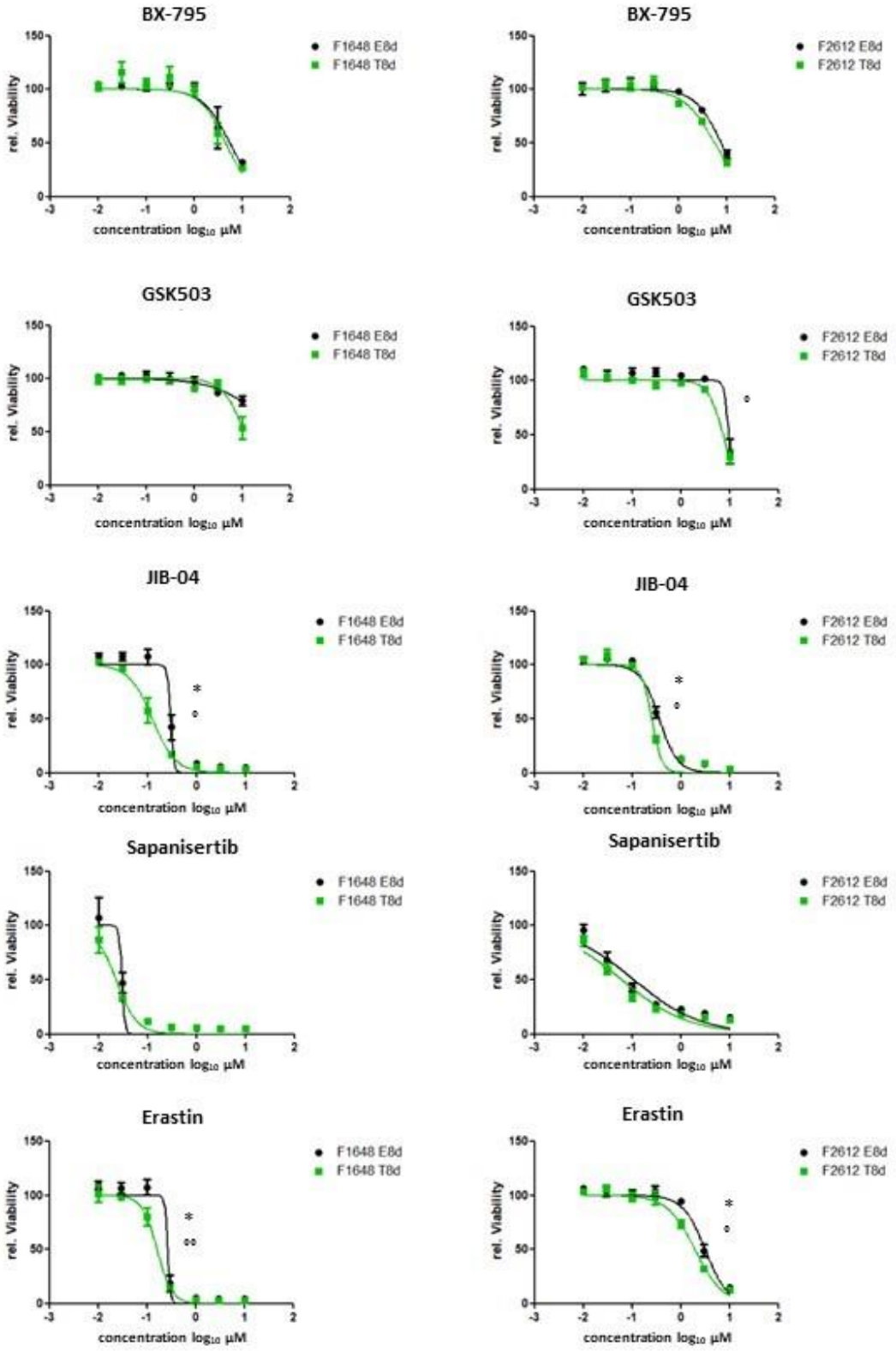

Figure 18: ***Dose-response curves of the identified hits with cell viability assay****. After the screening, hits were validated (n=3 biologically independent samples) and dose-response were generated for F1648 and F2612. Measurement of cell viability after 72 hours by using CellTiter-Glo assay. Significance of the biological triplicates were calculated by using unpaired t-test (°p_{AUC} <0,05; °°p_{AUC} <0,01, *p_{IC50} <0,05). Data are presented as mean values +/- SEM.*

Table 22: ***Overview and comparison of IC_{50}- and AUC-values in cell viability assay****. n=3 biologically independent samples.*

		F1648 *HDAC-2* (+)	F1648 *HDAC-2* (-)	F2612 *HDAC-2* (+)	F2612 *HDAC-2* (-)
BX-795	**IC_{50} (µM)**	5,461	4,491	7,576	5,594
	AUC	605,8	562,5	698,2	612,7
	Reduction IC_{50}	17,76%		26,16%	
	Reduction AUC	7,15%		12,25%	
Erastin	**IC_{50} (µM)**	0,271	0,163	3,175	1,965
	AUC	149	125,6	256	232,4
	Reduction IC_{50}	39,85%		38,11%	
	Reduction AUC	15,70%		9,22%	
GSK503	**IC_{50} (µM)**	47,37	10,86	9,410	7,296
	AUC	863,9	799,0	791,7	713,6
	Reduction IC_{50}	77,07%		22,47%	
	Reduction AUC	7,51%		9,86%	
JIB-04	**IC_{50} (µM)**	0,2927	0,1231	0,3554	0,2496
	AUC	96,09	60,75	111,9	103,6
	Reduction IC_{50}	57,94%		29,77%	
	Reduction AUC	36,78%		7,42%	
Sapanisertib	**IC_{50} (µM)**	0,02976	0,02244	0,1083	0,06125
	AUC	53,44	56,03	192,9	159,4
	Reduction IC_{50}	24,69%		43,44%	
	Reduction AUC	-4,85%		17,37%	

We further evaluated *Erastin. Erastin* is a ferroptosis inducer, targeting the cystine-glutamate antiporter x_c^- and opens voltage dependent anion channels in the outer mitochondrial membrane (VDAC) and thus leads to ferroptosis, a non-apoptotic cell death (Yagoda et al., 2007; Dixon et al., 2012; Cao and Dixon, 2016; Conrad and Pratt, 2019).

Effect of *Erastin* treatment with the mean IC_{50}-value concentration of F2612 (2,57 µM) on *HDAC-2* proficient and deficient PDAC cells was visualized after 72 hours (figure 19).

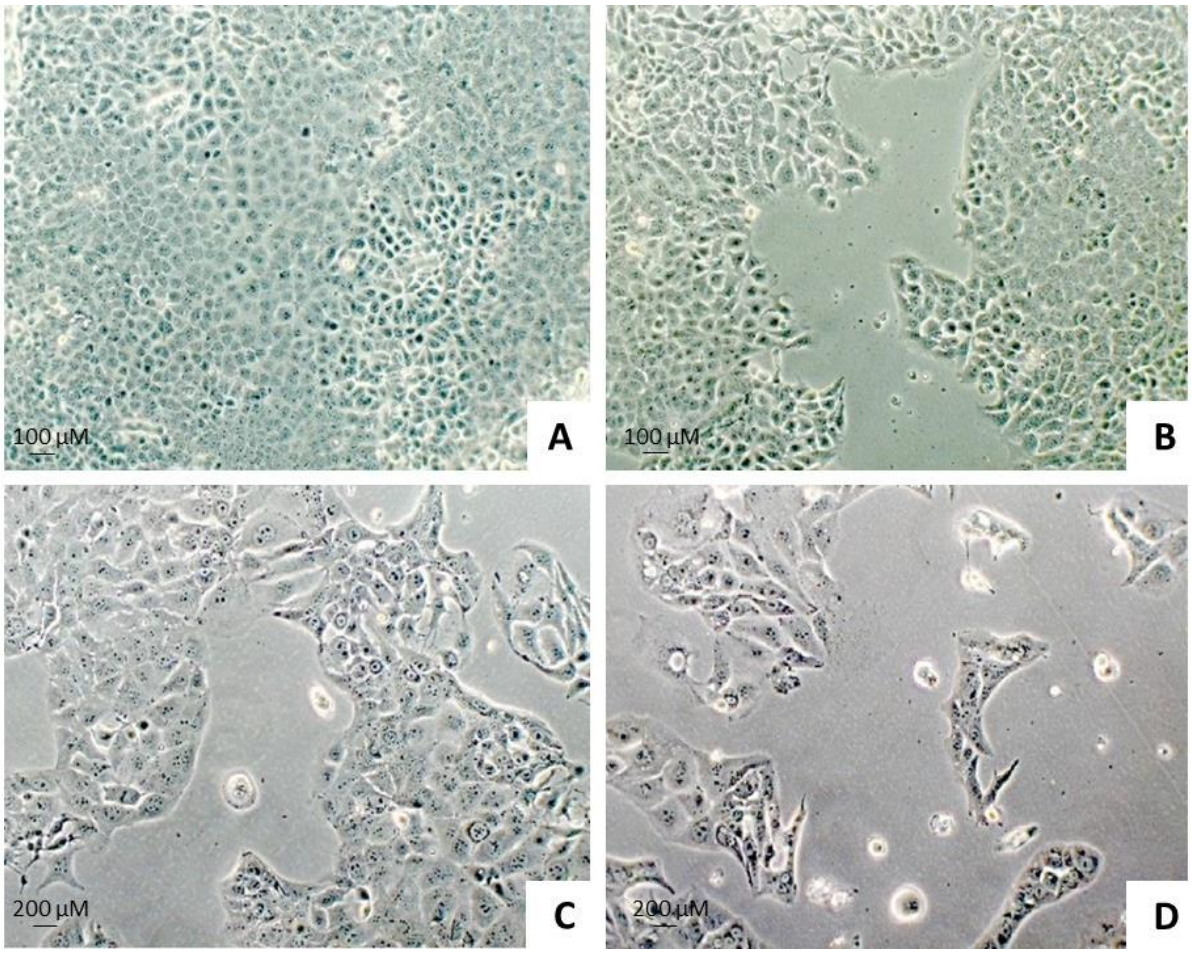

Figure 19: ***Pictures of cell lines treated with DMSO or 2,57 µM Erastin (F2612)****. Treatment of HDAC-2 proficient cells with (A) DMSO (control) or (C) Erastin 2,57 µM. Treatment of HDAC-2 deficient cells with (B) DMSO (control) or (D) Erastin 2,57 µM. The pictures taken were representative to the cell density in the dish.*

Next, we further validated the effect of *Erastin* in clonogenic assays (n=3) using the cell line F2612. We could confirm the reduction in clonogenic growth in *HDAC-2* deficient cell lines after 7 days of *Erastin* treatment, however the findings were not significant (figure 20). The clonogenic growth curve was used to determine AUC- and IC_{50}-values. Thus, for F2612 we observed a reduction of 42,59% for IC_{50}-value and 19,42% for AUC-value (table 23).

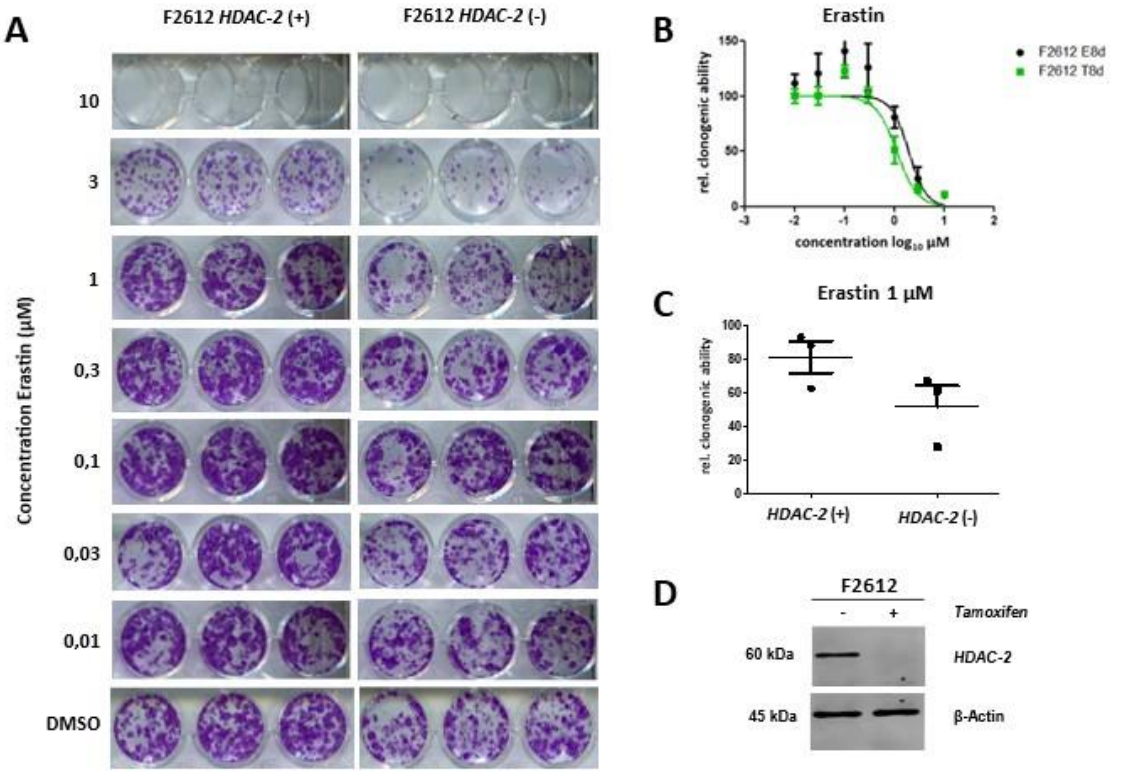

Figure 20: ***Validation of the effect of Erastin with clonogenic assay****. (A) Visualization of the clonogenic growth: HDAC-2 proficient and deficient cell line (F2612) treated with Erastin with indicated concentrations for 7 days. (B) Dose-response curve of clonogenic assay (n=3 biologically independent samples, ns). (C) Reduction of the relative clonogenic growth of HDAC-2 proficient and deficient cell lines (F2612) treated with Erastin 1 µM (ns, two-tailed unpaired t-test), as this concentration showed the biggest difference in clonogenic growth between proficient and deficient cells. (D) Indicated murine PDAC cell lines were treated with ethanol or Tamoxifen. Knock-out of HDAC-2 was confirmed on a protein level using Western Blot analysis. ß-actin was used as a loading control. All data are presented as mean values +/- SEM.*

Table 23: ***Clonogenic assay mean IC_{50}- and AUC-values and its reductions****. Mean IC_{50}- and AUC-values and its reductions comparing HDAC—2 proficient and deficient cells from the clonogenic assay experiments (n=3 biologically independent samples) with Erastin (F2612): the combination of HDAC-2 deficiency and Erastin treatment show a reduction of 42,59% for IC_{50}- and a reduction of 19,42% for AUC-value.*

	F2612 *HDAC-2* (+)	**F2612 *HDAC-2* (-)**
IC50 (µM)	1,965	1,128
AUC	277,1	223,3
Reduction IC_{50}	42,59% (ns)	
Reduction AUC	19,42% (ns)	

Analysis of combination of *Erastin* and *MS-275* with *HDAC-2* proficient cells

To evaluate if the observed effects in the genetic models were reproducible and could be translated in an actual pharmacological treatment, *HDAC-2* proficient cell lines F2612 and F1648 were receiving a treatment with *Erastin* and *MS-275*. Cell viability assay *CellTiterGlo* was performed for evaluation.

The results showed a reduction of cell viability in cell lines receiving the combination of *Erastin* and *MS-275* compared to those receiving either one of them (figure 21). For F1648 cell line receiving the combination of *Erastin* and *MS-275* 2 µM (n=2) we

observed a reduction of IC_{50}-value of 57,93% and a significant reduction of AUC-value of 25,30%, in F2612 we observed for this drug combination (n=2) a reduction of IC_{50}-value of 69,01% and a reduction of AUC-value of 26,80%. In cell lines treated with Erastin and MS-275 4 µM, we observed in F1648 (n=2) a reduction of IC_{50}-value of 97,23% and a significant reduction of AUC-value of 51,24% and in F2612 we observed for this drug combination (n=2) a reduction of IC_{50}-value of 98,45% and a reduction of AUC-value of 49,74%.

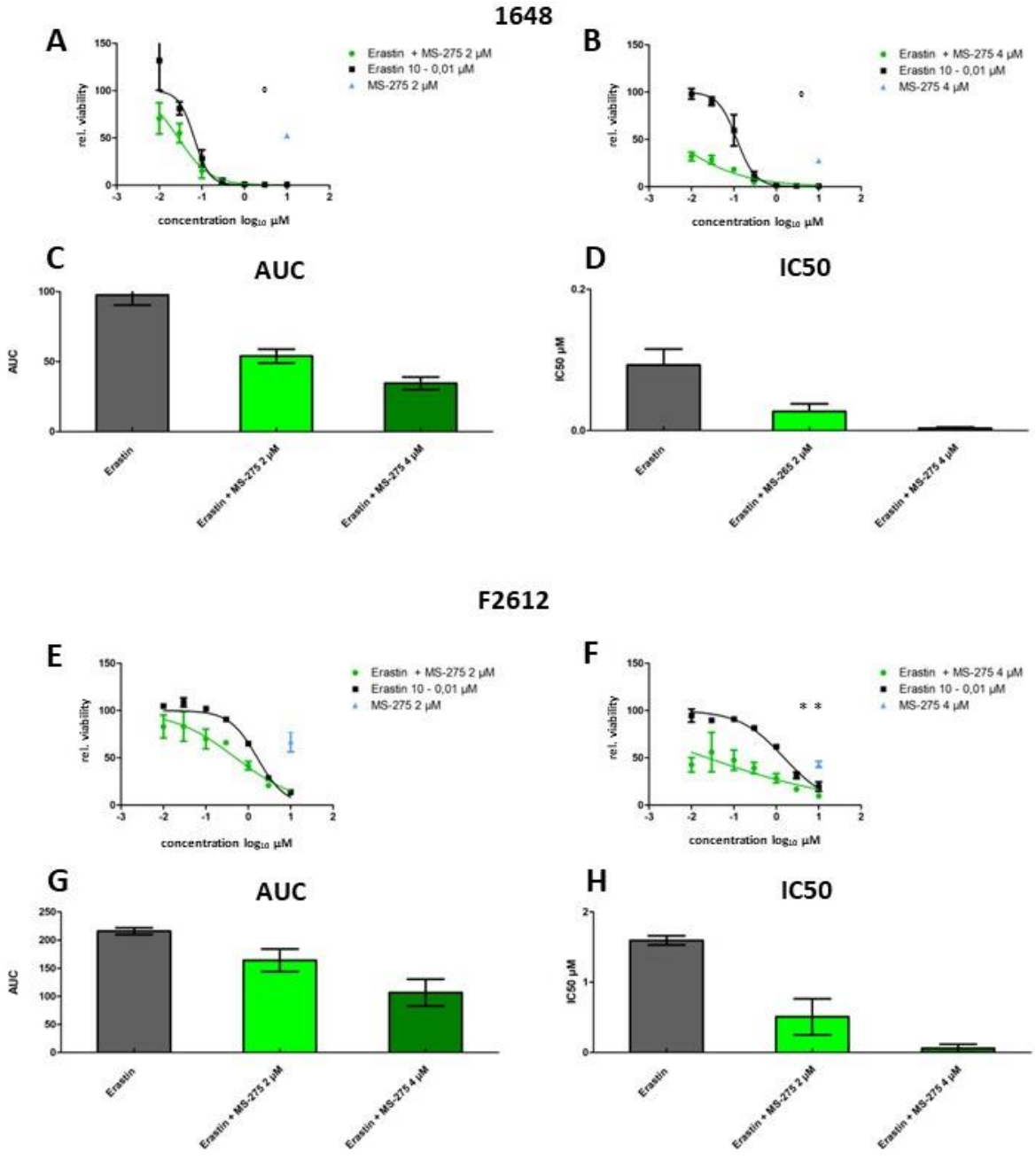

Figure 21: ***Combination treatment of HDAC-2 proficient cell lines F2612 and F1648 with Erastin and MS-275 using cell viability assay****. Treatment of (A) F1648 and EB) F2612 with Erastin and MS-275 2 µM. Treatment of (B) F1648 and (F) F2612 with Erastin and MS-275 4 µM. Comparison of AUC-values of the duplicates of (C) F1648 and (G) F2612. Comparison of IC_{50}-values of the duplicates of (D) F1648 and (H) F2612. Significance of the biological duplicates were calculated by using unpaired t-test (°p_{AUC} <0,05; **p_{IC50} <0,01). All data are presented as mean values +/- SEM (n=2 biologically independent samples). The presented data were generated with the support of Lukas Krauß.*

Analysis of synergy

Based on the results, we next wanted to evaluate if synergy between *Erastin* and *MS-275* exists. Therefore, we used the online tool *SynergyFinder* (https://synergyfinder.fimm.fi). We calculated the synergy score for clonogenic assay in *HDAC-2* proficient cell line F2612 (n=3) (figure 22). *SynergyFinder* compares the observed drug combination responses (e.g. dose-response matrix) with the expected responses calculated by means of synergy scoring models (reference model), leading to classification of synergy or antagonism depending on the observed deviation (Ianevski et al., 2022). The used reference model was the *Zero interaction potency model* (*ZIP-model*). The ZIP-model quantifies the degree of synergy and the expected response as if the single drugs wouldn't affect the potency of each other and it models the drug interaction by comparing the change in potency of the dose-response curves of each drug with the dose-response curve of the combination (Yadav et al., 2015; SynergyFinder, 2020). For each measured dose combination, an individual synergy score is visualized to find the most synergistic area. The synergy score is averaged over all the measured dose combinations. *SynergyFinder* defines the results of the synergy score as followed:

- ZIP < -10 antagonistic
- -10 < ZIP < 10 additive
- ZIP > 10 synergistic

With help of *SynergyFinder* we were able to show existing synergy between *Erastin* and *MS-275* with a summery synergistic score of 14,05 and a most synergistic area score of 18,95 (figure 23 A – C). The best synergy (34,07) was observed for a combination of 1µM *MS-275* and 0,3 µM *Erastin*. To determine significance of the findings, one-way analysis of variance with Bonferroni's multiple comparison test was performed showing a significant difference between cells treated with *Erastin* 0,3 µM in combination with *MS-275* 1 µM compared to cells only treated with *MS-275* 1 µM (figure 23 F). Generated combination dose-response-curves of the multi-dimensional synergy of combinations (MuSyC) reference model revealed that a synergistic potency shift with a fold change of 4,59 for *Erastin* treated cells induced by *MS-275* can be detected (figure 23 D) as well as a synergistic potency shift with a fold change of 21,44 for cells treated with *MS-275* induced by *Erastin* (figure 22 E).

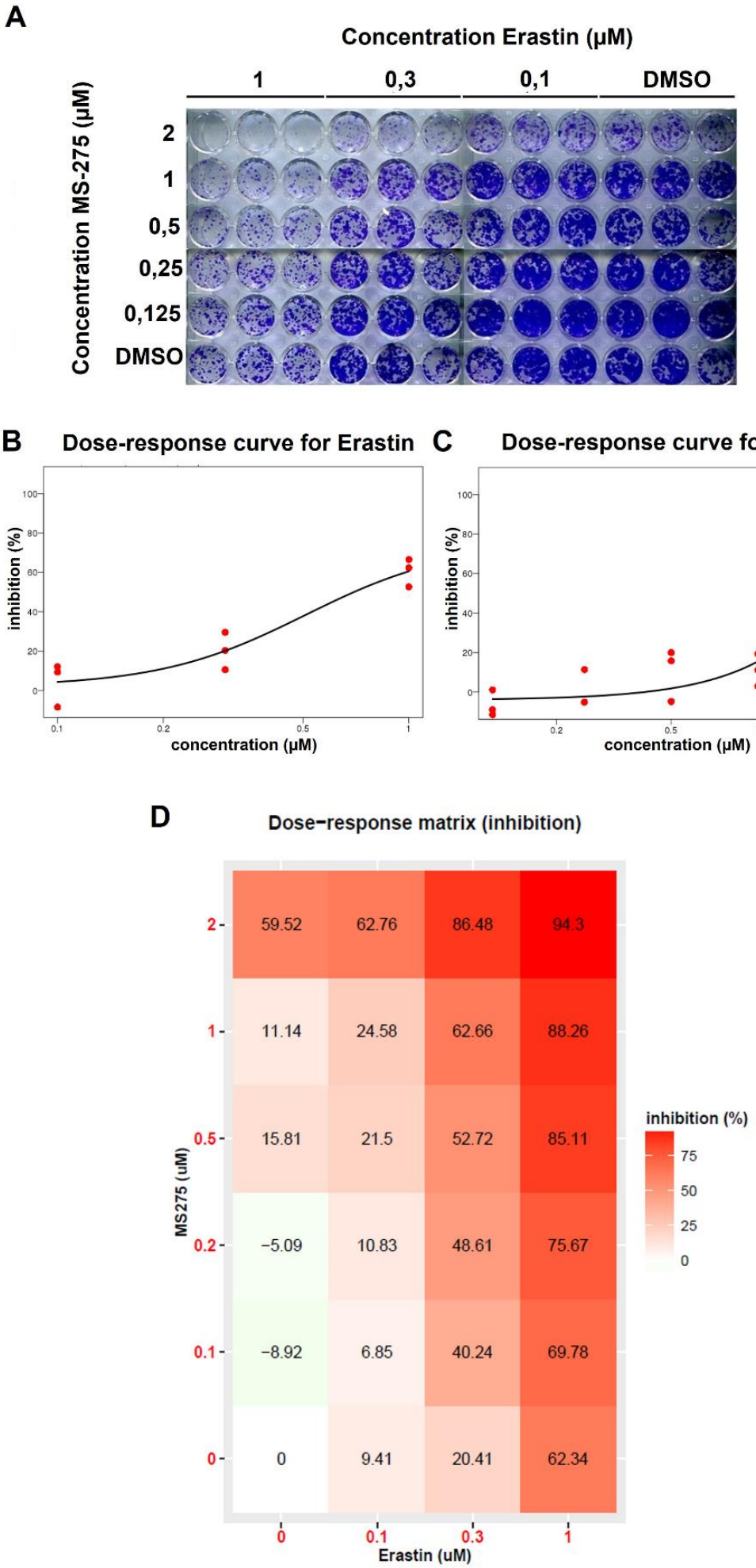
A
Concentration Erastin (µM)
1
0,3
0,1
DMSO
Concentration MS-275 (µM)
2
1
0,5
0,25
0,125
DMSO
B
Dose-response curve for Erastin
inhibition (%)
concentration (µM)
C
Dose-response curve for MS-275
inhibition (%)
concentration (µM)
D
Dose−response matrix (inhibition)
MS275 (uM)
2
1
0.5
0.2
0.1
0
59.52
62.76
86.48
94.3
11.14
24.58
62.66
88.26
15.81
21.5
52.72
85.11
−5.09
10.83
48.61
75.67
−8.92
6.85
40.24
69.78
0
9.41
20.41
62.34
0
0.1
0.3
1
Erastin (uM)
inhibition (%)
75
50
25
0

Figure 22: ***SynergyFinder matrix and input dose-response curves****. (A) Matrix generated with clonogenic assay: HDAC-2 proficient cell line (F2612) treated with Erastin and MS-275 with indicated concentrations for 7 days. Dose-response curves generated with clonogenic assay (n=3 biologically independent samples) after treatment with (B) Erastin or (C) MS-275. (D) Dose-response matrix generated by SynergyFinder showing inhibiton of cell viability after combination treatment of Erastin and MS-275 with indicated concentrations. The presented data were generated with the support of Lukas Krauß.*

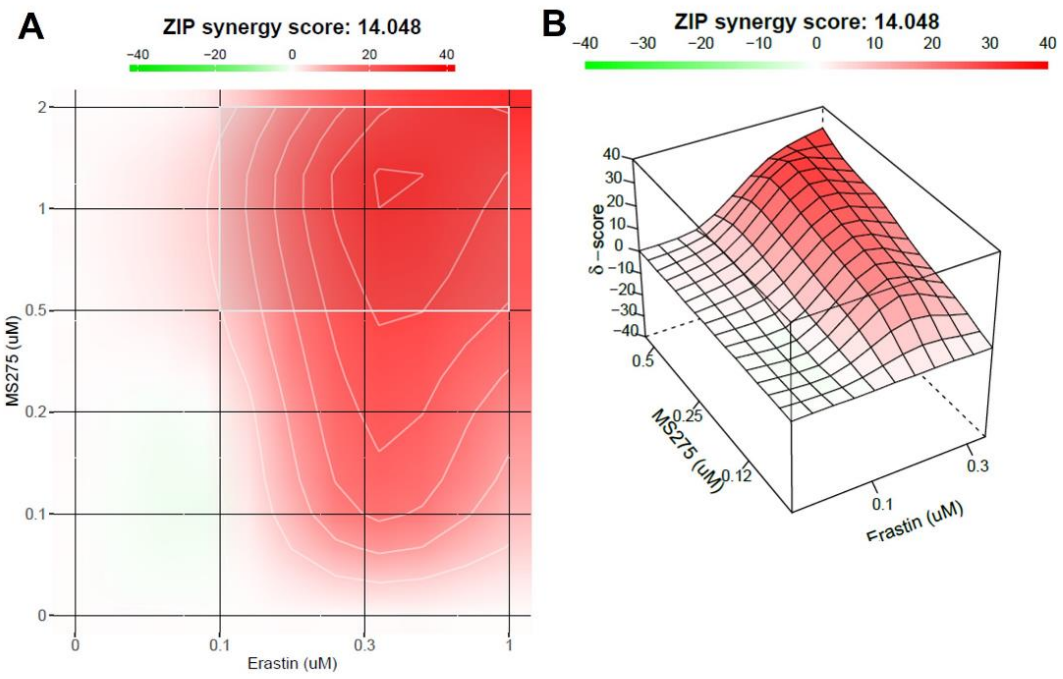

C

Drug combination	Synergy score	Most synergistic area score	Method
Erastin - MS275	14.05	18.95	ZIP

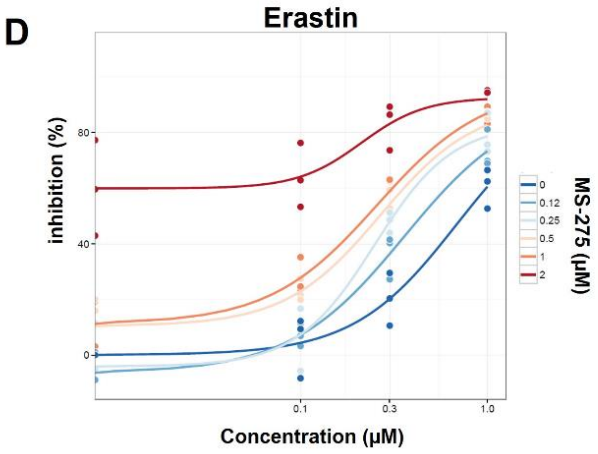

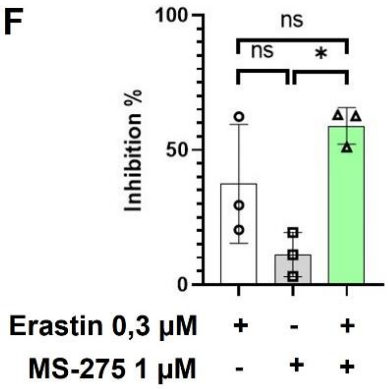

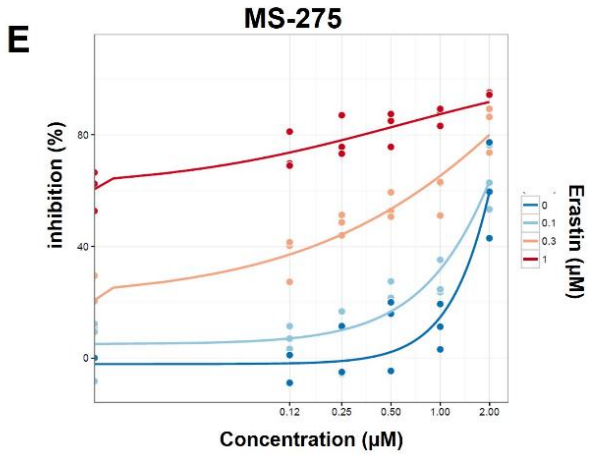

*Figure 23: **Visualization of synergy between Erastin and MS-275**. (A) 2D and (B) 3D synergy map highlighting synergistic regions, showing (C) a summery synergy score of 14,05 and a most synergistic area score of 18,95 (using ZIP-model). (D) Combination dose-response curves of the multi-dimensional synergy of combinations (MuSyC) reference model showing a synergistic potency shift of Erastin treated cells induced by MS-275 (fold change: 4,59) or (E) a synergistic potency shift of MS-275 treated cells induced by Erastin (fold change 21,44). (F) Significant difference in cell viability between cells treated with Erastin 0,3 µM and MS-275 1 µM compared to cells only treated with MS-275 1 µM (One-way ANOVA with Bonferroni's multiple comparison test). n=3 biologically independent samples.*

Analysis of RNA-sequencing data

RNA-sequencing data of *HDAC-2* cell lines F2612 and F1648 previously generated were used. The data were analyzed regarding genes relevant for induction of ferroptosis and HDAC inhibition as well as genes which are relevant in the pathways showing positive enrichment in *HDAC-2* proficient cell lines in GSEA (see below). SLC7A11 and VDAC2 are direct targets of *Erastin* (Conrad and Pratt, 2019; Zhao et al., 2020). GPX4 is an important enzyme for detoxification of reactive oxygen species and needs glutathione as cofactor (Yang et al., 2014). EIF2AK4 is a kinase, leading to phosphorylation of the eucaryotic translation initiation factor eIF2α, which activates the integrated stress response against cellular stress via ATF4 (table 24) (Suragani et al., 2012; B'chir et al., 2013; Wortel et al., 2017).

*Table 24: **Extract from the RNA-sequencing data necessary for the thesis**. (NA = no data) The Log2 Fold Change (Log2FC) is a ratio comparing the gene expression between HDAC-2-proficient and -deficient cells. A negative Log2FC equals a lower expression in the deficient cells, while a positive Log2FC means a higher expression in the deficient cells. The p-value as indicator for significance shows, that not all data from the sequencing are statistically significant. Especially ATF4 shows significantly lower resp. higher expression in the HDAC-2-deficient cells in both cell lines.*

	F2612		**F1648**	
	Log2FC	p-value	Log2FC	p-value
SLC7A11	-0,96	0,181	-0,62	0,003
ATF4	-0,69	0,003	-0,33	0,002
EIF2AK4	-0,13	0,4	0,09	0,155
GPX4	0,11	0,524	0,01	0,926
VDAC2	0,15	0,252	-0,13	0,255

Analysis of Gene set enrichment analysis

Gene set enrichment analysis (GSEA) using the previously generated RNA-sequencing data of *HDAC-2* cell lines F2612 and F1648 was performed to determine the behavior of the cell lines after *HDAC-2* knock-out. We overlapped the results from each cell line. We confirmed five enriched Reactome pathways in *HDAC-2* proficient cell lines, including the transport of amino acids across the plasma membrane, the response of kinases to amino acid deficiency and heme deprivation and the cellular response to starvation (figure 24).

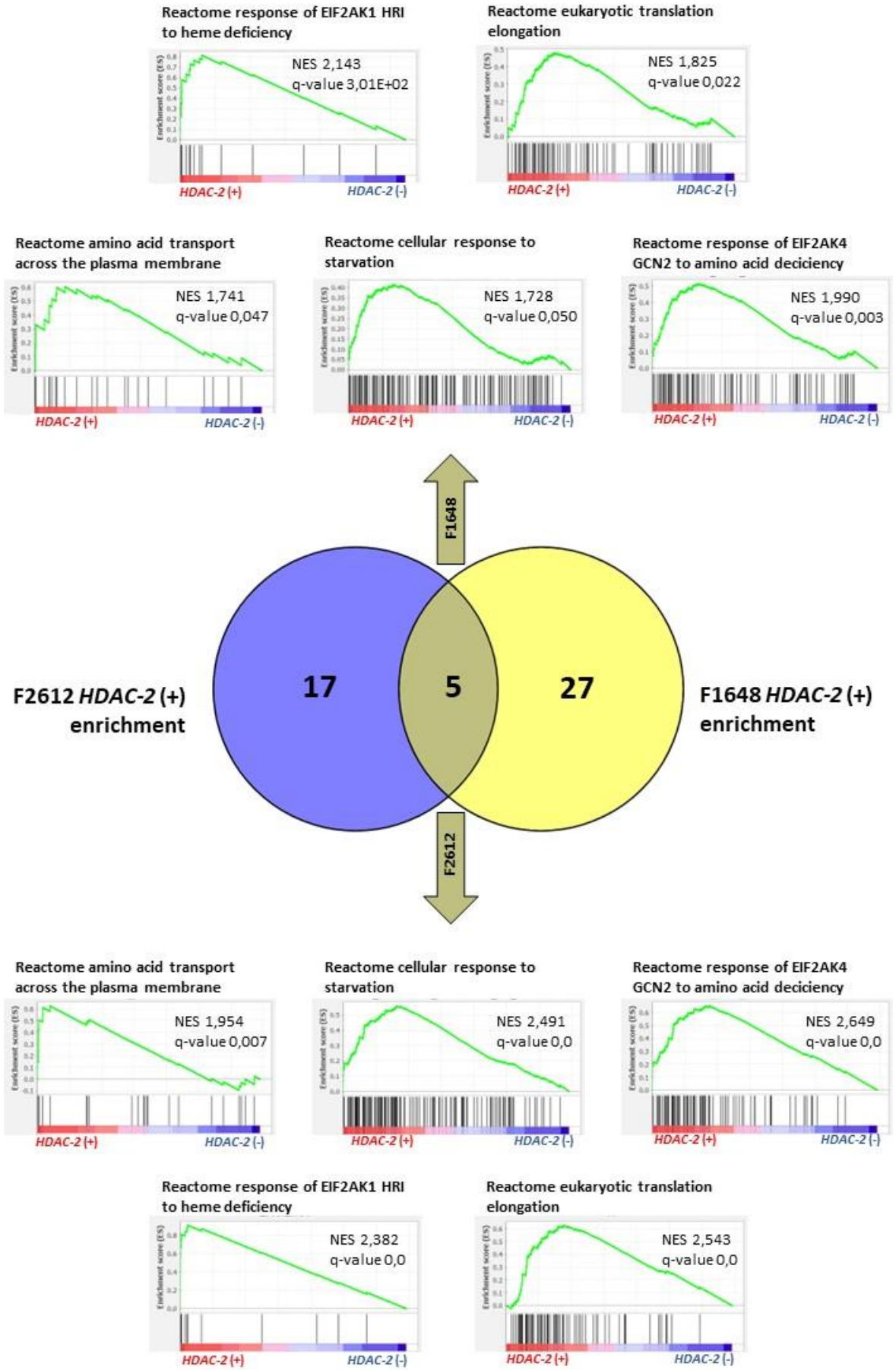
Reactome response of EIF2AK1 HRI to heme deficiency
NES 2,143
q-value 3,01E+02
HDAC-2 (+)
HDAC-2 (-)
Reactome eukaryotic translation elongation
NES 1,825
q-value 0,022
HDAC-2 (+)
HDAC-2 (-)
Reactome amino acid transport across the plasma membrane
NES 1,741
q-value 0,047
HDAC-2 (+)
HDAC-2 (-)
Reactome cellular response to starvation
NES 1,728
q-value 0,050
HDAC-2 (+)
HDAC-2 (-)
Reactome response of EIF2AK4 GCN2 to amino acid deciciency
NES 1,990
q-value 0,003
HDAC-2 (+)
HDAC-2 (-)
F1648
F2612 HDAC-2 (+) enrichment
17
5
27
F1648 HDAC-2 (+) enrichment
F2612
Reactome amino acid transport across the plasma membrane
NES 1,954
q-value 0,007
HDAC-2 (+)
HDAC-2 (-)
Reactome cellular response to starvation
NES 2,491
q-value 0,0
HDAC-2 (+)
HDAC-2 (-)
Reactome response of EIF2AK4 GCN2 to amino acid deciciency
NES 2,649
q-value 0,0
HDAC-2 (+)
HDAC-2 (-)
Reactome response of EIF2AK1 HRI to heme deficiency
NES 2,382
q-value 0,0
HDAC-2 (+)
HDAC-2 (-)
Reactome eukaryotic translation elongation
NES 2,543
q-value 0,0
HDAC-2 (+)
HDAC-2 (-)

Figure 24: ***Gene set enrichment analysis of F1648 and F2612****. RNA-sequencing data of HDAC-2 cell lines F2612 and F1648 were analyzed with GSEA. Five pathways show a significant negative enrichment in both HDAC-2 cell lines, the enrichment plots for the depicted reactome pathway signatures are shown.*

Discussion and interpretation of the results

With a 5-year-survival of 11%, pancreatic cancer has a very poor prognosis and is predicted to be the third leading cause of cancer related deaths in women and fourth leading cause of cancer related deaths in men by 2040 (Jain and Bhardwaj, 2021; Rahib et al., 2021; Siegel et al., 2022). It is mostly diagnosed in advanced stages, meaning that surgery, as only way to cure the disease, is often not possible anymore (Wagner et al., 2004; Park et al., 2021). This highlights the necessity for drug-based therapies. Although chemotherapeutic schemes like FOLFIRINOX are available, due to therapy resistance of the cancer the success is often limited (Jain and Bhardwaj, 2021). This shows the importance of new drug-based therapeutic strategies.

HDACi like *Vorinostat* seem to be promising anti-cancer agents, as *Vorinostat* has already been approved by the FDA for treatment of refractory cutaneous T-cell lymphomas (Falkenberg and Johnstone, 2014). Different studies also see potentials of HDACi for treatment of pancreatic cancer, e.g. to overcome chemotherapy resistances (Roca et al., 2022). While studies in the past showed HDACi as potential partner within a drug-combination, many clinical trials did not show the expected success, especially the utility of HDACi as single agent (Hontecillas-Prieto et al., 2020). To find new potential combination-based drug therapies for treatment of pancreatic cancer, a drug screening was established using isogenic murine *HDAC-2* proficient and deficient PDAC cell lines as a model system. The response to 101 drugs with different mode of actions was tested in the drug screening experiment. Based on the results of the unbiased screening with *HDAC-2* proficient and deficient cells, *Erastin* was further evaluated as a potential partner for a combination therapy with HDACi.

In both *HDAC-2* cell lines, cell lines treated with *Erastin* showed a significant reduction of cell viability. Those findings were reproducible performing different assays such as clonogenic assay, although significance has not always been confirmed. Further investigations and validations are necessary, e.g. by using different models such as primary human PDAC cell lines or a larger cohort of murine PDAC cell lines.

To determine if the observed results in the knock-out screening could be translated into actual pharmacological treatments, a treatment of *HDAC-2* proficient cell lines with actual compounds was necessary. After combination treatment with *Erastin* and *MS-275* (class-I-HDACi), we confirmed reduced cell viability and synergistic effects.

Erastin was originally found in a compound screening as a small molecule that killed cancer cells which were overexpressing Small T oncoprotein (*ST*) and oncogenic *RAS*, leading to its name *Erastin* ("**E**radicator of ***RAS*** and ***ST***-expressing cells") (Dolma et al., 2003). Although *KRAS* is the most frequently mutated oncogene in PDAC (Hong et al., 2011), ferroptosis induced by *Erastin* is not only relevant in *RAS*-mutated cancer cells and can be induced regardless of the *RAS*-status (Conrad and Pratt, 2019). *Erastin* has a poor water solubility and has an unstable metabolism in the body, limiting

its in-vivo use. However, after chemical manipulation, *Erastin* (like Piperazine-*Erastin* or Imidazole Ketone *Erastin* (IKE)) could be a good option for cancer treatment *in vivo,* what has already been shown in the past in mouse lymphoma models by Zhang et al., where a treatment with IKE showed reduced tumor growth (Zhang et al., 2019; Zhao et al., 2020). *Erastin* induces ferroptosis. Ferroptosis is an iron-dependent oxidative non-apoptotic cell death. Induction of ferroptosis leads to increase and accumulation of lipid peroxidation, lipid peroxids/lipid-ROS/reactive oxygen species (ROS), depletion of plasma membrane polyunsaturated fatty acids and cell damage (Cao and Dixon, 2016; Liu et al., 2021). One important antioxidant system is the x_c^- -GSH-glutathione peroxidase 4 system, which leads to detoxification of reactive oxygen species and inhibits ferroptosis with the help of glutathione (GSH) (Yang et al., 2014; Zhao et al., 2020).

Erastin induces ferroptotic cell death by irreversibly inhibiting the cystine-glutamate antiporter x_c^- and simultaneously opens voltage dependent anion channels (VDAC) 2 and 3 (Yagoda et al., 2007; Dixon et al., 2012; Cao and Dixon, 2016; Conrad and Pratt, 2019):

Due to inhibition of x_c^-, the uptake of cystine decreases while the concentration of glutamate increases. This could lead to a lower synthesis and faster depletion of glutathione (GSH), which is an important antioxidant in the cell by reducing the concentration of reactive oxygen species (ROS) and acts as a cofactor for glutathione peroxidase (GPX). GPX4 catalyzes reactions to reduce toxic lipid peroxide PLOOH (lipid-ROS), produced from polyunsaturated fatty acids (PUFA) from the cell membrane, to nontoxic lipid-alcohols PL-OH by using GSH as cofactor (Yang et al., 2014; Imai et al., 2017). This makes GPX4 a regulator of ferroptosis. A low concentration of GSH consequently leads to a higher concentration of ROS and especially lipid-ROS, due to reduced ROS detoxification. This increase of ROS-levels due to *Erastin*-treatment could lead to imbalance and to oxidative cell death, more specifically ferropotosis (Yang et al., 2014).

Another important effect of *Erastin* is the opening of VDAC channels. VDAC proteins are responsible for the exchange of metabolites and other substrates through the mitochondrial membrane (e.g. ATP or respiratory substrates) (Maldonado and Lemasters, 2012; Zhao et al., 2020). Together with the complexes I, III and IV of the respiratory chain, closed VDACs are also necessary to provide a stable mitochondrial membrane potential. Due to an opening of the VDAC channels, the mitochondrial membrane potential increases due to hyperpolarization (DeHart et al., 2018). The effect of the reopening of VDAC results in a reverse of the Warburg metabolism, meaning an increase in oxidative phosphorylation, ROS-synthesis and decrease of glycolysis (Yagoda et al., 2007; Imai et al., 2017; Maldonado, 2017; Zhao et al., 2020).

Zille et al. assumed that class-I-HDACi promote ferroptosis induced by *Erastin* in fibrosarcoma cancer cells (Zille et al., 2019). Beside the effects mentioned in the introduction, HDACi like *MS-275*, *Domatinostat* or *Vorinostat* (=SAHA) lead to increasing ROS-levels (Ruefli et al., 2001; Zhang and Zhong, 2014; Roca et al., 2022).

Analyzing RNA-sequencing data using GSEA after *HDAC-2* knock-out revealed negative enrichment of the EIF2AK4-EIF2A/eIF2α-ATF4 pathway, amino acid deprivation, amino acid transport across the plasma membrane and the elongation of

translation. Also, the data from the RNA-sequencing showed a significant downregulation of ATF4 after *HDAC-2* knock-out. These findings are strong hints for the postulated lower x_c^- -expression mediated by reduced ATF4-expression via lower expression of x_c^- -subunit SLC7A11 initiated by HDACi, what Wolf et al. and Lewerenz et al. showed in glioma cells (Lewerenz et al., 2012; Wolf et al., 2014; Koppula et al., 2018).

ATF4 is part of the Integrated Stress Response (ISR)-pathway, which is necessary for responding to cellular stress (B'chir et al., 2013; Masson, 2019). Important ways for activation of this pathway are amino acid deprivation and heme deprivation and hypoxia, both sensed by specific protein kinases GCN2 (EIF2AK4; general control non-depressible protein 2) and HRI (EIF2AK1; heme-regulated eIF2α kinase) (Suragani et al., 2012; Wortel et al., 2017; Masson, 2019). Both kinases lead to phosphorylation of the eukaryotic translation initiation factor eIF2α. After phosphorylation, eIF2α reduces translation of mRNA and activates a transcriptional stress response via ATF4 (Masson, 2019). A central regulator for GCN2 activity is deacetylated tRNA as tRNA synthetase enzymes fail to aminoacetylate tRNA due to amino acid deprivation (Zaborske et al., 2009) (figure 25).

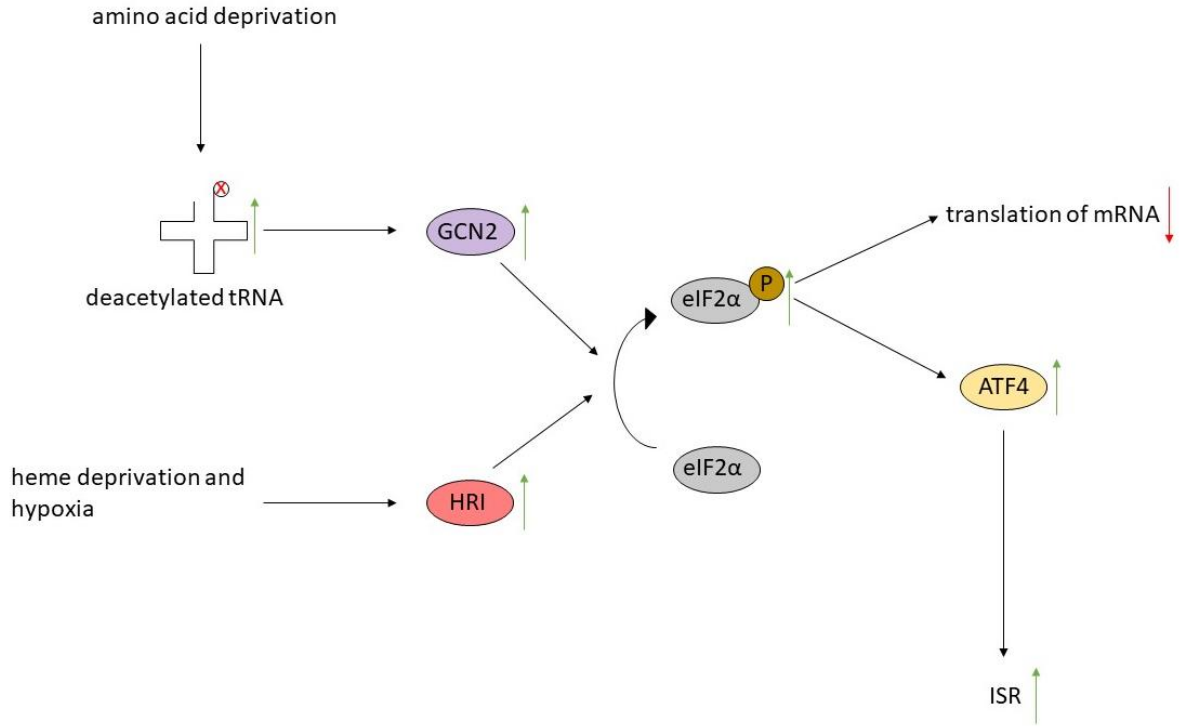

*Figure 25: **eIF2α-ATF4 pathway**. Heme deprivation and hypoxia lead to activation of HRI (heme-regulated eIF2α kinase) and amino acid deprivation leads to increasing levels of deacetylated tRNA which activates GCN2 (general control non-depressible protein 2). Both kinases induce phosphorylation of eIF2α, which reduces translation and increases ATF4-induced stress response.*

The downregulation of ATF4 mRNA may contribute to the increased *Erastin* sensitivity of *HDAC*-2 deficient murine PDAC cells. However, further experiments using cells with *ATF4* knock-out could be treated with *Erastin* to investigate changes in sensitivity. This could be further validated by reconstituting *ATF4* in these knock-out lines.

GPX4 is also necessary to reduce oxidative stress. Results published by Wang et al. showed that HDACi *Quisinostat* lead to downregulation of GPX4 (Wang et al., 2021).

However, the analyzed RNA-sequencing data did not confirm the mentioned regulation of GPX4.

Suggesting that *Erastin* or HDACi lead to higher oxidative stress due to higher levels of ROS, a combination of both agents should further increase ROS-levels. Such higher ROS-levels, due to a combination of HDACi and inhibition of x_c^-, have already been detected with ROS-measurement in human breast cancer cells and human colon cancer cells: the ROS-levels were higher after a combination of HDACi and x_c^--inhibitors than either one of the agents alone (Miyamoto et al., 2020). Yang et al. also showed, that class-I-HDACi enhances ferroptotic cell death after *Erastin* treatment in lung cancer cells and were able to show similar results regarding cell lethality and ROS-levels after a combination of *Vorinostat* and *Erastin* like Miyamoto et al. (Yang et al., 2020). This could explain the observed results, however ROS-measurements have not been performed. As the combination of *Vorinostat* and *Erastin* showed similar effects on apoptosis as each drug alone, Yang et al. are convinced that the combination lead to ferroptosis (Yang et al., 2020).

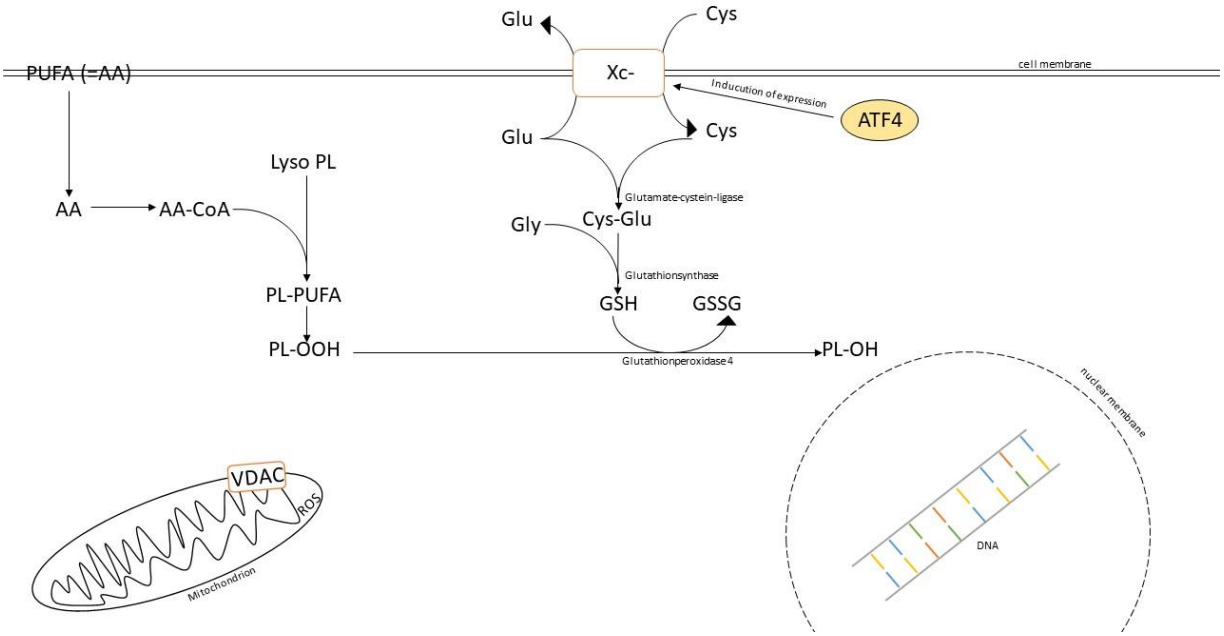

*Figure 26: **Regular pathway in the cell**. Antiporter x_c^-, which expression is influenced by ATF4, is responsible for transporting cystine in exchange for glutamate into the cell to build glutathione (GSH). GSH is necessary for the GPX4-catalyzed reduction of lipid-ROS (PL-OOH) to nontoxic lipid-alcohols (PL-OH). Characteristic for a cancer cell, VDAC is closed due to bonding of free tubulin. Due to the closed VDAC in the mitochondrial membrane, the mitochondrial membrane potential stays stable.*

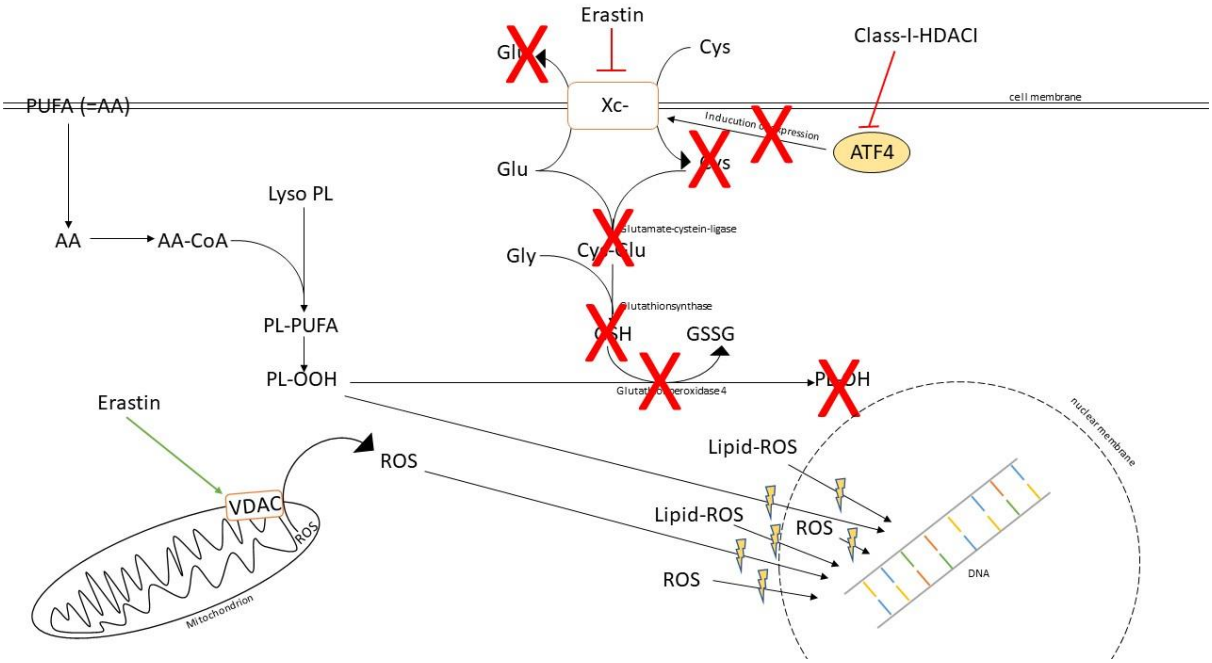

*Figure 27: **Inhibition with Erastin and Class-I-HDACi**. Erastin induces ferroptosis by irreversibly inhibiting x_c^-, which leads to a reduced production and faster depletion of glutathione (GSH). Decreasing detoxification of lipid-ROS is the consequence. Lipid-ROS can induce increasing DNA-damage. Erastin also leads to opening of VDAC, which induces oxidative phosphorylation and consequently increases ROS-production in the mitochondria and transport of ROS from the mitochondria into the cytoplasm. Those higher ROS-levels lead to increasing DNA-damage. HDAC-inhibition could enhance the DNA-damaging effects of Erastin induced ROS-levels by reducing the expression of x_c^- via reduced expression of ATF4.*

The figures 26 and 27 show the hypothesis of possible interactions leading to the observed synergistic effects of a cotreatment of HDACi and *Erastin*: the combination of increasing ROS-levels due to different mechanisms (x_c^--inhibition, lower x_c^--expression, reduced GSH-production and VDAC-opening) lead to much higher oxidative stress within the cells, leading to increasing cell lethality. With the data collected for this thesis, the described suspected mechanism of how HDACi and *Erastin* could interact cannot be confirmed for PDAC, but the data can give a hint for such interaction and working mechanism, which must be addressed in future experiments.

To understand how both drugs synergistically interact and to evaluate the postulated working mechanism of a combination of *Erastin* with HDACi in PDAC cells, further investigations are necessary. Therefore, more validations of the experiments using *Erastin* and *MS-275* in different concentrations and with different assays should be performed as well as ROS-measurements (like those of Myamoto et al. or Roca et al.). To evaluate, if the effect is caused by ferroptosis, experiments using ferrostatin (binds the necessary iron for ferroptosis) to reverse the effect should be performed. Also, DNA-damage should be measured to evaluate if the increasing ROS-levels lead to increasing DNA-damage. Furthermore GSH-measurement could be performed to measure the depletion and decreased production of GSH due to the inhibition. The presented observations suggest, the combination could also interact with the cellular metabolism (Zhao et al., 2020), which require further investigations. In case that further investigations show promising results, the tolerability has to be evaluated for a potential clinical use in the future. As previously mentioned, *Erastin* would need further chemical manipulation prior to *in-vivo* use, while *MS-275* already has a dosage form for oral use

and showed to be well tolerated in earlier phase-I-trials at a dose of 6 mg/m^2 with no severe side effects (Kummar et al., 2007).

The other promising hit *JIB-04*, a pan-selective Jumonji histone demethylase inhibitor, needs further investigations too.

Besides surgery, drug-based therapies are and will be the most important instrument in the fight against PDAC. The presented data show promising results for a therapy combining *MS-275* and *Erastin*, but further investigations are necessary. The goal of most of the therapies in medicine are the healing and recovery of the patient. Sometimes, certain therapies alone can achieve this goal and sometimes, therapies are part of a holistic concept. Maybe the combination of *Erastin* and HDACi could be a useful radiosensitizer with the advantage that additional to the ROS-production induced by radiotherapy, the drug-combination would lead to increasing ROS-levels as well (Zhao et al., 2020). Experiments using *Erastin* as radiosensitizer, e.g. to increase the sensitivity of breast cancer to γ-rays, seem promising (Cobler et al., 2018). Radiotherapy already plays a role in neoadjuvant treatment of borderline-resectable pancreatic cancer (Leitlinienprogramm Onkologie, 2021). But even if new drug-based therapies show increased survival-rates or symptom-free lifetime instead of curation from cancer, it would be a great success too.

Supplement

Table 25: F2612 IC_{50}- and AUC-values from the screening according to drug (NA = no results)

	***HDAC-2* (+) IC_{50}**	***HDAC-2* (+) AUC**	***HDAC-2* (-) IC_{50}**	***HDAC-2* (-) AUC**
4EGI-1	15,11	285,9	27,03	287,6
A1210477	35,56	313	NA	386
A-196	435,6	297,8	NA	324,1
Abexinostat	0,6466	180	0,2793	152,4
Adavosertib	0,09242	104,3	0,09105	107,9
Alisertinib	0	271,6	20,16	278,1
Alpelisib	4,361	253,7	2,953	232,7
AZD1208	0,009101	288,1	NA	279,3
AZD5153	0,6457	173,5	0,4078	168,5
AZD6738	0,8379	179,7	0,7216	195,1
AZD7762	0,06647	98,85	0,08121	108,8
BAY-876	0,02951	79,34	0,05292	91,4
BI-78D3	27,8	294,7	0	285,9
BI-847325	0,02261	66,16	0,09609	105,4
BI-D1870	10,27	281,1	7,839	269,2
Birinapant	NA	293,4	114,7	275,1
BRD4770	2,947	269,3	1,795	234,2
BX-795	7,726	288,1	4,955	261,1
BX-912	26,09	290,6	21,6	302,8
C646	959,2	280,1	24,14	316,9
CB-839	0,3399	157,4	2,448	224,9

CPI-455 HCl	138,2	271	NA	384,1
Crenigacestat	5,33E-15	286	1397	261,1
CUDC-101	2,337	221	1,507	218,2
CW069	33,77	306,6	259,4	281,8
EED226	0	298,8	NA	372
Elesclomol	0,01892	50,66	0,0145	33,76
Entrectinib	1,957	245,3	3	266,4
Enzastaurin	315,2	277,4	0	287,7
Epacadostat	44,61	307,5	31,27	303,8
EPZ004777	113,9	290,2	67,51	291,4
Erastin	3,642	253,8	1,905	224,3
Erdafitinib	6,517	303,9	5,499	247,3
Galunisertib	30,07	300	65,21	249,7
GDC-0152	18,8	306,1	89,49	283,1
GSK J1	0	290,2	137,2	282
GSK2656157	15,36	309,7	53,54	270,8
GSK2830371	147,6	283,4	0	290,7
GSK503	8,401	298,5	6,289	278,6
GSK591	10,85	254,4	16,06	249,6
HTH-01-015	2,348	225,4	2,939	234,1
Indirubin	6,38E-07	274,3	97,39	306,8
Ispinesib	4,165	243,7	1,926	200,4
JIB-04	0,3012	166,3	0,2615	163,7
JSH-23	NA	314,3	17,79	316,9
KU-60019	10,03	279,5	5,997	279,2
Lapatinib	6,918	236,2	4,083	241,8
Linsitinib	28,02	288,4	176,4	274,3
LJH685	6,88E-11	234	28,59	280,3
LLY-283	22,14	292,7	193,7	279,8
LLY-507	1,926	233,7	1,834	231,7
Luminespib	0,01018	54,04	0,01102	63,01
LY2109761	49,39	315,6	80,43	320,1
MI-463	1,774	230	1,964	236,1
MI-503	34,67	302,4	26,44	284,2
Milciclib	0,4067	182,2	0,5132	187
MK-2206 2HCl	3,209	250	2,627	231,1
ML264	NA	311,1	25,54	303,4
ML324	8,627	283,8	4,328	274,2
MS023	22,2	280,3	24,27	276
MX69	22,62	312,2	1987	272,7
Napabucasin	2,853	246,3	1,433	224,1
NMS-873	5,713	277,3	11,25	318,8
NSC87877	14,99	302,4	27,18	286,9
NVP-CGM097	7,74	275,7	22,78	254,6
Orantinib	NA	366,9	140,5	294,6
OTX015	3,691	523	0,4406	216,4
P22077	34,78	273,6	16,23	291,4
Pelitinib	0,7849	185,3	1,216	205,6
Pevonedistat	1,463	232,2	1,85	246,9
PFI-2 HCl	35,91	285,4	16,13	309,1

Poziotinib	10,78	277,3	4,904	240,1
Pracinostat	0,2924	221,7	0,2529	153,1
PRT4165	0	293,4	NA	375,7
PTC-209 HBr	2,111	242,6	1,549	221,2
PX-478 2HCl	NA	308,1	1074	280,8
PYR-41	14,08	320,7	12,36	330,9
Ralimetinib	14,64	300,5	62,55	265,1
RI-1	8,851	288,9	10,47	299,4
Rigosertib	1,168	196,9	0,7741	185
RO5126766	0,5125	166,9	0,4285	159,8
Ruxolitinib	NA	305,2	11,72	305,7
Sabutoclax	2,711	231,1	3,755	246,6
Salubrinal	NA	299,8	25,3	310,7
Sapanisertib	0,06672	102,8	0,05146	94,93
Saracatinib	0,8597	187,1	1,7	220
Selisistat	111,5	293,2	102,5	286,4
SF1670	2,605	244,5	4,199	268,7
SGC707	1,97E+07	278,7	11,1	307,5
SMER28	85,79	262,4	NA	367,8
Spautin-1	2,857	255	4,853	264,6
STF-083010	30,52	291,5	59,82	285,8
Thiomyristoyl	10,5	307,8	NA	381,8
Trametinib	0,02682	73,68	0,02608	74,87
Ulixertinib	0,5078	168,5	1,012	203,8
UNC0379	1,17	213,4	0,9608	196,6
UNC0638	1,447	184,2	1,302	217,7
UNC1999	3,8	268,6	3,969	266,5
Veliparib	NA	326,1	11879	274,3
Vemurafenib	15,35	306,1	NA	314,1
WZ4003	4,621	245,3	3,246	236,8

Table 26: F1648 IC_{50}- and AUC-values from the screening according to value (NA = no results)

	***HDAC-2* (+) IC_{50}**	***HDAC-2* (+) AUC**	***HDAC-2* (-) IC_{50}**	***HDAC-2* (-) AUC**
4EGI-1	68,02	264,3	329,9	312,1
A1210477	11,42	312,6	115,6	295,2
A-196	NA	310,9	18400	293,2
Abexinostat	0,05504	90,09	0,0973	107,4
Adavosertib	0,1198	121,3	0,1274	117,4
Alisertinib	10,28	339,3	NA	376,2
Alpelisib	2,79	265,1	4,239	237,1
AZD1208	NA	335,8	35,54	282,3
AZD5153	0,01549	38,56	0,05777	97,2
AZD6738	0,9869	211,8	1,826	240,3
AZD7762	0,101	118,2	0,1466	118,2
BAY-876	0,07139	104	0,3603	153,3
BI-78D3	8,61	283,1	9,047	280

BI-847325	0,04285	70,87	0,1127	113,3
BI-D1870	5,129	256,4	9,282	318,2
Birinapant	NA	330,7	NA	303
BRD4770	1,225	208,2	1,769	214,6
BX-795	9,448	285,3	5,576	272,6
BX-912	10,6	299,6	0	252,4
C646	0,0002006	301	16,17	301,5
CB-839	16,95	273,1	179,3	300,2
CPI-455 HCl	78,91	289,9	NA	314,9
Crenigacestat	4969	280,5	NA	321,1
CUDC-101	0,9813	218,4	1,263	220,4
CW069	0,1964	264,5	26,74	266,8
EED226	49,28	300,1	87,47	285,3
Elesclomol	0,0007202	27,76	NA	376,7
Entrectinib	0,4156	153,2	1,309	232,8
Enzastaurin	NA	321,3	0	288
Epacadostat	NA	324,2	NA	364,2
EPZ004777	21,87	345,8	10,78	304,4
Erastin	0,2456	149,8	0,1964	132
Erdafitinib	5,877	241,7	25,43	252,5
Galunisertib	94,5	248,3	40,75	286,3
GDC-0152	274,2	286,2	NA	303,7
GSK J1	111,2	277,4	0	249,2
GSK2656157	NA	510,2	NA	349,8
GSK2830371	1577	265,5	411,9	278,4
GSK503	91,16	288	9,899	282,9
GSK591	NA	323,5	16,58	290,7
HTH-01-015	3,223	256,5	9,014	295,6
Indirubin	NA	386,1	30,95	294,9
Ispinesib	3,793	268,3	8,576	394,1
JIB-04	0,3488	170,4	0,1277	116,6
JSH-23	NA	355,4	13,47	322,2
KU-60019	6,307	259,6	7,143	263,8
Lapatinib	NA	352,9	NA	364,3
Linsitinib	0	232,1	10,81	319,6
LJH685	NA	323,2	NA	346,3
LLY-283	0	283,4	1,38E+11	265,1
LLY-507	NA	331,8	6,581	300,9
Luminespib	NA	17,5	0	14,65
LY2109761	0	292,8	NA	342,5
MI-463	2,799	273,4	2,808	255,5
MI-503	211,7	306,2	300,1	258,2
Milciclib	0,8452	207	0,4738	165,6
MK-2206 2HCl	9,265	310,4	NA	325,9
ML264	23,64	267,3	35,33	281,2
ML324	1,45	219,4	1,491	225,6
MS023	NA	353,1	NA	341,8
MX69	1,96E+08	272,2	2987	293,1
Napabucasin	2,867	248,6	3,656	258,2
NMS-873	6,516	272,8	0	296,8

NSC87877	19,15	315,5	87,8	261,8
NVP-CGM097	NA	380,7	0	277,7
Orantinib	NA	329,7	1,263	283,7
OTX015	0,03833	74,21	0,0892	109,8
P22077	10,25	291,1	NA	321,6
Pelitinib	0,8837	193,1	1,524	238,4
Pevonedistat	2,023	261,1	1,864	236,2
PFI-2 HCl	NA	295,6	36,27	307,6
Poziotinib	0,473	161,3	0,6378	169,9
Pracinostat	0,02683	66,6	1,176	208,2
PRT4165	NA	321,1	28,67	307,1
PTC-209 HBr	1,353	199,2	2,664	277,2
PX-478 2HCl	2,44E+07	254,5	NA	353,1
PYR-41	17,63	305,4	78214	233,1
Ralimetinib	193,9	260,9	NA	322,7
RI-1	4,865	240,7	NA	302,9
Rigosertib	0,2809	174,6	0,7395	193,8
RO5126766	0,3319	157,2	NA	371,7
Ruxolitinib	4,49E+10	927,3	NA	1039
Sabutoclax	6,479	295,2	8,52	276,3
Salubrinal	NA	305,8	10,68	303
Sapanisertib	0,03167	75,94	0,02706	53,73
Saracatinib	1,069	222,8	1,696	210,2
Selisistat	1,27E+11	284,1	62,25	292,1
SF1670	0,6443	178,3	0,8965	211,7
SGC707	81,79	302,4	NA	300,5
SMER28	NA	308	0	294,8
Spautin-1	11834	299,2	46,63	288,9
STF-083010	0,001016	269,6	NA	323
Thiomyristoyl	0	273,5		314,7
Trametinib	0,01539	49,04	0,9956	203,8
Ulixertinib	1,301	223,4	3,954	255,5
UNC0379	1,383	231,3	8,903	292,2
UNC0638	2,758	281,8	2,578	282,2
UNC1999	4,741	277,3	7,615	284,6
Veliparib	17285	257,9	1299	275,2
Vemurafenib	NA	346,3	NA	306,5
WZ4003	9,231	293	8,707	304,5

Table 27: Overview over the calculated z-scores of the IC_{50}- and AUC-values (rounded to two decimals).

	F1648 z-scores				**F2612 z-scores**			
	***HDAC-2* (+)**		***HDAC-2* (-)**		***HDAC-2* (+)**		***HDAC-2* (-)**	
	IC_{50}	**AUC**	**IC_{50}**	**AUC**	**IC_{50}**	**AUC**	**IC50**	**AUC**
4EGI-1	-0,28	-1,19	1,48	1,26	-0,64	-0,08	-0,56	0,01
A1210477	-0,78	-0,35	1,13	-0,78	-0,34	-0,34	-0,99	1,47
A-196	-0,74	0,32	0,71	-0,96	-0,71	-0,62	-0,74	1,26
Abexinostat	-0,80	-1,03	-0,64	-0,61	1,40	1,15	0,04	0,48
Adavosertib	0,65	1,08	1,06	0,59	-0,82	-1,06	-0,89	-0,61
Alisertinib	0,01	0,46	-1,01	1,19	-1,01	-0,89	0,99	-0,76

Alpelisib	-0,96	1,20	0,79	-0,67	0,94	0,44	-0,76	-0,96
AZD1208	-0,71	1,49	0,71	-0,53	-0,71	-0,31	-0,71	-0,64
AZD5153	-0,89	-1,26	-0,75	-0,35	1,21	0,84	0,42	0,76
AZD6738	-0,21	0,20	1,46	1,29	-0,51	-1,04	-0,74	-0,45
AZD7762	0,06	0,78	1,37	0,78	-0,93	-1,32	-0,51	-0,24
BAY-876	-0,37	-0,09	1,49	1,43	-0,64	-0,85	-0,49	-0,48
BI-78D3	-0,23	-0,45	-0,20	-0,94	1,40	1,39	-0,97	0,00
BI-847325	-0,60	-0,76	1,03	1,02	-1,08	-0,95	0,64	0,69
BI-D1870	-1,34	-0,93	0,52	1,39	0,96	0,00	-0,13	-0,45
Birinapant	NA	1,30	NA	0,11	NA	-0,31	NA	-1,10
BRD4770	-0,98	-0,85	-0,23	-0,62	1,40	1,37	-0,19	0,10
BX-795	1,23	0,69	-0,66	-0,34	0,39	0,91	-0,96	-1,26
BX-912	-0,34	0,57	-1,25	-1,46	0,98	0,18	0,60	0,71
C646	-0,53	0,07	-0,49	0,11	1,50	-1,31	-0,48	1,13
CB-839	-0,38	0,55	1,49	0,98	-0,57	-1,30	-0,55	-0,22
CPI-455 HCl	-0,71	-0,51	-2,59	0,00	0,71	-0,89	-2,59	1,40
Crenigacestat	1,11	-0,27	-0,83	1,36	-0,83	-0,05	-0,28	-1,04
CUDC-101	-0,93	-0,78	-0,44	0,64	1,39	1,06	-0,03	-0,92
CW069	-0,66	-0,80	-0,44	-0,68	-0,38	1,38	1,49	0,10
EED226	0,08	-0,36	0,96	-0,73	-1,04	-0,39	-1,04	1,48
Elesclomol	-1,12	-0,56	-1,20	1,50	0,79	-0,42	0,33	-0,52
Entrectinib	-1,20	-1,44	-0,31	0,17	0,34	0,42	1,16	0,85
Enzastaurin	-0,58	1,45	-0,58	-0,29	1,15	-0,85	-0,58	-0,31
Epacadostat	-4,02	-0,03	-4,02	1,42	0,71	-0,63	-0,71	-0,76
EPZ004777	-0,67	1,45	-0,91	-0,14	1,28	-0,68	0,30	-0,64
Erastin	-0,77	-0,69	-0,80	-0,99	1,31	1,09	0,25	0,59
Erdafitinib	-0,51	-0,68	1,50	-0,31	-0,44	1,48	-0,55	-0,49
Galunisertib	1,29	-0,87	-0,59	0,58	-0,96	1,11	0,26	-0,82
GDC-0152	1,11	-0,73	-0,97	0,76	-0,82	0,96	-0,29	-0,99
GSK J1	0,68	0,15	-0,86	-1,43	-0,86	0,87	1,04	0,41
GSK2656157	#WERT!	1,43	-1,28	-0,10	-0,71	-0,48	0,71	-0,85
GSK2830371	1,46	-1,32	-0,17	-0,10	-0,54	0,37	-0,75	1,06
GSK503	1,50	0,12	-0,46	-0,48	-0,49	1,34	-0,55	-0,98
GSK591	-4,57	1,27	0,66	0,32	-1,15	-0,73	0,49	-0,87
HTH-01-015	-0,37	0,11	1,49	1,36	-0,65	-0,88	-0,46	-0,60
Indirubin	-0,86	1,44	-0,24	-0,42	-0,86	-0,84	1,10	-0,18
Ispinesib	-0,29	-0,10	1,41	1,41	-0,16	-0,40	-0,95	-0,92
JIB-04	0,94	0,64	-1,39	-1,49	0,44	0,48	0,02	0,37
JSH-23	-5,12	1,48	-0,71	-0,26	-5,12	-0,68	0,71	-0,54
KU-60019	-0,58	-1,06	-0,12	-0,65	1,45	0,87	-0,75	0,84
Lapatinib	-2,74	0,78	-2,74	0,95	0,71	-0,90	-0,71	-0,82
Linsitinib	-0,65	-1,28	-0,52	1,13	-0,31	0,27	1,49	-0,12
LJH685	-0,71	0,55	-0,71	1,02	-0,71	-1,25	0,71	-0,32
LLY-283	-0,50	0,27	1,50	-1,32	-0,50	1,09	-0,50	-0,04
LLY-507	-1,27	1,15	1,15	0,53	-0,56	-0,82	-0,59	-0,86
Luminespib	-1,15	-0,80	-1,15	-0,91	0,51	0,67	0,64	1,04
LY2109761	-1,07	-1,22	-1,07	1,21	0,15	-0,11	0,92	0,12
MI-463	0,85	1,25	0,87	0,34	-1,03	-0,95	-0,68	-0,64
MI-503	0,51	0,84	1,16	-1,35	-0,80	0,67	-0,86	-0,16
Milciclib	1,46	1,26	-0,44	-1,16	-0,78	-0,19	-0,24	0,09
MK-2206 2HCl	1,15	0,68	-1,37	1,01	-0,50	-0,64	-0,65	-1,05
ML264	-0,72	-1,17	1,14	-0,47	-4,49	1,01	-0,42	0,63
ML324	-0,75	-0,95	-0,73	-0,76	1,38	1,00	0,10	0,71
MS023	-15,87	1,00	-15,87	0,72	-0,71	-0,81	0,71	-0,91
MX69	1,50	-0,80	-0,50	0,29	-0,50	1,29	-0,50	-0,78
Napabucasin	0,18	0,30	1,03	0,96	0,16	0,14	-1,37	-1,40
NMS-873	0,14	-0,89	-1,27	0,26	-0,03	-0,67	1,17	1,30
NSC87877	-0,53	1,03	1,48	-1,29	-0,65	0,47	-0,30	-0,21
NVP-CGM097	-0,88	1,47	-0,88	-0,34	-0,21	-0,38	1,09	-0,75
Orantinib	-0,72	0,29	-0,71	-0,93	-0,72	1,28	0,71	-0,64

OTX015	-0,58	-0,77	-0,55	-0,59	1,49	1,43	-0,35	-0,07
P22077	-0,80	-0,17	-1,60	1,36	1,12	-1,04	-0,33	-0,15
Pelitinib	-0,65	-0,53	1,25	1,40	-0,94	-0,87	0,34	0,00
Pevonedistat	0,94	1,32	0,27	-0,61	-1,42	-0,92	0,21	0,22
PFI-2 HCl	-2,55	-0,34	0,59	0,73	0,56	-1,26	-1,15	0,87
Poziotinib	-0,77	-0,91	-0,74	-0,75	1,36	1,16	0,15	0,50
Pracinostat	-0,81	-1,36	1,46	0,65	-0,29	0,84	-0,36	-0,13
PRT4165	-0,71	-0,09	0,71	-0,48	-0,71	-0,86	-0,71	1,42
PTC-209 HBr	-0,96	-1,08	1,26	1,27	0,32	0,23	-0,63	-0,42
PX-478 2HCl	0,71	-1,06	-0,71	1,28	-0,71	0,21	-0,71	-0,44
PYR-41	-0,50	0,18	1,50	-1,46	-0,50	0,52	-0,50	0,75
Ralimetinib	1,12	-0,89	-0,97	1,20	-0,82	0,45	-0,30	-0,75
RI-1	-1,11	-1,47	-2,79	0,69	0,27	0,21	0,83	0,57
Rigosertib	-1,27	-1,30	0,00	0,62	1,18	0,93	0,09	-0,26
RO5126766	-1,02	-0,54	-4,69	1,50	0,98	-0,45	0,05	-0,51
Ruxolitinib	0,71	0,72	-0,71	1,00	-0,71	-0,86	-0,71	-0,86
Sabutoclax	0,42	1,14	1,20	0,49	-1,01	-1,08	-0,61	-0,54
Salubrinal	-1,74	0,21	-0,71	-0,39	-1,74	-1,09	0,71	1,27
Sapanisertib	-0,68	-0,27	-0,94	-1,29	1,23	0,96	0,39	0,60
Saracatinib	-0,61	0,79	0,84	0,01	-1,09	-1,41	0,85	0,62
Selisistat	1,50	-1,10	-0,50	0,72	-0,50	0,97	-0,50	-0,58
SF1670	-0,87	-1,21	-0,72	-0,36	0,31	0,48	1,28	1,09
SGC707	-0,58	0,40	-0,58	0,25	1,15	-1,46	-0,58	0,80
SMER28	-0,71	-0,01	-0,71	-0,31	0,71	-1,04	-0,71	1,35
Spautin-1	1,50	1,08	-0,50	0,58	-0,50	-1,06	-0,50	-0,60
STF-083010	-1,01	-1,02	-1,01	1,36	0,01	-0,04	0,99	-0,30
Thiomyristoyl	-0,71	-1,01	-0,71	-0,10	0,71	-0,26	-0,71	1,38
Trametinib	-0,52	-0,73	1,50	1,48	-0,49	-0,38	-0,49	-0,36
Ulixertinib	-0,25	0,29	1,47	1,17	-0,77	-1,22	-0,44	-0,25
UNC0379	-0,44	-0,05	1,50	1,41	-0,50	-0,48	-0,55	-0,88
UNC0638	0,98	0,83	0,74	0,84	-0,76	-1,17	-0,96	-0,49
UNC1999	-0,16	0,37	1,46	1,24	-0,70	-0,68	-0,60	-0,93
Veliparib	0,88	-0,86	-1,09	-0,28	-1,25	1,44	0,21	-0,31
Vemurafenib	NA	1,47	NA	-0,62	NA	-0,64	NA	-0,22
WZ4003	0,94	0,68	0,76	1,02	-0,62	-0,73	-1,08	-0,98

Table 28: Overview over Δ z-scores in IC_{50}- and AUC-value of F1648 and F2612

	F1648 IC50 Δ z-score	F2612 IC50 Δ z-score	F1648 AUC Δ z-score	F2612 AUC Δ z-score
4EGI-1	1,76550817	0,08036069	2,44569544	0,0869808
A-1210477	1,9104283	-0,6520909	-0,4307476	1,80715953
A-196	1,44850535	-0,0342918	-1,2711136	1,8887168
Abexinostat	0,1567889	-1,3627203	0,42061856	-0,670657
Adavosertib	0,40716947	-0,0733977	-0,4905143	0,45278243
Alisertib	-1,0197744	1,99986879	0,73436944	0,12936047
Alpelisib	1,74805193	-1,6985901	-1,8667911	-1,4000933
AZD1208	1,4145758	-0,0003622	-2,016134	-0,3316258
AZD5153	0,14108767	-0,7938684	0,91337203	-0,0778796
AZD6738	1,67645723	-0,2323585	1,09872284	0,59369585
AZD7762	1,30833058	0,42291212	1,5543E-15	1,07682075
BAY-876	1,85841107	0,15058462	1,51875142	0,37152418
BI-78D3	0,03727943	-2,3715521	-0,4899744	-1,3908952
BI-847325	1,63452051	1,7194641	1,77730405	1,64368161

BI-D1870	1,85743991	-1,087271	2,32037642	-0,4468039
Birinapant	NA	NA	-1,1942873	-0,7890057
BRD4770	0,75069696	-1,5897112	0,23294003	-1,2775305
BX-795	-1,88131	-1,3463611	-1,0211129	-2,17087
BX-912	-0,9065271	-0,3839912	-2,0331548	0,52551883
C646	0,03418647	-1,9769201	0,03309378	2,43570222
CB-839	1,8730803	0,02432178	0,43273622	1,07784852
CPI-455 HCl	-1,8821992	-3,2964128	0,50539172	2,28639216
Crenigacestat	-1,9390403	0,54514779	1,62324374	-0,9955362
CUDC-101	0,48219351	-1,4207335	1,41895131	-1,9865318
CW069	0,2203647	1,87317796	0,11875737	-1,2805143
EED226	0,87088358	0	-0,3774687	1,86693998
Elesclomol	-0,07587	-0,4656279	2,05343196	-0,0994526
Entrectinib	0,8907245	0,82552036	1,60916944	0,4265512
Enzastaurin	0	-1,7320508	-1,7422858	0,53890522
Epacadostat	0	-1,4142136	1,44685018	-0,1338336
EPZ004777	-0,2351975	-0,9838424	-1,5898832	0,04608357
Erastin	-0,0300817	-1,0620294	-0,3048647	-0,5052534
Erdafitinib	2,00710373	-0,1044971	0,3762092	-1,9716149
Galunisertib	-1,8765199	1,22680763	1,45579	-1,9270062
GDC-0152	-2,0792624	0,53604324	1,48300203	-1,9490884
GSK J1	-1,5340417	1,89272049	-1,5838032	-0,4605385
GSK2656157	NA	1,41421356	-1,5258728	-0,3700527
GSK2830371	-1,6276314	-0,2061955	1,21557553	0,68788383
GSK503	-1,9577068	-0,0508814	-0,5947143	-2,3205518
GSK591	5,23228024	1,64416044	-0,9487737	-0,1388449
HTH-01-015	1,86199993	0,19002624	1,24774384	0,27763098
Indirubin	0,62197208	1,9571522	-1,8639634	0,66424134
Ispinesib	1,69819239	-0,7949514	1,51211872	-0,5204669
JIB-04	-2,3267987	-0,4177924	-2,1306026	-0,1029659
JSH-23	4,40959645	5,82381002	-1,7395635	0,13623088
KU-60019	0,45467418	-2,1934222	0,40641725	-0,0290298
Lapatinib	0	-1,4142136	0,16463162	0,08087168
Linsitinib	0,13096875	1,79770053	2,40903359	-0,3881986
LJH685	0	1,41421356	0,46636033	0,93473954
LLY-283	2	2,49E-09	-1,5955325	-1,1247197
LLY-507	2,42437558	-0,0338919	-0,6189611	-0,0400622
Luminespib	0	0,13693476	-0,1148828	0,36157852
LY2109761	0	0,76524115	2,43947132	0,22087768
MI-463	0,01651093	0,34856406	-0,9084344	0,3095782
MI-503	0,65453645	-0,060937	-2,1902591	-0,8304732
Milciclib	-1,9014069	0,54523381	-2,429152	0,28164081
MK-2206	-2,5204174	-0,1583252	0,33768903	-0,4117628
ML264	1,86351444	4,07135661	0,6906255	-0,3825767
ML324	0,01212339	-1,2711818	0,1881511	-0,2913307
MS023	0	1,41421356	-0,2803018	-0,1066635
MX69	-1,9999865	2,0035E-05	1,09417086	-2,0679306
Napabucasin	0,85237086	-1,5340515	0,66577895	-1,5396138
NMS-873	-1,412486	1,20026629	1,14212898	1,97493136
NSC87877	2,01568513	0,35791991	-2,3267547	-0,6715959

NVP-CGM097	0	1,29842055	-1,8180081	-0,3724269
Orantinib	0,01282814	1,4270417	-1,2221417	-1,920888
OTX015	0,02890467	-1,8468989	0,17452956	-1,5035337
P22077	-0,801375	-1,4502933	1,52987308	0,89284396
Pelitinib	1,90397124	1,28190224	1,93501417	0,86712555
Pevonedistat	-0,6681419	1,62623226	-1,9270891	1,13767912
PFI-2	3,14698501	-1,7162218	1,07796873	2,12898824
Poziotinib	0,03402659	-1,2132298	0,15366529	-0,6646917
Pracinostat	2,26952978	-0,0780097	2,01070246	-0,9741115
PRT4165	1,41421356	0	-0,3881485	2,28175847
PTC-209	2,2168975	-0,9503405	2,34799562	-0,6441937
PX-478	-1,4142758	6,2251E-05	2,34120247	-0,6482234
PYR-41	1,9999248	-4,399E-05	-1,6353773	0,23071713
Ralimetinib	-2,0892113	0,51621512	2,09233224	-1,1985204
RI-1	-1,6865444	0,56125701	2,1593979	0,36452858
Rigosertib	1,26366251	-1,085383	1,91780377	-1,1886388
RO5126766	-3,6725479	-0,9294788	2,03742693	-0,0674393
Ruxolitinib	-1,4142136	3,6882E-10	0,28356104	0,0012693
Sabutoclax	0,77455157	0,39619394	-0,6549327	0,5371141
Salubrinal	1,03309171	2,44730528	-0,6059929	2,35904396
Sapanisertib	-0,251168	-0,8314151	-1,0152773	-0,3597583
Saracatinib	1,45102406	1,94464995	-0,7773003	2,02961753
Selisistat	-2	-1,418E-10	1,81927848	-1,5463867
SF1670	0,15228977	0,96252933	0,84880271	0,61500076
SGC707	-7,206E-06	-1,7320539	-0,1492401	2,26216576
SMER28	0	-1,4142136	-0,2994491	2,39105564
Spautin-1	-1,9951615	0,00033785	-0,5001754	0,46618286
STF-083010	-3,397E-05	0,97955433	2,38768489	-0,2548652
Thiomyristoyl	0	-1,4142136	0,90942285	1,63342938
Trametinib	2,01504228	-0,0015212	2,21122286	0,01700281
Ulixertinib	1,72037818	0,32695615	0,88139595	0,96926097
UNC0379	1,94329943	-0,0540609	1,4605132	-0,4029002
UNC0638	-0,2391262	-0,1926295	0,00820477	0,68714961
UNC1999	1,62324006	0,09545149	0,87583886	-0,2519536
Veliparib	-1,9659704	1,46088845	0,58500416	-1,751631
Vemurafenib	NA	NA	-2,0882776	0,41975429
WZ4003	-0,1765105	-0,4631716	0,34002742	-0,2513246

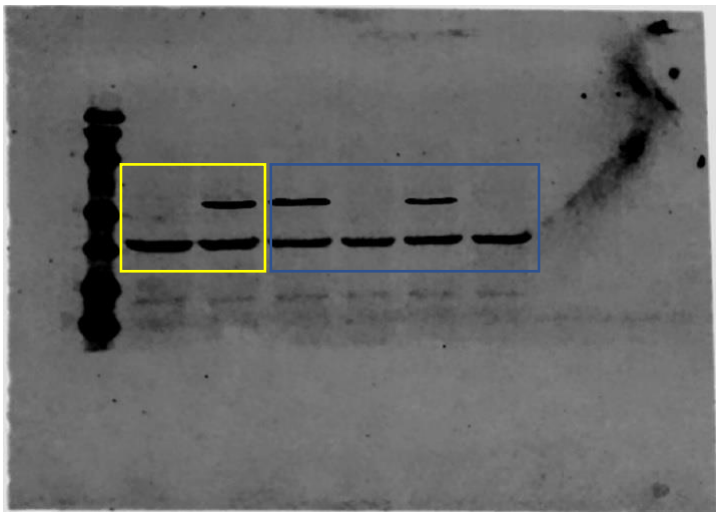

Figure 28: Western Blots (from left to right): F1648 PPT P13 T8d (not used) – F1648 PPT P13 E8d (not used) – F2612 PPT P14 E8d (Screen 1) – F2612 PPT P14 T8d (Screen 1) – F2612 PPT P15 E8d (Screen 2) – F2612 PPT P15 T8d (Screen 2); used in figure 16, the blue frame marks the used part of the blot for the figure, the yellow frame marks a part of the blot which got inverted prior to adding to the figure.

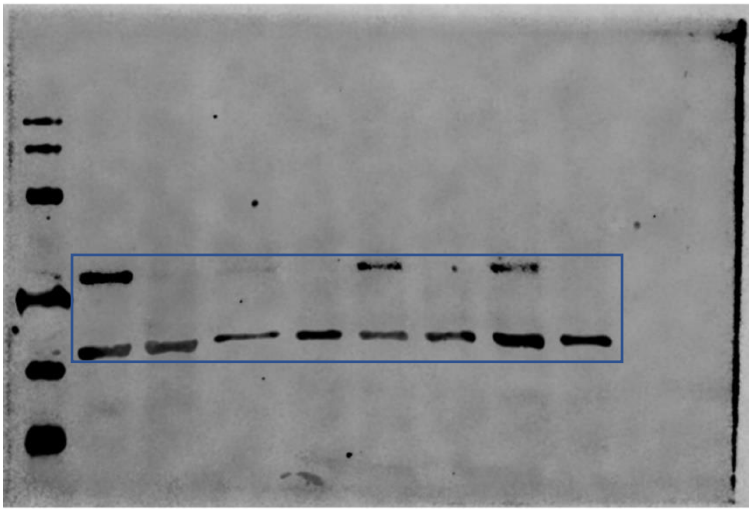

Figure 29: Western Blots (from left to right): F2612 PPT P16 E8d (Screen 3) – F2612 PPT P16 T8d (Screen 3) – F2612 PPT P17 E8d (Screen 4) – F2612 PPT P17 T8d (Screen 4) – F2612 PPT P10 E8d (Screen 5) – F2612 PPT P10 T8d (Screen 5) – F2612 PPT P11 E8d (Screen 6) – F2612 PPT P11 T8d (Screen 6); used in figure 16, the blue frame marks the used part of the blot for the figure.

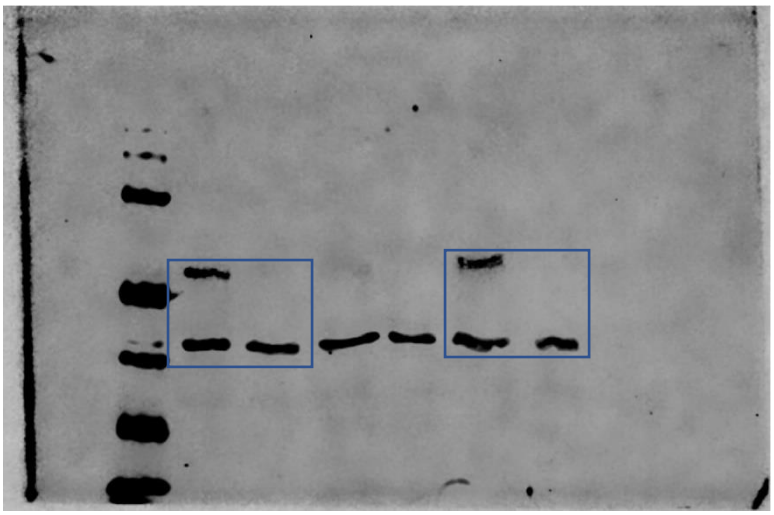

Figure 30: F2612 PPT P12 E8d (Screen 7) – F2612 PPT P12 T8d (Screen 7) – F2612 PPT P13 E8d – F2612 PPT P13 T8d – F2612 PPT P15 E8d (Screen 8+9) – F2612 PPT P15 T8d (Screen 8+9); used in figure 16, the blue frame marks the used part of the blot for the figure.

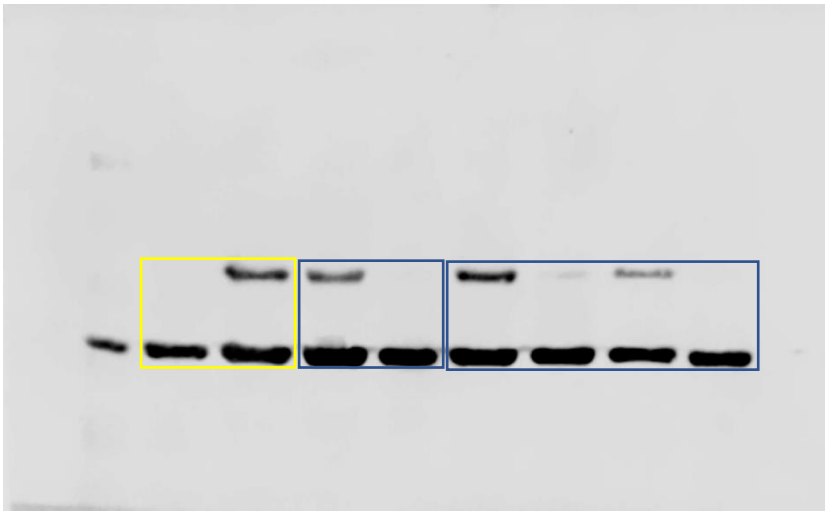

Figure 31: Western Blots (from left to right): F1648 PPT P12 T8d (Screen 1+2) – F1648 PPT P12 E8d (Screen 1+2) - F1648 PPT P13 E8d (Screen 3) – F1648 PPT P13 T8d (Screen 3) – F1648 PPT P16 E8d (Screen 6) – F1648 PPT P16 T8d (Screen 6) – F1648 PPT P17 E8d (Screen 7) – F1648 PPT P17 T8d (Screen 7); used in figure 16, the blue frame marks the used part of the blot for the figure, the yellow frame marks a part of the blot which got inverted prior to adding to the figure.

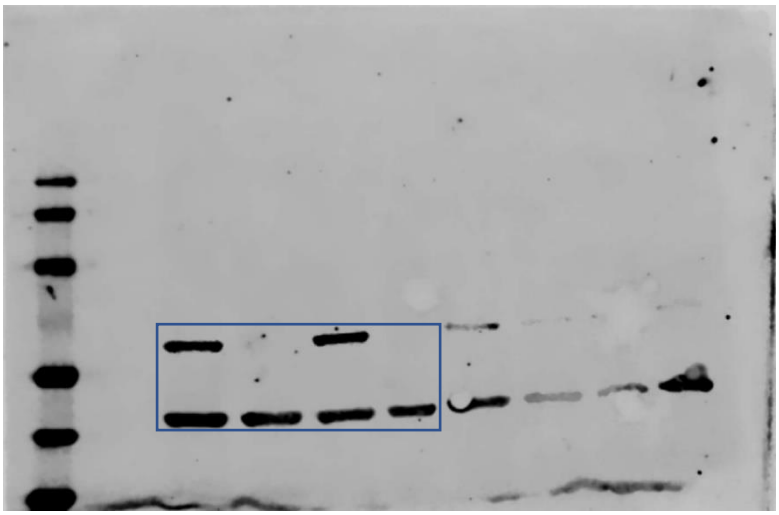

Figure 32: Western Blots (from left to right): F1648 PPT P14 E8d (Screen 4) – F1648 PPT P14 T8d (Screen 4) – F1648 PPT P15 E8d (Screen 5) – F1648 PPT P15 T8d (Screen 5) – F2800 PPT P11 E8d (not used) – F2800 PPT P11 T8d (not used) – F2800 PPT P12 E8d (not used) – F2800 PPT P12 T8d (not used); used in figure 16, the blue frame marks the used part of the blot for the figure.

Figure 33: Western Blots: F1648 PPT P18 E8d (Screen 8+9) – P1648 PPT P18 T8d (Screen 8+9); used in figure 16, the blue frame marks the used part of the blot for the figure.

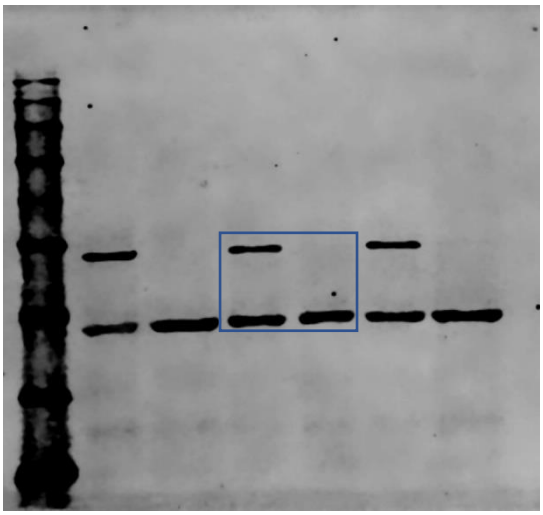

Figure 34: Western Blots (from left to right): F1648 PPT P13 E8d – F1648 PPT P13 T8d – F2612 PPT P11 E8d (used for Clonogenic assay) – F2612 PPT P11 T8d (used for Clonogenic assay) – F2800 PPT P25 E8d – F2800 PPT P25 T8d; used in figure 20, the blue frame marks the used part of the blot for the figure.

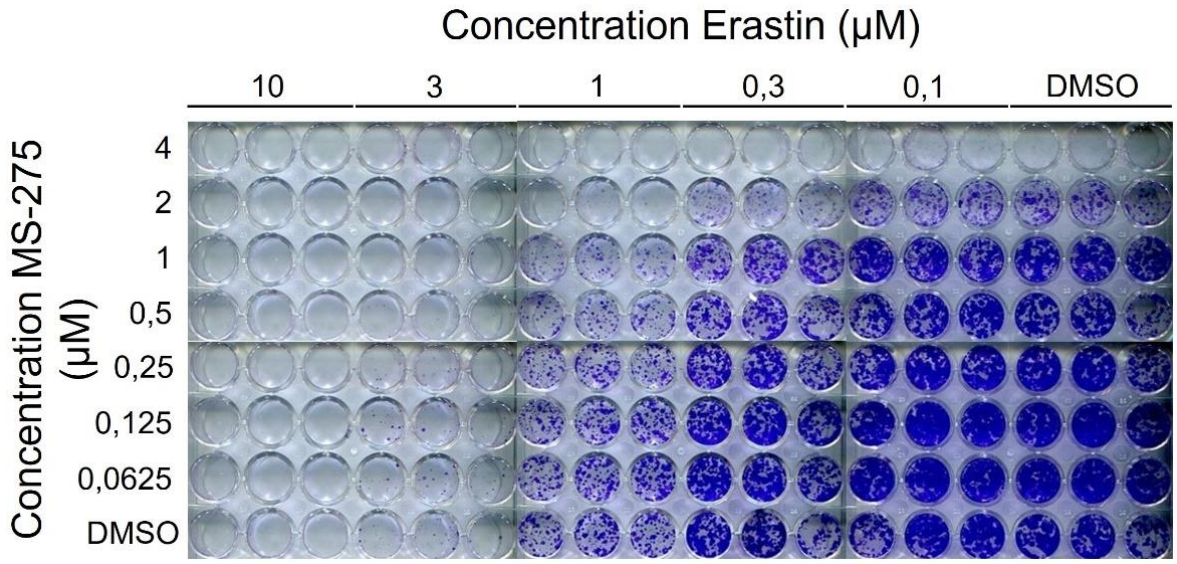

Figure 35: F2612 Clonogenic assay synergy matrix, for use in figure 22 the figure got processed.

Figure 36: Result of the screening for plagiarism with iThenticate (September 26th, 2022).

Screening of a drug library in HDAC-2 proficient and deficient murine pancreatic ductal adenocarcinoma cells to identify new potential combination therapies

Nach Marc Kidess

WORTZAHL 23943

UHRZEIT DER ÜBERMITTLUNG 26-SEPT.-2022 06:28PM

ARBEITS-ID 90908003

Technische Universität München
Fakultät für Medizin

Screening of a drug library in *HDAC-2* proficient and deficient murine pancreatic ductal adenocarcinoma cells to identify new potential combination therapies

Vollständiger Abdruck der von der Fakultät für Medizin der Technischen Universität München zur Erlangung eines

Doktors der Medizin (Dr. med.)

genehmigten Dissertation.

Vorsitz: ……

Prüfer*innen der Dissertation:

1. ……
2. ……
3. ……

Die Dissertation wurde am .. . .. . …. bei der Technischen Universität München eingereicht und durch die Fakultät für Medizin am .. . .. . …. angenommen.

TECHNISCHE UNIVERSITÄT MÜNCHEN

Klinik und Poliklinik für Innere Medizin II
Klinikum rechts der Isar
(Direktor: Univ.-Prof. Dr. med. Roland M. Schmid)

Screening of a drug-library in *HDAC-2* proficient and deficient murine pancreatic ductal adenocarcinoma cells to identify new potential combination therapies

Dissertation

vorgelegt von

2022

Contents

List of abbreviations

µl	Microliter
µM	Micromolar
°C	Degree Celsius
APS	Ammonium persulfate
ATP	Adenosine triphosphate
AUC	Area under the curve
BRCA	BReast CAncer-gen
BSA	Bovine serum albumin
CNS	Central nervous system
CO_2	Carbon dioxide
CTCL	Cutaneous T-cell lymphomas
Ctrl	Control
DAMPs	Damage-associated molecular pattern molecules
DMEM	Dulbecco's Modified DMEM
DMSO	Dimethyl sulfoxide
DNA	Deoxyribonucleic acid
EDTA	Ethylenediaminetetraacetate
EtOH	Ethanol
E8D	Ethanol treatment for 8 days; *HDAC-2* (+)
FCS/FBS	Fetal calf/bovine serum
FDA	U.S. Food and Drug Administration
FOLFIRINOX	*Flourouracil*, *Leucovorin*, *Irinotecan*, *Oxaliplatin*
g/gr	Grams
GSEA	Gene set enrichment analysis
GSH	Glutathione
GTP	Guanosine triphosphate
h	Hour(s)
HAT	Histone acetyltransferase
HCl	Hydrochloric acid
HDAC	Histone deacetylase
HDACi	Histone deacetylase inhibitor
HPV	Human papillomavirus
H_2O	Water
IC_{50}	Half-maximal inhibitory concentration
Ig	Immunoglobulin
IKE	Imidazole Ketone Erastin
IPMN	Intraductal papillary mucinous neoplasm
KRAS	V-Ki-ras2 Kirsten Rat sarcoma viral oncogene homolog
mA	Milliampere
MAPK	Mitogen-activated protein kinase
MCN	Mucinous cystic neoplasms
ml	Milliliter
mM	Milimolar
MS-275	Entinostat
MuSyC	Multi-dimensional synergy of combinations reference model
mTOR	Mechanistic target of rapamycin
NAC	N-acetylcysteine
NaCl	Sodium chloride

NAD^+/NADH	Nicotinamide adenine dinucleotide
nM	Nanomolar
ns	Not significant
KCl	Potassium chloride
PanIN	Pancreatic intraepithelial neoplasia
PARP	Poly-ADP-ribose-polymerase
PBS	Phosphate buffered saline
PDAC	Pancreatic ductal adenocarcinoma
Pen Strep	Penicillin, Streptomycin
PL-OH	Nontoxic lipid alcohols
PLOOH	Toxic lipid peroxids
PUFA	Polyunsaturated fatty acids
RAS	Rat sarcoma viral oncogene homolog
RNA	Ribonucleic acid
ROS	Reactive oxygen species
rpm	Rotations per minute
R0	In the microscope, no more remaining cancer cells remaining at the primary tumor site/on the resectate can be seen
SAHA	Suberanilohydroxamic acid/Vorinostat
SASP	Salazosulfapyridine
SDS	Sodium dodecyl sulfate
ST	Small T oncoprotein
TEMED	N, N, N', N' - Tetramethylethyldiamine
TRIS	Tris(hydroxymethyl)-aminomethane
T75	Medium-sized culture bottle
T8d	Tamoxifen treatment for 8 days; *HDAC-2* (-)
US/U.S.	United States of America
UV	Ultraviolet
V	Voltage
VDAC	Voltage dependent anion channels

Introduction

Anatomy and physiology of pancreas

The pancreas is a secondary retroperitoneal organ in the upper abdomen, which can be divided into head, body and tail. It has exocrine functions (98% of the pancreas) and endocrine functions (1-3%), which makes it a central organ in the human body (Welsch et al., 2014; Schünke et al., 2015). It is located on the height of the second lumbal vertebra and its head is located next to the descendent duodenum (Schünke et al., 2015) (figure 1).

The exocrine pancreas is a serous gland with epithelial cells organized in acini with apical zymogene granula, producing a lot of pancreatic secret (1500-3000 ml/day), enzymes (e.g. amylase) and proenzymes (e.g. trypsinogen), which are released into the pancreatic duct for secretion into the chymus in the duodenum to catalyze the digestion of proteins, carbohydrates or fatty acids (Pape et al., 2014; Welsch et al., 2014; Schünke et al., 2015). Besides the metabolic enzymes, the exocrine pancreas

also produces bicarbonate in its epithelial cells of the intercalated duct to neutralize the acidic chymus coming from the stomach (Pape et al., 2014).

1-3% of the pancreatic tissue are the Langerhans insula, which represent the endocrine pancreas (Welsch et al., 2014). Depending on the metabolic situation, different hormones like insulin or glucagon are getting released into the blood and do their duty at the targeting tissue, e.g. hepatocytes (Pape et al., 2014). The main type of cells (60-70%) in the endocrine pancreas are the β-cells which produce insulin, followed by α-cells (20%) (glucagon) and 10-15 % δ-cells (somatostatin) (Pape et al., 2014; Rassow et al., 2016).

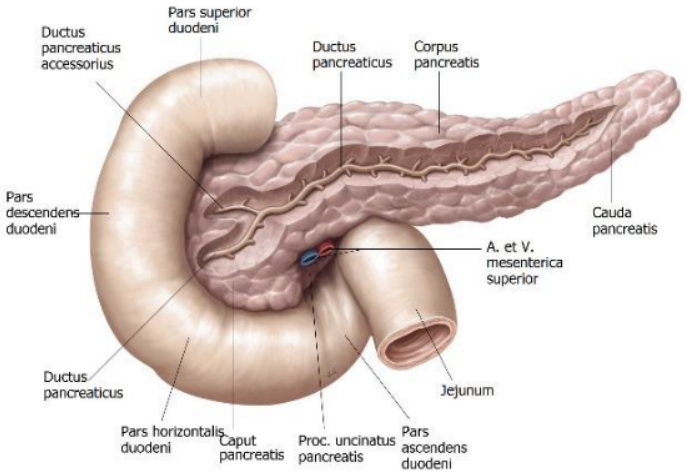

*Figure 1: **Anatomy of the pancreas.** From Gilroy, Atlas of Anatomy, 1st ed. Abb. 13.34. Illustrator: Markus Voll, ©2019 Thieme Medical Publishers. Inc. All Rights Reserved. (Gilroy, 2009).*

Pancreatic ductal adenocarcinoma (PDAC)

According to the recent 2022 cancer statistics, 32,970 US-men and 29,240 US-women will be newly diagnosed with pancreatic cancer (figure 2) in 2022 and with 25,970 estimated deaths of male patients and 23,860 estimated deaths of female patients (figure 3) in 2022, pancreatic cancer is one of the deadliest cancers (Siegel et al., 2022). In 2018, pancreatic cancer was the 4th deadliest cancer in the United States after cancers of the lung and bronchus, breast-/prostate cancer and cancer of the colon and rectum (Siegel et al., 2021).

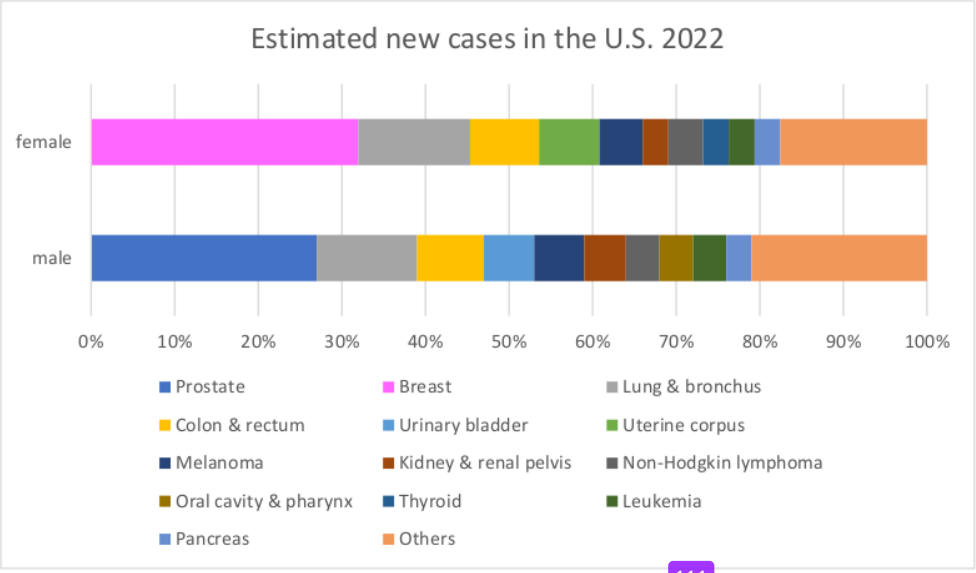

*Figure 2: **Estimated new cancer cases 2022**. With 3% of all new cancer diagnoses, pancreatic cancer is the 8th most common new cancer for women and the 10th most common new cancer for men. The results shown here are in whole or part based upon data generated by Siegel et al. CA: a Cancer Journal for Clinicians. 2022. (Siegel et al., 2022).*

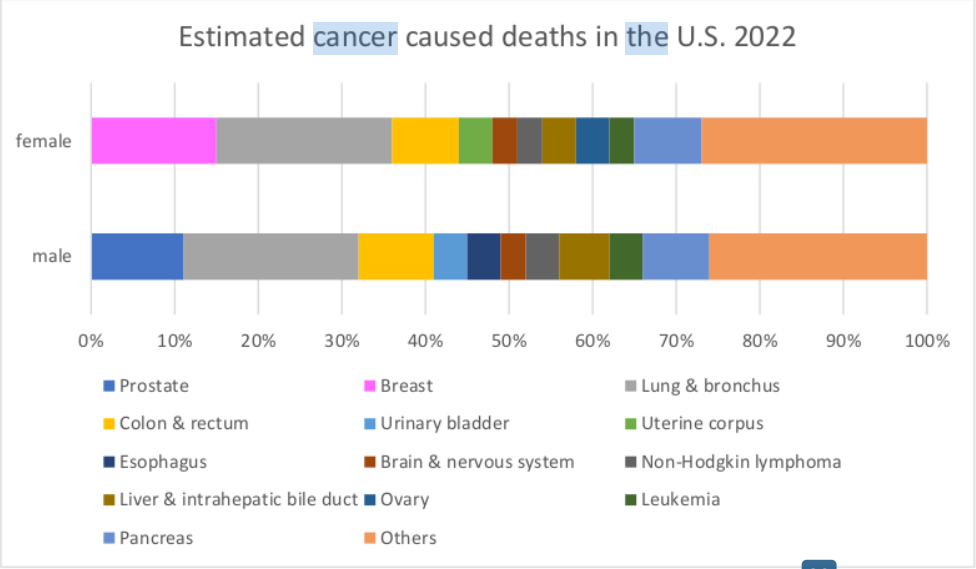

*Figure 3: **Estimated cancer caused deaths 2022**. Pancreatic cancer is the 4th deadliest cancer. The results shown here are in whole or part based upon data generated by Siegel et al. CA: a Cancer Journal for Clinicians. 2022. (Siegel et al., 2022).*

The 5-year-survival of pancreatic cancer is 11%, the lowest 5-year-survival percentage of all cancers (Siegel et al., 2022). Even if the cancer survival for the most cancers in general improved over the last years (e.g. because of new techniques of diagnosis, therapy or vaccinations like HPV-vaccination), it is not the case for pancreatic cancer:

pancreatic cancer is mostly diagnosed at advanced or metastasized stages and therefore mostly has a poor prognosis and survival (Siegel et al., 2021).

The most common cancer of the pancreas is the pancreatic ductal adenocarcinoma (PDAC) (Cascinu et al., 2010; Renz-Polster et al., 2013). Typically for a cancer entity, PDAC also harbours many genetic mutations. The most frequent driver genes are *KRAS*, *CDKN2A*, *SMAD4/DPC4* and *TP53* (Jones et al., 2008; Hong et al., 2011; Zamboni et al., 2013; Esposito et al., 2014). Accumulation of genetic mutations lead to development and progression of precursor lesions, including pancreatic intraepithelial neoplasia (PanIN; most frequent precursor lesion) (figure 4), intraductal papillary mucinous neoplasia (IPMN) and mucinous cystic neoplasms (MCN) (Esposito et al., 2014).

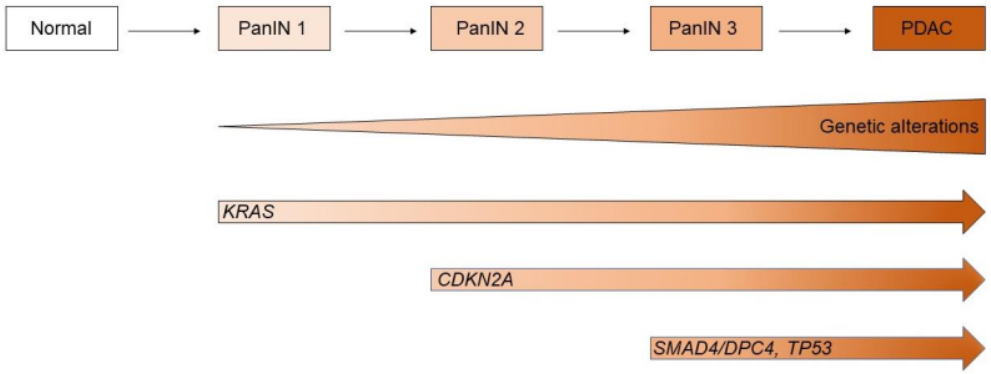

*Figure 4: **Development of PDAC**. Development of PDAC and its precursor lesions (PanIN) due to accumulation of genetic mutations of genes like KRAS, CDKN2A, SMAD4/DPC4 and TP53. The figure presented is based on a figure generated by Li et al. Cell stress. 2019. (Li et al., 2019)*

PanIN lesions can be classified into three grades: PanIN-1A and -1B as early and low-grade lesions, PanIN-2 are intermediate-grade lesions and PanIN-3 as carcinoma in situ (Zamboni et al., 2013; Distler et al., 2014). PanIN lesions are just detectable under the microscope (lesion usually < 5mm) and not reliable via imaging (computed tomography, magnetic resonance imaging or endoscopic ultrasonography) (Ott et al., 2007; Canto et al., 2012; Zamboni et al., 2013; Esposito et al., 2014). Although PanIN-lesions are not easy to detect, they offer an opportunity to cure a neoplasia before it develops into an invasive pancreatic cancer (Zamboni et al., 2013).

The most frequently mutated oncogene (>95 %) is *KRAS* (Hruban et al., 1993; Jones et al., 2008; Hong et al., 2011). *KRAS* codes for a membrane-bound GTP-binding protein, the KRAS protein, which fulfills several functions in the cell, e.g. proliferation or cellular survival: after bondage with GTP, KRAS protein gets activated. This leads to activation of more than 80 downstream signaling pathways and effector proteins, e.g. mTOR (mechanistic target of rapamycin), MAPK (mitogen-activated protein kinase), as well as activation of nuclear transcription factors (e.g. MYC) leading to stimulation of proliferation, dedifferentiation and tumor progression (Buscail et al., 2020). The activating *KRAS*-mutation leads to constitutive signaling of this pathway, as the mutation leads to reduced hydrolysis of GTP to GDP and reduced inactivation of KRAS (Waters and Der, 2018; Hafezi et al., 2021). Also found in the PanIN-lesions (PDAC precursor lesion), *KRAS*-mutation seems to be one of the earliest events in the

genesis of PDAC (figure 4) (Tada et al., 1996; Moskaluk et al., 1997; Jones et al., 2008).

Current recommendations for treatment of PDAC

The recommendation for PDAC treatment depends on the clinical stage. In this context, a differentiation can be made between localized resectable disease (10-15% of the newly diagnosed patients), locally advanced disease (30-35%) and metastatic disease (50-55%). Resectability is defined as the ability to remove the cancer completely, considered when there is no or minimal contact with major vessels (e.g. hepatic artery) (Park et al., 2021).

The only possibility to cure patients from PDAC is surgery (Wagner et al., 2004; Doi et al., 2008; Leitlinienprogramm Onkologie, 2021). The goal is the complete resection in healthy tissue (R0), which shows the best long-term survival rate (Wagner et al., 2004; Fusai et al., 2008; Hartwig et al., 2011). The best surgical procedure depends on the tumors location within the pancreas (e.g. pancreaticoduodenectomy for tumor in the pancreas head). But even after reaching the R0-status after surgery, the 5-year-survival rate is 24,2% (Wagner et al., 2004; Leitlinienprogramm Onkologie, 2021). Although data varies between different observations, several studies in the past showed a benefit for patients receiving adjuvant chemotherapy (Principe et al., 2021). Patients with resectable disease should receive surgery in combination with adjuvant chemotherapy to increase the progression-free survival and overall survival after R0-resection. Therefore an adjuvant chemotherapy should be performed with modified FOLFIRINOX (fluorouracil, oxaliplatin, irinotecan, leucovorin) (overall survival 54,4% (Conroy et al., 2018)) or a combination of gemcitabine and capecitabine (overall survival 28% (Neoptolemos et al., 2017)) or gemcitabine alone (overall survival 25,5% (Neoptolemos et al., 2017)), depending on the patients functional status (Park et al., 2021).

Patients with borderline resectable or locally advanced tumors should receive neoadjuvant chemotherapy to eradicate metastasis or to increase the chances for downstaging and surgery. Therefore, these patients should receive modified FOLFIRINOX or a combination of gemcitabine and albumin-bound paclitaxel (Park et al., 2021).

Patients suffering from metastatic disease should receive palliative care, including chemotherapy (gemcitabine and albumin-bound paclitaxel or modified FOLFIRINOX), symptomatic therapy (e.g. with potent pain killers) and supportive care (e.g. placement of an endobiliary metallic stent in patients with biliary obstruction) (Park et al., 2021).

Not only in other types of cancer like chronic myeloid leukemia, also in PDAC targeted therapies start to establish: due to the POLO trial (U.S. Federal Government), patients with BRCA-gen mutation and metastatic pancreatic cancer showed longer progression-free survival when treated with a PARP (poly adenosinde diohosphate-ribose) polymerase)-inhibitor Olaparib (Golan et al., 2019). In 2019, the FDA approved Olaparib for maintenance treatment for patients with *BRCA*-mutated metastatic PDAC (U.S. Food and Drug Administration, 2019).

Histone deacetylases (HDAC), HDAC-inhibitors and their role in PDAC

Histones are proteins interacting with the DNA and after binding lead to regulation of DNA-packing. The binding of DNA lead to a tighter and more compact form of DNA, called heterochromatin, and reduces gene transcription (Mariño-Ramírez et al., 2005). The unit of DNA wrapped around histone proteins is called nucleosome (Mariño-Ramírez et al., 2005). Nucleosomes consist of 8 histone sub-units (H2A, H2B, H3, H4) and about 146 base pairs wrapped around (figure 5 A) (Singh and Mueller-Planitz, 2021). Besides of the mentioned function of controlled DNA condensation, they also play an important role in transcription process (Singh and Mueller-Planitz, 2021). Histone deacetylases (*HDAC*) are necessary to change the chromatin structure by removing acetylation from the histone proteins (Venugopal and Evans, 2011). This regulates the expression of target genes (Feng et al., 2014). Due to the removal of the acetylation from the Ɛ-amino group of lysines at the N-terminal tail of histone proteins, heterochromatin gets formed, which inhibits the transcription of genes (Yang and Seto, 2008; Haberland et al., 2009). Essential to fulfill their functions, HDACs (especially class I, see below) are part and catalytic core of multiple co-repressor complexes (Kelly et al., 2018). The three major co-repressor complexes are Sin3, CoREST (co-repressor for element-1-silencing transcription factor) and NuRD (nucleosome remodeling and deacetylation), all containing DNA-binding motifs, directing HDACs, with the help of transcription factors, to the specific chromatin regions (Kelly and Cowley, 2013).

HDACs also affect non-histone proteins, which are involved in different functions (e.g. chaperon proteins, enzymes for cell motility, enzymes of the adaptive immune system or metabolic enzymes) or transcription factors (e.g. *p53*) (Feng et al., 2014; Roche and Bertrand, 2016; Shvedunova and Akhtar, 2022). The deacetylation of histones also lead to epigenetic repression and is important for transcriptional regulation or the control of the cell cycle (Roche and Bertrand, 2016). The antagonistic reaction is catalyzed by histone acetyltransferases (HAT) (figure 4). They add an acetyl group to histones and thereby relax the structure of the chromatin (euchromatin) to increase the transcription of genes (Epping and Bernards, 2009; Lane and Chabner, 2009).

HDACs are zinc- or NAD^+-dependent enzymes which means, that they need Zn^{2+} (class I, II, IV) or NAD^+ (class III) for deacetylation (Yang and Seto, 2008; Seto and Yoshida, 2014; Roche and Bertrand, 2016). Phylogenetic analysis showed homology of the human HDAC with those of yeast, so that the 18 HDAC molecules can be classified into four classes (Schneider et al., 2010; Feng et al., 2014; Seto and Yoshida, 2014). Class I HDACs contain HDACs 1, 2, 3 and 8 and are homologue to those of yeast RPD3, class II HDACs contain HDAC 4, 5, 6, 7, 9 and 10, which are homologue to those of yeast HDA1, HDACs of class III are related to yeast Sir2 and class IV HDAC contains HDAC 11, showing homologies with class I and II HDAC's (Schneider et al., 2010; Feng et al., 2014; Seto and Yoshida, 2014; Damaskos et al., 2015). HDAC's are localized in the cytoplasm and/or the nucleus (Damaskos et al., 2015).

HDAC-expressions and -overexpressions, especially of class I HDACs, can be found in a lot of human malignancies (e.g. ovarian cancer and prostate cancer) (Weichert, 2009; Schneider et al., 2010; Li and Seto, 2016; Shinke et al., 2018; Rana et al., 2020). Also in 56% of PDAC, high expression of *HDAC-1* is reported (Miyake et al., 2008;

Schneider et al., 2010). Together with the expression of HIF-1α, it could predict a poor prognosis (Miyake et al., 2008; Schneider et al., 2010). In their experiments, Wang et al. found the expression of class I and class II HDAC in all of their PDAC cell lines in variable levels (Wang et al., 2012). *HDAC-2* shows high expression in moderately differentiated and undifferentiated PDAC (Schneider et al., 2010) and seems to facilitate PDAC metastasis (Krauß et al., 2022). Depletion of *HDAC-2* can make PDAC cells more sensible to etoposide, a topoisomerase II inhibitor, or the tumor necrosis factor-related apoptosis-inducing ligand (TRAIL) (Fritsche et al., 2009; Schüler et al., 2010). *HDAC-7* shows high expression levels in PDAC too (Ouaïssi et al., 2008).

HDAC-inhibitors (HDACi) can inhibit all HDAC isoforms (pan-HDACi, e.g. Vorinostat) or specific isoforms (isoform-selective-HDACi, e.g. *MS-275, a class I inhibitor*) (Eckschlager et al., 2017). Based on their chemical structures, HDACi can be divided into five groups: hydroxamate/hydroxamic acid, short-chain fatty acids, benzamide, cyclic peptide and sirtuin inhibitors (Seto and Yoshida, 2014; Damaskos et al., 2015; Roche and Bertrand, 2016; Eckschlager et al., 2017). A central mechanism of HDACi is the binding to the Zn^{2+} ion in the catalytic domain of class I HDAC, which is essential for the deacetylation catalyzed by HDACs, which leads to higher expressions of the target genes.

Inhibition of HDAC's prevent the deacetylation of lysine of histones which consequently leads to more acetylated lysine groups. Deacetylated lysine groups have a positive charge. With the binding acetylation, this positive charge gets neutralized, leading to reduced interaction with the negatively charged DNA (Damaskos et al., 2015). This leads to an increasing transcription of genes in the control of e.g. cell cycle (e.g. increased expression of *CDKN1A*), differentiation, angiogenesis (e.g. downregulation of *VEGF*) or apoptosis (e.g. by influencing the expression of death inducing genes) (Richon and O'Brien, 2002; Damaskos et al., 2015; Eckschlager et al., 2017) which in turn leads to an inhibition of cancer growth. Due to the relaxed chromatin structure, the access of polymerases or transcription factors to the DNA is much easier, leading to the described increase in transcription (Richon and O'Brien, 2002; Damaskos et al., 2015) (figure 5 B).

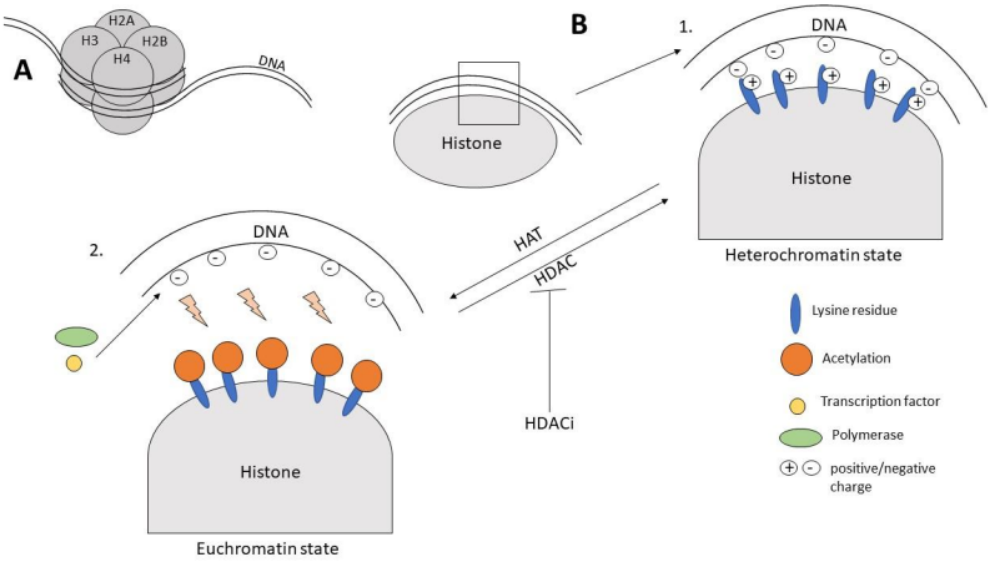

Figure 5: ***Nucleosome and mode of action of HDAC and HAT****. (A) Nucleosome consists of 8 histone subunits (H2A, H2B, H3, H4), formed by two molecules of each histone protein, and DNA wrapped around it. (B) Due to negative charged DNA and positive charged lysine residues from the histone, the histone binds with the DNA (heterochromatin, 1.). After acetylation of lysine, catalyzed by histone acetyltransferase (HAT), the positive charge gets neutralized, leading to lose DNA (euchromatin, 2.). Now, polymerases, transcription factors, etc. can access the DNA, leading to transcription. The antagonistic effect is catalyzed by histone deacetylase (HDAC), leading to compact chromatin structure. Inhibitors of histone deacetylases (HDACi) lead to increasing expression of proteins necessary for inhibition of the cell cycle, differentiation or apoptosis (Aktories, 2017).*

Another important effect of HDACi seems to be the regulation of proteins that are relevant for DNA repair (e.g. KU70 or FEN1) and are regulated by acetylation and may be increased by HDAC inhibition (Eckschlager et al., 2017), because due to the acetylation of proteins like KU70 (induces repair of double-strand brakes by binding DNA endings), the binding to the DNA for its repair is reduced (Bose et al., 2014). Inhibition of *HDAC-1* and *HDAC-2* decreases the DNA-damage repair process (double strand brakes), mediated by BAL-associated protein (BBAP) (Bhaskara, 2015; Eckschlager et al., 2017). BBAP is part of protecting cells against DNA-damage (see below) (Eckschlager et al., 2017). DNA-damage due to problems in DNA repairment causes genome instability, which can lead to cell death (Bhaskara, 2015; Li et al., 2020). HDACi can also induce reactive oxygen species (ROS), which could lead to higher oxidative stress and cell death (Ruefli et al., 2001; Trachootham et al., 2006; Wolf et al., 2014).

HDACi can be promising anti-cancer agents, e.g. *Vorinostat* has been approved for treating refractory cutaneous T cell lymphomas (CTCL) by the U.S. Food and Drug Administration (FDA) (table 1) (Duvic et al., 2007; Falkenberg and Johnstone, 2014). Also recent studies show the potential of HDACi as effective drugs in solid tumors, e.g. triple negative breast cancer (Fedele et al., 2017).

Table 1: ***Overview of HDACi approved by the FDA or in phase-3-trials****. The results shown here are in whole or part based upon data generated by Nepali and Liou. Journal of biomedical science 28, 27. 2021 (Nepali and Liou, 2021) and Li et al. Frontiers in Cell and Developmental Biology 8:576946. 2020 (Li et al., 2020).*

FDA-approved HDACi		HDACi in phase-III-trial	
Vorinostat/SAHA (Cutaneus T cell lymphoma)	Pan HDACi	**Givinostat** (Polycythaemia vera)	Hydroxomate HDACi
Romidepsin (Cutaneus T cell lymphoma, peripheral T cell lymphoma)	Class I HDACi	**Abexinostat** (Renal cell carcinoma)	Pan HDACi
Belinostat (Peripheral T cell lymphoma)	Pan HDACi	**Entinostat/MS-275** (Hormone receptor-positive, locally advanced or metastatic breast cancer)	Class I HDACi
Panobinostat (Multiple myeloma)	Pan HDACi	**Tucidinostat** (advanced, hormone receptor-positive, breast cancer)	HDACi of HDAC 1, 2, 3, 10
		Pracinostat (intermediate/ high-risk Myelofibrosis)	Class I, II, IV (except HDAC 6) HDACi
		Tacedinaline (Non-small lung cancer, pancreatic cancer)	Inhibits HDAC 1-3
		Valproic acid (Flioblastoma)	Class I/II HDACi

Knock-out model: dual-recombinase system

Isogenic models offer the opportunity to determine the effect of individual genes on cancer development and to investigate and focus on the implications of addressing these genes. Therefore, PDAC cells of genetically engineered mouse models were used to evaluate the effect of *HDAC-2* knock-out. Therefore, an inducible dual-recombinase system has been developed in the past by combining flippase-*FRT* and Cre-*loxP* recombination systems (Schönhuber et al., 2014). This means, that the mice expresses Flippase (Flp)-recombinase, which is directed by (pancreas specific) *Pdx1* promoter, which activates the expression of CreER by removing the FSF-stop-cassette (FRT-stop-FRT). CreER is a recombinase fused with an estrogen receptor which can be activated by Tamoxifen (also called $CreER^T$ (Cre estrogen receptor tamoxifen)) (Kim et al., 2018). The FRT-stop-FRT cassette is located between the *CreER*-gene and its promotor $Rosa26^{CAG}$ and prevents the expression of CreER. After activation of Pdx1-Flp, the expression of CreER is induced (figure 6) (Schönhuber et al., 2014). The activation of oncogenic $Kras^{G12D}$ is similarly regulated, while exons 2-6 of the *Trp53* gene (Wu et al., 2017) are flanked by FRT sites leading to *Trp53* inactivation due to

Pdx1-Flp activity. Both lead to development of murine PanIN lesions and PDAC (Schönhuber et al., 2014).

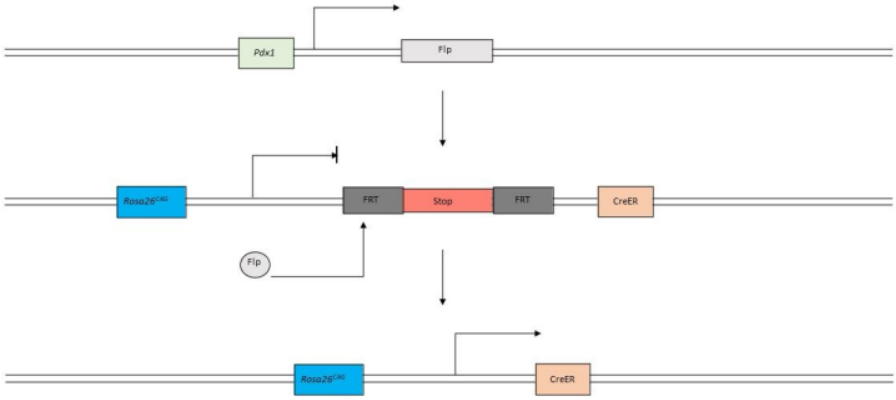

*Figure 6: **Knock-out model**. As "inhibitor" of CreER-expression, FSF-cassette is located between the CreER-gene and its promotor. After Pdx1-Flp activation, the FSF-cassette gets removed, leading to expression of CreER.*

The Cre/loxP-system can be used for selectively excising genes out of the DNA and binding the remaining DNA-endings together.

To get a Tamoxifen-inducible Cre/loxP-system, the Cre recombinase was fused with an estrogen receptor (CreER^{T}; see above). A new version of this fusion protein is called CreER^{T2}, a mutated form of CreER^{T} which is more sensitive towards Tamoxifen treatment (Kristianto et al., 2017; Kim et al., 2018). Treatment with Tamoxifen leads to an induction of Cre activity, as CreER^{T2} is normally located in the cytoplasm and bond to heat shock protein 90 (Schönhuber et al., 2014; Kim et al., 2018). Tamoxifen disrupts this interaction between CreER^{T2} and heat shock protein 90, which leads to translocation of CreER^{T2} into the nucleus for interaction with *loxP* sites (Schönhuber et al., 2014; Kim et al., 2018). *loxP* sites are necessary for recognition of the target gene region by Cre as the targeted gene region is flanked by the genetic sequence of *loxP* (flanked by *loxP* = floxed). After recognition, Cre excises the floxed sequence of the targeted gene(s) (figure 7) (Kim et al., 2018). The floxed regions used in our model were *HDAC-2 exons 2-4*. Consequently, after a treatment with Tamoxifen, the cells were deficient of *HDAC-2*.

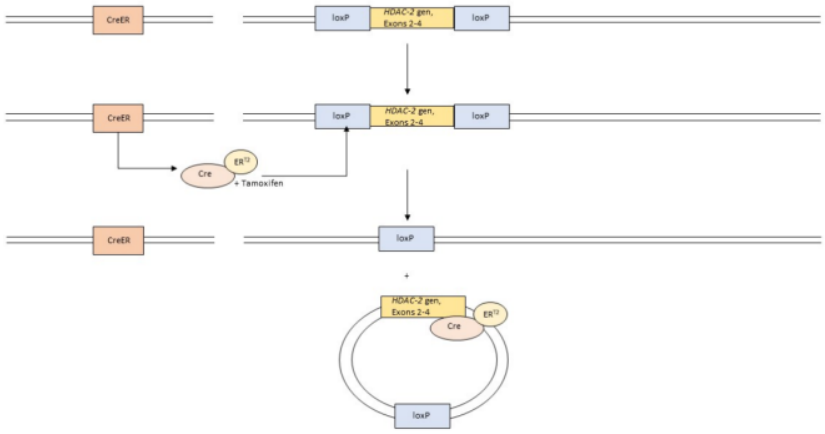

Figure 7: ***Scheme of the HDAC-2 knock-out mechanism****. Exon 2-4 of HDAC-2 gene is floxed and gets exercised by CreER^{T2} after Tamoxifen treatment. This leads to HDAC-2 knock-out.*

Objective

In the past, HDACi as anti-cancer drugs in pancreatic cancer failed in clinical studies regarding relevant antitumor effects (Arlt and Schäfer, 2016). To find effective, specific and novel combination therapies, an unbiased drug screen was implemented containing 101 drugs with different mode of actions (tables 1 – 9). Therefore, two *HDAC-2* proficient (*HDAC-2 (+)*) and deficient (*HDAC-2 (-)*) murine cell lines were treated with the drug library. The goal was to find new potential therapies against PDAC with an HDAC-2 inhibitor as a combination partner. Goal of this thesis is to explore new possibilities and potential therapeutical solutions in the fight against PDAC. The results are presented in the following.

Material and Methods

Material

Cell lines

Table 2: ***Cell lines****.*

Cell line	Genotype	Morphology	Date isolated	Source
PPT-F1648	*FSF-Kras$^{G12D/+}$, FSF-Trp$^{53del/+}$, Pdx1-Flp, R26$^{CAG-FSF-CreERT2/+}$,*	Mesenchymal	01.06.2012	Department of Internal Medicine II, Klinikum rechts

	Pdk$^{loxP/+}$, *Hdac2*$^{loxP/loxP}$			der Isar, Technical
PPT-F2612	*FSF-Kras*$^{G12D/+}$, *FSF-Trp*$^{53del/+}$, *Pdx1-Flp, R26*$^{CAG-FSF-CreERT2/FSF-CreERT2}$, *Hdac2*$^{loxP/loxP}$	Epithelial	17.04.2013	University of Munich

Reagents

Table 3: ***Reagents****.*

Product – Reagents	Manufacturer
30% Acrylamide/Bisacrylamide-stock solution (29:1)	Carl Roth, Karlsruhe
4-Hydroxytamoxifen	Sigma-Aldrich, Steinheim
Ammonium Persulfate (APS)	Sigma-Aldrich, Steinheim
Agarose	Sigma-Aldrich, Steinheim
Aqua 1000 ml	B. Braun Melsungen AG, Melsungen
Bovine serum albumin	Sigma-Aldrich, Steinheim
Bradford reagent 5x	Serva, Heidelberg
Crystal Violet	Sigma-Aldrich, Steinheim
ddH$_2$O	SAV Liquid Production GmbH, Flintsbach am Inn
imethyl sulfoxide (DMSO)	Carl Roth, Karlsruhe
Dulbecco's Modified DMEM; high glucose	Sigma-Aldrich, Steinheim
Dulbecco's Phosphate Buffered Saline	Sigma-Aldrich, Steinheim
Ethanol Absolut	Otto Fischar, Saarbrücken
Ethanol 100%	Merck, Darmstadt
Ethylenediaminetetraacetate (EDTA)	Invitrogen GmbH, Karlsruhe
Fetal Calf Serum (FCS)	bco, Schwerte
Glycerol	Sigma-Aldrich, Steinheim
Glycine	Sigma-Aldrich, Steinheim
Isopropanol	Carl Roth, Karlsruhe
ethanol	Carl Roth, Karlsruhe
PageRuler Prestained Protein Ladder	Thermo Scientific, Schwerte
(Penicillin-Streptomycin-solution (Pen Strep)	Gibco, Schwerte
Phosphatase-Inhibitor-Mix	Serva, Heidelberg
Potassium chloride	Merck, Darmstadt
wdered milk	Carl Roth, Karlsruhe
Protease inhibitor cocktail tablets	Roche Diagnostics GmbH, Mannheim
RLT-Buffer	Qiagen GmbH, Hilden
Sodium Chloride	Merck, Darmstadt
Sodium Dodecyl Sulfate pellets	Serva, Heidelberg

Sodium hydrogen phosphate	Fluka, Steinheim
Tetramethylethylenediamine (TEMED)	Carl Roth, Karlsruhe
Tris Pufferan	Carl Roth, Karlsruhe
Trypan Blue 0,4%, 0,85% NaCl	Lonza, Walkersville, MD
Tween 20	Carl Roth, Karlsruhe
β-Mercaptoethanol	Carl Roth, Karlsruhe

Kits and Assays

Table 4: ***Kits and Assays.***

Kits and Assays	**Manufacturer**
***CellTiterGlo* Luminescent Cell Viability Assay**	Promega Corporation, Madison

Antibodies

Table 5: ***Antibodies.***

Antibody	**Dilution**	**Species of origin**	**Catalogue number**	**Manufacturer**	**RRID**
Anti-mouse IgG (H+L) (DyLight™ 680 Conjugate)	1:10000	Goat	5470	Cell Signaling Technology, Leiden	AB10696895
Anti-rabbit IgG (H+L) (DyLight™ 800 4X PEG Conjugate)	1:10000	Goat	5151	Cell Signaling Technology, Leiden	AB10697505
Hdac2 (D6S5P)	1:500	Rabbit	57156	Cell Signaling Technology, Leiden	AB2756828
β-Actin	1:5000	Mouse	A5316	Sigma-Aldrich, Steinheim	AB476743

Drugs

All drugs used for the screening (listed under "b. Methods – Cell culture: Drug screening", table 12-20) were purchased from *Selleck Chemicals Llc* (www.selleckchem.com).

Table 6: ***Drugs.***

Product – Reagents	**Manufacturer**
Entinostat (*MS-275*) E-3866	LC Labratories, Woburn

Buffer/Medium/Solution

Table 7: ***Buffer/Medium/Solution.***

Buffer/Medium/Solution	Composition
Dulbecco's Modified DMEM, high glucose (supplemented with FBS and Pen Strep)	- 500 ml DMEM - 10% (v/v) FBS - 1% Pen Strep
EDTA-Solution (0.05%) for cell culture, 50 ml	- 2,5 ml EDTA 1% - 47,5 ml PBS
Freezing Medium	- 70 ml DMEM - 20 ml FCS - 10 ml DMSO
IP-Buffer (pH 7,9)	- 150 mM NaCl - 1 mM EDTA - 1% Triton X-100 - 50 mM TRIS
Laemmli (1x), 100 ml	- 20 ml Laemmli (5x) - 80 ml ddH_2O
Laemmli (5x)	- 0,3 M TRIS - 50% (v/v) Glycerine - 0,35 M SDS (pH 6,8) - 50 mg Bromophenol blue - 5% (v/v) β-Mercaptoethanol
Lysis buffer	- 200 µl IP-Buffer - 2 µl Phosphatase inhibitor - Protease inhibitor (25x)
PBS (10x) 1l, pH 7,4	- 80 gr. NaCl - 2 gr. KCl - 14,4 gr. Na_2HPO_4 - 800 ml ddH_2O - with HCl to pH 7,4 - fill up with ddH_2O to 1l
Protease inhibitor (25x)	- 1 protease inhibitor cocktail tablet - 2 ml ddH_20
RIPA-buffer	- 4,206 gr. NaCl - 3,028 gr. TRIS - 2,5 gr. Sodiumdeoxychelate - 0,5 gr. SDS - 5 ml NPO_4 - 25x Protease - 100x Phosphatase - H_2O
Running buffer (10x) 1l	- 10 gr. SDS - 30 gr. TRIS - 144 gr. Glycin - fill up with ddH_2O to 1l
Separation gel (10%), two gels	- 6150 µl ddH_20 - 3900 µl separation gel buffer - 4950 µl acrylamide 30%

	- 150 µl SDS 10% - 75 µl APS 10% - 22,5 µl TEMED
Separation gel buffer (1,5 M TRIS/HCl pH 8,8), 100 ml	- 18,171 gr TRIS - 50 ml ddH_2O - with HCl to pH 8,8 - fill up with ddH_2O to 100 ml
Skim Milk	- 500 ml PBS - 25 gr Powdered milk
Stacking gel (2x), two gels	- 4500 µl ddH_20 - 1950 µl collection gel buffer - 1125 µl acrylamide 30% - 75 µl SDS 10% - 37,5 µl APS 10% - 15 µl TEMED
Stacking gel buffer (0,5 M TRIS/HCl pH 6,8), 100 ml	- 6 gr. TRIS - 50 ml ddH_2O - with HCl to pH 6,8 - fill up with ddH_2O to 100 ml
Transfer buffer 1l, pH 8,3	- 2,9 gr. Glycin - 5,8 gr. TRIS - 700 ml ddH_2O - 3,7 ml SDS 10% - 200 ml Ethanol - fill up with ddH_2O to 1l

Devices

Table 8: ***Devices.***

Product	Manufacturer
Anthos Photometer 2001	Anthos Mikrosysteme, Krefeld
AxioCam MRc	Carl Zeiss, Oberkochen
Axiovert 25 Inverse microscope	Carl Zeiss, Oberkochen
Centrifuge 5415 R	Eppendorf, Hamburg
Centrifuge 5451R	Eppendorf, Hamburg
CLARIOstar Plate Reader	BMG Labtech, Ortenberg
CO_2 Incubator	Sanyo, München
Combitips advanced 0,2 ml, 1 ml, 2,5 ml, 5 ml, 10 ml	Eppendorf, Hamburg
FLUOstar optima	BMG Labtech, Ortenberg
LICOR Odyssey	LI-CO, Lincoln, NE
Mini-PROTEAN Tetra Cell	Bio-Rad, Hercules
Mini-Trans-Blot Cell	Bio-Rad, Hercules
Multipette E3x	Eppendorf, Hamburg
Multiscan RC	ThermoFisher Scientific, Waltham
Nebauer Kammer	Assitent, Sondheim vor der Rhön
Pipettes 10 µl, 100 µl, 200 µl, 1000 µl	Eppendorf, Hamburg
PowerPac HC Power Supply	Bio-Rad, Hercules
Rotina 280	Hettich Zentrifugen, Tuttlingen

Rotina 46 R	Hettich Zentrifugen, Tuttlingen
Shaker	Henning GmbH, Berlin
Stripettor Ultra Pipet Controller	Corning, Corning
Thermomixer compact	Eppendorf, Hamburg
Vortex Genie 2	Bender & Hobein AG, Zurich

Software

*Table 9: **Software**.*

Product	Manufacturer	RRID
Axio Version 4.3	Carl Zeiss, Jena	SCR_021351
Flourstar optima ogramm Version 1.30-0	BMG Labtechnologies, Ortenberg	-
Graph Pad Prism 5	Graph Pad Software, La Jolla, CA	SCR_002798
Image Studio Software Version 5.2.5	Li-COR, Lincoln, NE	SCR_015795
Microsoft Excel 2016	Microsoft Corporation, Redmond, WA	SCR_016137
Microsoft PowerPoint 2016	Microsoft Corporation, Redmond, WA	-

Online Tools/Databases

*Table 10: **Online Tools/Databases**.*

Product	Internet-adress	RRID
ClustVis	https://biit.cs.ut.ee/clustvis/	SCR_017133
Gene set enrichment analysis 4.0.3, BROAD Institute	https://www.gsea-msigdb.org/	SCR_016863
ynergyFinder 3.0	https://synergyfinder.fimm.fi	SCR_019318
Venny 2.1	https://bioinfogp.cnb.csic.es/tools/venny/	SCR_016561

Various materials

*Table 11: **Various materials**.*

Product	Manufacturer
5 ml Polystrene Round-Bottom Tube	BD Falcon,
Assay Plates, 96 wells	Corning, Corning
Cell Culture Flasks 50 ml, 250 ml, 550 ml	Greiner Bio One, Frickenhausen
Cell Scr er	Sarstedt, Newton
Cellstar tubes 15 ml, 50 ml	Greiner Bio-One GmbH, Kremsmünster
CellTrics 3 m	Sysmex, Görlitz
Clear Line Filter Tips 10 µl, 100 µl, 200 µl, 1000 µl	Biosigma, Cona
Injekt-F 1ml	B. Braun Melsungen AG, Melsungen
Pasteur Pipettes	Hirschmann Laborgeräte GmbH & Co. KG, Eberstadt

Serological Pipette 2 ml, 5 ml, 10 ml, 25 ml, 50 ml	Greiner Bio-One GmbH, Kremsmünster
Tissue Culture Dish 100 x 20 mm	Corning, Corning
Tissue Culture Plate 96 Well	Corning, Corning
Whatman Papier 3MM Chr	GE Healthcare Life Sciences, Freiburg
Amersham Protran 0,2 µm NC	GE Healthcare Life Sciences, Freiburg
100 Sterican 0,45 x 25 mm Gr. 18	B. Braun Melsungen AG, Melsungen

Methods

Cell culture: preparing Medium

The medium used for the experiments was *Dulbecco's Modified Eagle's Medium – high Glucose* 500 ml bottles (DMEM). 50 ml fetal calf serum (FCS) and 5 ml of the Penicillin-Streptomycin solution was added to DMEM prior to use.

Cell culture: washing cells and exchange of medium

After aspirating the DMEM from the T75-cell culture flask, 5 ml PBS was added to wash the cells and to remove media residue. After 30 seconds of incubation the PBS got removed. Finally, 10 ml of new DMEM was added.

Cell culture: freezing cells

To freeze cells, the cells were grown till 80% confluency in a T75-flask. First, the cells were washed (see Cell culture: washing cells/exchanging of medium). After removing the PBS, 1 ml EDTA 0,05% was added to the cells to detach them from the flask, followed by resuspending them in 10 ml of DMEM. After detaching, the suspension was filled into 15 ml falcon-tubes and centrifuged at 1000 rpm for 5 minutes. Subsequently the supernatant was aspirated, and the cell pellet was resuspended and singularized with 4 ml freezing medium. After preparation of the cryo-tubes, 1 ml of the suspension was filled in each of the tubes. The tubes were frozen at -80°C and transferred into liquid nitrogen tanks after one week.

Cell culture: thawing cells

The frozen samples were thawed in the 37°C water bath. After thawing, the samples were transferred in a falcon tube filled with 5 ml DMEM. Subsequently they were put into the centrifuge at 1000 rpm for 5 minutes. Afterwards the supernatant was aspirated and another 10 ml DMEM was added to the tubes to resuspend and singularize the cells. Afterwards the whole suspension was transferred into a T75-culture flask and put into the incubator.

Cell culture: splitting cells

To split cells, the cells were grown till 80% confluency in a T75-flask. First, the cells were washed (see Cell culture: washing cells/exchanging of medium). After aspirating the PBS, 1 ml EDTA 0,05% was added to the cells to detach them. While the cells detached from the bottom of the flask, the new flasks/dishes were prepared by filling them with DMEM:

- T75 bottle: 10 ml
- 10 cm-dish: 5 ml

Depending on the cell line, after 5 (F1648) to 10 (F2612) minutes of incubation with EDTA, the cells were detached with 10 ml DMEM and singularized. Next, 0,5-1 ml of the suspension was transferred into the previously prepared flask respectively 0,5 ml in the 10 cm-dish.

Cell culture: drug screening

The drug library was divided into nine screens, containing 5-12 different compounds. The following descriptions of the drugs are copied from the official descriptions of www.selleckchem.com (viewed October 13th, 2019) where the compounds were bought (Selleck Chemicals).

*Table 12: **Drugs of screen 1 with mode of action (Selleck Chemicals).***

Veliparib	Potent inhibitor of PARP1 and PARP2
Linsitinib	Selective inhibitor of IGF-1R
Pelitinib	Potent irreversible inhibitor of EGFR
Galunisertib	Potent inhibitor of TGFβ-receptor I (TβRI)
GDC-0152	Antagonist of XIAP-BIR3, ML-IAP-BIR3, cIAP1-BIR3 and cIAP2-BIR3
UNC1999	Selective inhibitor of EZH2 and EZH1
SF1670	Highly potent and specific PTEN inhibitor
4EGI-1	Competitive eIF4E/eIF4g interaction inhibitor
CB-839	Potent and selective glutaminase inhibitor
Ulixertinib	Potent and reversible ERK1/ERK2 inhibitor
Sabutoclax	Pan-Bcl-2 inhibitor, including Bcl-xL, Bcl-2, Mcl-1 and Bfl-1
Saracatinib	Potent Src inhibitor

*Table 13: **Drugs of screen 2 with mode of action (Selleck Chemicals).***

Alisertib	Selective Aurora A inhibitor
Ispinesib	Potent, specific and reversible inhibitor of KSP (kinesin spindle protein)
Indirubin	Potent cyclin-dependent kinases and GSK-3β inhibitor
Birinapant	SMAC mimetic antagonist, mostly to cIAP1
Crenigacestat	Oral Notch inhibitor
WZ4003	Highly specific NUAK kinase inhibitor
PTC-209 HBr	Hydrobromide salt of PTC209, a potent and selective BMI-1 inhibitor

AZD6738	Selective ATR kinase inhibitor
LJH685	Potent pan-RSK inhibitor
UNC0638	Potent, selective and cell-penetrant chemical probe for G9a and GLP
Lapatinib	Potent EGFR and ErbB2 inhibitor
CUDC-101	Potent multi-targeted inhibitor against HDAC, EGFR and Her2

*Table 14: **Drugs of screen 3 with mode of action (Selleck Chemicals).***

Orantinib	Potent against PDGFR autophosphorylation
Trametinib	Highly specific and potent MEK1/2 inhibitor
GSK2656157	ATP-competitive and highly selective inhibitor of PERK
RO5126766	Dual RAF/MEK inhibitor
HTH-01-015	Potent and selective NUAK1 inhibitor
UNC0379	Selective, substrate competitive inhibitor of N-lysine methyltransferase SETD8
STF-083010	Specific IRE1α endonuclease inhibitor
NVP-CGM097	Highly potent and selective MDM2 inhibitor
RI-1	RAD51 inhibitor
Elesclomol	Potent oxidative stress inducer
Vemurafenib	Inhibitor of B-RafV600E
Pracinostat	Potent pan-HDAC inhibitor

*Table 15: **Drugs of screen 4 with mode of action (Selleck Chemicals).***

Milciclib	Potent, ATP-competitive CDK inhibitor for CDK2
AZD1208	Potent Pim kinase inhibitor
Erastin	Ferroptosis activator by acting on mitochondrial VDAC, exhibiting selectivity for RAS-mutated tumor cells
CW069	Allosteric and selective inhibitor of microtubule motor protein HSET
GSK2830371	Allosteric Wip1 phosphatase inhibitor
GSK503	Potent and specific EZH2 methyltransferase inhibitor
Spautin-1	Potent and specific autophagy inhibitor, and inhibits the deubiquitinating activity of USP10 and USP13
GSK591	Potent and selective inhibitor of the arginine methyltransferase PRMT5
Enzastaurin	Potent PKCβ selective inhibitor
BX-795	Potent and specific PDK1 inhibitor
Adavosertib	Potent and selective Wee1 inhibitor
Sapanisertib	Potent and selective mTOR inhibitor

*Table 16: **Drugs of screen 5 with mode of action (Selleck Chemicals).***

Pevonedistat	Small molecule inhibitor of Nedd8 activating enzyme (NAE)
JIB-04	Pan-selective Jumonji histone demethylase inhibitor
JSH-23	Inhibitor of NF-κB transcriptional activity

LLY-507	Potent and selective inhibitor of protein-lysine methyltransferase SMYD2
MI-463	Potent inhibitor of Menin-MLL interaction
Epacadostat	Potent and selective indoleamine 2,3-dioxygenase (IDO1) inhibitor
MS023	Potent, selective and cell-active Type I PRMT inhibitor
Luminespib	Highly potent HSP90 inhibitor for HSP90α/β
BX-912	Potent and specific PDK1 inhibitor
AZD7762	Potent and selective inhibitor of Chk1
Alpelisib	Potent and selective PI3Kα inhibitor
PYR-41	Cell-permeable inhibitor of ubiquitin-activating enzyme E1, with no activity at E2

Table 17: ***Drugs of screen 6 with mode of action (Selleck Chemicals).***

NMS-873	Allosteric and specific p97 inhibitor
EPZ004777	Potent, selective DOT1L inhibitor
GSK-J1	Highly potent H3K27 histone demethylase inhibitor
MI-503	Potent and selective Menin-MLL inhibitor
Napabucasin	Stat3 and cancer cell stemness inhibitor
NSC87877	Cell-permeable inhibitor of SHP-1 and SHP-2
MK-2206 2HCl	Highly selective inhibitor of AKT1/2/3
Rigosertib	Non-ATP-competitive inhibitor of PLK1
Selisistat	Potent and selective SIRT1 inhibitor
BI-D1870	ATP-competitive inhibitor of S6 ribosome for RSK1/2/3/4
PFI-2 HCl	Potent selective and cell-active lysine methyltransferase SETD7 inhibitor
P22077	Inhibitor of ubiquitin-specific protease USP7 and USP47

Table 18: ***Drugs of screen 7 with mode of action (Selleck Chemicals).***

Poziotinib	Irreversible pan-Her inhibitor
BRD4770	Histone methyltransferase G9a inhibitor
SGC707	Potent, selective and cell-active allosteric inhibitor of protein arginine methyltransferase (PRMT3)
A-196	Potent and selective inhibitor of SUV420H1 and SUV420H2
ML264	Selectively inhibitor of kruppel-like factor 5 (KLF5)
Abexinostat	Pan-HDAC inhibitor mostly targeting HDAC-1
Ruxolitinib	Potent and selective JAK1/2 inhibitor
KU-60019	Improved analogue of KU-55933 (specific ATM inhibitor)
Salubrinal	Selective inhibitor of eIF2a dephosphorylation and inhibits ER stress-mediated apoptosis
C646	Inhibitor for histone acetyltransferase, and inhibits p300
ML324	Selective inhibitor of Jumonji histone demethylase (JMJD2)
OTX015	Potent BET bromodomain inhibitor

Table 19: ***Drugs of screen 8 with mode of action (Selleck Chemicals).***

PX-478 2HCl	Selective hypoxia-inducible-factor-1α (HIF-1α) inhibitor
BI-847325	elective dual MEK/Aurora kinase inhibitor
Entrectinib	Pan-TrkA/B/C, ROS1 and ALK inhibitor
BI-78D3	Competitive JNK inhibitor
SMER28	Small-mole enhancer (SMER) of autophagy
EED226	Potent and selective allosteric Polycomb repressive complex 2 (PRC2) inhibitor
Thiomyristoyl	Potent and specific SIRT2 inhibitor
PRT4165	Bmi1/Ring1A inhibitor
CPI-455 HCl	Specific K 5 inhibitor
LY2109761	Selective TGFβ-receptor type I/II (TβRI/II) dual inhibitor
AZD5153	tent and selective BET/BRD4 bromodomain inhibitor
A-1210477	Potent and selective MCL-1 inhibitor

Table 20: ***Drugs of screen 9 with mode of action (Selleck Chemicals).***

Erdafitinib	Potent and selective pan fibroblast growth factor receptor (FGFR) inhibitor
Ralimetinib	otent inhibitor of p38 MAPK
MX69	MDM2/XIAP inhibitor that binds to MDM2 RING protein
BAY-876	otent and selective GLUT1 inhibitor
LLY-283	Potent and selective SAM-competitive chemical probe for PRMT5

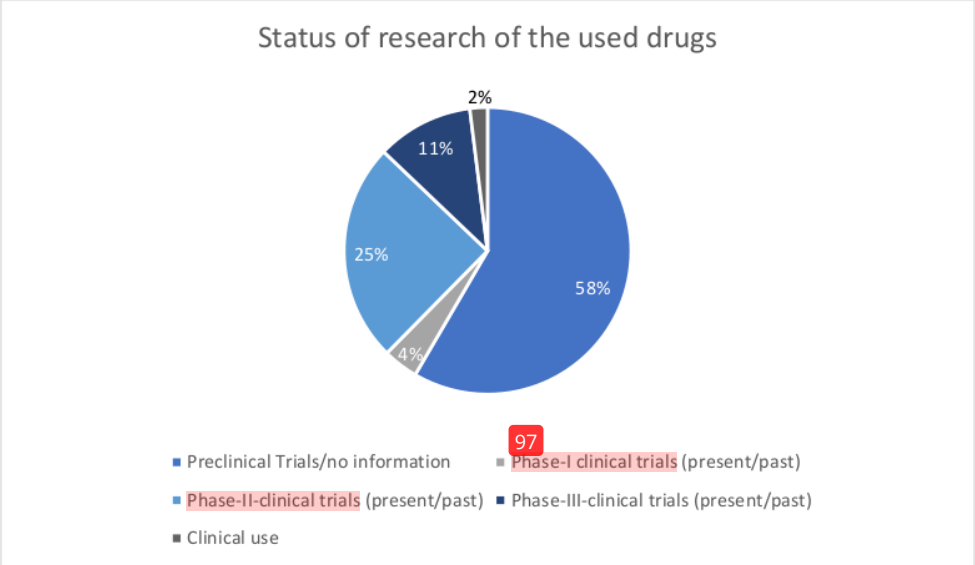

Figure 8: ***Developmental status of the drugs used in the screening.***

One screen needed 5 days to be completed:

Day 1:

After splitting the Tamoxifen (*HDAC-2* deficient)- and ethanol-treated (*HDAC-2* proficient) cells (see cell culture: splitting) to one 10 ml bottle and two 10 cm-dishes (for harvesting proteins), the cell suspension was put into a 50 ml Falcon-tube and singularized. Afterwards, 20 µl of the suspension was put into a 0,5 ml Eppendorf-Tube and 20 µl of Trypan Blue 0,4% was added, followed by another singularization of the cells. Next, the cells were counted with a Neubauer-chamber (see counting cells with Neubauer-chamber). In order to seed 1000 cells in 100 µl per well in the 96-well-plate later, dependent on the counting result, the cell suspension was diluted to 10000 cells/ml. The next step contained seeding the cells with a multistep pipette into the wells. After finishing this procedure, the cells were put in the incubator (37°C; 5% CO_2) until the next day.

Day 2:

To treat the cells with the drugs, the preparations of the right concentrations were necessary. The drugs were added to the cells on the 96-well-plate following the scheme in figure 9.

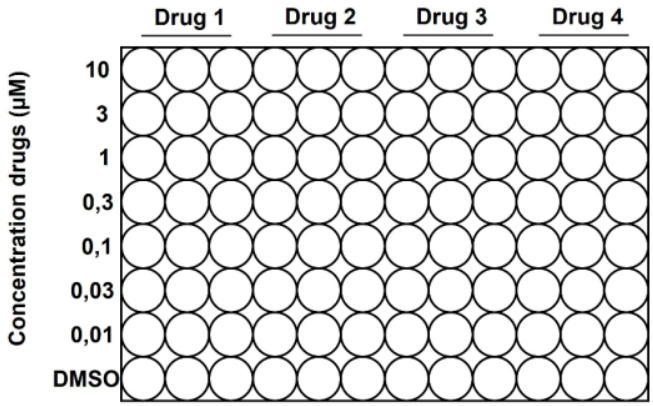

Figure 9: ***Layout of drugs and concentrations on a 96-well-plate.*** *On each plate, four drugs were tested. For every concentration, technical triplicates were performed. The prepared seven-point drug dilutions contained the indicated concentrations. Additionally, the cell lines were treated with the vehicle (DMSO/water) as control.*

In the beginning, the 1,5 ml Eppendorf tubes for the drug dilutions series (seven-point drug dilution: 10 µM – 0,01 µM) were prepared. The stock solutions of the drugs (10mM, frozen at -80°C) were thawed and diluted to 60 µM in DMEM. Afterwards the dilution series were prepared in a 1:3 manner. The DMSO-control was prepared similarly as the stock solutions of the drugs were dissolved in DMSO (exception *Ralimetinib*, which was diluted in H_2O).

20 µl of the drug dilution series and the control dilutions (DMSO/H_2O) were added to each well to achieve the final drug concentrations indicated in figure 9. In the end, the plates were incubated (37°C; 5% CO_2) for 72 hours.

Day 3 + 4:

Incubation in the incubator (37°C; 5% CO_2).

Day 5:

Initially, the *CellTiterGlo* was prepared following the instructions of the manufacturer (Promega Corporation), filled into aliquots and put into the freezer until further use. Prior to use, the *CellTiterGlo* aliquots were thawed. Afterwards, 25 µl *CellTiterGlo* was added to each well in a darkened room. Next, the plates were covered with aluminium foil and put on a shaker for 10 minutes. Afterwards, the plates were incubated for additional 20 minutes, followed by the measurement of the luminescence with the *Fluostar optima-photometer*.

*Figure 10: **Scheme of the screening procedure**. 24 hours after (A) seeding the cells into 96-well-plates, (B) the drug treatment was started. (C) After 72 hours, the CellTiterGlo reagent was added to the wells and after 30 minutes of incubation, (D) the cell viability was measured.*

The results were analyzed using the program *GraphPad Prism 5* after normalizing the raw data to the DMSO control. A scheme of the screening procedure can be viewed in figure 10.

Cell culture: counting cells with Neubauer-chamber

20 µl of the singularized cells were put into a 0,5 ml Eppendorf tube and mixed with 20 µl Trypan blue 0,4%. The chamber and the necessary cover glass were prepared by cleaning them with 80% ethanol, followed by fixing the cover glass on the chamber. Furthermore, 10 µl from the cell-dye suspension was applicated between the cover glass and the chamber. Subsequently, all cells in the 4 quadrants were counted. After counting, the following formula was used to calculate the cells per ml (x = number of cells, counted in all 4 chambers):

$$\frac{x}{2} \times 10^4 \; cells/ml$$

For every screening, 100 µl containing 1000 cells were seeded in every well of the 96-well-plates per cell line. Depending on the result, the cells were diluted to 10000 cells/ml (see above).

Cell culture: harvesting proteins

When the cells were seeded on day 1 of the screening, additionally cells were seeded to 10 cm dishes with 0,5 ml cell suspension into 5 ml DMEM. At 80% confluence in the dishes, the proteins were harvested to confirm the *HDAC-2* knock-out with WesternBlot later. Therefore, the lysis buffer was prepared, which contained 200 µl of IP-buffer, 2 µl phosphatase-inhibitor x100 and 8 µl protease-inhibitor x25 per cm-dish. After aspirating the medium and washing the dishes with 5 ml PBS, 200 µl of the lysis buffer was added on each dish, the cells were collected using a cell scraper. The cell suspension was filled into 1,5 ml Eppendorf tubes and they were blast-froze in liquid nitrogen before storing them in a freezer at -80°C until further use.

Cell viability assay *CellTiterGlo*

The *CellTiterGlo* assay is a method to indirectly measure the viability of cells by measuring the adenosine triphosphate (ATP) level of a cell population via luminescence. The assay binds and reacts with ATP: Catalyzed by luciferase, luciferin reacts together with ATP and O_2 to the luminescent product oxyluciferin (Promega Corporation). The luminescence emission signal is directly linked with ATP-level and cell viability (Promega Corporation).

The *CellTiterGlo* assay consists of 2 components which needed to be prepared prior to use according to the instructions of the manufacturer (Promega Corporation). The prepared reagent was frozen until further use.

The day the prepared *CellTiterGlo* was needed, aliquots were thawed 4 to 5 hours prior to use and therefore put into a darkened place. After thawing, the reagent was added to the 96-well-plates from the screening by adding 25 µl *CellTiterGlo* in each well under light-protection. Afterwards the plates were put on the shaker for 10 minutes, followed by 20 minutes incubation time without shaking, both under light-protection. After incubation, luminescent measurement of the plates with *Fluostar optima-photometer* was performed (gain: 1500, luminescent filter: lens from the top, room temperature).

Bradford reagent and measurement of the protein concentration of samples

The Bradford reagent is an assay used to measure the protein concentration of samples by a photometric measurement. The reagent contains triphenylmethane dye which builds complexes with nonpolar and cationic rests of the tertiary structure of protein. The resulting complex shows an absorption maximum at 595 nm, the reagent itself has an absorption maximum at 470 nm. By change of absorption maximum of a probe, protein concentrations can be measured by comparing them with a calibration curve.

First, the Bradford reagent was mixed with sterile water in a 1:5 manner in a 50 ml falcon tube. Meanwhile a 96-well-plate was prepared. The first 6 wells were necessary for the calibration curve, which was generated by adding BSA 1 µg/µl into the wells in indicated concentrations (figure 11). Meanwhile the protein samples for the measurement were thawed and centrifuged at 4°C for 15 minutes (16000 rpm).

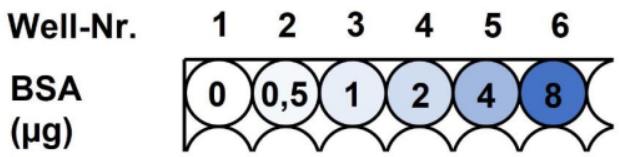

Figure 11: ***Occupancy for the BSA calibration curve****. To receive a calibration curve for the photometric measurement of protein concentration, the first six wells of the plate were used. Therefore, bovine serum albumin (BSA) in different concentrations was added to the prepared Bradford reagent: no BSA was added to the first well, the concentrations of the remaining five wells were 0,5 µg – 8 µg.*

For the sample wells, 1 µl of each sample was added into the prepared 300 µl Bradford reagent (n=3). A change of the color from green to blue was observed after adding standard or sample. Afterwards, the plate was put into the *Anthos-photometer* to measure the absorption at 595 nm.

Gel electrophoresis and WesternBlot

First, the electrophoresis chambers were prepared. Next, the separation gels were prepared and filled into ¾ of the electrophoresis chambers. To prevent formation of air bubbles, a few drops of isopropanol was added on top of the separation gel. After the separation gel polymerized entirely, the stacking gel was prepared and filled on top of the separation gel. A spacer was put into the polymerizing separation gel to form pockets for protein loading.

After the stacking gel polymerized, the protein samples were prepared. Depending on the protein concentrations of the harvested samples (measurement with Bradford reagent, see above), Laemmli-reagent and the protein samples were mixed in an eppendorf tube, to receive 2 µg/µl protein of each sample in the aliquot. Afterwards the aliquots were boiled up for 5 minutes at 95°C to denaturate the proteins. Meanwhile the gels were prepared by removing the spacer and the *Mini-PROTEAN Tetra Cell* were prepared by filling the trough with running buffer.

After the aliquots were boiled up for 5 minutes, 60 µg of protein per sample were filled into the foreseen pockets in the stacking gel. In one of the pockets 1 µl of the *PageRuler* marker was loaded to determine the size of the bands. After the gels were put in the trough, the electrophoresis was started using 80 V. After the samples reached the separation gel, the voltage was raised to 120 V.

Prior to use, one blotting membrane and six prepared Whatman papers were briefly incubated in transfer buffer. In the next step, three Whatman papers were stockpiled, followed by the gel and the blotting membrane, topped with the remaining three Whatman papers. To prevent air bubbles, the pile was smoothened and chucked into

the blotting device, which was put into the blotting chamber filled with transfer buffer. The blotting was started for 120 minutes at 350 mA.

After the blotting was completed, the blotting membrane was washed in PBS two times for 5 minutes, followed by a blocking process with 5% Skim Milk for 30 minutes. Furthermore, the blotting membrane was shrink-wrapped in plastic foil, followed by adding 3 ml of the primary antibody (solved in 5% skim milk/PBS) and putting it on a shaker at 4 °C overnight.

The next day, the primary antibody was aspirated and the membrane was washed two times with PBS for 10 minutes, before the membrane got shrink-wrapped again, followed by adding 3 ml of fluorescent secondary antibody. Again, the membrane was wrapped into aluminum foil to protect the antibodies from light and put on the shaker for 1 hour.

Afterwards, the antibodies were aspirated and the blotting membranes were washed two times with PBS for 10 minutes, before the blotting membrane were shrink-wrapped one last time in plastic foil and 3 ml of the prepared mixture of anti-β-Actin-antibody and the fluorescent secondary antibody were added, followed by wrapping the membrane into aluminum foil and incubating it on the shaker for 1 hour. Finally, the membranes were washed two times with PBS for 10 minutes, prior to scanning them by using *Li-COR-Odysee* (figure 12).

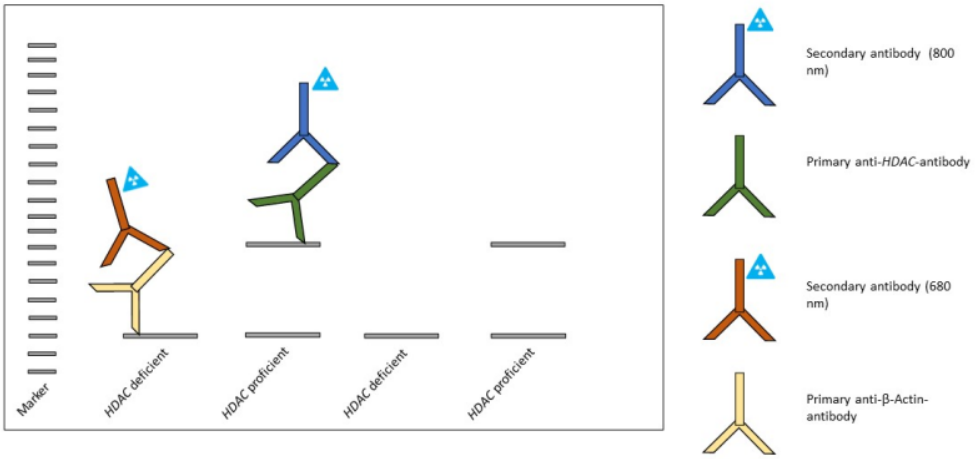

Figure 12: ***WesternBlot****. Draft of the knock-out measurement, exemplary for HDAC-2 knock-out: After the blotting, the membrane gets blocked with skim milk, to prevent untargeted bindings of the antibodies. The primary antibody binds the proteins. The secondary fluorescent antibody binds the primary antibody. The primary anti-β-Actin-antibody and the fluorescent secondary antibody were already mixed together in advance and are added to the membrane in the following step.*

RNA-sequencing

Previously generated and normalized RNA-sequencing data of the *HDAC-2* cell lines F2612 and F1648 were used. Briefly, mRNA was extracted from the Tamoxifen treated cell lines and control cell lines. After quality control with densitometry, RNA-sequencing

was carried out by the facility for genomics and proteomics of the *Deutsches Krebsforschungszentrum*. For more explicit description see Krauß et al., 2022.

The changes in gene expression between *HDAC-2* proficient and deficient cell lines were analyzed using the Log2 fold changes. To generate the Log2 transformed fold changes, the DeSeq2 package in RStudio was used (Krauß et al., 2022).

Cell culture: Tamoxifen treatment for *HDAC-2* knock-out

The dual recombinase system, used to induce *HDAC-2* knock-out in murine PDAC cell lines, has already been described previously (Schönhuber et al., 2014; Kim et al., 2018).

First, cells were seeded on 10 cm dishes and treated with 4-OH-Tamoxifen (diluted in 100% ethanol) for 8 days. This induced *HDAC-2* knock-out due to the recombinase system. Since 4-OH-Tamoxifen (dissolved in ethanol 100%) is less stable in solution and when exposed to UV-light, 600 nM 4-OH-Tamoxifen was added each day by changing the media supplemented with 4-OH-Tamoxifen and the cells were split every 2-3 days. The control cell lines were treated simultaneously with the same amount of vehicle (ethanol). After finishing the treatment, the cells were labeled with T8d (treatment with 4-OH-Tamoxifen -> *HDAC-2* knock-out) or E8d (treatment with ethanol -> no *HDAC-2* knock-out) and proteins were harvested to confirm the knock-out of *HDAC-2* with WesternBlot.

Cell culture: Clonogenic assay

24-well-plates were used and 1000 cells/well (*HDAC-2* proficient or deficient) singularized in 500 µl of DMEM were seeded. 24 hours later, the drug dilutions of *Erastin* (100 µl 6-fold concentration of the final indicated concentrations) were added to the wells (figure 13).

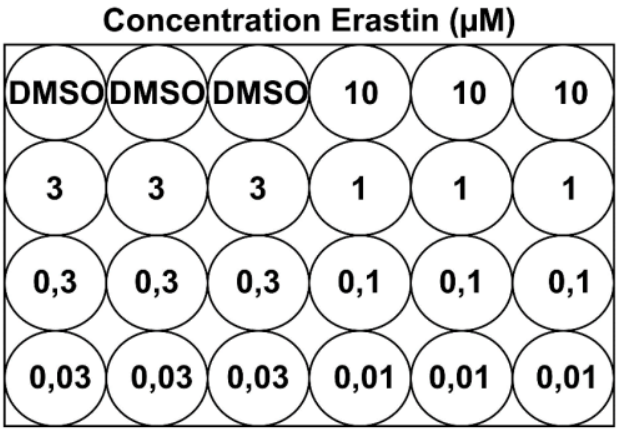

*Figure 13: **Clonogenic assay**. Layout of the 24-well-plates for the Erastin concentrations: after seeding 1000 cells in every well, drug dilutions of Erastin (0,01 µM – 10 µM) and, as Erastin was solved in DMSO, the DMSO control was added to the wells. To achieve technical triplicates, three wells were needed for every concentrations/control.*

DMEM was changed every second/third day. On day 7 after seeding the cells the medium was removed and the wells were washed carefully using 1 ml of PBS. After removing the PBS, each well was carefully filled with 200 µl of 0,2% *CrystalViolett*-solution, to fix and stain the cells. After 10 minutes of incubation, the *CrystalViolett* solution was removed, followed by washing the wells two times with 1 ml of water for 60 minutes. After the second washing process, the water was removed, and the plates were left for drying. After the plates were dry, they were scanned and subsequently 600 µl of 1% SDS was added to every well to solubilize the *CristalViolett* staining in the wells. After incubation of 2,5 hours, the *CLARIOstar-photometer* was used for photometric measurement.

Calculation of the z-score and definition of hits in the screening

The results of the IC_{50}-values and the AUC-values of the screening were analyzed by calculation of the z-scores. The z-score (z_i) is the amount of standard deviations (s) above or below a certain data (x_i) from the mean ($\bar{x}$).

$$z_i = \frac{x_i - \bar{x}}{s}$$

For example: $z_{IC50-Erastin\ F2612E8d} = \frac{x_{IC50-Erastin\ F2612E8d} - \overline{x_{IC50\ of\ Erastin\ in\ all\ tested\ cell\ lines}}}{Standarddeviation\ IC50\ all\ cell\ lines}$

Afterwards, the difference between the z-scores of the Tamoxifen-treated cell lines and the corresponding ethanol-treated cell lines was calculated:

$$\Delta z = z_{Tamoxifen} - z_{Ethanol}$$

A drug was defined as a hit when Δz-score of IC_{50} as well as Δz-score of AUC-values in both *HDAC-2* cell lines were <0. A negative Δz indicated a higher sensitivity of the tested drug in *HDAC-2* deficient cell lines. Afterwards the dose-response curves of the drugs were analyzed manually to confirm the observed results.

Cell culture: Combination treatment of *HDAC-2* proficient cells with *Erastin* and *MS-275*

To further validate the results from the screening, *HDAC-2* proficient cell lines F2612 and F1648 were treated with a combination treatment of *Erastin* and *MS-275*. Therefore, we performed cell viability assays using *CellTiterGlo* (for more information regarding *CellTiterGlo* see "Cell viability assay *CellTiterGlo*"). The cell lines were treated with *Erastin* (10-0,01 µM) and *MS-275* (2 µM or 4 µM) (figure 14). To determine the differences between the combination and a treatment with each compound alone, the cell lines were simultaneously treated with only *Erastin* or *MS-275*.

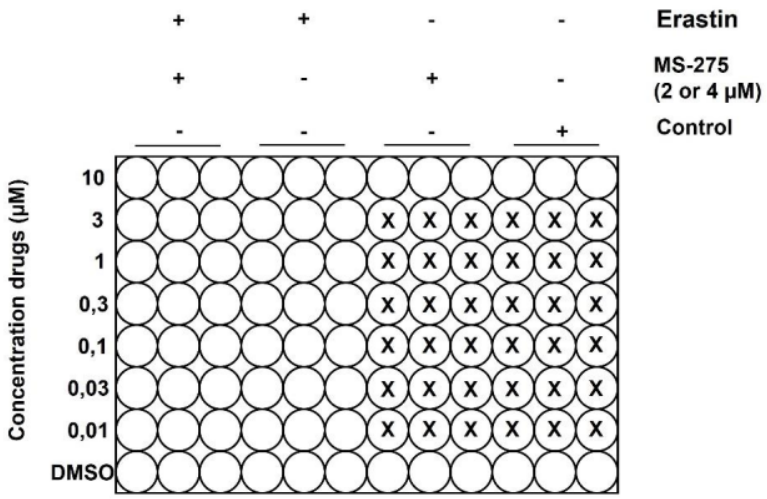

*Figure 14: **Layout for the validation experiments (Erastin + MS-275) with a 96-well-plate using cell viability assay**. HDAC-2 proficient cell lines were simultaneously treated with a combination of Erastin and MS-275 (2 or 4 µM), Erastin only and MS-275 only.*

Synergy Finder

To identify a potential synergy between *Erastin* and *MS-275*, the online tool *SynergyFinder* was used (https://synergyfinder.fimm.fi). It compares measured drug responses with expected drug combination responses calculated by means of synergy scoring models. The used synergy scoring model was the *Zero interaction model* (*ZIP-model*), which quantifies the degree of synergy and the expected response as the single compounds wouldn't affect the potency of each other and models the drug interaction by comparing the change in potency of each drug with the dose-response curve of the combination (Yadav et al., 2015; SynergyFinder, 2020; Ianevski et al., 2022).

Clonogenic assays (n=3) of F2612 were performed and measured as previously described (see "Clonogenic Assay"), six 24-well-plates were seeded, and the cells were treated with *Erastin* (3 µM – 0,1 µM) and *MS-275* (4 µM – 0,0625 µM) in technical triplicates (figure 15).

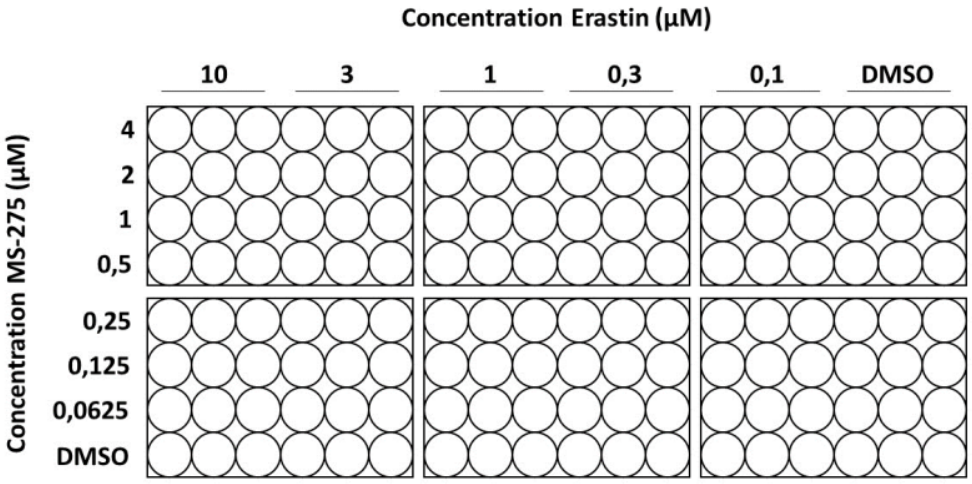

*Figure 15: **Clonogenic matrix for synergy finder**. Layout for the cell treatment with Erastin and MS-275 with indicated concentrations.*

To receive representative synergy scores after measurement, the highest (and lowest for MS-275) concentrations (10 and 3 μM for Erastin, 4 μM and 0,0625 μM for MS-275) were removed prior to analysis. Next, the values of the individual concentration treatments were uploaded as a table to the *SynergyFinder*-tool. "ZIP-model" as reference model and "Inhibition" as readout was chosen. All other settings were set to default. The tool subsequently calculated synergy scores (mean and highest), dose-response curves, dose-response matrix and visualized the synergy scores with 3D and 2D models. Furthermore, dose-response curves of the multi-dimensional synergy of combination (MuSyC) reference model were created by the tool. MuSyC reveals if an observed synergy is caused due to enhanced potency or/and efficacy of the compounds (Ianevski et al., 2022).

Gene set enrichment analysis (GSEA)

GSEA offers the possibility to compare *HDAC-2* proficient and deficient PDAC cells (F2612 and F1648) regarding significantly enriched pathways. Previously generated RNA-sequencing data were used and analyzed, using the software *GSEA 4.0.3* (Mootha et al., 2003; Subramanian et al., 2005). Briefly, rlog transformed countmatrix of RNA-sequencing data was used to compare *HDAC-2* proficient and deficient cell lines.

To detect overlapping positively or negatively enriched pathways in F2612 and F1648, the pathways with adjusted p-values <0,05 in F2612 and F1648 were compared using *Venny 2.1*.

Statistics

Unless stated otherwise, experiments were done in at least biological and technical triplicates. The screening was performed as one biological replicate in technical triplicates. Validation experiments were additionally performed in biological triplicates. For comparison of two independent kind of cell lines (*HDAC-2* proficient and deficient cell lines) regarding the consequences of the treatments, unpaired t-test (two tailed) was used to explore statistical significance, except for the evaluation of significance towards the findings from *SynergyFinder* (one-way analysis of variance with Bonferroni's multiple comparison test was used to determine significance). *GraphPad Prism 5* was used to visualize the results and perform the statistical calculations. No statistical method was used to predetermine sample size. The experiments were not randomized. The investigator was not blinded to allocation during experiments and outcome assessment.

Results

Drug screening and validations

To identify new HDACi-based combination therapies against PDAC, an explorative unbiased drug screening using 101 drugs targeting a variety of targets (see tables 12 – 20 in materials) in different concentrations was performed in two *HDAC-2* proficient and *HDAC-2* deficient PDAC cell lines (F1648, F2612). The knock-outs were confirmed on protein level by performing WesternBlots (figure 16).

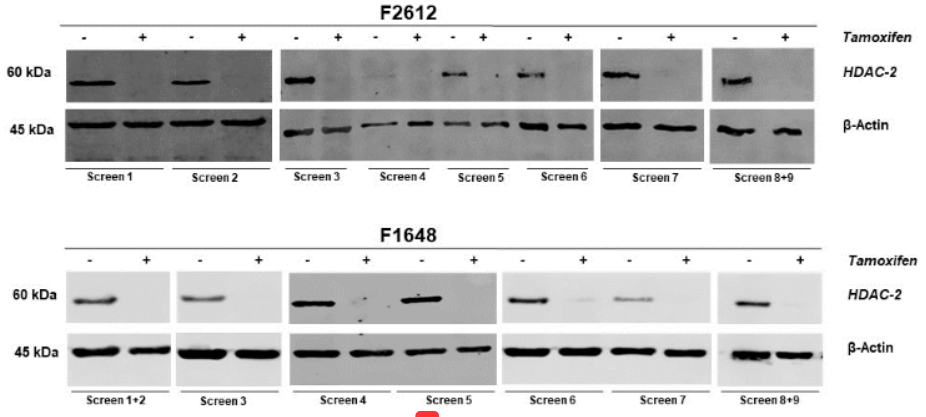

*Figure 16: **Tamoxifen induces HDAC knock-out in murine PDAC cell lines**. Indicated murine PDAC cell lines were treated with ethanol or Tamoxifen (600 nM, 8 days). Knock-out of HDAC-2 was confirmed on a protein level using Western Blot analysis. β-actin was used as a loading control.*

As a screening result, we observed differences in drug sensitivity between proficient and deficient cell lines. For analysis the IC_{50}- and AUC-values of the dose-response curves were used (tables 25 - 26) and the z-scores were calculated (table 27). Based on the IC_{50}- and AUC-values, the z-ratios (Δ z-scores) between proficient and deficient cell lines were calculated (table 28). A drug was defined as a hit, if z-ratios of IC_{50} and AUC were both negative in the *HDAC-2* cell lines F2612 and F1648, indicating increased drug sensitivity in *HDAC-2* deficient cell lines (figure 17 B, C and D).

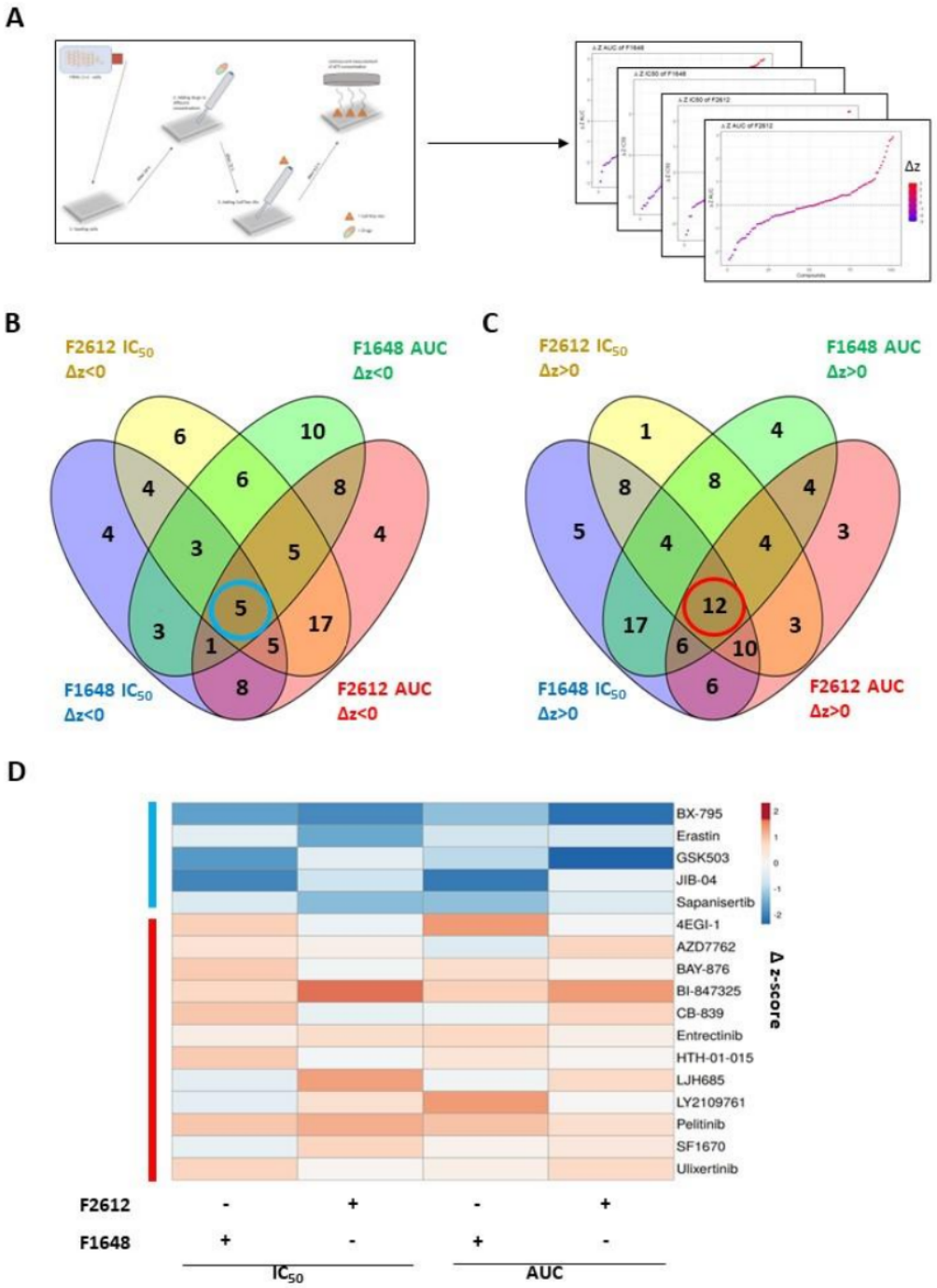

*Figure 17: **Definition of screening hits in HDAC-2 cell lines**. (A) Visualization of screening hits and analysis of the results. (B) shows the overlap of the calculated negative z-ratios. (C) shows the overlap of the calculated positive z-ratios. (D) Heatmap of the overlapping compounds (negative z-rations shown in blue, positive z-rations shown in red).*

Consequently, five drugs were identified as hits (figure 17 B and D and table 21). Furthermore, curve fitting was confirmed manually.

Table 21: Overview over Δz-scores of identified compound hits.

	Δz IC_{50} F1648	Δz IC_{50} F2612	Δz AUC F1648	Δz AUC F2612
BX-795	-1,881	-1,346	-1,021	-2,171
Erastin	-0,030	-1,062	-0,305	-0,505
GSK503	-1,958	-0,051	-0,595	-2,321
JIB-04	-2,327	-0,418	-2,131	-0,103
Sapanisertib	-0,251	-0,831	-1,015	-0,359

In order to validate the identified hits, we first repeated the viability experiments (figure 18) and were able to confirm the results of *Erastin* and *JIB-04*. For *Erastin*-treatment in *HDAC-2* deficient cell lines we observed a significant reduction of IC_{50}-values of 38,11% in F2612 and 39,85% in F1648 as well as a reduction of AUC-values of 9,22% in F2612 and 15,70% in F1648 compared to the *HDAC-2* proficient cell lines. For *JIB-04*-treatment in *HDAC-2* deficient cell lines we observed a significant reduction of IC_{50}-value of 29,77% in F2612 and 57,94% in F1648 as well as a reduction of AUC-value of 7,42% in F2612 and 36,78% in F1648 compared to *HDAC-2* proficient cell lines (table 22). To calculate the reduction of AUC- and IC_{50}-values, the following equation was used: $\text{Reduction}_{IC50/AUC} = (1 - \frac{T8d}{E8d}) \times 100$ [%].

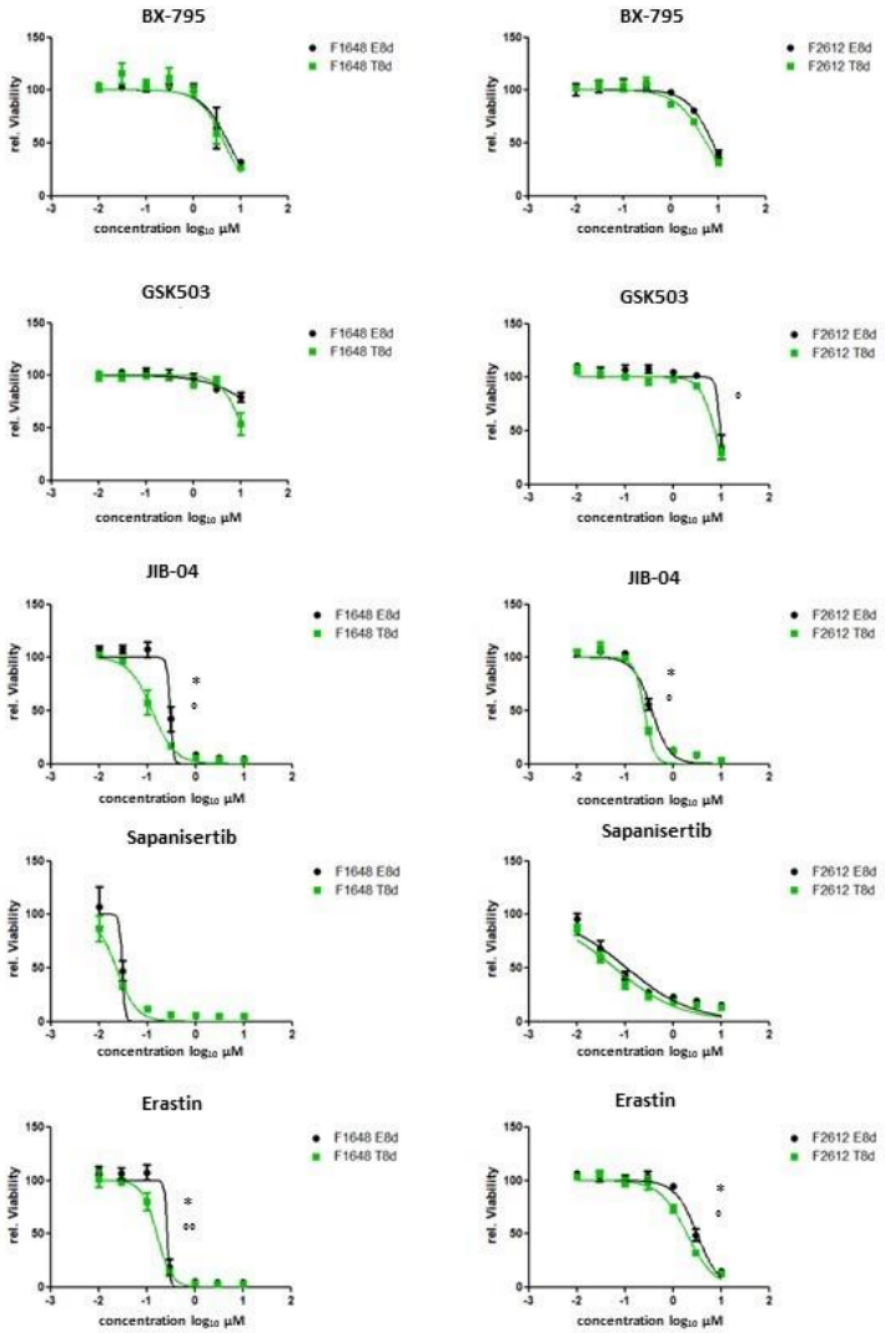

*Figure 18: **Dose-response curves of the identified hits with cell viability assay**. After the screening, hits were validated (n=3 biologically independent samples) and dose-response were generated for F1648 and F2612. Measurement of cell viability after 72 hours by using CellTiter-Glo assay. Significance of the biological triplicates were calculated by using unpaired t-test (°p_{AUC} <0,05; °°p_{AUC} <0,01, *p_{IC50} <0,05). Data are presented as mean values +/- SEM.*

Table 22: ***Overview and comparison of IC_{50}- and AUC-values in cell viability assay.*** *n=3 biologically independent samples.*

		F1648 *HDAC-2* (+)	F1648 *HDAC-2* (-)	F2612 *HDAC-2* (+)	F2612 *HDAC-2* (-)
BX-795	**IC_{50} (µM)**	5,461	4,491	7,576	5,594
	AUC	605,8	562,5	698,2	612,7
	Reduction IC_{50}	17,76%		26,16%	
	Reduction AUC	7,15%		12,25%	
Erastin	**IC_{50} (µM)**	0,271	0,163	3,175	1,965
	AUC	149	125,6	256	232,4
	Reduction IC_{50}	39,85%		38,11%	
	Reduction AUC	15,70%		9,22%	
GSK503	**IC_{50} (µM)**	47,37	10,86	9,410	7,296
	AUC	863,9	799,0	791,7	713,6
	Reduction IC_{50}	77,07%		22,47%	
	Reduction AUC	7,51%		9,86%	
JIB-04	**IC_{50} (µM)**	0,2927	0,1231	0,3554	0,2496
	AUC	96,09	60,75	111,9	103,6
	Reduction IC_{50}	57,94%		29,77%	
	Reduction AUC	36,78%		7,42%	
Sapanisertib	**IC_{50} (µM)**	0,02976	0,02244	0,1083	0,06125
	AUC	53,44	56,03	192,9	159,4
	Reduction IC_{50}	24,69%		43,44%	
	Reduction AUC	-4,85%		17,37%	

We further evaluated *Erastin*. *Erastin* is a ferroptosis inducer, targeting the cystine-glutamate antiporter x_c^- and opens voltage dependent anion channels in the outer mitochondrial membrane (VDAC) and thus leads to ferroptosis, a non-apoptotic cell death (Yagoda et al., 2007; Dixon et al., 2012; Cao and Dixon, 2016; Conrad and Pratt, 2019).

Effect of *Erastin* treatment with the mean IC_{50}-value concentration of F2612 (2,57 µM) on *HDAC-2* proficient and deficient PDAC cells was visualized after 72 hours (figure 19).

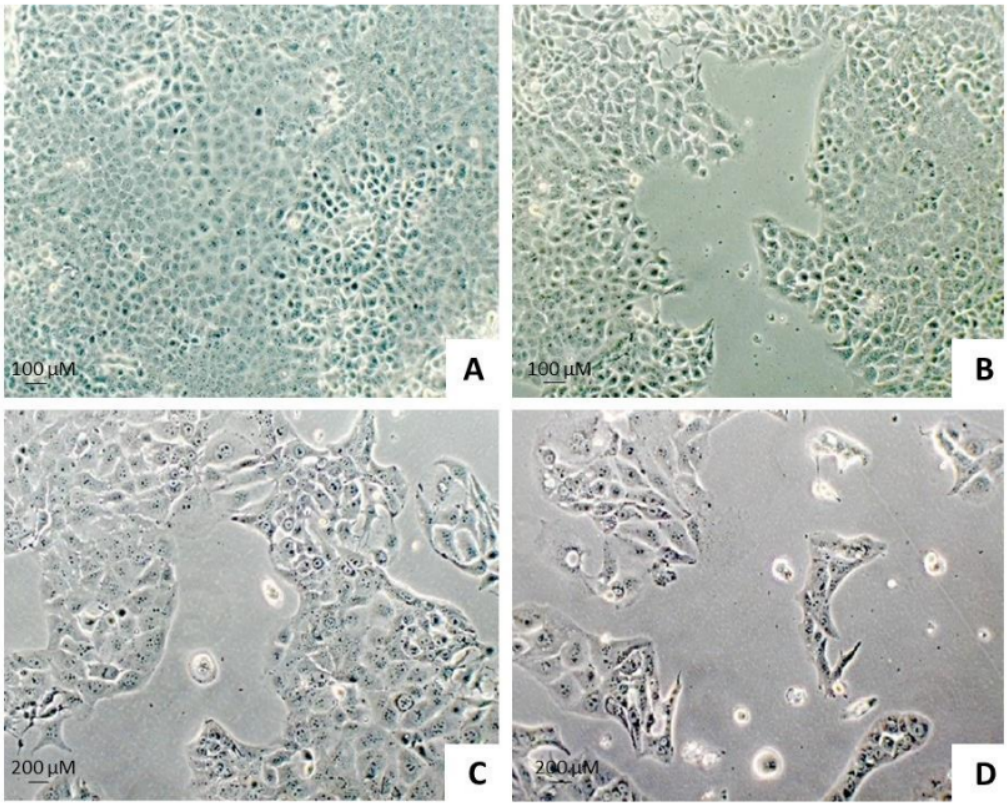

Figure 19: ***Pictures of cell lines treated with DMSO or 2,57 µM Erastin (F2612)****. Treatment of HDAC-2 proficient cells with (A) DMSO (control) or (C) Erastin 2,57 µM. Treatment of HDAC-2 deficient cells with (B) DMSO (control) or (D) Erastin 2,57 µM. The pictures taken were representative to the cell density in the dish.*

Next, we further validated the effect of *Erastin* in clonogenic assays (n=3) using the cell line F2612. We could confirm the reduction in clonogenic growth in *HDAC-2* deficient cell lines after 7 days of *Erastin* treatment, however the findings were not significant (figure 20). The clonogenic growth curve was used to determine AUC- and IC_{50}-values. Thus, for F2612 we observed a reduction of 42,59% for IC_{50}-value and 19,42% for AUC-value (table 23).

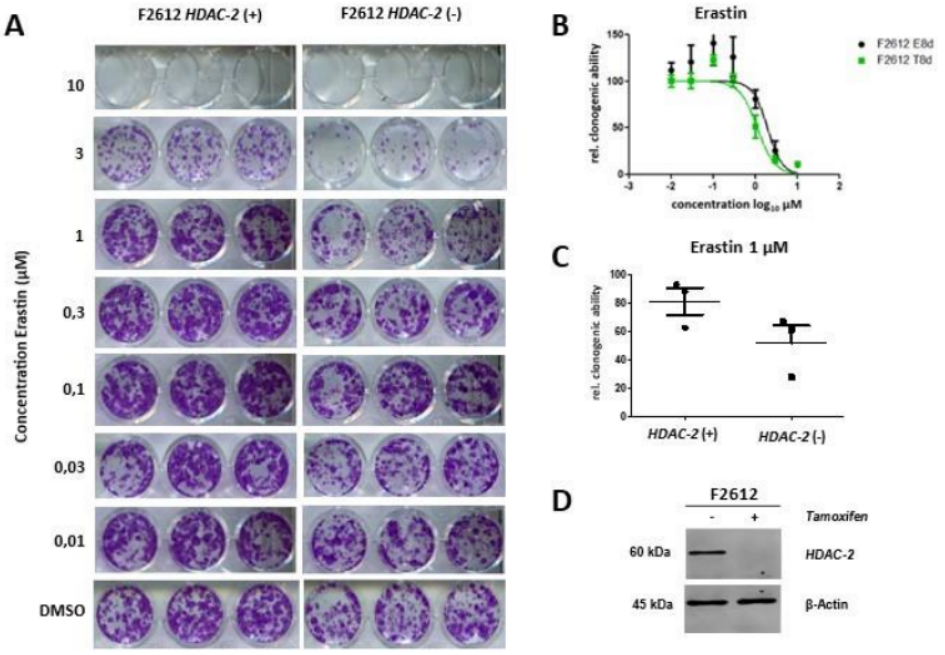

*Figure 20: **Validation of the effect of Erastin with clonogenic assay**. (A) Visualization of the clonogenic growth: HDAC-2 proficient and deficient cell line (F2612) treated with Erastin with indicated concentrations for 7 days. (B) Dose-response curve of clonogenic assay (n=3 biologically independent samples, ns). (C) Reduction of the relative clonogenic growth of HDAC-2 proficient and deficient cell lines (F2612) treated with Erastin 1 µM (ns, two-tailed unpaired t-test), this concentration showed the biggest difference in clonogenic growth between proficient and deficient cells. (D) Indicated urine PDAC cell lines were treated with ethanol or Tamoxifen. Knock-out of HDAC-2 was confirmed on a protein level using Western Blot analysis. β-actin was used as a loading control. All data are presented as mean values +/- SEM.*

*Table 23: **Clonogenic assay mean IC_{50}- and AUC-values and its reductions**. Mean IC_{50}- and AUC-values and its reductions comparing HDAC—2 proficient and deficient cells from the clonogenic assay experiments (n=3 biologically independent samples) with Erastin (F2612): the combination of HDAC-2 deficiency and Erastin treatment show a reduction of 42,59% for IC_{50}- and a reduction of 19,42% for AUC-value.*

	F2612 *HDAC-2* (+)	F2612 *HDAC-2* (-)
IC50 (µM)	1,965	1,128
AUC	277,1	223,3
Reduction IC_{50}	42,59% (ns)	
Reduction AUC	19,42% (ns)	

Analysis of combination of *Erastin* and *MS-275* with *HDAC-2* proficient cells

To evaluate if the observed effects in the genetic models were reproducible and could be translated in an actual pharmacological treatment, *HDAC-2* proficient cell lines F2612 and F1648 were receiving a treatment with *Erastin* and *MS-275*. Cell viability assay *CellTiterGlo* was performed for evaluation.

The results showed a reduction of cell viability in cell lines receiving the combination of *Erastin* and *MS-275* compared to those receiving either one of them (figure 21). For F1648 cell line receiving the combination of *Erastin* and *MS-275* 2 µM (n=2) we

observed a reduction of IC_{50}-value of 57,93% and a significant reduction of AUC-value of 25,30%, in F2612 we observed for this drug combination (n=2) a reduction of IC_{50}-value of 69,01% and a reduction of AUC-value of 26,80%. In cell lines treated with Erastin and MS-275 4 μM, we observed in F1648 (n=2) a reduction of IC_{50}-value of 97,23% and a significant reduction of AUC-value of 51,24% and in F2612 we observed for this drug combination (n=2) a reduction of IC_{50}-value of 98,45% and a reduction of AUC-value of 49,74%.

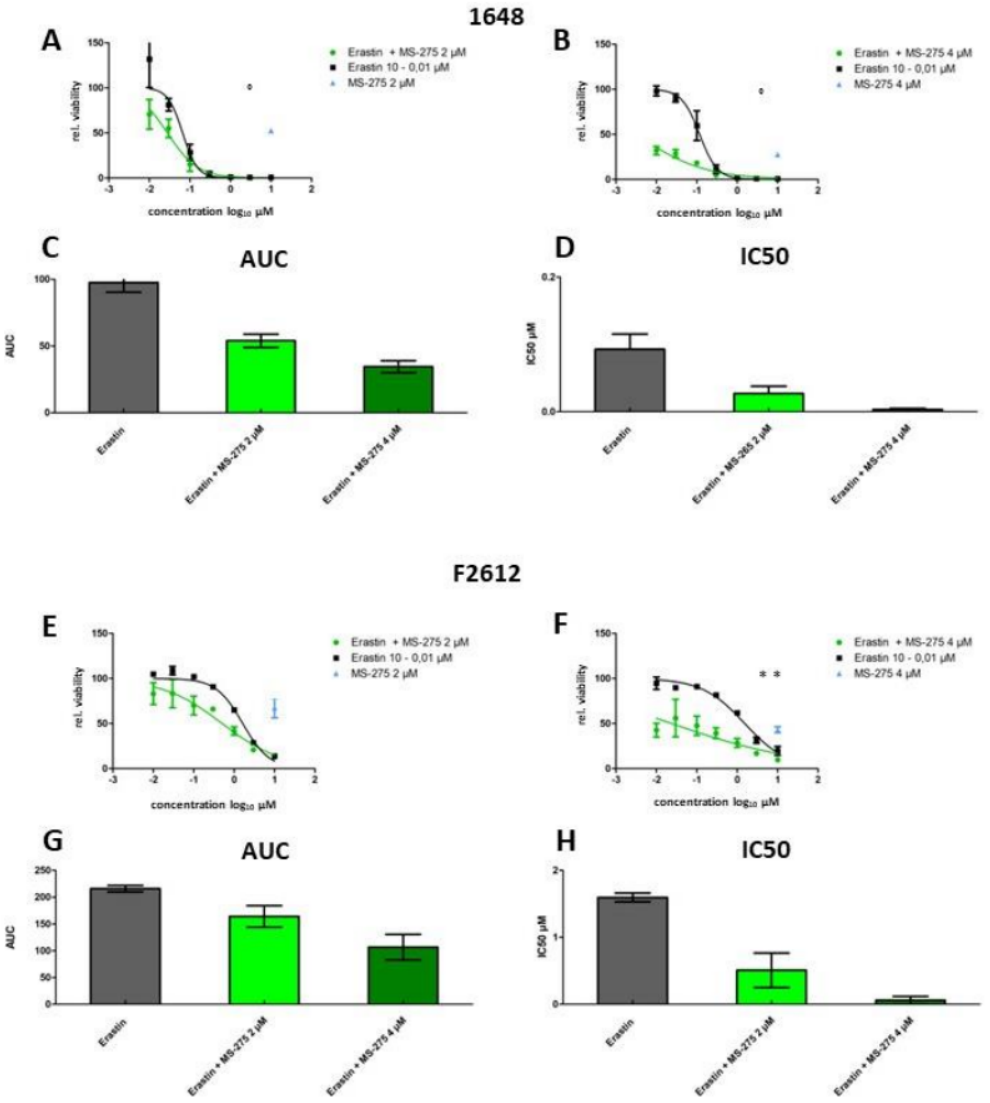

Figure 21: ***Combination treatment of HDAC-2 proficient cell lines F2612 and F1648 with Erastin and MS-275 using cell viability assay****. Treatment of (A) F1648 and EB) F2612 with Erastin and MS-275 2 µM. Treatment of (B) F1648 and (F) F2612 with Erastin and MS-275 4 µM. Comparison of AUC-values of the duplicates of (C) F1648 and (G) F2612. Comparison of IC_{50}-values of the duplicates of (D) F1648 and (H) F2612. Significance of the biological duplicates were calculated by using unpaired t-test (°p_{AUC} <0,05; **p_{IC50} <0,01). All data are presented as mean values +/- SEM (n=2 biologically independent samples). The presented data were generated with the support of Lukas Krauß.*

Analysis of synergy

Based on the results, we next wanted to evaluate if synergy between *Erastin* and *MS-275* exists. Therefore, we used the online tool *SynergyFinder* (https://synergyfinder.fimm.fi). We calculated the synergy score for clonogenic assay in *HDAC-2* proficient cell line F2612 (n=3) (figure 22). *SynergyFinder* compares the observed drug combination responses (e.g. dose-response matrix) with the expected responses calculated by means of synergy scoring models (reference model), leading to classification of synergy or antagonism depending on observed deviation (Ianevski et al., 2022). The used reference model was the *Zero interaction potency model* (*ZIP-model*). The ZIP-model quantifies the degree of synergy and the expected response as if the single drugs wouldn't affect the potency of each other and it models the drug interaction by comparing the change in potency of the dose-response curves of each drug with the dose-response curve of the combination (Yadav et al., 2015; SynergyFinder, 2020). For each measured dose combination, an individual synergy score is visualized to find the most synergistic area. The synergy score is averaged over all the measured dose combinations. *SynergyFinder* defines the results of the synergy score as followed:

- ZIP < -10 antagonistic
- -10 < ZIP < 10 additive
- ZIP > 10 synergistic

With help of *SynergyFinder* we were able to show existing synergy between *Erastin* and *MS-275* with a summery synergistic score of 14,05 and a most synergistic area score of 18,95 (figure 23 A – C). The best synergy (34,07) was observed for a combination of *µM MS-275* and 0,3 *µM Erastin*. To determine significance of the findings, one-way analysis of variance with Bonferroni's multiple comparison test was performed showing a significant difference between cells treated with *Erastin* 0,3 *µM* in combination with *MS-275* 1 *µM* compared to cells only treated with *MS-275* 1 *µM* (figure 23 F). Generated combination dose-response-curves of the multi-dimensional synergy of combinations (MuSyC) reference model revealed that a synergistic potency shift with a fold change of 4,59 for *Erastin* treated cells induced by *MS-275* can be detected (figure 23 D) as well as a synergistic potency shift with a fold change of 21,44 for cells treated with *MS-275* induced by *Erastin* (figure 22 E).

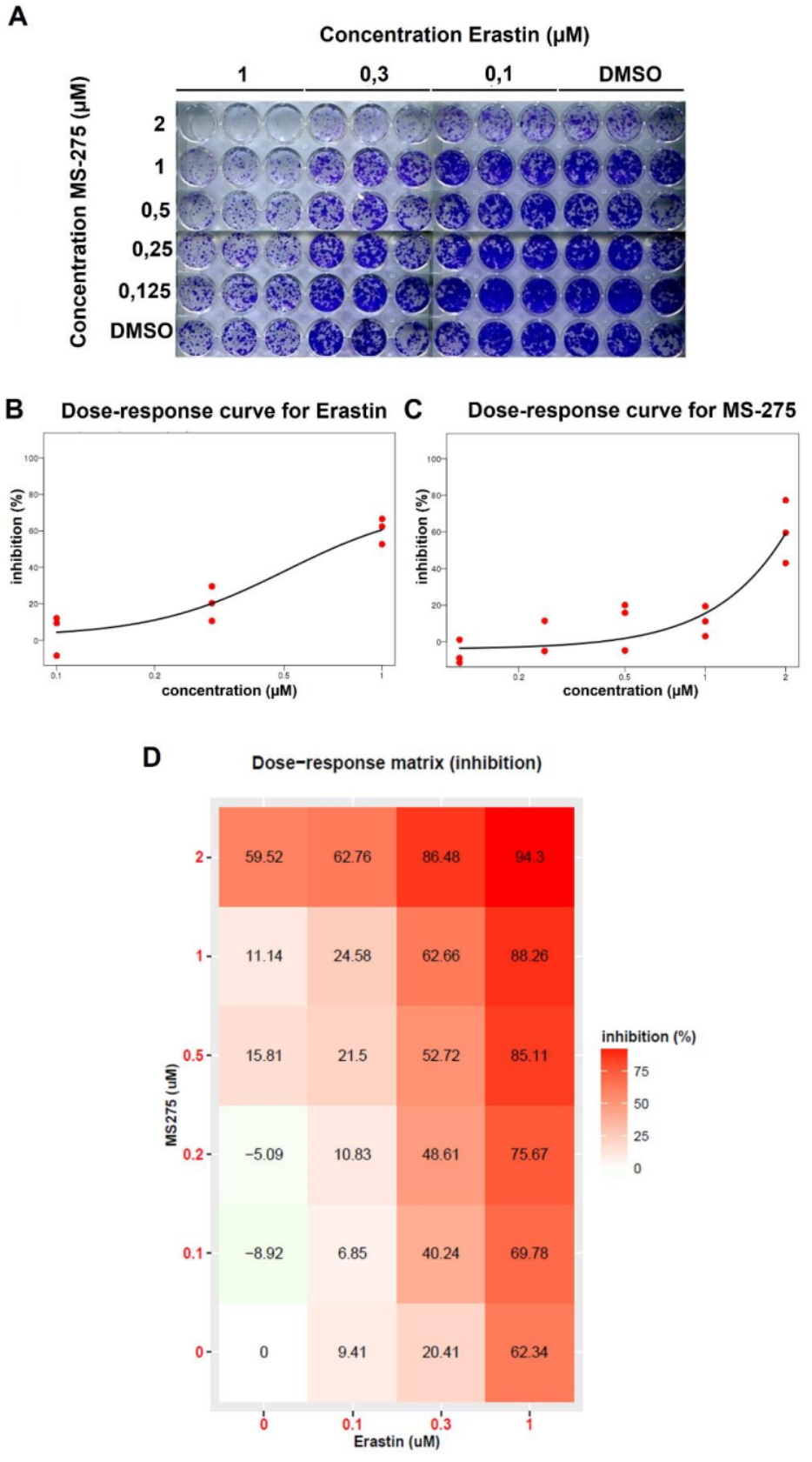
A
Concentration Erastin (µM)
1
0,3
0,1
DMSO
Concentration MS-275 (µM)
2
1
0,5
0,25
0,125
DMSO
B
Dose-response curve for Erastin
inhibition (%)
concentration (µM)
C
Dose-response curve for MS-275
inhibition (%)
concentration (µM)
D
Dose−response matrix (inhibition)
2
1
0.5
0.2
0.1
0
59.52
62.76
86.48
94.3
11.14
24.58
62.66
88.26
15.81
21.5
52.72
85.11
−5.09
10.83
48.61
75.67
−8.92
6.85
40.24
69.78
0
9.41
20.41
62.34
MS275 (uM)
0
0.1
0.3
1
Erastin (uM)
inhibition (%)
75
50
25
0

Figure 22: ***SynergyFinder matrix and input dose-response curves****. (A) Matrix generated with clonogenic assay: HDAC-2 proficient cell line (F2612) treated with Erastin and MS-275 with indicated concentrations for 7 days. Dose-response curves generated with clonogenic assay (n=3 biologically independent samples) after treatment with (B) Erastin or (C) MS-275. (D) Dose-response matrix generated by SynergyFinder showing inhibiton of cell viability after combination treatment of Erastin and MS-275 with indicated concentrations. The presented data were generated with the support of Lukas Krauß.*

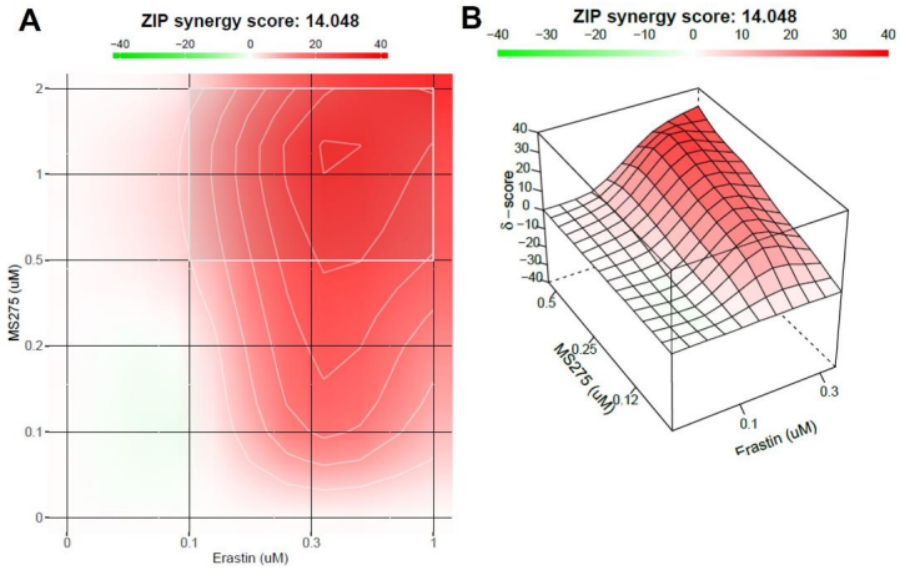

C

Drug combination	Synergy score	Most synergistic area score	Method
Erastin - MS275	14.05	18.95	ZIP

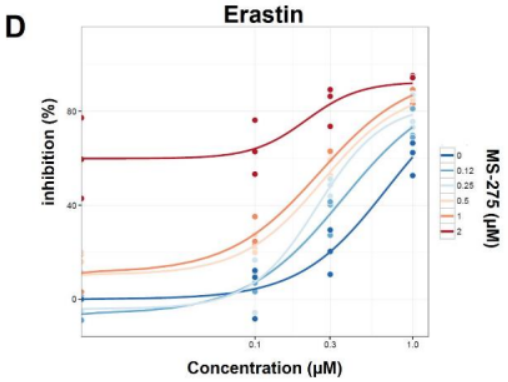

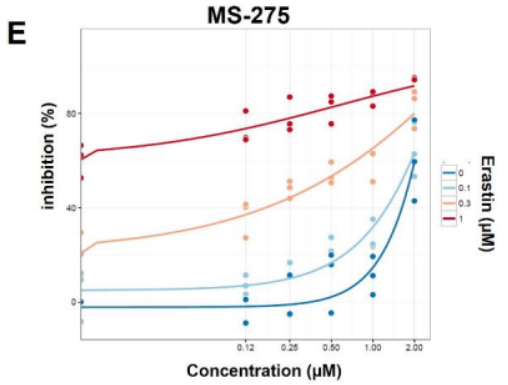

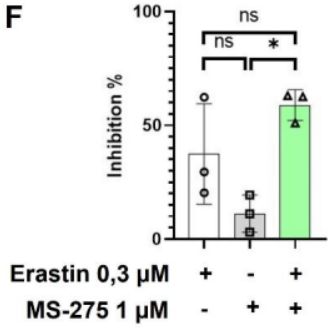

*Figure 23: **Visualization of synergy between Erastin and MS-275**. (A) 2D and (B) 3D synergy map highlighting synergistic regions, showing (C) a summery synergy score of 14,05 and a most synergistic area score of 18,95 (using ZIP-model). (D) Combination dose-response curves of the multi-dimensional synergy of combinations (MuSyC) reference model showing a synergistic potency shift of Erastin treated cells induced by MS-275 (fold change: 4,59) or (E) a synergistic potency shift of MS-275 treated cells induced by Erastin (fold change 21,44). (F) Significant difference in cell viability between cells treated with Erastin 0,3 µM and MS-275 1 µM compared to cells only treated with MS-275 1 µM (One-way ANOVA with Bonferroni's multiple comparison test). n=3 biologically independent samples.*

Analysis of RNA-sequencing data

RNA-sequencing data of *HDAC-2* cell lines F2612 and F1648 previously generated were used. The data were analyzed regarding genes relevant for induction of ferroptosis and HDAC inhibition as well as genes which are relevant in the pathways showing positive enrichment in *HDAC-2* proficient cell lines in GSEA (see below). SLC7A11 and VDAC2 are direct targets of *Erastin* (Conrad and Pratt, 2019; Zhao et al., 2020). GPX4 is an important enzyme for detoxification of reactive oxygen species and needs glutathione as cofactor (Yang et al., 2014). EIF2AK4 is a kinase, leading to phosphorylation of the eucaryotic translation initiation factor eIF2α, which activates the integrated stress response against cellular stress via ATF4 (table 24) (Suragani et al., 2012; B'chir et al., 2013; Wortel et al., 2017).

*Table 24: **Extract from the RNA-sequencing data necessary for the thesis**. (NA = no data) The Log2 Fold Change (Log2FC) is a ratio comparing the gene expression between HDAC-2-proficient and -deficient cells. A negative Log2FC equals a lower expression in the deficient cells, while a positive Log2FC means a higher expression in the deficient cells. The p-value as indicator for significance shows, that not all data from the sequencing are statistically significant. Especially ATF4 shows significantly lower resp. higher expression in the HDAC-2-deficient cells in both cell lines.*

	F2612		F1648	
	Log2FC	p-value	Log2FC	p-value
SLC7A11	-0,96	0,181	-0,62	0,003
ATF4	-0,69	0,003	-0,33	0,002
EIF2AK4	-0,13	0,4	0,09	0,155
GPX4	0,11	0,524	0,01	0,926
VDAC2	0,15	0,252	-0,13	0,255

Analysis of Gene set enrichment analysis

Gene set enrichment analysis (GSEA) using the previously generated RNA-sequencing data of *HDAC-2* cell lines F2612 and F1648 was performed to determine the behavior of the cell lines after *HDAC-2* knock-out. We overlapped the results from each cell line. We confirmed five enriched Reactome pathways in *HDAC-2* proficient cell lines, including the transport of amino acids across the plasma membrane, the response of kinases to amino acid deficiency and heme deprivation and the cellular response to starvation (figure 24).

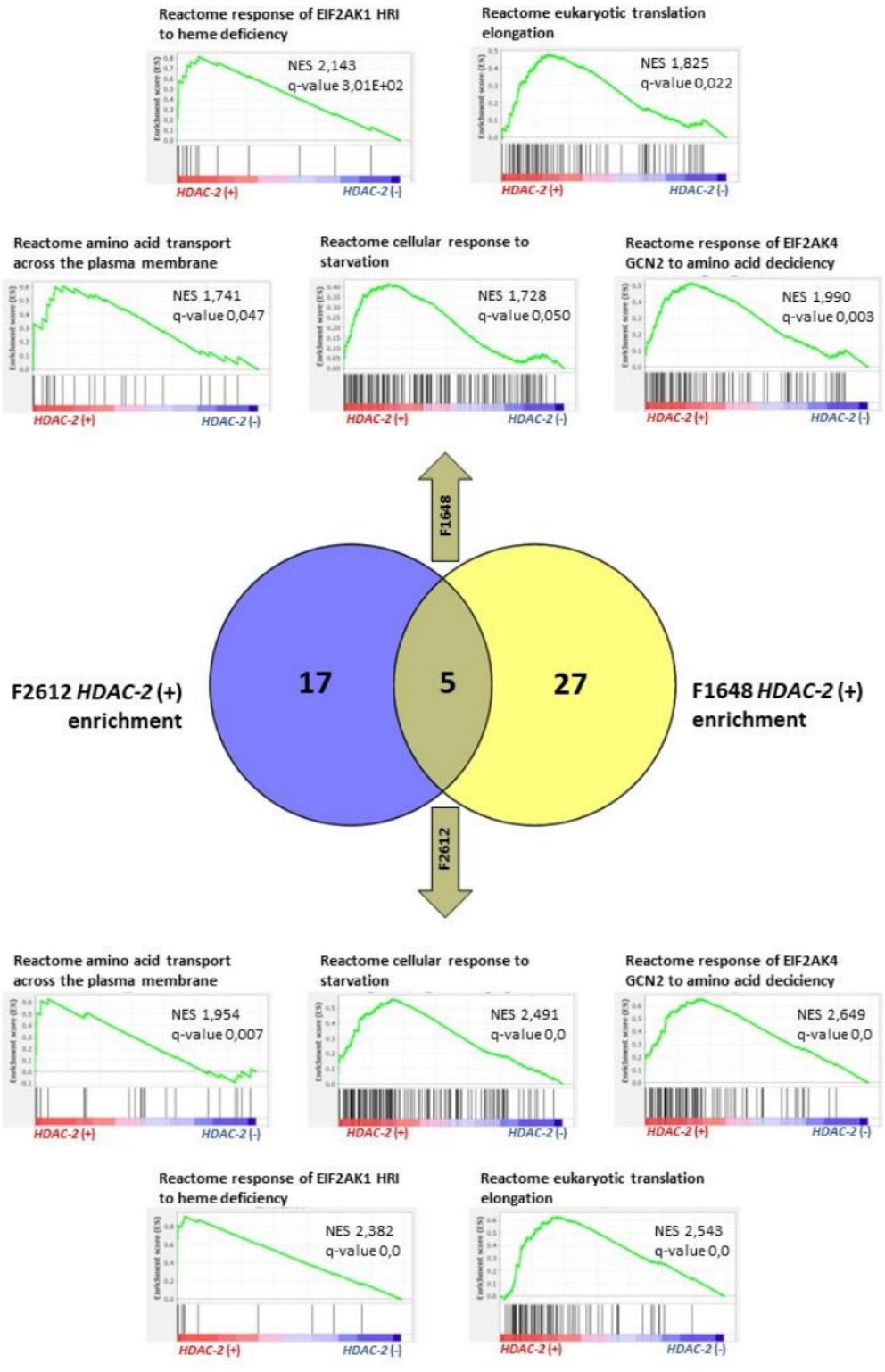
Reactome response of EIF2AK1 HRI to heme deficiency
NES 2,143
q-value 3,01E+02
HDAC-2 (+)
HDAC-2 (-)
Reactome eukaryotic translation elongation
NES 1,825
q-value 0,022
HDAC-2 (+)
HDAC-2 (-)
Reactome amino acid transport across the plasma membrane
NES 1,741
q-value 0,047
HDAC-2 (+)
HDAC-2 (-)
Reactome cellular response to starvation
NES 1,728
q-value 0,050
HDAC-2 (+)
HDAC-2 (-)
Reactome response of EIF2AK4 GCN2 to amino acid deciciency
NES 1,990
q-value 0,003
HDAC-2 (+)
HDAC-2 (-)
F1648
17
5
27
F2612 HDAC-2 (+) enrichment
F1648 HDAC-2 (+) enrichment
F2612
Reactome amino acid transport across the plasma membrane
NES 1,954
q-value 0,007
HDAC-2 (+)
HDAC-2 (-)
Reactome cellular response to starvation
NES 2,491
q-value 0,0
HDAC-2 (+)
HDAC-2 (-)
Reactome response of EIF2AK4 GCN2 to amino acid deciciency
NES 2,649
q-value 0,0
HDAC-2 (+)
HDAC-2 (-)
Reactome response of EIF2AK1 HRI to heme deficiency
NES 2,382
q-value 0,0
HDAC-2 (+)
HDAC-2 (-)
Reactome eukaryotic translation elongation
NES 2,543
q-value 0,0
HDAC-2 (+)
HDAC-2 (-)

*Figure 24: **Gene set enrichment analysis of F1648 and F2612**. RNA-sequencing data of HDAC-2 cell lines F2612 and F1648 were analyzed with GSEA. Five pathways show a significant negative enrichment in both HDAC-2 cell lines, the enrichment plots for the depicted reactome pathway signatures are shown.*

Discussion and interpretation of the results

With a 5-year-survival of 11%, pancreatic cancer has a very poor prognosis and is predicted to be the third leading cause of cancer related deaths in women and fourth leading cause of cancer related deaths in men by 2040 (Jain and Bhardwaj, 2021; Rahib et al., 2021; Siegel et al., 2022). It is mostly diagnosed in advanced stages, meaning that surgery, as only way to cure the disease, is often not possible anymore (Wagner et al., 2004; Park et al., 2021). This highlights the necessity for drug-based therapies. Although chemotherapeutic schemes like FOLFIRINOX are available, due to therapy resistance of the cancer the success is often limited (Jain and Bhardwaj, 2021). This shows the importance of new drug-based therapeutic strategies.

HDACi like *Vorinostat* seem to be promising anti-cancer agents, as *Vorinostat* has already been approved by the FDA for treatment of refractory cutaneous T-cell lymphomas (Falkenberg and Johnstone, 2014). Different studies also see potentials of HDACi for treatment of pancreatic cancer, e.g. to overcome chemotherapy resistances (Roca et al., 2022). While studies in the past showed HDACi as potential partner within a drug-combination, many clinical trials did not show the expected success, especially the utility of HDACi as single agent (Hontecillas-Prieto et al., 2020). To find new potential combination-based drug therapies for treatment of pancreatic cancer, a drug screening was established using isogenic murine *HDAC-2* proficient and deficient PDAC cell lines as a model system. The response to 101 drugs with different mode of actions was tested in the drug screening experiment. Based on the results of the unbiased screening with *HDAC-2* proficient and deficient cells, *Erastin* was further evaluated as a potential partner for a combination therapy with HDACi.

In both *HDAC-2* cell lines, cell lines treated with *Erastin* showed a significant reduction of cell viability. Those findings were reproducible performing different assays such as clonogenic assay, although significance has not always been confirmed. Further investigations and validations are necessary, e.g. by using different models such as primary human PDAC cell lines or a larger cohort of murine PDAC cell lines.

To determine if the observed results in the knock-out screening could be translated into actual pharmacological treatments, a treatment of *HDAC-2* proficient cell lines with actual compounds was necessary. After combination treatment with *Erastin* and *MS-275* (class-I-HDACi), we confirmed reduced cell viability and synergistic effects.

Erastin was originally found in a compound screening as a small molecule that killed cancer cells which were overexpressing Small T oncoprotein (*ST*) and oncogenic *RAS*, leading to its name *Erastin* ("Eradicator of ***RAS*** and ***ST***-expressing cells") (Dolma et al., 2003). Although *KRAS* is the most frequently mutated oncogene in PDAC (Hong et al., 2011), ferroptosis induced by *Erastin* is not only relevant in *RAS*-mutated cancer cells and can be induced regardless of the *RAS*-status (Conrad and Pratt, 2019). *Erastin* has a poor water solubility and has an unstable metabolism in the body, limiting

its in-vivo use. However, after chemical manipulation, *Erastin* (like Piperazine-*Erastin* or Imidazole Ketone *Erastin* (IKE)) could b good option for cancer treatment *in vivo,* what has already been shown in the past in mouse lymphom odels by Zhang et al., where a treatment with IKE showed reduc umor growth (Zhang et al., 2019; Zhao et al., 2020). *Erastin* induces ferroptosis. Ferroptosis is an iron-dependent oxidative non-apoptotic cell death. Induction of ferropt is leads to increase and accumulation of lipid peroxidation, lipid peroxids/lipid-ROS/reactive oxygen species (ROS), depletion of plasma mbrane polyunsaturated fatty acids and cell damage (Cao and Dixon, 2016; Liu et al., 2021). One i ortant antioxidant system is the x_c^- -GSH-glutathione peroxidase 4 system, which leads to detoxification of active oxygen species and inhibits ferroptosis with the help of glutathione (GSH) (Yang et al., 2014; Zhao et al., 2020).

Erastin induces ferroptotic cell death b reversibly inhibiting the cystine-glutamate antiporter x_c^- and simultane usly opens voltage dependent anion channels (VDAC) 2 and 3 (Yagoda et al., 2007; Dixon et al., 2012; Cao and Dixon, 2016; Conrad and Pratt, 2019):

Due to inhibition of x_c^-, the uptake of cystine decreases while the concentration of glutamate increases. This could lead to a lower synthesis and fa depletion of glutathione (GSH), which is an important antioxidant i e cell by reducing the concentration of reactive oxygen species (ROS) and acts as a cofactor for glutathione peroxidase (GPX). GPX4 catalyzes reactions to reduce toxic lipid peroxide PLOOH (lipid-ROS), oduced from polyunsaturated fatty acids (PUFA) from the cell mbrane, to nontoxic lipid-alcohols PL-OH by using GSH as cofactor (Yang et al., 2014; Imai et al., 2017). This makes GPX4 a regulator of ferroptosis. A low concentration of GSH consequently leads to a higher concentration of ROS and especially lipid-ROS, due to reduced ROS detoxification. This increase of ROS-levels due to *Erastin*-treatment could lead to imbalance and to oxidative cell death, more specifically ferropotosis (Yang et al., 2014).

Another important effect of *Erastin* e opening of VDAC channels. VDAC proteins are responsible for the exchange of metabolites and other substrates through the mitochondrial membrane (e.g. ATP or respiratory s strates) (Maldonado and Lemasters, 2012; Zhao et al., 2020). Together with the complexes I, III and IV of the respiratory chain, closed VDACs are also necessary to provide a stable mitochondrial membrane potential. Due to an opening of the VDAC channels, the mitochondrial membrane potential increases due to hyperpo ization (DeHart et al., 2018). The effect of the reopening of VDAC results in a reverse of the Warburg metabolism, meaning an increa n oxidative phosphorylation, ROS-synthesis and decrease of glycolysis (Yagoda et al., 2007; Imai et al., 2017; Maldonado, 2017; Zhao et al., 2020).

Zille et al. assumed that class-I-HDACi promote roptosis induced by *Erastin* in fibrosarcoma cancer cells (Zille et al., 2019). Beside the effects mentioned in the introduction, HDACi like *MS-275*, *Domatinostat* or *Vorinostat* (=SAHA) lead to increasing ROS-levels (Ruefli et al., 2001; Zhang and Zhong, 2014; Roca et al., 2022).

Analyzing RNA-sequencing data using GSEA after *HDAC-2* knock-out revealed negative enrichment o he EIF2AK4-EIF2A/eIF2α-ATF4 pathway, amino acid deprivation, amino acid transport across the plasma membrane and the elongation of

translation. Also, the data from the RNA-sequencing showed a significant downregulation of ATF4 after *HDAC-2* knock-out. These findings are strong hints for the postulated lower x_c^- -expression mediated by reduced ATF4-expression via lower expression of x_c^--subunit SLC7A11 initiated by HDACi, what Wolf et al. and Lewerenz et al. showed in glioma cells (Lewerenz et al., 2012; Wolf et al., 2014; Koppula et al., 2018).

ATF4 is part of the Integrated Stress Response (ISR)-pathway, which is necessary for responding to cellular stress (B'chir et al., 2013; Masson, 2019). Important ways for activation of this pathway are amino acid deprivation and heme deprivation and hypoxia, both sensed by specific protein kinases GCN2 (EIF2AK4; general control non-depressible protein 2) and HRI (EIF2AK1; heme-regulated eIF2α kinase) (Suragani et al., 2012; Wortel et al., 2017; Masson, 2019). Both kinases lead to phosphorylation of the eukaryotic translation initiation factor eIF2α. After phosphorylation, eIF2α reduces translation of mRNA and activates a transcriptional stress response via ATF4 (Masson, 2019). A central regulator for GCN2 activity is deacetylated tRNA as tRNA synthetase enzymes fail to aminoacetylate tRNA due to amino acid deprivation (Zaborske et al., 2009) (figure 25).

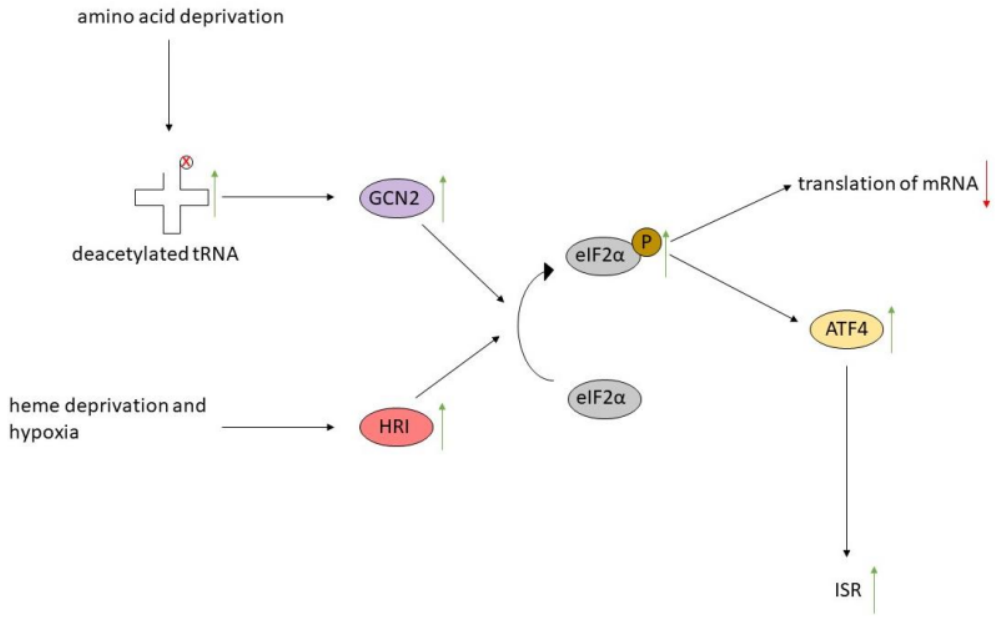

*Figure 25: **eIF2α-ATF4 pathway**. Heme deprivation and hypoxia lead to activation of HRI (heme-regulated eIF2α kinase) and amino acid deprivation leads to increasing levels of deacetylated tRNA which activates GCN2 (general control non-depressible protein 2). Both kinases induce phosphorylation of eIF2α, which reduces translation and increases ATF4-induced stress response.*

The downregulation of ATF4 mRNA may contribute to the increased *Erastin* sensitivity of *HDAC-2* deficient murine PDAC cells. However, further experiments using cells with *ATF4* knock-out could be treated with *Erastin* to investigate changes in sensitivity. This could be further validated by reconstituting *ATF4* in these knock-out lines.

GPX4 is also necessary to reduce oxidative stress. Results published by Wang et al. showed that HDACi *Quisinostat* lead to downregulation of GPX4 (Wang et al., 2021).

However, the analyzed RNA-sequencing data did not confirm the mentioned regulation of GPX4.

Suggesting that *Erastin* or HDACi lead to higher oxidative stress due to higher levels of ROS, a combination of both agents should further increase ROS-levels. Such higher ROS-levels, due to a combination of HDACi and inhibition of x_c^-, have already been detected with ROS-measurement in human breast cancer cells and human colon cancer cells: the ROS-levels were higher after a combination of HDACi and x_c^--inhibitors than either one of the agents alone (Miyamoto et al. 2020). Yang et al. also showed, that class-I-HDACi enhances ferroptotic cell death after *Erastin* treatment in lung cancer cells and were able to show similar results regarding cell lethality and ROS-levels after a combination of *Vorinostat* and *Erastin* like Miyamoto et al. (Yang et al., 2020). This could explain the observed results, however ROS-measurements have not been performed. As the combination of *Vorinostat* and *Erastin* showed similar effects on apoptosis as each drug alone, Yang et al. are convinced that the combination lead to ferroptosis (Yang et al., 2020).

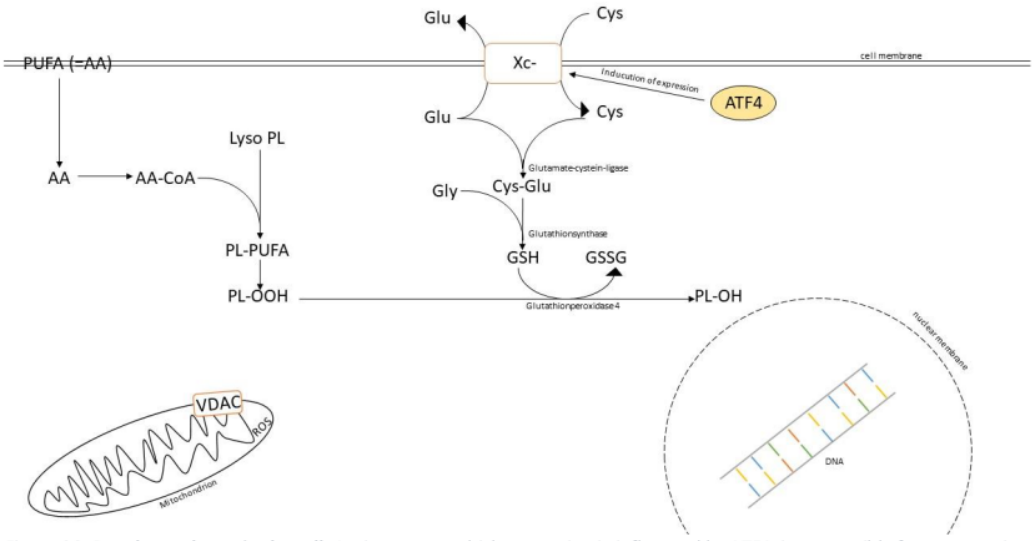

*Figure 26: **Regular pathway in the cell**. Antiporter x_c^-, which expression is influenced by ATF4, is responsible for transporting cystine in exchange for glutamate into the cell to build glutathione (GSH). GSH is necessary for the GPX4-catalyzed reduction of lipid-ROS (PL-OOH) to nontoxic lipid-alcohols (PL-OH). Characteristic for a cancer cell, VDAC is closed due to bonding of free tubulin. Due to the closed VDAC in the mitochondrial membrane, the mitochondrial membrane potential stays stable.*

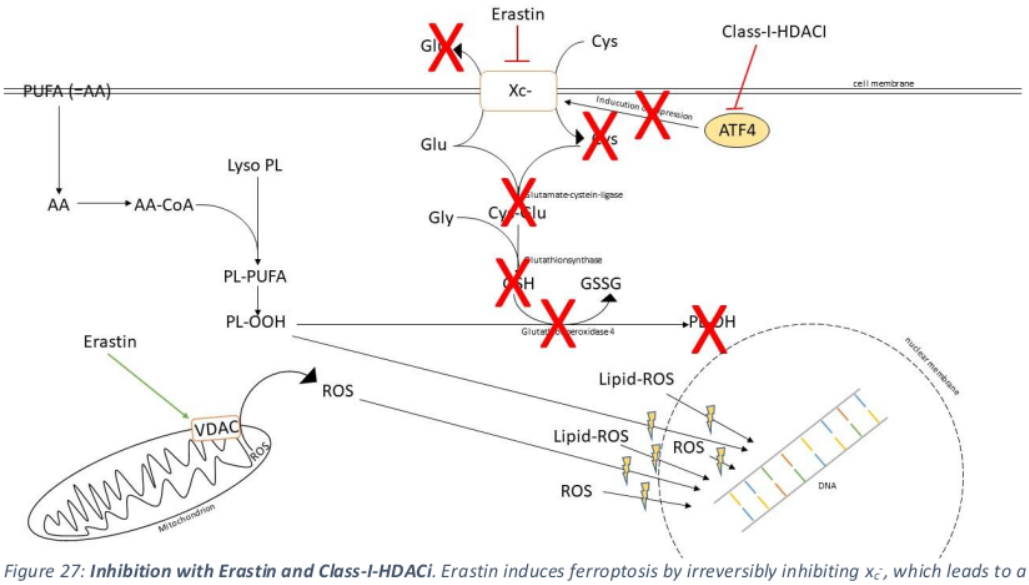

Figure 27: ***Inhibition with Erastin and Class-I-HDACi****. Erastin induces ferroptosis by irreversibly inhibiting x_c^-, which leads to a reduced production and faster depletion of glutathione (GSH). Decreasing detoxification of lipid-ROS is the consequence. Lipid-ROS can induce increasing DNA-damage. Erastin also leads to opening of VDAC, which induces oxidative phosphorylation and consequently increases ROS-production in the mitochondria and transport of ROS from the mitochondria into the cytoplasm. Those higher ROS-levels lead to increasing DNA-damage. HDAC-inhibition could enhance the DNA-damaging effects of Erastin induced ROS-levels by reducing the expression of x_c^- via reduced expression of ATF4.*

The figures 26 and 27 show the hypothesis of possible interactions leading to the observed synergistic effects of a cotreatment of HDACi and *Erastin*: the combination of increasing ROS-levels due to different mechanisms (x_c^--inhibition, lower x_c^--expression, reduced GSH-production and VDAC-opening) lead to much higher oxidative stress within the cells, leading to increasing cell lethality. With the data collected for this thesis, the described suspected mechanism of how HDACi and *Erastin* could interact cannot be confirmed for PDAC, but the data can give a hint for such interaction and working mechanism, which must be addressed in future experiments.

To understand how both drugs synergistically interact and to evaluate the postulated working mechanism of a combination of *Erastin* with HDACi in PDAC cells, further investigations are necessary. Therefore, more validations of the experiments using *Erastin* and *MS-275* in different concentrations and with different assays should be performed as well as ROS-measurements (like those of Myamoto et al. or Roca et al.). To evaluate, if the effect is caused by ferroptosis, experiments using ferrostatin (binds the necessary iron for ferroptosis) to reverse the effect should be performed. Also, DNA-damage should be measured to evaluate if the increasing ROS-levels lead to increasing DNA-damage. Furthermore GSH-measurement could be performed to measure the depletion and decreased production of GSH due to the inhibition. The presented observations suggest, the combination could also interact with the cellular metabolism (Zhao et al., 2020), which require further investigations. In case that further investigations show promising results, the tolerability has to be evaluated for a potential clinical use in the future. As previously mentioned, *Erastin* would need further chemical manipulation prior to *in-vivo* use, while *MS-275* already has a dosage form for oral use

and showed to be well tolerated in earlier phase-I-trials at a dose of 6 mg/m^2 with no severe side effects (Kummar et al., 2007).

The other promising hit *JIB-04*, a pan-selective Jumonji histone demethylase inhibitor, needs further investigations too.

Besides surgery, drug-based therapies are and will be the most important instrument in the fight against PDAC. The presented data show promising results for a therapy combining *MS-275* and *Erastin*, but further investigations are necessary. The goal of most of the therapies in medicine are the healing and recovery of the patient. Sometimes, certain therapies alone can achieve this goal and sometimes, therapies are part of a holistic concept. Maybe the combination of *Erastin* and HDACi could be a useful radiosensitizer with the advantage that additional to the ROS-production induced by radiotherapy, the drug-combination would lead to increasing ROS-levels well (Zhao et al., 2020). Experiments using *Erastin* as radiosensitizer, e.g. to increase the sensitivity of breast cancer to γ-rays, seem promising (Cobler et al., 2018). Radiotherapy already plays a role in neoadjuvant treatment of borderline-resectable pancreatic cancer (Leitlinienprogramm Onkologie, 2021). But even if new drug-based therapies show increased survival-rates or symptom-free lifetime instead of curation from cancer, it would be a great success too.

Supplement

Table 25: F2612 IC_{50}- and AUC-values from the screening according to drug (NA = no results)

	***HDAC-2* (+) IC_{50}**	***HDAC-2* (+) AUC**	***HDAC-2* (-) IC_{50}**	***HDAC-2* (-) AUC**
4EGI-1	15,11	285,9	27,03	287,6
A1210477	35,56	313	NA	386
A-196	435,6	297,8	NA	324,1
Abexinostat	0,6466	180	0,2793	152,4
Adavosertib	0,09242	104,3	0,09105	107,9
Alisertinib	0	271,6	20,16	278,1
Alpelisib	4,361	253,7	2,953	232,7
AZD1208	0,009101	288,1	NA	279,3
AZD5153	0,6457	173,5	0,4078	168,5
AZD6738	0,8379	179,7	0,7216	195,1
AZD7762	0,06647	98,85	0,08121	108,8
BAY-876	0,02951	79,34	0,05292	91,4
BI-78D3	27,8	294,7	0	285,9
BI-847325	0,02261	66,16	0,09609	105,4
BI-D1870	10,27	281,1	7,839	269,2
Birinapant	NA	293,4	114,7	275,1
BRD4770	2,947	269,3	1,795	234,2
BX-795	7,726	288,1	4,955	261,1
BX-912	26,09	290,6	21,6	302,8
C646	959,2	280,1	24,14	316,9
CB-839	0,3399	157,4	2,448	224,9

CPI-455 HCl	138,2	271	NA	384,1
Crenigacestat	5,33E-15	286	1397	261,1
CUDC-101	2,337	221	1,507	218,2
CW069	33,77	306,6	259,4	281,8
EED226	0	298,8	NA	372
Elesclomol	0,01892	50,66	0,0145	33,76
Entrectinib	1,957	245,3	3	266,4
Enzastaurin	315,2	277,4	0	287,7
Epacadostat	44,61	307,5	31,27	303,8
EPZ004777	113,9	290,2	67,51	291,4
Erastin	3,642	253,8	1,905	224,3
Erdafitinib	6,517	303,9	5,499	247,3
Galunisertib	30,07	300	65,21	249,7
GDC-0152	18,8	306,1	89,49	283,1
GSK J1	0	290,2	137,2	282
GSK2656157	15,36	309,7	53,54	270,8
GSK2830371	147,6	283,4	0	290,7
GSK503	8,401	298,5	6,289	278,6
GSK591	10,85	254,4	16,06	249,6
HTH-01-015	2,348	225,4	2,939	234,1
Indirubin	6,38E-07	274,3	97,39	306,8
Ispinesib	4,165	243,7	1,926	200,4
JIB-04	0,3012	166,3	0,2615	163,7
JSH-23	NA	314,3	17,79	316,9
KU-60019	10,03	279,5	5,997	279,2
Lapatinib	6,918	236,2	4,083	241,8
Linsitinib	28,02	288,4	176,4	274,3
LJH685	6,88E-11	234	28,59	280,3
LLY-283	22,14	292,7	193,7	279,8
LLY-507	1,926	233,7	1,834	231,7
Luminespib	0,01018	54,04	0,01102	63,01
LY2109761	49,39	315,6	80,43	320,1
MI-463	1,774	230	1,964	236,1
MI-503	34,67	302,4	26,44	284,2
Milciclib	0,4067	182,2	0,5132	187
MK-2206 2HCl	3,209	250	2,627	231,1
ML264	NA	311,1	25,54	303,4
ML324	8,627	283,8	4,328	274,2
MS023	22,2	280,3	24,27	276
MX69	22,62	312,2	1987	272,7
Napabucasin	2,853	246,3	1,433	224,1
NMS-873	5,713	277,3	11,25	318,8
NSC87877	14,99	302,4	27,18	286,9
NVP-CGM097	7,74	275,7	22,78	254,6
Orantinib	NA	366,9	140,5	294,6
OTX015	3,691	523	0,4406	216,4
P22077	34,78	273,6	16,23	291,4
Pelitinib	0,7849	185,3	1,216	205,6
Pevonedistat	1,463	232,2	1,85	246,9
PFI-2 HCl	35,91	285,4	16,13	309,1

Poziotinib	10,78	277,3	4,904	240,1
Pracinostat	0,2924	221,7	0,2529	153,1
PRT4165	0	293,4	NA	375,7
PTC-209 HBr	2,111	242,6	1,549	221,2
PX-478 2HCl	NA	308,1	1074	280,8
PYR-41	14,08	320,7	12,36	330,9
Ralimetinib	14,64	300,5	62,55	265,1
RI-1	8,851	288,9	10,47	299,4
Rigosertib	1,168	196,9	0,7741	185
RO5126766	0,5125	166,9	0,4285	159,8
Ruxolitinib	NA	305,2	11,72	305,7
Sabutoclax	2,711	231,1	3,755	246,6
Salubrinal	NA	299,8	25,3	310,7
Sapanisertib	0,06672	102,8	0,05146	94,93
Saracatinib	0,8597	187,1	1,7	220
Selisistat	111,5	293,2	102,5	286,4
SF1670	2,605	244,5	4,199	268,7
SGC707	1,97E+07	278,7	11,1	307,5
SMER28	85,79	262,4	NA	367,8
Spautin-1	2,857	255	4,853	264,6
STF-083010	30,52	291,5	59,82	285,8
Thiomyristoyl	10,5	307,8	NA	381,8
Trametinib	0,02682	73,68	0,02608	74,87
Ulixertinib	0,5078	168,5	1,012	203,8
UNC0379	1,17	213,4	0,9608	196,6
UNC0638	1,447	184,2	1,302	217,7
UNC1999	3,8	268,6	3,969	266,5
Veliparib	NA	326,1	11879	274,3
Vemurafenib	15,35	306,1	NA	314,1
WZ4003	4,621	245,3	3,246	236,8

Table 26: F1648 IC_{50}- and AUC-values from the screening according to value (NA = no results)

	***HDAC-2* (+) IC_{50}**	***HDAC-2* (+) AUC**	***HDAC-2* (-) IC_{50}**	***HDAC-2* (-) AUC**
4EGI-1	68,02	264,3	329,9	312,1
A1210477	11,42	312,6	115,6	295,2
A-196	NA	310,9	18400	293,2
Abexinostat	0,05504	90,09	0,0973	107,4
Adavosertib	0,1198	121,3	0,1274	117,4
Alisertinib	10,28	339,3	NA	376,2
Alpelisib	2,79	265,1	4,239	237,1
AZD1208	NA	335,8	35,54	282,3
AZD5153	0,01549	38,56	0,05777	97,2
AZD6738	0,9869	211,8	1,826	240,3
AZD7762	0,101	118,2	0,1466	118,2
BAY-876	0,07139	104	0,3603	153,3
BI-78D3	8,61	283,1	9,047	280

BI-847325	0,04285	70,87	0,1127	113,3
BI-D1870	5,129	256,4	9,282	318,2
Birinapant	NA	330,7	NA	303
BRD4770	1,225	208,2	1,769	214,6
BX-795	9,448	285,3	5,576	272,6
BX-912	10,6	299,6	0	252,4
C646	0,0002006	301	16,17	301,5
CB-839	16,95	273,1	179,3	300,2
CPI-455 HCl	78,91	289,9	NA	314,9
Crenigacestat	4969	280,5	NA	321,1
CUDC-101	0,9813	218,4	1,263	220,4
CW069	0,1964	264,5	26,74	266,8
EED226	49,28	300,1	87,47	285,3
Elesclomol	0,0007202	27,76	NA	376,7
Entrectinib	0,4156	153,2	1,309	232,8
Enzastaurin	NA	321,3	0	288
Epacadostat	NA	324,2	NA	364,2
EPZ004777	21,87	345,8	10,78	304,4
Erastin	0,2456	149,8	0,1964	132
Erdafitinib	5,877	241,7	25,43	252,5
Galunisertib	94,5	248,3	40,75	286,3
GDC-0152	274,2	286,2	NA	303,7
GSK J1	111,2	277,4	0	249,2
GSK2656157	NA	510,2	NA	349,8
GSK2830371	1577	265,5	411,9	278,4
GSK503	91,16	288	9,899	282,9
GSK591	NA	323,5	16,58	290,7
HTH-01-015	3,223	256,5	9,014	295,6
Indirubin	NA	386,1	30,95	294,9
Ispinesib	3,793	268,3	8,576	394,1
JIB-04	0,3488	170,4	0,1277	116,6
JSH-23	NA	355,4	13,47	322,2
KU-60019	6,307	259,6	7,143	263,8
Lapatinib	NA	352,9	NA	364,3
Linsitinib	0	232,1	10,81	319,6
LJH685	NA	323,2	NA	346,3
LLY-283	0	283,4	1,38E+11	265,1
LLY-507	NA	331,8	6,581	300,9
Luminespib	NA	17,5	0	14,65
LY2109761	0	292,8	NA	342,5
MI-463	2,799	273,4	2,808	255,5
MI-503	211,7	306,2	300,1	258,2
Milciclib	0,8452	207	0,4738	165,6
MK-2206 2HCl	9,265	310,4	NA	325,9
ML264	23,64	267,3	35,33	281,2
ML324	1,45	219,4	1,491	225,6
MS023	NA	353,1	NA	341,8
MX69	1,96E+08	272,2	2987	293,1
Napabucasin	2,867	248,6	3,656	258,2
NMS-873	6,516	272,8	0	296,8

NSC87877	19,15	315,5	87,8	261,8
NVP-CGM097	NA	380,7	0	277,7
Orantinib	NA	329,7	1,263	283,7
OTX015	0,03833	74,21	0,0892	109,8
P22077	10,25	291,1	NA	321,6
Pelitinib	0,8837	193,1	1,524	238,4
Pevonedistat	2,023	261,1	1,864	236,2
PFI-2 HCl	NA	295,6	36,27	307,6
Poziotinib	0,473	161,3	0,6378	169,9
Pracinostat	0,02683	66,6	1,176	208,2
PRT4165	NA	321,1	28,67	307,1
PTC-209 HBr	1,353	199,2	2,664	277,2
PX-478 2HCl	2,44E+07	254,5	NA	353,1
PYR-41	17,63	305,4	78214	233,1
Ralimetinib	193,9	260,9	NA	322,7
RI-1	4,865	240,7	NA	302,9
Rigosertib	0,2809	174,6	0,7395	193,8
RO5126766	0,3319	157,2	NA	371,7
Ruxolitinib	4,49E+10	927,3	NA	1039
Sabutoclax	6,479	295,2	8,52	276,3
Salubrinal	NA	305,8	10,68	303
Sapanisertib	0,03167	75,94	0,02706	53,73
Saracatinib	1,069	222,8	1,696	210,2
Selisistat	1,27E+11	284,1	62,25	292,1
SF1670	0,6443	178,3	0,8965	211,7
SGC707	81,79	302,4	NA	300,5
SMER28	NA	308	0	294,8
Spautin-1	11834	299,2	46,63	288,9
STF-083010	0,001016	269,6	NA	323
Thiomyristoyl	0	273,5		314,7
Trametinib	0,01539	49,04	0,9956	203,8
Ulixertinib	1,301	223,4	3,954	255,5
UNC0379	1,383	231,3	8,903	292,2
UNC0638	2,758	281,8	2,578	282,2
UNC1999	4,741	277,3	7,615	284,6
Veliparib	17285	257,9	1299	275,2
Vemurafenib	NA	346,3	NA	306,5
WZ4003	9,231	293	8,707	304,5

Table 27: Overview over the calculated z-scores of the IC_{50}- and AUC-values (rounded to two decimals).

	221648 z-scores				F2612 z-scores			
	HDAC-2 (+)		*HDAC-2* (-)		*HDAC-2* (+)		*HDAC-2* (-)	
	IC_{50}	AUC	IC_{50}	AUC	IC_{50}	AUC	IC50	AUC
4EGI-1	-0,28	-1,19	1,48	1,26	-0,64	-0,08	-0,56	0,01
A1210477	-0,78	-0,35	1,13	-0,78	-0,34	-0,34	-0,99	1,47
A-196	-0,74	0,32	0,71	-0,96	-0,71	-0,62	-0,74	1,26
Abexinostat	-0,80	-1,03	-0,64	-0,61	1,40	1,15	0,04	0,48
Adavosertib	0,65	1,08	1,06	0,59	-0,82	-1,06	-0,89	-0,61
Alisertinib	0,01	0,46	-1,01	1,19	-1,01	-0,89	0,99	-0,76

Alpelisib	-0,96	1,20	0,79	-0,67	0,94	0,44	-0,76	-0,96
AZD1208	-0,71	1,49	0,71	-0,53	-0,71	-0,31	-0,71	-0,64
AZD5153	-0,89	-1,26	-0,75	-0,35	1,21	0,84	0,42	0,76
AZD6738	-0,21	0,20	1,46	1,29	-0,51	-1,04	-0,74	-0,45
AZD7762	0,06	0,78	1,37	0,78	-0,93	-1,32	-0,51	-0,24
BAY-876	-0,37	-0,09	1,49	1,43	-0,64	-0,85	-0,49	-0,48
BI-78D3	-0,23	-0,45	-0,20	-0,94	1,40	1,39	-0,97	0,00
BI-847325	-0,60	-0,76	1,03	1,02	-1,08	-0,95	0,64	0,69
BI-D1870	-1,34	-0,93	0,52	1,39	0,96	0,00	-0,13	-0,45
Birinapant	NA	1,30	NA	0,11	NA	-0,31	NA	-1,10
BRD4770	-0,98	-0,85	-0,23	-0,62	1,40	1,37	-0,19	0,10
BX-795	1,23	0,69	-0,66	-0,34	0,39	0,91	-0,96	-1,26
BX-912	-0,34	0,57	-1,25	-1,46	0,98	0,18	0,60	0,71
C646	-0,53	0,07	-0,49	0,11	1,50	-1,31	-0,48	1,13
CB-839	-0,38	0,55	1,49	0,98	-0,57	-1,30	-0,55	-0,22
CPI-455 HCl	-0,71	-0,51	-2,59	0,00	0,71	-0,89	-2,59	1,40
Crenigacestat	1,11	-0,27	-0,83	1,36	-0,83	-0,05	-0,28	-1,04
CUDC-101	-0,93	-0,78	-0,44	0,64	1,39	1,06	-0,03	-0,92
CW069	-0,66	-0,80	-0,44	-0,68	-0,38	1,38	1,49	0,10
EED226	0,08	-0,36	0,96	-0,73	-1,04	-0,39	-1,04	1,48
Elesclomol	-1,12	-0,56	-1,20	1,50	0,79	-0,42	0,33	-0,52
Entrectinib	-1,20	-1,44	-0,31	0,17	0,34	0,42	1,16	0,85
Enzastaurin	-0,58	1,45	-0,58	-0,29	1,15	-0,85	-0,58	-0,31
Epacadostat	-4,02	-0,03	-4,02	1,42	0,71	-0,63	-0,71	-0,76
EPZ004777	-0,67	1,45	-0,91	-0,14	1,28	-0,68	0,30	-0,64
Erastin	-0,77	-0,69	-0,80	-0,99	1,31	1,09	0,25	0,59
Erdafitinib	-0,51	-0,68	1,50	-0,31	-0,44	1,48	-0,55	-0,49
Galunisertib	1,29	-0,87	-0,59	0,58	-0,96	1,11	0,26	-0,82
GDC-0152	1,11	-0,73	-0,97	0,76	-0,82	0,96	-0,29	-0,99
GSK J1	0,68	0,15	-0,86	-1,43	-0,86	0,87	1,04	0,41
GSK2656157	#WERT!	1,43	-1,28	-0,10	-0,71	-0,48	0,71	-0,85
GSK2830371	1,46	-1,32	-0,17	-0,10	-0,54	0,37	-0,75	1,06
GSK503	1,50	0,12	-0,46	-0,48	-0,49	1,34	-0,55	-0,98
GSK591	-4,57	1,27	0,66	0,32	-1,15	-0,73	0,49	-0,87
HTH-01-015	-0,37	0,11	1,49	1,36	-0,65	-0,88	-0,46	-0,60
Indirubin	-0,86	1,44	-0,24	-0,42	-0,86	-0,84	1,10	-0,18
Ispinesib	-0,29	-0,10	1,41	1,41	-0,16	-0,40	-0,95	-0,92
JIB-04	0,94	0,64	-1,39	-1,49	0,44	0,48	0,02	0,37
JSH-23	-5,12	1,48	-0,71	-0,26	-5,12	-0,68	0,71	-0,54
KU-60019	-0,58	-1,06	-0,12	-0,65	1,45	0,87	-0,75	0,84
Lapatinib	-2,74	0,78	-2,74	0,95	0,71	-0,90	-0,71	-0,82
Linsitinib	-0,65	-1,28	-0,52	1,13	-0,31	0,27	1,49	-0,12
LJH685	-0,71	0,55	-0,71	1,02	-0,71	-1,25	0,71	-0,32
LLY-283	-0,50	0,27	1,50	-1,32	-0,50	1,09	-0,50	-0,04
LLY-507	-1,27	1,15	1,15	0,53	-0,56	-0,82	-0,59	-0,86
Luminespib	-1,15	-0,80	-1,15	-0,91	0,51	0,67	0,64	1,04
LY2109761	-1,07	-1,22	-1,07	1,21	0,15	-0,11	0,92	0,12
MI-463	0,85	1,25	0,87	0,34	-1,03	-0,95	-0,68	-0,64
MI-503	0,51	0,84	1,16	-1,35	-0,80	0,67	-0,86	-0,16
Milciclib	1,46	1,26	-0,44	-1,16	-0,78	-0,19	-0,24	0,09
MK-2206 2HCl	1,15	0,68	-1,37	1,01	-0,50	-0,64	-0,65	-1,05
ML264	-0,72	-1,17	1,14	-0,47	-4,49	1,01	-0,42	0,63
ML324	-0,75	-0,95	-0,73	-0,76	1,38	1,00	0,10	0,71
MS023	-15,87	1,00	-15,87	0,72	-0,71	-0,81	0,71	-0,91
MX69	1,50	-0,80	-0,50	0,29	-0,50	1,29	-0,50	-0,78
Napabucasin	0,18	0,30	1,03	0,96	0,16	0,14	-1,37	-1,40
NMS-873	0,14	-0,89	-1,27	0,26	-0,03	-0,67	1,17	1,30
NSC87877	-0,53	1,03	1,48	-1,29	-0,65	0,47	-0,30	-0,21
NVP-CGM097	-0,88	1,47	-0,88	-0,34	-0,21	-0,38	1,09	-0,75
Orantinib	-0,72	0,29	-0,71	-0,93	-0,72	1,28	0,71	-0,64

OTX015	-0,58	-0,77	-0,55	-0,59	1,49	1,43	-0,35	-0,07
P22077	-0,80	-0,17	-1,60	1,36	1,12	-1,04	-0,33	-0,15
Pelitinib	-0,65	-0,53	1,25	1,40	-0,94	-0,87	0,34	0,00
Pevonedistat	0,94	1,32	0,27	-0,61	-1,42	-0,92	0,21	0,22
PFI-2 HCl	-2,55	-0,34	0,59	0,73	0,56	-1,26	-1,15	0,87
Poziotinib	-0,77	-0,91	-0,74	-0,75	1,36	1,16	0,15	0,50
Pracinostat	-0,81	-1,36	1,46	0,65	-0,29	0,84	-0,36	-0,13
PRT4165	-0,71	-0,09	0,71	-0,48	-0,71	-0,86	-0,71	1,42
PTC-209 HBr	-0,96	-1,08	1,26	1,27	0,32	0,23	-0,63	-0,42
PX-478 2HCl	0,71	-1,06	-0,71	1,28	-0,71	0,21	-0,71	-0,44
PYR-41	-0,50	0,18	1,50	-1,46	-0,50	0,52	-0,50	0,75
Ralimetinib	1,12	-0,89	-0,97	1,20	-0,82	0,45	-0,30	-0,75
RI-1	-1,11	-1,47	-2,79	0,69	0,27	0,21	0,83	0,57
Rigosertib	-1,27	-1,30	0,00	0,62	1,18	0,93	0,09	-0,26
RO5126766	-1,02	-0,54	-4,69	1,50	0,98	-0,45	0,05	-0,51
Ruxolitinib	0,71	0,72	-0,71	1,00	-0,71	-0,86	-0,71	-0,86
Sabutoclax	0,42	1,14	1,20	0,49	-1,01	-1,08	-0,61	-0,54
Salubrinal	-1,74	0,21	-0,71	-0,39	-1,74	-1,09	0,71	1,27
Sapanisertib	-0,68	-0,27	-0,94	-1,29	1,23	0,96	0,39	0,60
Saracatinib	-0,61	0,79	0,84	0,01	-1,09	-1,41	0,85	0,62
Selisistat	1,50	-1,10	-0,50	0,72	-0,50	0,97	-0,50	-0,58
SF1670	-0,87	-1,21	-0,72	-0,36	0,31	0,48	1,28	1,09
SGC707	-0,58	0,40	-0,58	0,25	1,15	-1,46	-0,58	0,80
SMER28	-0,71	-0,01	-0,71	-0,31	0,71	-1,04	-0,71	1,35
Spautin-1	1,50	1,08	-0,50	0,58	-0,50	-1,06	-0,50	-0,60
STF-083010	-1,01	-1,02	-1,01	1,36	0,01	-0,04	0,99	-0,30
Thiomyristoyl	-0,71	-1,01	-0,71	-0,10	0,71	-0,26	-0,71	1,38
Trametinib	-0,52	-0,73	1,50	1,48	-0,49	-0,38	-0,49	-0,36
Ulixertinib	-0,25	0,29	1,47	1,17	-0,77	-1,22	-0,44	-0,25
UNC0379	-0,44	-0,05	1,50	1,41	-0,50	-0,48	-0,55	-0,88
UNC0638	0,98	0,83	0,74	0,84	-0,76	-1,17	-0,96	-0,49
UNC1999	-0,16	0,37	1,46	1,24	-0,70	-0,68	-0,60	-0,93
Veliparib	0,88	-0,86	-1,09	-0,28	-1,25	1,44	0,21	-0,31
Vemurafenib	NA	1,47	NA	-0,62	NA	-0,64	NA	-0,22
WZ4003	0,94	0,68	0,76	1,02	-0,62	-0,73	-1,08	-0,98

Table 28: Overview over Δ z-scores in IC_{50}- and AUC-value of F1648 and F2612

	F1648 IC50 Δ z-score	F2612 IC50 Δ z-score	F1648 AUC Δ z-score	F2612 AUC Δ z-score
4EGI-1	1,76550817	0,08036069	2,44569544	0,0869808
A-1210477	1,9104283	-0,6520909	-0,4307476	1,80715953
A-196	1,44850535	-0,0342918	-1,2711136	1,8887168
Abexinostat	0,1567889	-1,3627203	0,42061856	-0,670657
Adavosertib	0,40716947	-0,0733977	-0,4905143	0,45278243
Alisertib	-1,0197744	1,99986879	0,73436944	0,12936047
Alpelisib	1,74805193	-1,6985901	-1,8667911	-1,4000933
AZD1208	1,4145758	-0,0003622	-2,016134	-0,3316258
AZD5153	0,14108767	-0,7938684	0,91337203	-0,0778796
AZD6738	1,67645723	-0,2323585	1,09872284	0,59369585
AZD7762	1,30833058	0,42291212	1,5543E-15	1,07682075
BAY-876	1,85841107	0,15058462	1,51875142	0,37152418
BI-78D3	0,03727943	-2,3715521	-0,4899744	-1,3908952
BI-847325	1,63452051	1,7194641	1,77730405	1,64368161

BI-D1870	1,85743991	-1,087271	2,32037642	-0,4468039
Birinapant	NA	NA	-1,1942873	-0,7890057
BRD4770	0,75069696	-1,5897112	0,23294003	-1,2775305
BX-795	-1,88131	-1,3463611	-1,0211129	-2,17087
BX-912	-0,9065271	-0,3839912	-2,0331548	0,52551883
C646	0,03418647	-1,9769201	0,03309378	2,43570222
CB-839	1,8730803	0,02432178	0,43273622	1,07784852
CPI-455 HCl	-1,8821992	-3,2964128	0,50539172	2,28639216
Crenigacestat	-1,9390403	0,54514779	1,62324374	-0,9955362
CUDC-101	0,48219351	-1,4207335	1,41895131	-1,9865318
CW069	0,2203647	1,87317796	0,11875737	-1,2805143
EED226	0,87088358	0	-0,3774687	1,86693998
Elesclomol	-0,07587	-0,4656279	2,05343196	-0,0994526
Entrectinib	0,8907245	0,82552036	1,60916944	0,4265512
Enzastaurin	0	-1,7320508	-1,7422858	0,53890522
Epacadostat	0	-1,4142136	1,44685018	-0,1338336
EPZ004777	-0,2351975	-0,9838424	-1,5898832	0,04608357
Erastin	-0,0300817	-1,0620294	-0,3048647	-0,5052534
Erdafitinib	2,00710373	-0,1044971	0,3762092	-1,9716149
Galunisertib	-1,8765199	1,22680763	1,45579	-1,9270062
GDC-0152	-2,0792624	0,53604324	1,48300203	-1,9490884
GSK J1	-1,5340417	1,89272049	-1,5838032	-0,4605385
GSK2656157	NA	1,41421356	-1,5258728	-0,3700527
GSK2830371	-1,6276314	-0,2061955	1,21557553	0,68788383
GSK503	-1,9577068	-0,0508814	-0,5947143	-2,3205518
GSK591	5,23228024	1,64416044	-0,9487737	-0,1388449
HTH-01-015	1,86199993	0,19002624	1,24774384	0,27763098
Indirubin	0,62197208	1,9571522	-1,8639634	0,66424134
Ispinesib	1,69819239	-0,7949514	1,51211872	-0,5204669
JIB-04	-2,3267987	-0,4177924	-2,1306026	-0,1029659
JSH-23	4,40959645	5,82381002	-1,7395635	0,13623088
KU-60019	0,45467418	-2,1934222	0,40641725	-0,0290298
Lapatinib	0	-1,4142136	0,16463162	0,08087168
Linsitinib	0,13096875	1,79770053	2,40903359	-0,3881986
LJH685	0	1,41421356	0,46636033	0,93473954
LLY-283	2	2,49E-09	-1,5955325	-1,1247197
LLY-507	2,42437558	-0,0338919	-0,6189611	-0,0400622
Luminespib	0	0,13693476	-0,1148828	0,36157852
LY2109761	0	0,76524115	2,43947132	0,22087768
MI-463	0,01651093	0,34856406	-0,9084344	0,3095782
MI-503	0,65453645	-0,060937	-2,1902591	-0,8304732
Milciclib	-1,9014069	0,54523381	-2,429152	0,28164081
MK-2206	-2,5204174	-0,1583252	0,33768903	-0,4117628
ML264	1,86351444	4,07135661	0,6906255	-0,3825767
ML324	0,01212339	-1,2711818	0,1881511	-0,2913307
MS023	0	1,41421356	-0,2803018	-0,1066635
MX69	-1,9999865	2,0035E-05	1,09417086	-2,0679306
Napabucasin	0,85237086	-1,5340515	0,66577895	-1,5396138
NMS-873	-1,412486	1,20026629	1,14212898	1,97493136
NSC87877	2,01568513	0,35791991	-2,3267547	-0,6715959

NVP-CGM097	0	1,29842055	-1,8180081	-0,3724269
Orantinib	0,01282814	1,4270417	-1,2221417	-1,920888
OTX015	0,02890467	-1,8468989	0,17452956	-1,5035337
P22077	-0,801375	-1,4502933	1,52987308	0,89284396
Pelitinib	1,90397124	1,28190224	1,93501417	0,86712555
Pevonedistat	-0,6681419	1,62623226	-1,9270891	1,13767912
PFI-2	3,14698501	-1,7162218	1,07796873	2,12898824
Poziotinib	0,03402659	-1,2132298	0,15366529	-0,6646917
Pracinostat	2,26952978	-0,0780097	2,01070246	-0,9741115
PRT4165	1,41421356	0	-0,3881485	2,28175847
PTC-209	2,2168975	-0,9503405	2,34799562	-0,6441937
PX-478	-1,4142758	6,2251E-05	2,34120247	-0,6482234
PYR-41	1,9999248	-4,399E-05	-1,6353773	0,23071713
Ralimetinib	-2,0892113	0,51621512	2,09233224	-1,1985204
RI-1	-1,6865444	0,56125701	2,1593979	0,36452858
Rigosertib	1,26366251	-1,085383	1,91780377	-1,1886388
RO5126766	-3,6725479	-0,9294788	2,03742693	-0,0674393
Ruxolitinib	-1,4142136	3,6882E-10	0,28356104	0,0012693
Sabutoclax	0,77455157	0,39619394	-0,6549327	0,5371141
Salubrinal	1,03309171	2,44730528	-0,6059929	2,35904396
Sapanisertib	-0,251168	-0,8314151	-1,0152773	-0,3597583
Saracatinib	1,45102406	1,94464995	-0,7773003	2,02961753
Selisistat	-2	-1,418E-10	1,81927848	-1,5463867
SF1670	0,15228977	0,96252933	0,84880271	0,61500076
SGC707	-7,206E-06	-1,7320539	-0,1492401	2,26216576
SMER28	0	-1,4142136	-0,2994491	2,39105564
Spautin-1	-1,9951615	0,00033785	-0,5001754	0,46618286
STF-083010	-3,397E-05	0,97955433	2,38768489	-0,2548652
Thiomyristoyl	0	-1,4142136	0,90942285	1,63342938
Trametinib	2,01504228	-0,0015212	2,21122286	0,01700281
Ulixertinib	1,72037818	0,32695615	0,88139595	0,96926097
UNC0379	1,94329943	-0,0540609	1,4605132	-0,4029002
UNC0638	-0,2391262	-0,1926295	0,00820477	0,68714961
UNC1999	1,62324006	0,09545149	0,87583886	-0,2519536
Veliparib	-1,9659704	1,46088845	0,58500416	-1,751631
Vemurafenib	NA	NA	-2,0882776	0,41975429
WZ4003	-0,1765105	-0,4631716	0,34002742	-0,2513246

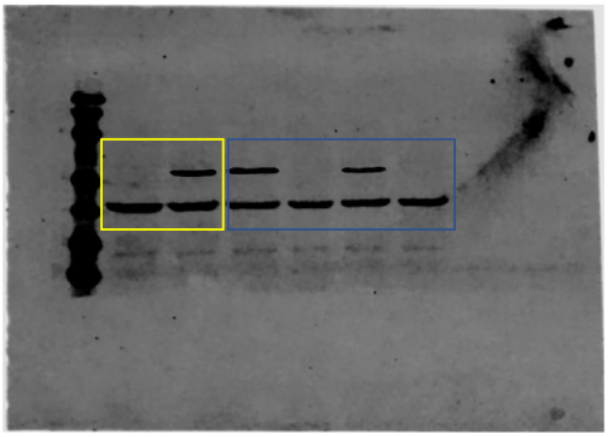

Figure 28: Western Blots (from left to right): F1648 PPT P13 T8d (not used) – F1648 PPT P13 E8d (not used) – F2612 PPT P14 E8d (Screen 1) – F2612 PPT P14 T8d (Screen 1) – F2612 PPT P15 E8d (Screen 2) – F2612 PPT P15 T8d (Screen 2); used in figure 16, the blue frame marks the used part of the blot for the figure, the yellow frame marks a part of the blot which got inverted prior to adding to the figure.

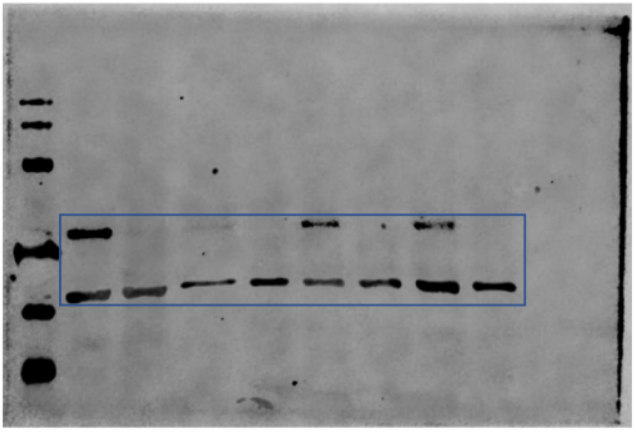

Figure 29: Western Blots (from left to right): F2612 PPT P16 E8d (Screen 3) – F2612 PPT P16 T8d (Screen 3) – F2612 PPT P17 E8d (Screen 4) – F2612 PPT P17 T8d (Screen 4) – F2612 PPT P10 E8d (Screen 5) – F2612 PPT P10 T8d (Screen 5) – F2612 PPT P11 E8d (Screen 6) – F2612 PPT P11 T8d (Screen 6); used in figure 16, the blue frame marks the used part of the blot for the figure.

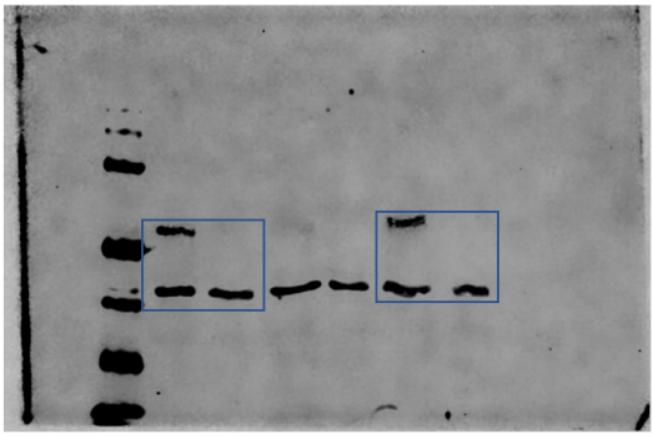

Figure 30: F2612 PPT P12 E8d (Screen 7) – F2612 PPT P12 T8d (Screen 7) – F2612 PPT P13 E8d – F2612 PPT P13 T8d – F2612 PPT P15 E8d (Screen 8+9) – F2612 PPT P15 T8d (Screen 8+9); used in figure 16, the blue frame marks the used part of the blot for the figure.

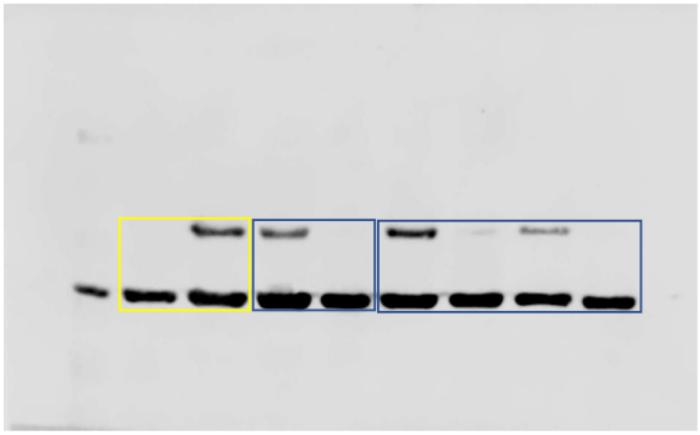

Figure 31: Western Blots (from left to right): F1648 PPT P12 T8d (Screen 1+2) – F1648 PPT P12 E8d (Screen 1+2) - F1648 PPT P13 E8d (Screen 3) – F1648 PPT P13 T8d (Screen 3) – F1648 PPT P16 E8d (Screen 6) – F1648 PPT P16 T8d (Screen 6) – F1648 PPT P17 E8d (Screen 7) – F1648 PPT P17 T8d (Screen 7); used in figure 16, the blue frame marks the used part of the blot for the figure, the yellow frame marks a part of the blot which got inverted prior to adding to the figure.

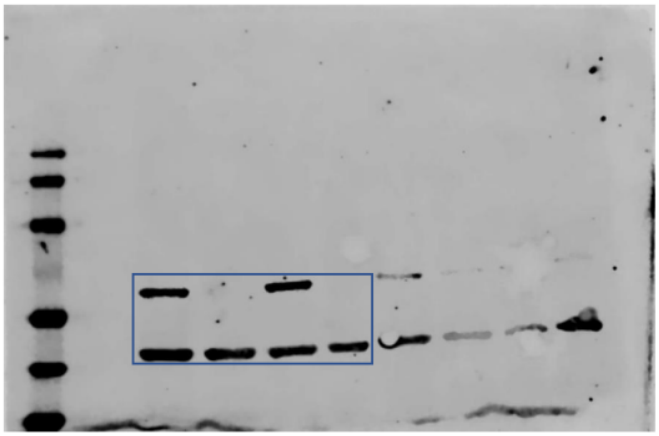

Figure 32: Western Blots (from left to right): F1648 PPT P14 E8d (Screen 4) – F1648 PPT P14 T8d (Screen 4) – F1648 PPT P15 E8d (Screen 5) – F1648 PPT P15 T8d (Screen 5) – F2800 PPT P11 E8d (not used) – F2800 PPT P11 T8d (not used) – F2800 PPT P12 E8d (not used) – F2800 PPT P12 T8d (not used); used in figure 16, the blue frame marks the used part of the blot for the figure.

Figure 33: Western Blots: F1648 PPT P18 E8d (Screen 8+9) – P1648 PPT P18 T8d (Screen 8+9); used in figure 16, the blue frame marks the used part of the blot for the figure.

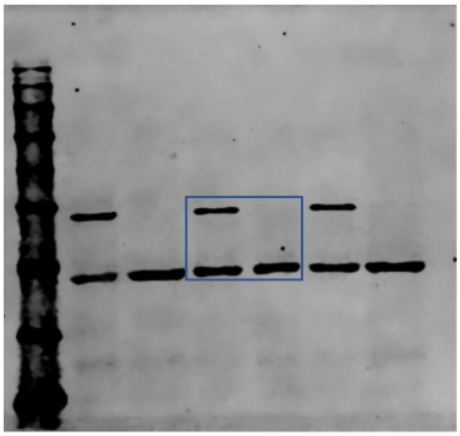

Figure 34: Western Blots (from left to right): F1648 PPT P13 E8d – F1648 PPT P13 T8d – F2612 PPT P11 E8d (used for Clonogenic assay) – F2612 PPT P11 T8d (used for Clonogenic assay) – F2800 PPT P25 E8d – F2800 PPT P25 T8d; used in figure 20, the blue frame marks the used part of the blot for the figure.

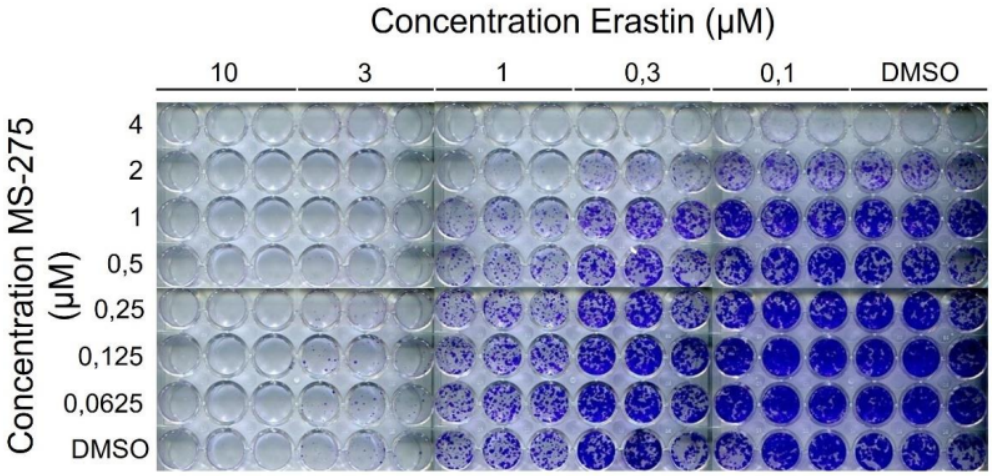

Figure 35: F2612 Clonogenic assay synergy matrix, for use in figure 22 the figure got processed.

Figure 36: Result of the screening for plagiarism with iThenticate (September 29th, 2022).

References

Aktories, K. (2017). Allgemeine und Spezielle Pharmakologie und Toxikologie. Begründet Von W. Forth, D. Henschler, W. Rummel (Philadelphia: Urban & Fischer Verlag GmbH & Co. KG).

Arlt, A., and Schäfer, H. (2016). Investigational histone deacetylase inhibitors for treating pancreatic adenocarcinoma. Expert opinion on investigational drugs *25*, 1251-1254. https://doi.org/10.1080/13543784.2016.1240167.

B'chir, W., Maurin, A.-C., Carraro, V., Averous, J., Jousse, C., Muranishi, Y., Parry, L., Stepien, G., Fafournoux, P., and Bruhat, A. (2013). The eIF2α/ATF4 pathway is essential for stress-induced autophagy gene expression. Nucleic acids research *41*, 7683-7699. https://doi.org/10.1093/nar/gkt563.

Bhaskara, S. (2015). Histone deacetylases 1 and 2 regulate DNA replication and DNA repair: potential targets for genome stability-mechanism-based therapeutics for a subset of cancers. Cell cycle (Georgetown, Tex.) *14*, 1779-1785. https://doi.org/10.1080/15384101.2015.1042634.

Bose, P., Dai, Y., and Grant, S. (2014). Histone deacetylase inhibitor (HDACI) mechanisms of action: emerging insights. Pharmacology & therapeutics *143*, 323-336. https://doi.org/10.1016/j.pharmthera.2014.04.004.

Buscail, L., Bournet, B., and Cordelier, P. (2020). Role of oncogenic KRAS in the diagnosis, prognosis and treatment of pancreatic cancer. Nature reviews. Gastroenterology & hepatology *17*, 153-168. https://doi.org/10.1038/s41575-019-0245-4.

Canto, M.I., Hruban, R.H., Fishman, E.K., Kamel, I.R., Schulick, R., Zhang, Z., Topazian, M., Takahashi, N., Fletcher, J., and Petersen, G., et al. (2012). Frequent detection of pancreatic lesions in asymptomatic high-risk individuals. Gastroenterology *142*, 796-804; quiz e14-5. https://doi.org/10.1053/j.gastro.2012.01.005.

Cao, J.Y., and Dixon, S.J. (2016). Mechanisms of ferroptosis. Cellular and molecular life sciences : CMLS *73*, 2195-2209. https://doi.org/10.1007/s00018-016-2194-1.

Cascinu, S., Falconi, M., Valentini, V., and Jelic, S. (2010). Pancreatic cancer: ESMO Clinical Practice Guidelines for diagnosis, treatment and follow-up. Annals of oncology : official journal of the European Society for Medical Oncology *21 Suppl 5*, v55-8. https://doi.org/10.1093/annonc/mdq165.

Cobler, L., Zhang, H., Suri, P., Park, C., and Timmerman, L.A. (2018). xCT inhibition sensitizes tumors to γ-radiation via glutathione reduction. Oncotarget *9*, 32280-32297. https://doi.org/10.18632/oncotarget.25794.

Conrad, M., and Pratt, D.A. (2019). The chemical basis of ferroptosis. Nature chemical biology *15*, 1137-1147. https://doi.org/10.1038/s41589-019-0408-1.

Conroy, T., Hammel, P., Hebbar, M., Ben Abdelghani, M., Wei, A.C., Raoul, J.-L., Choné, L., Francois, E., Artru, P., and Biagi, J.J., et al. (2018). FOLFIRINOX or

Gemcitabine as Adjuvant Therapy for Pancreatic Cancer. The New England journal of medicine *379*, 2395-2406. https://doi.org/10.1056/NEJMoa1809775.

Damaskos, C., Garmpis, N., Karatzas, T., Nikolidakis, L., Kostakis, I.D., Garmpi, A., Karamaroudis, S., Boutsikos, G., Damaskou, Z., and Kostakis, A., et al. (2015). Histone Deacetylase (HDAC) Inhibitors: Current Evidence for Therapeutic Activities in Pancreatic Cancer. Anticancer research *35*, 3129-3135.

DeHart, D.N., Fang, D., Heslop, K., Li, L., Lemasters, J.J., and Maldonado, E.N. (2018). Opening of voltage dependent anion channels promotes reactive oxygen species generation, mitochondrial dysfunction and cell death in cancer cells. Biochemical pharmacology *148*, 155-162. https://doi.org/10.1016/j.bcp.2017.12.022.

Distler, M., Aust, D., Weitz, J., Pilarsky, C., and Grützmann, R. (2014). Precursor lesions for sporadic pancreatic cancer: PanIN, IPMN, and MCN. BioMed research international *2014*, 474905. https://doi.org/10.1155/2014/474905.

Dixon, S.J., Lemberg, K.M., Lamprecht, M.R., Skouta, R., Zaitsev, E.M., Gleason, C.E., Patel, D.N., Bauer, A.J., Cantley, A.M., and Yang, W.S., et al. (2012). Ferroptosis: an iron-dependent form of nonapoptotic cell death. Cell *149*, 1060-1072. https://doi.org/10.1016/j.cell.2012.03.042.

Doi, R., Imamura, M., Hosotani, R., Imaizumi, T., Hatori, T., Takasaki, K., Funakoshi, A., Wakasugi, H., Asano, T., and Hishinuma, S., et al. (2008). Surgery versus radiochemotherapy for resectable locally invasive pancreatic cancer: final results of a randomized multi-institutional trial. Surgery today *38*, 1021-1028. https://doi.org/10.1007/s00595-007-3745-8.

Dolma, S., Lessnick, S.L., Hahn, W.C., and Stockwell, B.R. (2003). Identification of genotype-selective antitumor agents using synthetic lethal chemical screening in engineered human tumor cells. Cancer cell *3*, 285-296. https://doi.org/10.1016/s1535-6108(03)00050-3.

Duvic, M., Talpur, R., Ni, X., Zhang, C., Hazarika, P., Kelly, C., Chiao, J.H., Reilly, J.F., Ricker, J.L., and Richon, V.M., et al. (2007). Phase 2 trial of oral vorinostat (suberoylanilide hydroxamic acid, SAHA) for refractory cutaneous T-cell lymphoma (CTCL). Blood *109*, 31-39. https://doi.org/10.1182/blood-2006-06-025999.

Eckschlager, T., Plch, J., Stiborova, M., and Hrabeta, J. (2017). Histone Deacetylase Inhibitors as Anticancer Drugs. International journal of molecular sciences *18*. https://doi.org/10.3390/ijms18071414.

Epping, M.T., and Bernards, R. (2009). Molecular basis of the anti-cancer effects of histone deacetylase inhibitors. The international journal of biochemistry & cell biology *41*, 16-20. https://doi.org/10.1016/j.biocel.2008.07.020.

Esposito, I., Konukiewitz, B., Schlitter, A.M., and Klöppel, G. (2014). Pathology of pancreatic ductal adenocarcinoma: facts, challenges and future developments. World journal of gastroenterology *20*, 13833-13841. https://doi.org/10.3748/wjg.v20.i38.13833.

Falkenberg, K.J., and Johnstone, R.W. (2014). Histone deacetylases and their inhibitors in cancer, neurological diseases and immune disorders. Nature reviews. Drug discovery *13*, 673-691. https://doi.org/10.1038/nrd4360.

Fedele, P., Orlando, L., and Cinieri, S. (2017). Targeting triple negative breast cancer with histone deacetylase inhibitors. Expert opinion on investigational drugs *26*, 1199-1206. https://doi.org/10.1080/13543784.2017.1386172.

Feng, W., Zhang, B., Cai, D., and Zou, X. (2014). Therapeutic potential of histone deacetylase inhibitors in pancreatic cancer. Cancer letters *347*, 183-190. https://doi.org/10.1016/j.canlet.2014.02.012.

Fritsche, P., Seidler, B., Schüler, S., Schnieke, A., Göttlicher, M., Schmid, R.M., Saur, D., and Schneider, G. (2009). HDAC2 mediates therapeutic resistance of pancreatic cancer cells via the BH3-only protein NOXA. Gut *58*, 1399-1409. https://doi.org/10.1136/gut.2009.180711.

Fusai, G., Warnaar, N., Sabin, C.A., Archibong, S., and Davidson, B.R. (2008). Outcome of R1 resection in patients undergoing pancreatico-duodenectomy for pancreatic cancer. European journal of surgical oncology : the journal of the European Society of Surgical Oncology and the British Association of Surgical Oncology *34*, 1309-1315. https://doi.org/10.1016/j.ejso.2008.01.017.

Gilroy, A.M. (2009). Atlas of anatomy. Winkingskull.com (New York, Stuttgart: Thieme).

Golan, T., Hammel, P., Reni, M., van Cutsem, E., Macarulla, T., Hall, M.J., Park, J.-O., Hochhauser, D., Arnold, D., and Oh, D.-Y., et al. (2019). Maintenance Olaparib for Germline BRCA-Mutated Metastatic Pancreatic Cancer. The New England journal of medicine *381*, 317-327. https://doi.org/10.1056/NEJMoa1903387.

Haberland, M., Montgomery, R.L., and Olson, E.N. (2009). The many roles of histone deacetylases in development and physiology: implications for disease and therapy. Nature reviews. Genetics *10*, 32-42. https://doi.org/10.1038/nrg2485.

Hafezi, S., Saber-Ayad, M., and Abdel-Rahman, W.M. (2021). Highlights on the Role of KRAS Mutations in Reshaping the Microenvironment of Pancreatic Adenocarcinoma. International journal of molecular sciences *22*. https://doi.org/10.3390/ijms221910219.

Hartwig, W., Hackert, T., Hinz, U., Gluth, A., Bergmann, F., Strobel, O., Büchler, M.W., and Werner, J. (2011). Pancreatic cancer surgery in the new millennium: better prediction of outcome. Annals of surgery *254*, 311-319. https://doi.org/10.1097/SLA.0b013e31821fd334.

Hong, S.-M., Park, J.Y., Hruban, R.H., and Goggins, M. (2011). Molecular signatures of pancreatic cancer. Archives of pathology & laboratory medicine *135*, 716-727. https://doi.org/10.1043/2010-0566-RA.1.

Hontecillas-Prieto, L., Flores-Campos, R., Silver, A., Álava, E. de, Hajji, N., and García-Domínguez, D.J. (2020). Synergistic Enhancement of Cancer Therapy Using HDAC Inhibitors: Opportunity for Clinical Trials. Frontiers in genetics *11*, 578011. https://doi.org/10.3389/fgene.2020.578011.

Hruban, R.H., van Mansfeld, A.D., Offerhaus, G.J., van Weering, D.H., Allison, D.C., Goodman, S.N., Kensler, T.W., Bose, K.K., Cameron, J.L., and Bos, J.L. (1993). K-ras oncogene activation in adenocarcinoma of the human pancreas. A study of 82 carcinomas using a combination of mutant-enriched polymerase chain reaction analysis and allele-specific oligonucleotide hybridization. The American journal of pathology *143*, 545-554.

Ianevski, A., Giri, A.K., and Aittokallio, T. (2022). SynergyFinder 3.0: an interactive analysis and consensus interpretation of multi-drug synergies across multiple samples. Nucleic acids research. https://doi.org/10.1093/nar/gkac382.

Imai, H., Matsuoka, M., Kumagai, T., Sakamoto, T., and Koumura, T. (2017). Lipid Peroxidation-Dependent Cell Death Regulated by GPx4 and Ferroptosis. Current topics in microbiology and immunology *403*, 143-170. https://doi.org/10.1007/82_2016_508.

Jain, A., and Bhardwaj, V. (2021). Therapeutic resistance in pancreatic ductal adenocarcinoma: Current challenges and future opportunities. World journal of gastroenterology *27*, 6527-6550. https://doi.org/10.3748/wjg.v27.i39.6527.

Jones, S., Zhang, X., Parsons, D.W., Lin, J.C.-H., Leary, R.J., Angenendt, P., Mankoo, P., Carter, H., Kamiyama, H., and Jimeno, A., et al. (2008). Core signaling pathways in human pancreatic cancers revealed by global genomic analyses. Science (New York, N.Y.) *321*, 1801-1806. https://doi.org/10.1126/science.1164368.

Kelly, R.D.W., Chandru, A., Watson, P.J., Song, Y., Blades, M., Robertson, N.S., Jamieson, A.G., Schwabe, J.W.R., and Cowley, S.M. (2018). Histone deacetylase (HDAC) 1 and 2 complexes regulate both histone acetylation and crotonylation in vivo. Scientific reports *8*, 14690. https://doi.org/10.1038/s41598-018-32927-9.

Kelly, R.D.W., and Cowley, S.M. (2013). The physiological roles of histone deacetylase (HDAC) 1 and 2: complex co-stars with multiple leading parts. Biochemical Society transactions *41*, 741-749. https://doi.org/10.1042/BST20130010.

Kidess, A., Schmid, S.C., Pollak, S., Gschwend, J.E., Berberat, P.O., and Autenrieth, M.E. (2021). Virtueller Praktikumstag Urologie : Studentenunterricht an der Technischen Universität München in Zeiten der COVID-19-Pandemie. Der Urologe. Ausg. A *60*, 484-490. https://doi.org/10.1007/s00120-020-01431-2.

Kim, H., Kim, M., Im, S.-K., and Fang, S. (2018). Mouse Cre-LoxP system: general principles to determine tissue-specific roles of target genes. Laboratory animal research *34*, 147-159. https://doi.org/10.5625/lar.2018.34.4.147.

Koppula, P., Zhang, Y., Zhuang, L., and Gan, B. (2018). Amino acid transporter SLC7A11/xCT at the crossroads of regulating redox homeostasis and nutrient dependency of cancer. Cancer communications (London, England) *38*, 12. https://doi.org/10.1186/s40880-018-0288-x.

Krauß, L., Urban, B.C., Hastreiter, S., Schneider, C., Wenzel, P., Hassan, Z., Wirth, M., Lankes, K., Terrasi, A., and Klement, C., et al. (2022). HDAC2 Facilitates Pancreatic Cancer Metastasis. Cancer research *82*, 695-707. https://doi.org/10.1158/0008-5472.CAN-20-3209.

Kristianto, J., Johnson, M.G., Zastrow, R.K., Radcliff, A.B., and Blank, R.D. (2017). Spontaneous recombinase activity of Cre-ERT2 in vivo. Transgenic research *26*, 411-417. https://doi.org/10.1007/s11248-017-0018-1.

Kummar, S., Gutierrez, M., Gardner, E.R., Donovan, E., Hwang, K., Chung, E.J., Lee, M.-J., Maynard, K., Kalnitskiy, M., and Chen, A., et al. (2007). Phase I trial of MS-275, a histone deacetylase inhibitor, administered weekly in refractory solid tumors and lymphoid malignancies. Clinical cancer research : an official journal of the American Association for Cancer Research *13*, 5411-5417. https://doi.org/10.1158/1078-0432.CCR-07-0791.

Lane, A.A., and Chabner, B.A. (2009). Histone deacetylase inhibitors in cancer therapy. Journal of clinical oncology : official journal of the American Society of Clinical Oncology *27*, 5459-5468. https://doi.org/10.1200/JCO.2009.22.1291.

Leitlinienprogramm Onkologie (2021). S3-Leitlinie zum exokrinen Pankreaskarzinom. Kurzversion.

Lewerenz, J., Sato, H., Albrecht, P., Henke, N., Noack, R., Methner, A., and Maher, P. (2012). Mutation of ATF4 mediates resistance of neuronal cell lines against oxidative stress by inducing xCT expression. Cell death and differentiation *19*, 847-858. https://doi.org/10.1038/cdd.2011.165.

Li, G., Tian, Y., and Zhu, W.-G. (2020). The Roles of Histone Deacetylases and Their Inhibitors in Cancer Therapy. Frontiers in cell and developmental biology *8*, 576946. https://doi.org/10.3389/fcell.2020.576946.

Li, J.-T., Wang, Y.-P., Yin, M., and Lei, Q.-Y. (2019). Metabolism remodeling in pancreatic ductal adenocarcinoma. Cell stress *3*, 361-368. https://doi.org/10.15698/cst2019.12.205.

Li, Y., and Seto, E. (2016). HDACs and HDAC Inhibitors in Cancer Development and Therapy. Cold Spring Harbor perspectives in medicine *6*. https://doi.org/10.1101/cshperspect.a026831.

Liu, J., Kang, R., and Tang, D. (2021). The Art of War: Ferroptosis and Pancreatic Cancer. Frontiers in pharmacology *12*, 773909. https://doi.org/10.3389/fphar.2021.773909.

Maldonado, E.N. (2017). VDAC-Tubulin, an Anti-Warburg Pro-Oxidant Switch. Frontiers in oncology *7*, 4. https://doi.org/10.3389/fonc.2017.00004.

Maldonado, E.N., and Lemasters, J.J. (2012). Warburg revisited: regulation of mitochondrial metabolism by voltage-dependent anion channels in cancer cells. The Journal of pharmacology and experimental therapeutics *342*, 637-641. https://doi.org/10.1124/jpet.112.192153.

Mariño-Ramírez, L., Kann, M.G., Shoemaker, B.A., and Landsman, D. (2005). Histone structure and nucleosome stability. Expert review of proteomics *2*, 719-729. https://doi.org/10.1586/14789450.2.5.719.

Masson, G.R. (2019). Towards a model of GCN2 activation. Biochemical Society transactions *47*, 1481-1488. https://doi.org/10.1042/BST20190331.

Miyake, K., Yoshizumi, T., Imura, S., Sugimoto, K., Batmunkh, E., Kanemura, H., Morine, Y., and Shimada, M. (2008). Expression of hypoxia-inducible factor-1alpha, histone deacetylase 1, and metastasis-associated protein 1 in pancreatic carcinoma: correlation with poor prognosis with possible regulation. Pancreas *36*, e1-9. https://doi.org/10.1097/MPA.0b013e31815f2c2a.

Miyamoto, K., Watanabe, M., Boku, S., Sukeno, M., Morita, M., Kondo, H., Sakaguchi, K., Taguchi, T., and Sakai, T. (2020). xCT Inhibition Increases Sensitivity to Vorinostat in a ROS-Dependent Manner. Cancers *12*. https://doi.org/10.3390/cancers12040827.

Mootha, V.K., Lindgren, C.M., Eriksson, K.-F., Subramanian, A., Sihag, S., Lehar, J., Puigserver, P., Carlsson, E., Ridderstråle, M., and Laurila, E., et al. (2003). PGC-1alpha-responsive genes involved in oxidative phosphorylation are coordinately downregulated in human diabetes. Nature genetics *34*, 267-273. https://doi.org/10.1038/ng1180.

Moskaluk, C.A., Hruban, R.H., and Kern, S.E. (1997). p16 and K-ras gene mutations in the intraductal precursors of human pancreatic adenocarcinoma. Cancer research *57*, 2140-2143.

Neoptolemos, J.P., Palmer, D.H., Ghaneh, P., Psarelli, E.E., Valle, J.W., Halloran, C.M., Faluyi, O., O'Reilly, D.A., Cunningham, D., and Wadsley, J., et al. (2017). Comparison of adjuvant gemcitabine and capecitabine with gemcitabine monotherapy in patients with resected pancreatic cancer (ESPAC-4): a multicentre, open-label, randomised, phase 3 trial. The Lancet *389*, 1011-1024. https://doi.org/10.1016/S0140-6736(16)32409-6.

Nepali, K., and Liou, J.-P. (2021). Recent developments in epigenetic cancer therapeutics: clinical advancement and emerging trends. Journal of biomedical science *28*, 27. https://doi.org/10.1186/s12929-021-00721-x.

Ott, C., Heinmöller, E., Gaumann, A., Schölmerich, J., and Klebl, F. (2007). Intraepitheliale Neoplasien (PanIN) und intraduktale papillär-muzinöse Neoplasien (IPMN) des Pankreas als Vorläufer des Pankreaskarzinoms. Medizinische Klinik (Munich, Germany : 1983) *102*, 127-135. https://doi.org/10.1007/s00063-007-1013-8.

Ouaïssi, M., Sielezneff, I., Silvestre, R., Sastre, B., Bernard, J.-P., Lafontaine, J.S., Payan, M.J., Dahan, L., Pirrò, N., and Seitz, J.F., et al. (2008). High histone deacetylase 7 (HDAC7) expression is significantly associated with adenocarcinomas of the pancreas. Annals of surgical oncology *15*, 2318-2328. https://doi.org/10.1245/s10434-008-9940-z.

Pape, H.-C., Klinke, R., Brenner, B., and Silbernagl, S. (2014). Physiologie (s.l.: Georg Thieme Verlag KG).

Park, W., Chawla, A., and O'Reilly, E.M. (2021). Pancreatic Cancer: A Review. JAMA *326*, 851-862. https://doi.org/10.1001/jama.2021.13027.

Principe, D.R., Underwood, P.W., Korc, M., Trevino, J.G., Munshi, H.G., and Rana, A. (2021). The Current Treatment Paradigm for Pancreatic Ductal Adenocarcinoma and Barriers to Therapeutic Efficacy. Frontiers in oncology *11*, 688377. https://doi.org/10.3389/fonc.2021.688377.

Promega Corporation. CellTiter-Glo Luminescent Cell Viability Assay Technical Bulletin #TB288.

Rahib, L., Wehner, M.R., Matrisian, L.M., and Nead, K.T. (2021). Estimated Projection of US Cancer Incidence and Death to 2040. JAMA network open *4*, e214708. https://doi.org/10.1001/jamanetworkopen.2021.4708.

Rana, Z., Diermeier, S., Hanif, M., and Rosengren, R.J. (2020). Understanding Failure and Improving Treatment Using HDAC Inhibitors for Prostate Cancer. Biomedicines *8*. https://doi.org/10.3390/biomedicines8020022.

Rassow, J., Hauser, K., Netzker, R., and Deutzmann, R. (2016). Biochemie (Stuttgart: Thieme).

Renz-Polster, H., Krautzig, S., Bätge, B., and Stoll, M. (2013). Basislehrbuch Innere Medizin. Kompakt - greifbar - verständlich ; [Plus im Web, mediscript (München: Elsevier Urban & Fischer).

Richon, V.M., and O'Brien, J.P. (2002). Histone deacetylase inhibitors: a new class of potential therapeutic agents for cancer treatment. Clinical cancer research : an official journal of the American Association for Cancer Research *8*, 662-664.

Roca, M.S., Moccia, T., Iannelli, F., Testa, C., Vitagliano, C., Minopoli, M., Camerlingo, R., Riso, G. de, Cecio, R. de, and Bruzzese, F., et al. (2022). HDAC class I inhibitor domatinostat sensitizes pancreatic cancer to chemotherapy by targeting cancer stem cell compartment via FOXM1 modulation. Journal of experimental & clinical cancer research : CR *41*, 83. https://doi.org/10.1186/s13046-022-02295-4.

Roche, J., and Bertrand, P. (2016). Inside HDACs with more selective HDAC inhibitors. European journal of medicinal chemistry *121*, 451-483. https://doi.org/10.1016/j.ejmech.2016.05.047.

Ruefli, A.A., Ausserlechner, M.J., Bernhard, D., Sutton, V.R., Tainton, K.M., Kofler, R., Smyth, M.J., and Johnstone, R.W. (2001). The histone deacetylase inhibitor and chemotherapeutic agent suberoylanilide hydroxamic acid (SAHA) induces a cell-death pathway characterized by cleavage of Bid and production of reactive oxygen species. Proceedings of the National Academy of Sciences of the United States of America *98*, 10833-10838. https://doi.org/10.1073/pnas.191208598.

Schneider, G., Krämer, O.H., Fritsche, P., Schüler, S., Schmid, R.M., and Saur, D. (2010). Targeting histone deacetylases in pancreatic ductal adenocarcinoma. Journal of cellular and molecular medicine *14*, 1255-1263. https://doi.org/10.1111/j.1582-4934.2009.00974.x.

Schönhuber, N., Seidler, B., Schuck, K., Veltkamp, C., Schachtler, C., Zukowska, M., Eser, S., Feyerabend, T.B., Paul, M.C., and Eser, P., et al. (2014). A next-generation dual-recombinase system for time- and host-specific targeting of pancreatic cancer. Nature medicine *20*, 1340-1347. https://doi.org/10.1038/nm.3646.

Schüler, S., Fritsche, P., Diersch, S., Arlt, A., Schmid, R.M., Saur, D., and Schneider, G. (2010). HDAC2 attenuates TRAIL-induced apoptosis of pancreatic cancer cells. Molecular cancer *9*, 80. https://doi.org/10.1186/1476-4598-9-80.

Schünke, M., Schulte, E., Schumacher, U., Voll, M., and Wesker, K. (2015). Prometheus Lernatlas LernAtlas der Anatomie - Innere Organe (Stuttgart: Thieme).

Selleck Chemicals. www. selleckchem.com. http://selleckchem.com/products/. October 13th, 2019.

Seto, E., and Yoshida, M. (2014). Erasers of histone acetylation: the histone deacetylase enzymes. Cold Spring Harbor perspectives in biology *6*, a018713. https://doi.org/10.1101/cshperspect.a018713.

Shinke, G., Yamada, D., Eguchi, H., Iwagami, Y., Asaoka, T., Noda, T., Wada, H., Kawamoto, K., Gotoh, K., and Kobayashi, S., et al. (2018). Role of histone deacetylase in distant metastasis of pancreatic ductal cancer. Cancer science *109*, 2520-2531. https://doi.org/10.1111/cas.13700.

Shvedunova, M., and Akhtar, A. (2022). Modulation of cellular processes by histone and non-histone protein acetylation. Nature reviews. Molecular cell biology *23*, 329-349. https://doi.org/10.1038/s41580-021-00441-y.

Siegel, R.L., Miller, K.D., Fuchs, H.E., and Jemal, A. (2021). Cancer Statistics, 2021. CA: a cancer journal for clinicians *71*, 7-33. https://doi.org/10.3322/caac.21654.

Siegel, R.L., Miller, K.D., Fuchs, H.E., and Jemal, A. (2022). Cancer statistics, 2022. CA: a cancer journal for clinicians. https://doi.org/10.3322/caac.21708.

Singh, A.K., and Mueller-Planitz, F. (2021). Nucleosome Positioning and Spacing: From Mechanism to Function. Journal of molecular biology *433*, 166847. https://doi.org/10.1016/j.jmb.2021.166847.

Subramanian, A., Tamayo, P., Mootha, V.K., Mukherjee, S., Ebert, B.L., Gillette, M.A., Paulovich, A., Pomeroy, S.L., Golub, T.R., and Lander, E.S., et al. (2005). Gene set enrichment analysis: a knowledge-based approach for interpreting genome-wide expression profiles. Proceedings of the National Academy of Sciences of the United States of America *102*, 15545-15550. https://doi.org/10.1073/pnas.0506580102.

Suragani, R.N.V.S., Zachariah, R.S., Velazquez, J.G., Liu, S., Sun, C.-W., Townes, T.M., and Chen, J.-J. (2012). Heme-regulated eIF2α kinase activated Atf4 signaling pathway in oxidative stress and erythropoiesis. Blood *119*, 5276-5284. https://doi.org/10.1182/blood-2011-10-388132.

SynergyFinder (2020). SynergyFinder - User Documentation. https://synergyfinder.fimm.fi/synergy/synfin_docs/. 9.1.2022.

Tada, M., Ohashi, M., Shiratori, Y., Okudaira, T., Komatsu, Y., Kawabe, T., Yoshida, H., Machinami, R., Kishi, K., and Omata, M. (1996). Analysis of K-ras gene mutation in hyperplastic duct cells of the pancreas without pancreatic disease. Gastroenterology *110*, 227-231. https://doi.org/10.1053/gast.1996.v110.pm8536861.

Trachootham, D., Zhou, Y., Zhang, H., Demizu, Y., Chen, Z., Pelicano, H., Chiao, P.J., Achanta, G., Arlinghaus, R.B., and Liu, J., et al. (2006). Selective killing of oncogenically transformed cells through a ROS-mediated mechanism by beta-phenylethyl isothiocyanate. Cancer cell *10*, 241-252. https://doi.org/10.1016/j.ccr.2006.08.009.

U.S. Federal Government. Olaparib in gBRCA Mutated Pancreatic Cancer Whose Disease Has Not Progressed on First Line Platinum-Based Chemotherapy (POLO). https://clinicaltrials.gov/ct2/show/NCT02184195. 15.05.2022.

U.S. Food and Drug Administration (2019). FDA approves olaparib for gBRCAm metastatic pancreatic adenocarcinoma. https://www.fda.gov/drugs/resources-information-approved-drugs/fda-approves-olaparib-gbrcam-metastatic-pancreatic-adenocarcinoma. November 13, 2021.

Venugopal, B., and Evans, T.R.J. (2011). Developing histone deacetylase inhibitors as anti-cancer therapeutics. Current medicinal chemistry *18*, 1658-1671. https://doi.org/10.2174/092986711795471284.

Wagner, M., Redaelli, C., Lietz, M., Seiler, C.A., Friess, H., and Büchler, M.W. (2004). Curative resection is the single most important factor determining outcome in patients with pancreatic adenocarcinoma. The British journal of surgery *91*, 586-594. https://doi.org/10.1002/bjs.4484.

Wang, G., He, J., Zhao, J., Yun, W., Xie, C., Taub, J.W., Azmi, A., Mohammad, R.M., Dong, Y., and Kong, W., et al. (2012). Class I and class II histone deacetylases are potential therapeutic targets for treating pancreatic cancer. PloS one *7*, e52095. https://doi.org/10.1371/journal.pone.0052095.

Wang, X., Liu, K., Gong, H., Li, D., Chu, W., Zhao, D., Wang, X., and Xu, D. (2021). Death by histone deacetylase inhibitor quisinostat in tongue squamous cell carcinoma via apoptosis, pyroptosis, and ferroptosis. Toxicology and applied pharmacology *410*, 115363. https://doi.org/10.1016/j.taap.2020.115363.

Waters, A.M., and Der, C.J. (2018). KRAS: The Critical Driver and Therapeutic Target for Pancreatic Cancer. Cold Spring Harbor perspectives in medicine *8*. https://doi.org/10.1101/cshperspect.a031435.

Weichert, W. (2009). HDAC expression and clinical prognosis in human malignancies. Cancer letters *280*, 168-176. https://doi.org/10.1016/j.canlet.2008.10.047.

Welsch, U., Deller, T., and Kummer, W. (2014). Lehrbuch Histologie (München: Elsevier Urban & Fischer).

Wolf, I.M.L., Fan, Z., Rauh, M., Seufert, S., Hore, N., Buchfelder, M., Savaskan, N.E., and Eyüpoglu, I.Y. (2014). Histone deacetylases inhibition by SAHA/Vorinostat normalizes the glioma microenvironment via xCT equilibration. Scientific reports *4*, 6226. https://doi.org/10.1038/srep06226.

Wortel, I.M.N., van der Meer, L.T., Kilberg, M.S., and van Leeuwen, F.N. (2017). Surviving Stress: Modulation of ATF4-Mediated Stress Responses in Normal and Malignant Cells. Trends in endocrinology and metabolism: TEM *28*, 794-806. https://doi.org/10.1016/j.tem.2017.07.003.

Wu, J., Liu, X., Nayak, S.G., Pitarresi, J.R., Cuitiño, M.C., Yu, L., Hildreth, B.E., Thies, K.A., Schilling, D.J., and Fernandez, S.A., et al. (2017). Generation of a pancreatic cancer model using a Pdx1-Flp recombinase knock-in allele. PloS one *12*, e0184984. https://doi.org/10.1371/journal.pone.0184984.

Yadav, B., Wennerberg, K., Aittokallio, T., and Tang, J. (2015). Searching for Drug Synergy in Complex Dose-Response Landscapes Using an Interaction Potency Model. Computational and structural biotechnology journal *13*, 504-513. https://doi.org/10.1016/j.csbj.2015.09.001.

Yagoda, N., Rechenberg, M. von, Zaganjor, E., Bauer, A.J., Yang, W.S., Fridman, D.J., Wolpaw, A.J., Smukste, I., Peltier, J.M., and Boniface, J.J., et al. (2007). RAS-RAF-MEK-dependent oxidative cell death involving voltage-dependent anion channels. Nature *447*, 864-868. https://doi.org/10.1038/nature05859.

Yang, H., Zhao, L., Gao, Y., Yao, F., Marti, T.M., Schmid, R.A., and Peng, R.-W. (2020). Pharmacotranscriptomic Analysis Reveals Novel Drugs and Gene Networks Regulating Ferroptosis in Cancer. Cancers *12*. https://doi.org/10.3390/cancers12113273.

Yang, W.S., SriRamaratnam, R., Welsch, M.E., Shimada, K., Skouta, R., Viswanathan, V.S., Cheah, J.H., Clemons, P.A., Shamji, A.F., and Clish, C.B., et al. (2014). Regulation of ferroptotic cancer cell death by GPX4. Cell *156*, 317-331. https://doi.org/10.1016/j.cell.2013.12.010.

Yang, X.-J., and Seto, E. (2008). The Rpd3/Hda1 family of lysine deacetylases: from bacteria and yeast to mice and men. Nature reviews. Molecular cell biology *9*, 206-218. https://doi.org/10.1038/nrm2346.

Zaborske, J.M., Narasimhan, J., Jiang, L., Wek, S.A., Dittmar, K.A., Freimoser, F., Pan, T., and Wek, R.C. (2009). Genome-wide Analysis of tRNA Charging and Activation of the eIF2 Kinase Gcn2p*♦. The Journal of biological chemistry *284*, 25254-25267. https://doi.org/10.1074/jbc.M109.000877.

Zamboni, G., Hirabayashi, K., Castelli, P., and Lennon, A.M. (2013). Precancerous lesions of the pancreas. Best practice & research. Clinical gastroenterology *27*, 299-322. https://doi.org/10.1016/j.bpg.2013.04.001.

Zhang, J., and Zhong, Q. (2014). Histone deacetylase inhibitors and cell death. Cellular and molecular life sciences : CMLS *71*, 3885-3901. https://doi.org/10.1007/s00018-014-1656-6.

Zhang, Y., Tan, H., Daniels, J.D., Zandkarimi, F., Liu, H., Brown, L.M., Uchida, K., O'Connor, O.A., and Stockwell, B.R. (2019). Imidazole Ketone Erastin Induces Ferroptosis and Slows Tumor Growth in a Mouse Lymphoma Model. Cell chemical biology *26*, 623-633.e9. https://doi.org/10.1016/j.chembiol.2019.01.008.

Zhao, Y., Li, Y., Zhang, R., Wang, F., Wang, T., and Jiao, Y. (2020). The Role of Erastin in Ferroptosis and Its Prospects in Cancer Therapy. OncoTargets and therapy *13*, 5429-5441. https://doi.org/10.2147/OTT.S254995.

Zille, M., Kumar, A., Kundu, N., Bourassa, M.W., Wong, V.S.C., Willis, D., Karuppagounder, S.S., and Ratan, R.R. (2019). Ferroptosis in Neurons and Cancer Cells Is Similar But Differentially Regulated by Histone Deacetylase Inhibitors. eNeuro *6*. https://doi.org/10.1523/ENEURO.0263-18.2019.

Screening of a drug library in HDAC-2 proficient and deficient murine pancreatic ductal adenocarcinoma cells to identify new potential combination therapies

ECHTHEITSBERICHT

29 %
ÄHNLICHKEITSINDEX

HAUPTQUELLEN

1	d-nb.info Internet	414 Wörter —	2 %
2	ouci.dntb.gov.ua Internet	345 Wörter —	1 %
3	www.biorxiv.org Internet	345 Wörter —	1 %
4	www.selleckchem.com Internet	293 Wörter —	1 %
5	www.mdpi.com Internet	240 Wörter —	1 %
6	link.springer.com Internet	192 Wörter —	1 %
7	hdl.handle.net Internet	190 Wörter —	1 %
8	rupress.org Internet	163 Wörter —	1 %
9	journals.biologists.com Internet	119 Wörter —	< 1 %

10	elifesciences.org Internet	115 Wörter — < 1 %
11	www.frontiersin.org Internet	110 Wörter — < 1 %
12	academicrepository.khas.edu.tr Internet	93 Wörter — < 1 %
13	www.spandidos-publications.com Internet	88 Wörter — < 1 %
14	www.nature.com Internet	85 Wörter — < 1 %
15	etheses.whiterose.ac.uk Internet	81 Wörter — < 1 %
16	refubium.fu-berlin.de Internet	76 Wörter — < 1 %
17	edoc.ub.uni-muenchen.de Internet	71 Wörter — < 1 %
18	openscience.ub.uni-mainz.de Internet	71 Wörter — < 1 %
19	www.fda.gov Internet	70 Wörter — < 1 %
20	aacrjournals.org Internet	68 Wörter — < 1 %
21	Newbold, Andrea, Katrina J Falkenberg, Miles H. Prince, and Ricky W Johnstone. "How do tumor cells respond to HDAC inhibition?", FEBS Journal, 2016.	66 Wörter — < 1 %

Crossref

22	mdpi-res.com Internet	65 Wörter —	< 1 %
23	www.springermedizin.de Internet	63 Wörter —	< 1 %
24	Han, Jong Jin. "Investigating the Role of Adipocyte Yap in Glucose Homeostasis and Adipose Tissue Fibrosis", University of Toronto (Canada), 2021 ProQuest	62 Wörter —	< 1 %
25	docserv.uni-duesseldorf.de Internet	61 Wörter —	< 1 %
26	mediatum.ub.tum.de Internet	58 Wörter —	< 1 %
27	Lisa Nguyen, Michelle Westerhoff, Leonie Thewes, Wasco Wruck, Andreas S. Reichert, Carsten Berndt, James Adjaye. "JNK signalling regulates self-renewal of proliferative urine-derived renal progenitor cells via inhibition of ferroptosis", Cold Spring Harbor Laboratory, 2022 Crossref Posted Content	56 Wörter —	< 1 %
28	addi.ehu.es Internet	56 Wörter —	< 1 %
29	www.medchemexpress.com Internet	52 Wörter —	< 1 %
30	Steinhart, Zachary. "Genome-wide CRISPR Screens to Uncover Novel Therapeutic Targets in Wnt-β-catenin Driven Gastrointestinal Cancers.", University of Toronto (Canada), 2019 ProQuest	50 Wörter —	< 1 %

31	Yibo Liu, Yuanjian Fang, Zeyu Zhang, Yujie Luo, Anke Zhang, Cameron Lenahan, Sheng Chen. "Ferroptosis: An emerging therapeutic target in stroke", Journal of Neurochemistry, 2021 Crossref	50 Wörter — < 1 %
32	Lief E. Fenno, Charu Ramakrishnan, Yoon Seok Kim, Kathryn E. Evans et al. "Comprehensive Dual- and Triple-Feature Intersectional Single-Vector Delivery of Diverse Functional Payloads to Cells of Behaving Mammals", Neuron, 2020 Crossref	48 Wörter — < 1 %
33	naturalcancerhandbook.com Internet	48 Wörter — < 1 %
34	www.zora.uzh.ch Internet	48 Wörter — < 1 %
35	ueg.eu Internet	47 Wörter — < 1 %
36	www.repository.cam.ac.uk Internet	47 Wörter — < 1 %
37	www.tandfonline.com Internet	47 Wörter — < 1 %
38	Xiuyi Wu, Shanglin Jin, Yiwen Yang, Xiaoli Lu, Xiaoxi Dai, Zhongyi Xu, Chengfeng Zhang, Leihong Flora Xiang. "Altered expression of ferroptosis markers and iron metabolism reveals a potential role of ferroptosis in vitiligo", Pigment Cell & Melanoma Research, 2022 Crossref	46 Wörter — < 1 %
39	www.oncotarget.com Internet	46 Wörter — < 1 %

40	m.scirp.org Internet	45 Wörter — < 1 %
41	www.biomedexperts.com Internet	45 Wörter — < 1 %
42	i-cirena.ubfc.fr Internet	44 Wörter — < 1 %
43	Ronan Talty, Marcus Bosenberg. "The role of ferroptosis in melanoma", Pigment Cell & Melanoma Research, 2021 Crossref	43 Wörter — < 1 %
44	coek.info Internet	43 Wörter — < 1 %
45	digibug.ugr.es Internet	43 Wörter — < 1 %
46	discovery.ucl.ac.uk Internet	43 Wörter — < 1 %
47	www.scholars.northwestern.edu Internet	43 Wörter — < 1 %
48	citeseerx.ist.psu.edu Internet	42 Wörter — < 1 %
49	docksci.com Internet	42 Wörter — < 1 %
50	www.neoplasia.com Internet	42 Wörter — < 1 %
51	erc.bioscientifica.com Internet	

		41 Wörter — < 1 %
52	rdrr.io Internet	41 Wörter — < 1 %
53	acikbilim.yok.gov.tr Internet	40 Wörter — < 1 %
54	acris.aalto.fi Internet	37 Wörter — < 1 %
55	academictree.org Internet	36 Wörter — < 1 %
56	www.preprints.org Internet	36 Wörter — < 1 %
57	"Textbook of Pancreatic Cancer", Springer Science and Business Media LLC, 2021 Crossref	34 Wörter — < 1 %
58	thesis.honors.olemiss.edu Internet	34 Wörter — < 1 %
59	www.hh.um.es Internet	33 Wörter — < 1 %
60	ndl.ethernet.edu.et Internet	32 Wörter — < 1 %
61	revista.spcir.com Internet	32 Wörter — < 1 %
62	www.iieta.org Internet	32 Wörter — < 1 %

63	Bhagwan Yadav, Krister Wennerberg, Tero Aittokallio, Jing Tang. "Searching for Drug Synergy in Complex Dose–Response Landscapes Using an Interaction Potency Model", Computational and Structural Biotechnology Journal, 2015 Crossref	31 Wörter — < 1 %
64	www.koreascience.or.kr Internet	31 Wörter — < 1 %
65	ascopost.com Internet	30 Wörter — < 1 %
66	digitalcommons.library.tmc.edu Internet	30 Wörter — < 1 %
67	elib.uni-stuttgart.de Internet	30 Wörter — < 1 %
68	www.ncbi.nlm.nih.gov Internet	30 Wörter — < 1 %
69	discovery.dundee.ac.uk Internet	29 Wörter — < 1 %
70	etds.lib.ncku.edu.tw Internet	29 Wörter — < 1 %
71	nbn-resolving.de Internet	29 Wörter — < 1 %
72	theses.gla.ac.uk Internet	29 Wörter — < 1 %
73	utsouthwestern.pure.elsevier.com Internet	28 Wörter — < 1 %

74	"Ferroptosis in Health and Disease", Springer Science and Business Media LLC, 2019 Crossref	26 Wörter — < 1 %
75	cronfa.swan.ac.uk Internet	26 Wörter — < 1 %
76	lra.le.ac.uk Internet	26 Wörter — < 1 %
77	neuro.unboundmedicine.com Internet	26 Wörter — < 1 %
78	www.science.org Internet	25 Wörter — < 1 %
79	escholarship.org Internet	24 Wörter — < 1 %
80	www.wjgnet.com Internet	24 Wörter — < 1 %
81	Wungki Park, Akhil Chawla, Eileen M. O'Reilly. "Pancreatic Cancer", JAMA, 2021 Crossref	23 Wörter — < 1 %
82	www.escholar.manchester.ac.uk Internet	22 Wörter — < 1 %
83	"Ferroptosis: Mechanism and Diseases", Springer Science and Business Media LLC, 2021 Crossref	21 Wörter — < 1 %
84	Ivan Corbeski, Xiaohu Guo, Bruna V. Eckhardt, Domenico Fasci et al. "Chaperoning of the histone octamer by the acidic domain of DNA repair factor APLF", Cold Spring Harbor Laboratory, 2022	21 Wörter — < 1 %

Crossref Posted Content

85	api.crossref.org Internet	20 Wörter — < 1 %
86	etj.bioscientifica.com Internet	20 Wörter — < 1 %
87	www.scirp.org Internet	20 Wörter — < 1 %
88	Bourne, Krystyn Zimmer. "Regulation of BACE1 promoter activity by nuclear factor-kappaB", Proquest, 20111109 ProQuest	19 Wörter — < 1 %
89	Wagner, Sarah. "Biomarker Discovery for Disease Progression and Metastasis in Prostate Cancer: A Multi-Omic Approach.", Nottingham Trent University (United Kingdom), 2020 ProQuest	19 Wörter — < 1 %
90	jultika.oulu.fi Internet	19 Wörter — < 1 %
91	arthritis-research.biomedcentral.com Internet	18 Wörter — < 1 %
92	diposit.ub.edu Internet	18 Wörter — < 1 %
93	journals.plos.org Internet	18 Wörter — < 1 %
94	nmbu.brage.unit.no Internet	18 Wörter — < 1 %

www.dovepress.com

95	Internet	18 Wörter — < 1 %
96	kclpure.kcl.ac.uk Internet	17 Wörter — < 1 %
97	mdpi.com Internet	17 Wörter — < 1 %
98	portlandpress.com Internet	17 Wörter — < 1 %
99	repositori.upf.edu Internet	17 Wörter — < 1 %
100	Meijer, Alfred J., Séverine Lorin, Edward F. Blommaart, and Patrice Codogno. "Regulation of autophagy by amino acids and MTOR-dependent signal transduction", Amino Acids, 2015. Crossref	16 Wörter — < 1 %
101	orca.cf.ac.uk Internet	16 Wörter — < 1 %
102	www.revistacomunicar.com Internet	16 Wörter — < 1 %
103	Eva Hellsberg, Gerhard F. Ecker, Anna Stary-Weinzinger, Lucy R. Forrest. "A structural model of the human serotonin transporter in an outward-occluded state", Cold Spring Harbor Laboratory, 2019 Crossref Posted Content	15 Wörter — < 1 %
104	cyberleninka.org Internet	15 Wörter — < 1 %
105	kjronline.org Internet	

15 Wörter — < 1 %

106 qmro.qmul.ac.uk
Internet
15 Wörter — < 1 %

107 Alnefaie, Ghaliah Obaid F. "Epigenetic Sensitisation of Chemotherapeutic Compounds in Non- Small Cell Lung Cancer", The University of Liverpool (United Kingdom), 2020
ProQuest
14 Wörter — < 1 %

108 Loncar, Ana. "Development and characterization of a polymerization deficient actin monomer and longitudinal actin dimer", Proquest, 20111003
ProQuest
14 Wörter — < 1 %

109 Panpan Hu, Yi Xu, Yanjiao Jiang, Jie Huang, Yi Liu, Dapeng Wang, Ting Tao, Zengxian Sun, Yun Liu. "The mechanism of the imbalance between proliferation and ferroptosis in pulmonary artery smooth muscle cells based on the activation of SLC7A11", European Journal of Pharmacology, 2022
Crossref
14 Wörter — < 1 %

110 Translation and Its Regulation in Cancer Biology and Medicine, 2014.
Crossref
14 Wörter — < 1 %

111 en.wikipedia.org
Internet
14 Wörter — < 1 %

112 immuneweb.xxmu.edu.cn
Internet
14 Wörter — < 1 %

113 opendata.uni-halle.de
Internet

14 Wörter — < 1 %

114 opus.bibliothek.uni-wuerzburg.de
Internet
14 Wörter — < 1 %

115 "Urothelial Carcinoma", Springer Science and Business Media LLC, 2018
Crossref
13 Wörter — < 1 %

116 Maskrey, Taber S.. "Synthetic Studies of Heterocyclic and Bioactive Agents", University of Pittsburgh, 2022
ProQuest
13 Wörter — < 1 %

117 Sykes, Paul David. "Development and in vitro Characterisation of a Super-paramagnetic Hybrid Nanoparticle for Multi-modal Targeted Drug Delivery in Pancreatic Cancer.", The University of Liverpool (United Kingdom), 2020
ProQuest
13 Wörter — < 1 %

118 Yilong Zou, Stuart L. Schreiber. "Progress in Understanding Ferroptosis and Challenges in Its Targeting for Therapeutic Benefit", Cell Chemical Biology, 2020
Crossref
13 Wörter — < 1 %

119 gut.bmj.com
Internet
13 Wörter — < 1 %

120 medlem.foreningssupport.se
Internet
13 Wörter — < 1 %

121 "Pancreatic Cancer", Springer Science and Business Media LLC, 2018
Crossref
12 Wörter — < 1 %

122 Gaupel, Ann-Christin. "A functional genomics approach to investigate the mechanism of action of the histone deacetylase inhibitor CG-1521.", Proquest, 2014.
ProQuest
12 Wörter — < 1 %

123 Herrmann, Mareike(Brand, Eva). "Analysis of sAC expression and function as a co-factor of CREB", Münster University, Germany, Document Server, 2012.
Publikationen
12 Wörter — < 1 %

124 Jasmin Sponagel, Jill K. Jones, Cheryl Frankfater, Shanshan Zhang et al. "Sex Differences in Brain Tumor Glutamine Metabolism Reveal Sex-Specific Vulnerabilities to Treatment", Cold Spring Harbor Laboratory, 2021
Crossref Posted Content
12 Wörter — < 1 %

125 Jiaming Qian, Hong Yang, Jingnan Li, Jian Wang. "Chapter 16 Characterization of the Molecular Genetic Mechanisms that Contribute to Pancreatic Cancer Carcinogenesis", IntechOpen, 2012
Crossref
12 Wörter — < 1 %

126 Nguyen, Son Ngoc. "Defining the Nature of CD8+ T Cell Responses in Lymphoid Tissues of HIV-1 Elite Controllers: An Implication for HIV Cure.", University of Pennsylvania, 2020
ProQuest
12 Wörter — < 1 %

127 Yuan Zhang, Man Wang, Wenguang Chang. "Iron dyshomeostasis and ferroptosis in Alzheimer's disease: Molecular mechanisms of cell death and novel therapeutic drugs and targets for AD", Frontiers in Pharmacology, 2022
Crossref
12 Wörter — < 1 %

128	dx.doi.org Internet	12 Wörter — < 1 %
129	www.cureus.com Internet	12 Wörter — < 1 %
130	Papadopoli, David. "The Impact of AMPK Signalling and Clinical Therapeutics on Cancer Metabolism", McGill University (Canada), 2020 ProQuest	11 Wörter — < 1 %
131	Takashi Kumagai, Naoki Wakimoto, Dong Yin, Sigal Gery et al. "Histone deacetylase inhibitor, suberoylanilide hydroxamic acid (Vorinostat, SAHA) profoundly inhibits the growth of human pancreatic cancer cells", International Journal of Cancer, 2007 Crossref	11 Wörter — < 1 %
132	breast-cancer-research.biomedcentral.com Internet	11 Wörter — < 1 %
133	cancerci.biomedcentral.com Internet	11 Wörter — < 1 %
134	docs.di.fc.ul.pt Internet	11 Wörter — < 1 %
135	emboj.embopress.org Internet	11 Wörter — < 1 %
136	epdf.pub Internet	11 Wörter — < 1 %
137	epub.uni-regensburg.de Internet	11 Wörter — < 1 %
138	helda.helsinki.fi	

Internet

11 Wörter — < 1 %

139 livrepository.liverpool.ac.uk
Internet

11 Wörter — < 1 %

140 onlinelibrary.wiley.com
Internet

11 Wörter — < 1 %

141 www.cs.princeton.edu
Internet

11 Wörter — < 1 %

142 www.embopress.org
Internet

11 Wörter — < 1 %

143 Aleksandr Ianevski, Liye He, Tero Aittokallio, Jing Tang. "SynergyFinder: a web application for analyzing drug combination dose–response matrix data", Bioinformatics, 2017
Crossref

10 Wörter — < 1 %

144 Gutierrez, Helga Nayelli Palma. "Induction of Differentiation of a Human Pancreas-Derived Cell Line Towards an Endocrine Cell Fate", The University of Manchester (United Kingdom), 2021
ProQuest

10 Wörter — < 1 %

145 Majeed, Safa. "Targeting the Ubiquitin Proteasome System for the Treatment of Small Cell Lung Cancer", University of Toronto (Canada), 2020
ProQuest

10 Wörter — < 1 %

146 Sang Jun Yoon, Joseph A Combs, Aimee Falzone, Nicolas Prieto-Farigua et al. "The Origin Of Cysteine and its Catabolism in Mammalian Tissues and Tumors", Cold Spring Harbor Laboratory, 2022
Crossref Posted Content

10 Wörter — < 1 %

147	acikerisim.iku.edu.tr Internet	10 Wörter — < 1 %
148	creativecommons.org Internet	10 Wörter — < 1 %
149	dokumen.pub Internet	10 Wörter — < 1 %
150	pure.amc.nl Internet	10 Wörter — < 1 %
151	rucforsk.ruc.dk Internet	10 Wörter — < 1 %
152	symposium.cshlp.org Internet	10 Wörter — < 1 %
153	tuprints.ulb.tu-darmstadt.de Internet	10 Wörter — < 1 %
154	Bayat Mokhtari, Reza . "Acetazolamide Potentiates the Anti-Tumor Efficacy of Sulforaphane and HDAC Inhibitor, MS-275, on Bronchial Carcinoids and Neuroblastoma.", University of Toronto (Canada), 2019 ProQuest	9 Wörter — < 1 %
155	Dwaipayan Adhya, Anirban Basu. "Epigenetic modulation of host: new insights into immune evasion by viruses", Journal of Biosciences, 2010 Crossref	9 Wörter — < 1 %
156	Fuhao Huang, Jinlong Pang, Liansong Xu, Wenwen Niu, Yaoshuai Zhang, Shanshan Li, Xian Li. "Hedyotis diffusa injection induces ferroptosis via the	9 Wörter — < 1 %

Bax/Bcl2/VDAC2/3 axis in lung adenocarcinoma", Phytomedicine, 2022
Crossref

157 Giulio Spinozzi, Valentina Tini, Alessio Ferrari, Ilaria Gionfriddo et al. "SiCoDEA: a simple, fast and complete app for analyzing the effect of individual drugs and their combinations", Cold Spring Harbor Laboratory, 2022 — 9 Wörter — < 1 %
Crossref Posted Content

158 MARILITA M. MOSCHOS, MARIA DETTORAKI, SOFIA ANDROUDI, DIMITRIOS KALOGEROPOULOS et al. "The Role of Histone Deacetylase Inhibitors in Uveal Melanoma: Current Evidence", Anticancer Research, 2018 — 9 Wörter — < 1 %
Crossref

159 Nattramilarasu, Praveen Kumar. "Campylobacter concisus Impairs Colonic Epithelial Sodium Channel Function and Aggravates Epithelial Barrier Dysfunction via Mucosal Immune Activation", Freie Universitaet Berlin (Germany), 2022 — 9 Wörter — < 1 %
ProQuest

160 Schmidt, Kamila. "In Vitro Analysis of Volatile Organic Compounds in Search of Potential Biomarkers of Lung Cancer", University of Salford (United Kingdom), 2021 — 9 Wörter — < 1 %
ProQuest

161 Weichert, W.. "HDAC expression and clinical prognosis in human malignancies", Cancer Letters, 20090808 — 9 Wörter — < 1 %
Crossref

162 Williams, Dylan. "The Role of Nrf2 in Pancreatic Cancer and the Evaluation of Brusatol as a Chemotherapeutic Agent", The University of Liverpool (United — 9 Wörter — < 1 %

Kingdom)
ProQuest

163	Yilei Zhang, Li Zhuang, Boyi Gan. "BAP1 suppresses tumor development by inducing ferroptosis upon SLC7A11 repression", Molecular & Cellular Oncology, 2018 Crossref	9 Wörter — < 1 %
164	bio-protocol.org Internet	9 Wörter — < 1 %
165	clinicalepigeneticsjournal.biomedcentral.com Internet	9 Wörter — < 1 %
166	digitalcommons.wayne.edu Internet	9 Wörter — < 1 %
167	effiloop.com Internet	9 Wörter — < 1 %
168	macau.uni-kiel.de Internet	9 Wörter — < 1 %
169	nrs.harvard.edu Internet	9 Wörter — < 1 %
170	open.uct.ac.za Internet	9 Wörter — < 1 %
171	publikationen.ub.uni-frankfurt.de Internet	9 Wörter — < 1 %
172	qspace.library.queensu.ca Internet	9 Wörter — < 1 %
173	sedici.unlp.edu.ar Internet	

9 Wörter — < 1 %

174 www.patentguru.com
Internet
9 Wörter — < 1 %

175 "Translational Pancreatic Cancer Research", Springer Science and Business Media LLC, 2020
Crossref
8 Wörter — < 1 %

176 Arroja, Raquel Esteves. "Studying the Role of Hypoxia in Glioblastoma", Universidade do Algarve (Portugal), 2022
ProQuest
8 Wörter — < 1 %

177 Avila, Jacqueli. "The role of Notch1 in K-ras induced pancreatic ductal adenocarcinoma", Proquest, 2014.
ProQuest
8 Wörter — < 1 %

178 Ayyıldız, Zeynep Ozge. "Validation of Prognostic Biomarkers for Overall Survival in Melanoma Patients undergoing Autologous Vaccination", Bilkent Universitesi (Turkey)
ProQuest
8 Wörter — < 1 %

179 Christos Damaskos, Nikolaos Garmpis, Dimitrios Dimitroulis, Anna Garmpi et al. "The Role of SNHG15 in the Pathogenesis of Hepatocellular Carcinoma", Journal of Personalized Medicine, 2022
Crossref
8 Wörter — < 1 %

180 Erika Bourguet, Katarzyna Ozdarska, Gautier Moroy, Jérôme Jeanblanc, Mickaël Naassila. "Class I HDAC Inhibitors: Potential New Epigenetic Therapeutics for Alcohol Use Disorder (AUD)", Journal of Medicinal Chemistry, 2017
Crossref
8 Wörter — < 1 %

181 Jong Kyong Kim, Guangyan Kan, Yu Mao, Zhixuan Wu, Xionghong Tan, Heng He, Chunsik Lee. "UHRF1 downmodulation enhances antitumor effects of histone deacetylase inhibitors in retinoblastoma by augmenting oxidative stress - mediated apoptosis", Molecular Oncology, 2019
Crossref
8 Wörter — < 1 %

182 Maria New, Heidi Olzscha, Nicholas B. La Thangue. "HDAC inhibitor-based therapies: Can we interpret the code?", Molecular Oncology, 2012
Crossref
8 Wörter — < 1 %

183 Minlin Jiang, Meng Qiao, Chuanliang Zhao, Juan Deng, Xuefei Li, Caicun Zhou. "Targeting ferroptosis for cancer therapy: exploring novel strategies from its mechanisms and role in cancers", Translational Lung Cancer Research, 2020
Crossref
8 Wörter — < 1 %

184 Mittermaier, Stephanie. "Characterisation of Functional and Sensory Properties of Lupin Proteins.", Friedrich-Alexander-Universitaet Erlangen-Nuernberg (Germany), 2021
ProQuest
8 Wörter — < 1 %

185 N Stojanovic, Z Hassan, M Wirth, P Wenzel et al. "HDAC1 and HDAC2 integrate the expression of p53 mutants in pancreatic cancer", Oncogene, 2016
Crossref
8 Wörter — < 1 %

186 Rihan Hai, Deyi Yang, Feifei Zheng, Weiqin Wang, Xing Han, Ann M. Bode, Xiangjian Luo. "The emerging roles of HDACs and their therapeutic implications in cancer", European Journal of Pharmacology, 2022
Crossref
8 Wörter — < 1 %

187 S Spiegel. "Endogenous modulators and pharmacological inhibitors of histone deacetylases in cancer therapy", Oncogene, 07/04/2011 — 8 Wörter — < 1 %
Crossref

188 Sangiliyandi Gurunathan, Min-hee Kang, Jin-Hoi Kim. "Combination Effect of Silver Nanoparticles and Histone Deacetylases Inhibitor in Human Alveolar Basal Epithelial Cells", Molecules, 2018 — 8 Wörter — < 1 %
Crossref

189 Völk, Helmut. "Etablierung eines Infektionsmodells in Säugerzellen zur Charakterisierung des Pathogenitätsfaktors SpvB von Salmonella enterica", Universität Ulm. Medizinische Fakultät, 2012. — 8 Wörter — < 1 %
Publikationen

190 Ziyan Y. Pessetto, Bin Chen, Hani Alturkmani, Stephen Hyter et al. "In silico and in vitro drug screening identifies new therapeutic approaches for Ewing sarcoma", Oncotarget, 2016 — 8 Wörter — < 1 %
Crossref

191 Zuo, Chong. "A Thesis on Macrophage Proliferation Machinery Drives Immunosuppression and PDAC Progression ", Washington University in St. Louis — 8 Wörter — < 1 %
ProQuest

192 academic.oup.com — 8 Wörter — < 1 %
Internet

193 bmccancer.biomedcentral.com — 8 Wörter — < 1 %
Internet

194 cdr.lib.unc.edu

	Internet	8 Wörter — < 1 %
195	digitalcommons.usf.edu Internet	8 Wörter — < 1 %
196	ediss.uni-goettingen.de Internet	8 Wörter — < 1 %
197	edoc.unibas.ch Internet	8 Wörter — < 1 %
198	encyclopedia.pub Internet	8 Wörter — < 1 %
199	gentaur.com Internet	8 Wörter — < 1 %
200	pdffox.com Internet	8 Wörter — < 1 %
201	pubs.acs.org Internet	8 Wörter — < 1 %
202	pure.manchester.ac.uk Internet	8 Wörter — < 1 %
203	pure.rug.nl Internet	8 Wörter — < 1 %
204	repisalud.isciii.es Internet	8 Wörter — < 1 %
205	savoirs.usherbrooke.ca Internet	8 Wörter — < 1 %
206	studentsrepo.um.edu.my	

	Internet	8 Wörter — < 1 %
207	test.dovepress.com Internet	8 Wörter — < 1 %
208	theses.ncl.ac.uk Internet	8 Wörter — < 1 %
209	unsworks.unsw.edu.au Internet	8 Wörter — < 1 %
210	www.cell.com Internet	8 Wörter — < 1 %
211	www.ijbs.com Internet	8 Wörter — < 1 %
212	www.research.manchester.ac.uk Internet	8 Wörter — < 1 %
213	www.researchgate.net Internet	8 Wörter — < 1 %
214	Cancer Treatment and Research, 2016. Crossref	7 Wörter — < 1 %
215	Hanna, Thomas A. R.. "Molecular Analysis of Circulating Tumour Cells in Pancreatic Cancer.", The University of Liverpool (United Kingdom), 2020 ProQuest	7 Wörter — < 1 %
216	Tyler, Emily Rose. "Analysis of Sociodemographic and Disease Factors Associated with Psychological Distress among Newly Diagnosed Cancer Patients", Georgetown University, 2022 ProQuest	7 Wörter — < 1 %

217 Xiaobing Tian, Shengliang Zhang, Lanlan Zhou, Attila A. Seyhan, Liz Hernandez Borrero, Yiqun Zhang, Wafik S. El-Deiry. "Targeting the Integrated Stress Response in Cancer Therapy", Frontiers in Pharmacology, 2021
Crossref
7 Wörter — < 1 %

218 de Andrade Gaspar, Mariana Amaral Colaco. "Pancreatic Cancer. New Screening Biomarkers and Detection Methods", Universidade de Lisboa (Portugal)
ProQuest
7 Wörter — < 1 %

219 Alm, Petter. "Environmental Regulation of Metabolism: From Transgenerational Effects of Nutrition to Acute Effects of Exercise.", Karolinska Institutet (Sweden), 2021
ProQuest
6 Wörter — < 1 %

220 Erol, Nihal Oztolan. "Genetic Analysis of Nitrogen Use Efficiency in Arabidopsis thaliana", Wageningen University and Research, 2021
ProQuest
6 Wörter — < 1 %

221 J. Alfer. "Class I histone deacetylase expression in the human cyclic endometrium and endometrial adenocarcinomas", Human Reproduction, 09/27/2007
Crossref
6 Wörter — < 1 %

222 Luigi Formisano, Natascia Guida, Giusy Laudati, Luigi Mascolo, Gianfranco Di Renzo, Lorella M. T. Canzoniero. "MS-275 Inhibits Aroclor 1254–Induced SH-SY5Y Neuronal Cell Toxicity by Preventing the Formation of the HDAC3/REST Complex on the Synapsin-1 Promoter", Journal of Pharmacology and Experimental Therapeutics, 2015
Crossref
6 Wörter — < 1 %

223 Ozhan Ocal, Victor Pashkov, Rahul K. Kollipara, Yalda Zolghadri et al. " A rapid screen for
6 Wörter — < 1 %

pancreatic ductal adenocarcinoma therapeutics ", Disease Models & Mechanisms, 2015
Crossref

224 Shen, Shengnan. "Investigation on the Role of Myricanol in Regulating the Remodeling of Skeletal Muscle and Adipose Tissue.", Universidade de Macau (People's Republic of China), 2020 — 6 Wörter — < 1 %
ProQuest

225 Thompson, Rachael H. "Developing Therapeutic Approaches to Enhance Tumour-Specific Immunity in Breast Cancer", The University of Manchester (United Kingdom) — 6 Wörter — < 1 %
ProQuest

226 Tomas Eckschlager, Johana Plch, Marie Stiborova, Jan Hrabeta. "Histone Deacetylase Inhibitors as Anticancer Drugs", International Journal of Molecular Sciences, 2017 — 6 Wörter — < 1 %
Crossref

227 Watanabe, Marina. "Co-targeting Epigenetic and Oncogenic Enzymes in HER2+ Breast Cancer", Harvard University, 2022 — 6 Wörter — < 1 %
ProQuest

228 Wen-Qing Zhuo, Yi Wen, Hui-Jun Luo, Zhu-Lin Luo, Li Wang. "Mechanisms of ferroptosis in chronic kidney disease", Frontiers in Molecular Biosciences, 2022 — 6 Wörter — < 1 %
Crossref

229 orcid.org — 6 Wörter — < 1 %
Internet

ZITATE AUSSCHLIESSEN	AUS	QUELLEN AUSSCHLIESSEN	AUS
BIBLIOGRAFIE AUSSCHLIESSEN	AUS	ÜBEREINSTIMMUNGEN AUSSCHLIESSEN	AUS

Acknowledgements

I would like to thank Prof. Dr. Günter Schneider that he admitted me in his lab to work on my thesis. Also, I would like to thank my supervisor Lukas Krauß and all other members of AG Schneider for their support and patience, especially Carolin Schneider, Aylin Aydemir, Bettina Urban, Katharina Lankes, Felix Orben, Markus Rösch, Franziska Genevaux and Daniel Göke. Further I would like to thank my mentor Dr. Michael Autenrieth from the Department of Urology of Klinikum rechts der Isar for his engagement during the mentorship, especially during the COVID-19 pandemic (Kidess et al., 2021), Prof. Dr. Roland Schmid that I could work on my thesis at his Department of Internal Medicine II, all my friends and my fellow students from the universities of Regensburg and Munich, I was privileged to meet, and everyone who supported me during the time of my thesis or in my life. Special thanks to my mother who supported me my whole life and always believed in me. This thesis is dedicated to all the mentioned peoples, to my family, to the patients suffering from pancreatic cancer and to Dr. Helmut Baur, my mentor without whom I would not be a physician today.

References

Aktories, K. (2017). Allgemeine und Spezielle Pharmakologie und Toxikologie. Begründet Von W. Forth, D. Henschler, W. Rummel (Philadelphia: Urban & Fischer Verlag GmbH & Co. KG).

Arlt, A., and Schäfer, H. (2016). Investigational histone deacetylase inhibitors for treating pancreatic adenocarcinoma. Expert opinion on investigational drugs *25*, 1251-1254. https://doi.org/10.1080/13543784.2016.1240167.

B'chir, W., Maurin, A.-C., Carraro, V., Averous, J., Jousse, C., Muranishi, Y., Parry, L., Stepien, G., Fafournoux, P., and Bruhat, A. (2013). The eIF2α/ATF4 pathway is essential for stress-induced autophagy gene expression. Nucleic acids research *41*, 7683-7699. https://doi.org/10.1093/nar/gkt563.

Bhaskara, S. (2015). Histone deacetylases 1 and 2 regulate DNA replication and DNA repair: potential targets for genome stability-mechanism-based therapeutics for a subset of cancers. Cell cycle (Georgetown, Tex.) *14*, 1779-1785. https://doi.org/10.1080/15384101.2015.1042634.

Bose, P., Dai, Y., and Grant, S. (2014). Histone deacetylase inhibitor (HDACI) mechanisms of action: emerging insights. Pharmacology & therapeutics *143*, 323-336. https://doi.org/10.1016/j.pharmthera.2014.04.004.

Buscail, L., Bournet, B., and Cordelier, P. (2020). Role of oncogenic KRAS in the diagnosis, prognosis and treatment of pancreatic cancer. Nature reviews. Gastroenterology & hepatology *17*, 153-168. https://doi.org/10.1038/s41575-019-0245-4.

Canto, M.I., Hruban, R.H., Fishman, E.K., Kamel, I.R., Schulick, R., Zhang, Z., Topazian, M., Takahashi, N., Fletcher, J., and Petersen, G., et al. (2012). Frequent

detection of pancreatic lesions in asymptomatic high-risk individuals. Gastroenterology *142*, 796-804; quiz e14-5. https://doi.org/10.1053/j.gastro.2012.01.005.

Cao, J.Y., and Dixon, S.J. (2016). Mechanisms of ferroptosis. Cellular and molecular life sciences : CMLS *73*, 2195-2209. https://doi.org/10.1007/s00018-016-2194-1.

Cascinu, S., Falconi, M., Valentini, V., and Jelic, S. (2010). Pancreatic cancer: ESMO Clinical Practice Guidelines for diagnosis, treatment and follow-up. Annals of oncology : official journal of the European Society for Medical Oncology *21 Suppl 5*, v55-8. https://doi.org/10.1093/annonc/mdq165.

Cobler, L., Zhang, H., Suri, P., Park, C., and Timmerman, L.A. (2018). xCT inhibition sensitizes tumors to γ-radiation via glutathione reduction. Oncotarget *9*, 32280-32297. https://doi.org/10.18632/oncotarget.25794.

Conrad, M., and Pratt, D.A. (2019). The chemical basis of ferroptosis. Nature chemical biology *15*, 1137-1147. https://doi.org/10.1038/s41589-019-0408-1.

Conroy, T., Hammel, P., Hebbar, M., Ben Abdelghani, M., Wei, A.C., Raoul, J.-L., Choné, L., Francois, E., Artru, P., and Biagi, J.J., et al. (2018). FOLFIRINOX or Gemcitabine as Adjuvant Therapy for Pancreatic Cancer. The New England journal of medicine *379*, 2395-2406. https://doi.org/10.1056/NEJMoa1809775.

Damaskos, C., Garmpis, N., Karatzas, T., Nikolidakis, L., Kostakis, I.D., Garmpi, A., Karamaroudis, S., Boutsikos, G., Damaskou, Z., and Kostakis, A., et al. (2015). Histone Deacetylase (HDAC) Inhibitors: Current Evidence for Therapeutic Activities in Pancreatic Cancer. Anticancer research *35*, 3129-3135.

DeHart, D.N., Fang, D., Heslop, K., Li, L., Lemasters, J.J., and Maldonado, E.N. (2018). Opening of voltage dependent anion channels promotes reactive oxygen species generation, mitochondrial dysfunction and cell death in cancer cells. Biochemical pharmacology *148*, 155-162. https://doi.org/10.1016/j.bcp.2017.12.022.

Distler, M., Aust, D., Weitz, J., Pilarsky, C., and Grützmann, R. (2014). Precursor lesions for sporadic pancreatic cancer: PanIN, IPMN, and MCN. BioMed research international *2014*, 474905. https://doi.org/10.1155/2014/474905.

Dixon, S.J., Lemberg, K.M., Lamprecht, M.R., Skouta, R., Zaitsev, E.M., Gleason, C.E., Patel, D.N., Bauer, A.J., Cantley, A.M., and Yang, W.S., et al. (2012). Ferroptosis: an iron-dependent form of nonapoptotic cell death. Cell *149*, 1060-1072. https://doi.org/10.1016/j.cell.2012.03.042.

Doi, R., Imamura, M., Hosotani, R., Imaizumi, T., Hatori, T., Takasaki, K., Funakoshi, A., Wakasugi, H., Asano, T., and Hishinuma, S., et al. (2008). Surgery versus radiochemotherapy for resectable locally invasive pancreatic cancer: final results of a randomized multi-institutional trial. Surgery today *38*, 1021-1028. https://doi.org/10.1007/s00595-007-3745-8.

Dolma, S., Lessnick, S.L., Hahn, W.C., and Stockwell, B.R. (2003). Identification of genotype-selective antitumor agents using synthetic lethal chemical screening in engineered human tumor cells. Cancer cell *3*, 285-296. https://doi.org/10.1016/s1535-6108(03)00050-3.

Duvic, M., Talpur, R., Ni, X., Zhang, C., Hazarika, P., Kelly, C., Chiao, J.H., Reilly, J.F., Ricker, J.L., and Richon, V.M., et al. (2007). Phase 2 trial of oral vorinostat (suberoylanilide hydroxamic acid, SAHA) for refractory cutaneous T-cell lymphoma (CTCL). Blood *109*, 31-39. https://doi.org/10.1182/blood-2006-06-025999.

Eckschlager, T., Plch, J., Stiborova, M., and Hrabeta, J. (2017). Histone Deacetylase Inhibitors as Anticancer Drugs. International journal of molecular sciences *18*. https://doi.org/10.3390/ijms18071414.

Epping, M.T., and Bernards, R. (2009). Molecular basis of the anti-cancer effects of histone deacetylase inhibitors. The international journal of biochemistry & cell biology *41*, 16-20. https://doi.org/10.1016/j.biocel.2008.07.020.

Esposito, I., Konukiewitz, B., Schlitter, A.M., and Klöppel, G. (2014). Pathology of pancreatic ductal adenocarcinoma: facts, challenges and future developments. World journal of gastroenterology *20*, 13833-13841. https://doi.org/10.3748/wjg.v20.i38.13833.

Falkenberg, K.J., and Johnstone, R.W. (2014). Histone deacetylases and their inhibitors in cancer, neurological diseases and immune disorders. Nature reviews. Drug discovery *13*, 673-691. https://doi.org/10.1038/nrd4360.

Fedele, P., Orlando, L., and Cinieri, S. (2017). Targeting triple negative breast cancer with histone deacetylase inhibitors. Expert opinion on investigational drugs *26*, 1199-1206. https://doi.org/10.1080/13543784.2017.1386172.

Feng, W., Zhang, B., Cai, D., and Zou, X. (2014). Therapeutic potential of histone deacetylase inhibitors in pancreatic cancer. Cancer letters *347*, 183-190. https://doi.org/10.1016/j.canlet.2014.02.012.

Fritsche, P., Seidler, B., Schüler, S., Schnieke, A., Göttlicher, M., Schmid, R.M., Saur, D., and Schneider, G. (2009). HDAC2 mediates therapeutic resistance of pancreatic cancer cells via the BH3-only protein NOXA. Gut *58*, 1399-1409. https://doi.org/10.1136/gut.2009.180711.

Fusai, G., Warnaar, N., Sabin, C.A., Archibong, S., and Davidson, B.R. (2008). Outcome of R1 resection in patients undergoing pancreatico-duodenectomy for pancreatic cancer. European journal of surgical oncology : the journal of the European Society of Surgical Oncology and the British Association of Surgical Oncology *34*, 1309-1315. https://doi.org/10.1016/j.ejso.2008.01.017.

Gilroy, A.M. (2009). Atlas of anatomy. Winkingskull.com (New York, Stuttgart: Thieme).

Golan, T., Hammel, P., Reni, M., van Cutsem, E., Macarulla, T., Hall, M.J., Park, J.-O., Hochhauser, D., Arnold, D., and Oh, D.-Y., et al. (2019). Maintenance Olaparib for Germline BRCA-Mutated Metastatic Pancreatic Cancer. The New England journal of medicine *381*, 317-327. https://doi.org/10.1056/NEJMoa1903387.

Haberland, M., Montgomery, R.L., and Olson, E.N. (2009). The many roles of histone deacetylases in development and physiology: implications for disease and therapy. Nature reviews. Genetics *10*, 32-42. https://doi.org/10.1038/nrg2485.

Hafezi, S., Saber-Ayad, M., and Abdel-Rahman, W.M. (2021). Highlights on the Role of KRAS Mutations in Reshaping the Microenvironment of Pancreatic Adenocarcinoma. International journal of molecular sciences *22*. https://doi.org/10.3390/ijms221910219.

Hartwig, W., Hackert, T., Hinz, U., Gluth, A., Bergmann, F., Strobel, O., Büchler, M.W., and Werner, J. (2011). Pancreatic cancer surgery in the new millennium: better prediction of outcome. Annals of surgery *254*, 311-319. https://doi.org/10.1097/SLA.0b013e31821fd334.

Hong, S.-M., Park, J.Y., Hruban, R.H., and Goggins, M. (2011). Molecular signatures of pancreatic cancer. Archives of pathology & laboratory medicine *135*, 716-727. https://doi.org/10.1043/2010-0566-RA.1.

Hontecillas-Prieto, L., Flores-Campos, R., Silver, A., Álava, E. de, Hajji, N., and García-Domínguez, D.J. (2020). Synergistic Enhancement of Cancer Therapy Using HDAC Inhibitors: Opportunity for Clinical Trials. Frontiers in genetics *11*, 578011. https://doi.org/10.3389/fgene.2020.578011.

Hruban, R.H., van Mansfeld, A.D., Offerhaus, G.J., van Weering, D.H., Allison, D.C., Goodman, S.N., Kensler, T.W., Bose, K.K., Cameron, J.L., and Bos, J.L. (1993). K-ras oncogene activation in adenocarcinoma of the human pancreas. A study of 82 carcinomas using a combination of mutant-enriched polymerase chain reaction analysis and allele-specific oligonucleotide hybridization. The American journal of pathology *143*, 545-554.

Ianevski, A., Giri, A.K., and Aittokallio, T. (2022). SynergyFinder 3.0: an interactive analysis and consensus interpretation of multi-drug synergies across multiple samples. Nucleic acids research. https://doi.org/10.1093/nar/gkac382.

Imai, H., Matsuoka, M., Kumagai, T., Sakamoto, T., and Koumura, T. (2017). Lipid Peroxidation-Dependent Cell Death Regulated by GPx4 and Ferroptosis. Current topics in microbiology and immunology *403*, 143-170. https://doi.org/10.1007/82_2016_508.

Jain, A., and Bhardwaj, V. (2021). Therapeutic resistance in pancreatic ductal adenocarcinoma: Current challenges and future opportunities. World journal of gastroenterology *27*, 6527-6550. https://doi.org/10.3748/wjg.v27.i39.6527.

Jones, S., Zhang, X., Parsons, D.W., Lin, J.C.-H., Leary, R.J., Angenendt, P., Mankoo, P., Carter, H., Kamiyama, H., and Jimeno, A., et al. (2008). Core signaling pathways in human pancreatic cancers revealed by global genomic analyses. Science (New York, N.Y.) *321*, 1801-1806. https://doi.org/10.1126/science.1164368.

Kelly, R.D.W., Chandru, A., Watson, P.J., Song, Y., Blades, M., Robertson, N.S., Jamieson, A.G., Schwabe, J.W.R., and Cowley, S.M. (2018). Histone deacetylase (HDAC) 1 and 2 complexes regulate both histone acetylation and crotonylation in vivo. Scientific reports *8*, 14690. https://doi.org/10.1038/s41598-018-32927-9.

Kelly, R.D.W., and Cowley, S.M. (2013). The physiological roles of histone deacetylase (HDAC) 1 and 2: complex co-stars with multiple leading parts. Biochemical Society transactions *41*, 741-749. https://doi.org/10.1042/BST20130010.

Kidess, M., Schmid, S.C., Pollak, S., Gschwend, J.E., Berberat, P.O., and Autenrieth, M.E. (2021). Virtueller Praktikumstag Urologie : Studentenunterricht an der Technischen Universität München in Zeiten der COVID-19-Pandemie. Der Urologe. Ausg. A *60*, 484-490. https://doi.org/10.1007/s00120-020-01431-2.

Kim, H., Kim, M., Im, S.-K., and Fang, S. (2018). Mouse Cre-LoxP system: general principles to determine tissue-specific roles of target genes. Laboratory animal research *34*, 147-159. https://doi.org/10.5625/lar.2018.34.4.147.

Koppula, P., Zhang, Y., Zhuang, L., and Gan, B. (2018). Amino acid transporter SLC7A11/xCT at the crossroads of regulating redox homeostasis and nutrient dependency of cancer. Cancer communications (London, England) *38*, 12. https://doi.org/10.1186/s40880-018-0288-x.

Krauß, L., Urban, B.C., Hastreiter, S., Schneider, C., Wenzel, P., Hassan, Z., Wirth, M., Lankes, K., Terrasi, A., and Klement, C., et al. (2022). HDAC2 Facilitates Pancreatic Cancer Metastasis. Cancer research *82*, 695-707. https://doi.org/10.1158/0008-5472.CAN-20-3209.

Kristianto, J., Johnson, M.G., Zastrow, R.K., Radcliff, A.B., and Blank, R.D. (2017). Spontaneous recombinase activity of Cre-ERT2 in vivo. Transgenic research *26*, 411-417. https://doi.org/10.1007/s11248-017-0018-1.

Kummar, S., Gutierrez, M., Gardner, E.R., Donovan, E., Hwang, K., Chung, E.J., Lee, M.-J., Maynard, K., Kalnitskiy, M., and Chen, A., et al. (2007). Phase I trial of MS-275, a histone deacetylase inhibitor, administered weekly in refractory solid tumors and lymphoid malignancies. Clinical cancer research : an official journal of the American Association for Cancer Research *13*, 5411-5417. https://doi.org/10.1158/1078-0432.CCR-07-0791.

Lane, A.A., and Chabner, B.A. (2009). Histone deacetylase inhibitors in cancer therapy. Journal of clinical oncology : official journal of the American Society of Clinical Oncology *27*, 5459-5468. https://doi.org/10.1200/JCO.2009.22.1291.

Leitlinienprogramm Onkologie (2021). S3-Leitlinie zum exokrinen Pankreaskarzinom. Kurzversion.

Lewerenz, J., Sato, H., Albrecht, P., Henke, N., Noack, R., Methner, A., and Maher, P. (2012). Mutation of ATF4 mediates resistance of neuronal cell lines against oxidative stress by inducing xCT expression. Cell death and differentiation *19*, 847-858. https://doi.org/10.1038/cdd.2011.165.

Li, G., Tian, Y., and Zhu, W.-G. (2020). The Roles of Histone Deacetylases and Their Inhibitors in Cancer Therapy. Frontiers in cell and developmental biology *8*, 576946. https://doi.org/10.3389/fcell.2020.576946.

Li, J.-T., Wang, Y.-P., Yin, M., and Lei, Q.-Y. (2019). Metabolism remodeling in pancreatic ductal adenocarcinoma. Cell stress *3*, 361-368. https://doi.org/10.15698/cst2019.12.205.

Li, Y., and Seto, E. (2016). HDACs and HDAC Inhibitors in Cancer Development and Therapy. Cold Spring Harbor perspectives in medicine *6*. https://doi.org/10.1101/cshperspect.a026831.

Liu, J., Kang, R., and Tang, D. (2021). The Art of War: Ferroptosis and Pancreatic Cancer. Frontiers in pharmacology *12*, 773909. https://doi.org/10.3389/fphar.2021.773909.

Maldonado, E.N. (2017). VDAC-Tubulin, an Anti-Warburg Pro-Oxidant Switch. Frontiers in oncology *7*, 4. https://doi.org/10.3389/fonc.2017.00004.

Maldonado, E.N., and Lemasters, J.J. (2012). Warburg revisited: regulation of mitochondrial metabolism by voltage-dependent anion channels in cancer cells. The Journal of pharmacology and experimental therapeutics *342*, 637-641. https://doi.org/10.1124/jpet.112.192153.

Mariño-Ramírez, L., Kann, M.G., Shoemaker, B.A., and Landsman, D. (2005). Histone structure and nucleosome stability. Expert review of proteomics *2*, 719-729. https://doi.org/10.1586/14789450.2.5.719.

Masson, G.R. (2019). Towards a model of GCN2 activation. Biochemical Society transactions *47*, 1481-1488. https://doi.org/10.1042/BST20190331.

Miyake, K., Yoshizumi, T., Imura, S., Sugimoto, K., Batmunkh, E., Kanemura, H., Morine, Y., and Shimada, M. (2008). Expression of hypoxia-inducible factor-1alpha, histone deacetylase 1, and metastasis-associated protein 1 in pancreatic carcinoma: correlation with poor prognosis with possible regulation. Pancreas *36*, e1-9. https://doi.org/10.1097/MPA.0b013e31815f2c2a.

Miyamoto, K., Watanabe, M., Boku, S., Sukeno, M., Morita, M., Kondo, H., Sakaguchi, K., Taguchi, T., and Sakai, T. (2020). xCT Inhibition Increases Sensitivity to Vorinostat in a ROS-Dependent Manner. Cancers *12*. https://doi.org/10.3390/cancers12040827.

Mootha, V.K., Lindgren, C.M., Eriksson, K.-F., Subramanian, A., Sihag, S., Lehar, J., Puigserver, P., Carlsson, E., Ridderstråle, M., and Laurila, E., et al. (2003). PGC-1alpha-responsive genes involved in oxidative phosphorylation are coordinately downregulated in human diabetes. Nature genetics *34*, 267-273. https://doi.org/10.1038/ng1180.

Moskaluk, C.A., Hruban, R.H., and Kern, S.E. (1997). p16 and K-ras gene mutations in the intraductal precursors of human pancreatic adenocarcinoma. Cancer research *57*, 2140-2143.

Neoptolemos, J.P., Palmer, D.H., Ghaneh, P., Psarelli, E.E., Valle, J.W., Halloran, C.M., Faluyi, O., O'Reilly, D.A., Cunningham, D., and Wadsley, J., et al. (2017). Comparison of adjuvant gemcitabine and capecitabine with gemcitabine monotherapy in patients with resected pancreatic cancer (ESPAC-4): a multicentre, open-label, randomised, phase 3 trial. The Lancet *389*, 1011-1024. https://doi.org/10.1016/S0140-6736(16)32409-6.

Nepali, K., and Liou, J.-P. (2021). Recent developments in epigenetic cancer therapeutics: clinical advancement and emerging trends. Journal of biomedical science *28*, 27. https://doi.org/10.1186/s12929-021-00721-x.

Ott, C., Heinmöller, E., Gaumann, A., Schölmerich, J., and Klebl, F. (2007). Intraepitheliale Neoplasien (PanIN) und intraduktale papillär-muzinöse Neoplasien (IPMN) des Pankreas als Vorläufer des Pankreaskarzinoms. Medizinische Klinik (Munich, Germany : 1983) *102*, 127-135. https://doi.org/10.1007/s00063-007-1013-8.

Ouaïssi, M., Sielezneff, I., Silvestre, R., Sastre, B., Bernard, J.-P., Lafontaine, J.S., Payan, M.J., Dahan, L., Pirrò, N., and Seitz, J.F., et al. (2008). High histone deacetylase 7 (HDAC7) expression is significantly associated with adenocarcinomas of the pancreas. Annals of surgical oncology *15*, 2318-2328. https://doi.org/10.1245/s10434-008-9940-z.

Pape, H.-C., Klinke, R., Brenner, B., and Silbernagl, S. (2014). Physiologie (s.l.: Georg Thieme Verlag KG).

Park, W., Chawla, A., and O'Reilly, E.M. (2021). Pancreatic Cancer: A Review. JAMA *326*, 851-862. https://doi.org/10.1001/jama.2021.13027.

Principe, D.R., Underwood, P.W., Korc, M., Trevino, J.G., Munshi, H.G., and Rana, A. (2021). The Current Treatment Paradigm for Pancreatic Ductal Adenocarcinoma and Barriers to Therapeutic Efficacy. Frontiers in oncology *11*, 688377. https://doi.org/10.3389/fonc.2021.688377.

Promega Corporation. CellTiter-Glo Luminescent Cell Viability Assay Technical Bulletin #TB288.

Rahib, L., Wehner, M.R., Matrisian, L.M., and Nead, K.T. (2021). Estimated Projection of US Cancer Incidence and Death to 2040. JAMA network open *4*, e214708. https://doi.org/10.1001/jamanetworkopen.2021.4708.

Rana, Z., Diermeier, S., Hanif, M., and Rosengren, R.J. (2020). Understanding Failure and Improving Treatment Using HDAC Inhibitors for Prostate Cancer. Biomedicines *8*. https://doi.org/10.3390/biomedicines8020022.

Rassow, J., Hauser, K., Netzker, R., and Deutzmann, R. (2016). Biochemie (Stuttgart: Thieme).

Renz-Polster, H., Krautzig, S., Bätge, B., and Stoll, M. (2013). Basislehrbuch Innere Medizin. Kompakt - greifbar - verständlich ; [Plus im Web, mediscript (München: Elsevier Urban & Fischer).

Richon, V.M., and O'Brien, J.P. (2002). Histone deacetylase inhibitors: a new class of potential therapeutic agents for cancer treatment. Clinical cancer research : an official journal of the American Association for Cancer Research *8*, 662-664.

Roca, M.S., Moccia, T., Iannelli, F., Testa, C., Vitagliano, C., Minopoli, M., Camerlingo, R., Riso, G. de, Cecio, R. de, and Bruzzese, F., et al. (2022). HDAC class I inhibitor domatinostat sensitizes pancreatic cancer to chemotherapy by targeting cancer stem cell compartment via FOXM1 modulation. Journal of experimental & clinical cancer research : CR *41*, 83. https://doi.org/10.1186/s13046-022-02295-4.

Roche, J., and Bertrand, P. (2016). Inside HDACs with more selective HDAC inhibitors. European journal of medicinal chemistry *121*, 451-483. https://doi.org/10.1016/j.ejmech.2016.05.047.

Ruefli, A.A., Ausserlechner, M.J., Bernhard, D., Sutton, V.R., Tainton, K.M., Kofler, R., Smyth, M.J., and Johnstone, R.W. (2001). The histone deacetylase inhibitor and chemotherapeutic agent suberoylanilide hydroxamic acid (SAHA) induces a cell-death pathway characterized by cleavage of Bid and production of reactive oxygen species. Proceedings of the National Academy of Sciences of the United States of America *98*, 10833-10838. https://doi.org/10.1073/pnas.191208598.

Schneider, G., Krämer, O.H., Fritsche, P., Schüler, S., Schmid, R.M., and Saur, D. (2010). Targeting histone deacetylases in pancreatic ductal adenocarcinoma. Journal of cellular and molecular medicine *14*, 1255-1263. https://doi.org/10.1111/j.1582-4934.2009.00974.x.

Schönhuber, N., Seidler, B., Schuck, K., Veltkamp, C., Schachtler, C., Zukowska, M., Eser, S., Feyerabend, T.B., Paul, M.C., and Eser, P., et al. (2014). A next-generation dual-recombinase system for time- and host-specific targeting of pancreatic cancer. Nature medicine *20*, 1340-1347. https://doi.org/10.1038/nm.3646.

Schüler, S., Fritsche, P., Diersch, S., Arlt, A., Schmid, R.M., Saur, D., and Schneider, G. (2010). HDAC2 attenuates TRAIL-induced apoptosis of pancreatic cancer cells. Molecular cancer *9*, 80. https://doi.org/10.1186/1476-4598-9-80.

Schünke, M., Schulte, E., Schumacher, U., Voll, M., and Wesker, K. (2015). Prometheus Lernatlas LernAtlas der Anatomie - Innere Organe (Stuttgart: Thieme).

Selleck Chemicals. www. selleckchem.com. http://selleckchem.com/products/. October 13th, 2019.

Seto, E., and Yoshida, M. (2014). Erasers of histone acetylation: the histone deacetylase enzymes. Cold Spring Harbor perspectives in biology *6*, a018713. https://doi.org/10.1101/cshperspect.a018713.

Shinke, G., Yamada, D., Eguchi, H., Iwagami, Y., Asaoka, T., Noda, T., Wada, H., Kawamoto, K., Gotoh, K., and Kobayashi, S., et al. (2018). Role of histone deacetylase 1 in distant metastasis of pancreatic ductal cancer. Cancer science *109*, 2520-2531. https://doi.org/10.1111/cas.13700.

Shvedunova, M., and Akhtar, A. (2022). Modulation of cellular processes by histone and non-histone protein acetylation. Nature reviews. Molecular cell biology *23*, 329-349. https://doi.org/10.1038/s41580-021-00441-y.

Siegel, R.L., Miller, K.D., Fuchs, H.E., and Jemal, A. (2021). Cancer Statistics, 2021. CA: a cancer journal for clinicians *71*, 7-33. https://doi.org/10.3322/caac.21654.

Siegel, R.L., Miller, K.D., Fuchs, H.E., and Jemal, A. (2022). Cancer statistics, 2022. CA: a cancer journal for clinicians. https://doi.org/10.3322/caac.21708.

Singh, A.K., and Mueller-Planitz, F. (2021). Nucleosome Positioning and Spacing: From Mechanism to Function. Journal of molecular biology *433*, 166847. https://doi.org/10.1016/j.jmb.2021.166847.

Subramanian, A., Tamayo, P., Mootha, V.K., Mukherjee, S., Ebert, B.L., Gillette, M.A., Paulovich, A., Pomeroy, S.L., Golub, T.R., and Lander, E.S., et al. (2005). Gene set enrichment analysis: a knowledge-based approach for interpreting genome-wide expression profiles. Proceedings of the National Academy of Sciences of the United States of America *102*, 15545-15550. https://doi.org/10.1073/pnas.0506580102.

Suragani, R.N.V.S., Zachariah, R.S., Velazquez, J.G., Liu, S., Sun, C.-W., Townes, T.M., and Chen, J.-J. (2012). Heme-regulated eIF2α kinase activated Atf4 signaling pathway in oxidative stress and erythropoiesis. Blood *119*, 5276-5284. https://doi.org/10.1182/blood-2011-10-388132.

SynergyFinder (2020). SynergyFinder - User Documentation. https://synergyfinder.fimm.fi/synergy/synfin_docs/. 9.1.2022.

Tada, M., Ohashi, M., Shiratori, Y., Okudaira, T., Komatsu, Y., Kawabe, T., Yoshida, H., Machinami, R., Kishi, K., and Omata, M. (1996). Analysis of K-ras gene mutation in hyperplastic duct cells of the pancreas without pancreatic disease. Gastroenterology *110*, 227-231. https://doi.org/10.1053/gast.1996.v110.pm8536861.

Trachootham, D., Zhou, Y., Zhang, H., Demizu, Y., Chen, Z., Pelicano, H., Chiao, P.J., Achanta, G., Arlinghaus, R.B., and Liu, J., et al. (2006). Selective killing of oncogenically transformed cells through a ROS-mediated mechanism by beta-phenylethyl isothiocyanate. Cancer cell *10*, 241-252. https://doi.org/10.1016/j.ccr.2006.08.009.

U.S. Federal Government. Olaparib in gBRCA Mutated Pancreatic Cancer Whose Disease Has Not Progressed on First Line Platinum-Based Chemotherapy (POLO). https://clinicaltrials.gov/ct2/show/NCT02184195. 15.05.2022.

U.S. Food and Drug Administration (2019). FDA approves olaparib for gBRCAm metastatic pancreatic adenocarcinoma. https://www.fda.gov/drugs/resources-information-approved-drugs/fda-approves-olaparib-gbrcam-metastatic-pancreatic-adenocarcinoma. November 13, 2021.

Venugopal, B., and Evans, T.R.J. (2011). Developing histone deacetylase inhibitors as anti-cancer therapeutics. Current medicinal chemistry *18*, 1658-1671. https://doi.org/10.2174/092986711795471284.

Wagner, M., Redaelli, C., Lietz, M., Seiler, C.A., Friess, H., and Büchler, M.W. (2004). Curative resection is the single most important factor determining outcome in patients with pancreatic adenocarcinoma. The British journal of surgery *91*, 586-594. https://doi.org/10.1002/bjs.4484.

Wang, G., He, J., Zhao, J., Yun, W., Xie, C., Taub, J.W., Azmi, A., Mohammad, R.M., Dong, Y., and Kong, W., et al. (2012). Class I and class II histone deacetylases are potential therapeutic targets for treating pancreatic cancer. PloS one *7*, e52095. https://doi.org/10.1371/journal.pone.0052095.

Wang, X., Liu, K., Gong, H., Li, D., Chu, W., Zhao, D., Wang, X., and Xu, D. (2021). Death by histone deacetylase inhibitor quisinostat in tongue squamous cell carcinoma via apoptosis, pyroptosis, and ferroptosis. Toxicology and applied pharmacology *410*, 115363. https://doi.org/10.1016/j.taap.2020.115363.

Waters, A.M., and Der, C.J. (2018). KRAS: The Critical Driver and Therapeutic Target for Pancreatic Cancer. Cold Spring Harbor perspectives in medicine *8*. https://doi.org/10.1101/cshperspect.a031435.

Weichert, W. (2009). HDAC expression and clinical prognosis in human malignancies. Cancer letters *280*, 168-176. https://doi.org/10.1016/j.canlet.2008.10.047.

Welsch, U., Deller, T., and Kummer, W. (2014). Lehrbuch Histologie (München: Elsevier Urban & Fischer).

Wolf, I.M.L., Fan, Z., Rauh, M., Seufert, S., Hore, N., Buchfelder, M., Savaskan, N.E., and Eyüpoglu, I.Y. (2014). Histone deacetylases inhibition by SAHA/Vorinostat normalizes the glioma microenvironment via xCT equilibration. Scientific reports *4*, 6226. https://doi.org/10.1038/srep06226.

Wortel, I.M.N., van der Meer, L.T., Kilberg, M.S., and van Leeuwen, F.N. (2017). Surviving Stress: Modulation of ATF4-Mediated Stress Responses in Normal and Malignant Cells. Trends in endocrinology and metabolism: TEM *28*, 794-806. https://doi.org/10.1016/j.tem.2017.07.003.

Wu, J., Liu, X., Nayak, S.G., Pitarresi, J.R., Cuitiño, M.C., Yu, L., Hildreth, B.E., Thies, K.A., Schilling, D.J., and Fernandez, S.A., et al. (2017). Generation of a pancreatic cancer model using a Pdx1-Flp recombinase knock-in allele. PloS one *12*, e0184984. https://doi.org/10.1371/journal.pone.0184984.

Yadav, B., Wennerberg, K., Aittokallio, T., and Tang, J. (2015). Searching for Drug Synergy in Complex Dose-Response Landscapes Using an Interaction Potency Model. Computational and structural biotechnology journal *13*, 504-513. https://doi.org/10.1016/j.csbj.2015.09.001.

Yagoda, N., Rechenberg, M. von, Zaganjor, E., Bauer, A.J., Yang, W.S., Fridman, D.J., Wolpaw, A.J., Smukste, I., Peltier, J.M., and Boniface, J.J., et al. (2007). RAS-RAF-MEK-dependent oxidative cell death involving voltage-dependent anion channels. Nature *447*, 864-868. https://doi.org/10.1038/nature05859.

Yang, H., Zhao, L., Gao, Y., Yao, F., Marti, T.M., Schmid, R.A., and Peng, R.-W. (2020). Pharmacotranscriptomic Analysis Reveals Novel Drugs and Gene Networks Regulating Ferroptosis in Cancer. Cancers *12*. https://doi.org/10.3390/cancers12113273.

Yang, W.S., SriRamaratnam, R., Welsch, M.E., Shimada, K., Skouta, R., Viswanathan, V.S., Cheah, J.H., Clemons, P.A., Shamji, A.F., and Clish, C.B., et al. (2014). Regulation of ferroptotic cancer cell death by GPX4. Cell *156*, 317-331. https://doi.org/10.1016/j.cell.2013.12.010.

Yang, X.-J., and Seto, E. (2008). The Rpd3/Hda1 family of lysine deacetylases: from bacteria and yeast to mice and men. Nature reviews. Molecular cell biology *9*, 206-218. https://doi.org/10.1038/nrm2346.

Zaborske, J.M., Narasimhan, J., Jiang, L., Wek, S.A., Dittmar, K.A., Freimoser, F., Pan, T., and Wek, R.C. (2009). Genome-wide Analysis of tRNA Charging and Activation of

the eIF2 Kinase Gcn2p*♦. The Journal of biological chemistry *284*, 25254-25267. https://doi.org/10.1074/jbc.M109.000877.

Zamboni, G., Hirabayashi, K., Castelli, P., and Lennon, A.M. (2013). Precancerous lesions of the pancreas. Best practice & research. Clinical gastroenterology *27*, 299-322. https://doi.org/10.1016/j.bpg.2013.04.001.

Zhang, J., and Zhong, Q. (2014). Histone deacetylase inhibitors and cell death. Cellular and molecular life sciences : CMLS *71*, 3885-3901. https://doi.org/10.1007/s00018-014-1656-6.

Zhang, Y., Tan, H., Daniels, J.D., Zandkarimi, F., Liu, H., Brown, L.M., Uchida, K., O'Connor, O.A., and Stockwell, B.R. (2019). Imidazole Ketone Erastin Induces Ferroptosis and Slows Tumor Growth in a Mouse Lymphoma Model. Cell chemical biology *26*, 623-633.e9. https://doi.org/10.1016/j.chembiol.2019.01.008.

Zhao, Y., Li, Y., Zhang, R., Wang, F., Wang, T., and Jiao, Y. (2020). The Role of Erastin in Ferroptosis and Its Prospects in Cancer Therapy. OncoTargets and therapy *13*, 5429-5441. https://doi.org/10.2147/OTT.S254995.

Zille, M., Kumar, A., Kundu, N., Bourassa, M.W., Wong, V.S.C., Willis, D., Karuppagounder, S.S., and Ratan, R.R. (2019). Ferroptosis in Neurons and Cancer Cells Is Similar But Differentially Regulated by Histone Deacetylase Inhibitors. eNeuro *6*. https://doi.org/10.1523/ENEURO.0263-18.2019.

Eidesstattliche Erklärung

Ich erkläre an Eides statt, dass ich die bei der promotionsführenden Einrichtung

Klinik und Poliklinik für Innere Medizin II, Klinikum rechts der Isar, Technische Universität München

---

der TUM zur Promotionsprüfung vorgelegte Arbeit mit dem Titel:

Screening of a drug-library in HDAC-2 proficient and deficient murine pancreatic ductal adenocarcinoma cells to identify new potential combination therapies

---

in Klinik und Poliklinik für Innere Medizin II, Klinikum rechts der Isar, Technische Universität München, Fakultät für Medizin

Fakultät, Institut, Lehrstuhl, Klinik, Krankenhaus, Abteilung

unter der Anleitung und Betreuung durch: Herrn Prof. Dr. med. Günter Schneider ohne sonstige Hilfe erstellt und bei der Abfassung nur die gemäß § 6 Ab. 6 und 7 Satz 2 angebotenen Hilfsmittel benutzt habe.

☒ Ich habe keine Organisation eingeschaltet, die gegen Entgelt Betreuerinnen und Betreuer für die Anfertigung von Dissertationen sucht, oder die mir obliegenden Pflichten hinsichtlich der Prüfungsleistungen für mich ganz oder teilweise erledigt.

☒ Ich habe die Dissertation in dieser oder ähnlicher Form in keinem anderen Prüfungsverfahren als Prüfungsleistung vorgelegt.

☒ Ich habe den angestrebten Doktorgrad noch nicht erworben und bin nicht in einem früheren Promotionsverfahren für den angestrebten Doktorgrad endgültig gescheitert.

Die öffentlich zugängliche Promotionsordnung der TUM ist mir bekannt, insbesondere habe ich die Bedeutung von § 28 (Nichtigkeit der Promotion) und § 29 (Entzug des Doktorgrades) zur Kenntnis genommen. Ich bin mir der Konsequenzen einer falschen Eidesstattlichen Erklärung bewusst.

Mit der Aufnahme meiner personenbezogenen Daten in die Alumni-Datei bei der TUM bin ich

☒ einverstanden, ☐ nicht einverstanden.

München, Datum, Unterschrift